Characterization of the Upper Arkansas River Basin, Chaffee County Colorado

Colorado School of Mines, Boise State University,
Imperial College London Geophysics Field Camp 2009

June 4, 2009

Abstract

Students specializing in geophysical investigations participated in a summer field session organized through the Colorado School of Mines, Boise State University, and Imperial College London in order to apply knowledge gained in the classroom. The 2009 Summer field session took place in Chaffee County, Colorado from May 10th through the 22nd before returning to Golden, Colorado for processing until June 5th.

For the fifth year, the students conducted geophysical surveys in the Poncha Springs and Mount Princeton Hot Springs area, where both near surface and deep geophysical techniques were used. The data collected builds on the geological understanding of the area, and therefore an increased understanding of geothermal activity in Chaffee County.

Just north of the Mount Princeton Hot Springs area the students conducted an investigation using seismic, gravity, and magnetics in order to help identify the large structures and basin fill associated with the Rio Grande Rift. At the area known as Mount Princeton Hot Springs, near surface geophysics was conducted to help understand the faulting and fractures that act as a conduit for hydrothermal flow. The methods used included high frequency 3D seismic, magnetics, gravity, D.C. resistivity, and self potential. Throughout the Mount Princeton area, passive seismic, vertical seismic profiling, and well logging were also used to better understand the geology and activity of the region.

Surveys were conducted in the Poncha Springs area as reconnaissance for future, more in depth, surveys. This data will give an initial understanding of surface manifestations and possible faulting associated with the Rio Grande Rift, the San Luis Valley, and the Upper Arkansas Basin. Methods used were D.C. resistivity, magnetics, electromagnetics, self potential, and gravity.

Following a thirteen day period of data acquisition in Chaffee County, the students returned to the Colorado School of Mines in Golden, Colorado for an additional two weeks of data processing. They drew many conclusions and made interpretations from the data collected.

In the Field of Pain the data suggest a 40 to 50 m thick unconsolidated layer overlying the fractured granitic basement. The DC profile shows a deep geothermal anomaly of low resistivity which correlates with a positive SP anomaly in the same region. In the Chalk Creek valley a shear zone extends from the north east to the south west, just south of the Chalk Cliffs. There appears to be an upward migration of the water through this shear zone which then flows along the porous sediments towards the south in this area.

At Poncha Springs, the high conductivity zones in the EM data and the low resistivity in the DC profiles suggest hot water distribution in the subsurface. The magnetic data suggests that a fault near the Boy Scout camp which acts a a conduit to hot water.

The deep seismic suggests that the depth to the basement is approximately 2000m. Also identified on the deep seismic are two major faults on the west end and two minors at the east end of the cross-section. An alteration zone is identified between the faults and a possible Precambrian northeast trending shear zone.

Acknowledgements

the students ensuring that the surveys ran smoothly and efficiently. CSM Alumni, Evan Genaud spent many hours helping students with seismic processing. Also a big thanks to Brian Passerella, the field equipment coordinator, for his tireless efforts to keep equipment running.

Students

Colorado School of Mines	Boise State University	Imperial College London
Bo Beins	Shannon Chollett	Yernur Akashev
Brandon Bush	Sean McShane	Akeem Akintayo
Joey Cohrs	Andrew Nies	Nafa Al Jahdhani
Sarah Devriese	Randi Walters	Ahmad Alghamamdi
Yuanzhong Fan	Horry Parker*	Kate Chapman
Farnoush Forghani	Antonio Pereira†	Anna Dawson
Renee Francese		Khushal Gohel
Roxy Frary		Hamizah Hj Hamzah
Leslie Godfrey		Nurbek Karatalov
Joyce Hoopes		Bakhytzhan Khairaliyev
Gordon Johnson		Christopher Leader
Colin Leek		Cristian Moncada Palacio
David Manthei		Tenice Nangoo
Craig Markey		Jeremy Soule
Michael Mitchell		Krystel-Maria St Clair
Cliff Preston		Christopher Swift
Orion Sandoval		Thomas Weight
Jessie Shirey		Victoria Wilson
Kristen Swaim		
Ariel Thomas		

---

[a]Horry Parker attends University of Georgia
[b]Antonio Pereira attends Texas A&M

Disclaimer

The information contained in this document is derived from a summer field camp for undergraduate and graduate students in Geophysics at the Colorado School of Mines, Boise State University, and the Imperial College London. The primary purpose of this camp is to teach students the hands-on use of a wide variety of geophysical methods. Secondarily, this camp focused on the issues associated with aquifer recharge dynamics in the Upper Arkansas Valley. However, the processing and interpretation of data gathered in the basin was done, mostly on a first-time basis, by students inexperienced in these activities. Therefore, the results should be regarded appropriately. Neither the Department of Geophysics nor the Colorado School of Mines guarantees the validity of the information presented in this document.

Contents

Chapter 1

Introduction

1.1   Background Information

Every year the Colorado School of Mines hosts a Geophysical field session, which gives an invaluable experience for students to refine the skills and reinforce their knowledge acquired in the classroom. The 2009 session was comprised of both graduate and undergraduate students in association with the Colorado School of Mines, Boise State University, and Imperial College London. The group visited Chaffee County, Colorado from May 11 to May 24(Figure 1.1). The goal was to investigate the geologic structure of the Upper Arkansas River Basin to give the local residents an understanding of the potential geothermal resources. Results from the 2009 field session build upon the work of previous field camps held in the Chaffee County area since 2005. To gain a comprehensive understanding of the Upper Arkansas River Valley structure, the students spent approximately two weeks in the field learning the local geology of the area and acquiring geophysical data in the Buena Vista, Salida, and Poncha Springs areas. The students spent an additional two weeks processing and interpreting the collected data. The students presented the processed data, interpretations, and understanding of the structure of the Upper Arkansas River Valley to Chaffee County on June 5, 2009 on the Colorado School of Mines campus.

The upper Arkansas River Basin has an unusually high heat flow in the subsurface. This is evident from surface manifistations in the form of hot springs displayed throughout the county. The unusually high heatflow has the potential for a significant economic impact on the region. The Department of Energy has flagged the area as a potential area for geothermal energy production. [1] There is current utilization of the areas hot water for tourism, small scale agriculture as well as for residential purposes. If Electricity generation via geothermal in this area is possible it would help the state of Colorado achieve its mandate of twenty percent of the states electricity generated by renewable/alternative sources by the year 2020. [2]

Three days of the field camp were devoted to understanding the local geology which allowed us to effectively interpret the geophysical data. Dr. Robert Raynolds, a geological

consultant with the Denver Museum of Nature and Science, gave the students a comprehensive overview of the structure and stratigraphy of the valley during visits to several outcrops. The students used the remaining time spent in Chaffee County to collect data using a variety of geophysical methods, such as seismic, magetics, electrical, electromagnetic, and gravity to assist in understanding the subsurface of the Upper Arkansas River Basin.

In order to facilitate the educational aspects of the field session the students rotated among the various methods each day. This was done to ensure that everyone worked with a variety of geophysical methods and their associated equipment. Methods such as deep seismic, magnetics, and gravity were used to better understand the structural geology of the area. Methods such as self-potential, DC resistivity, and electromagnetics helped characterize near surface water flow. The students used their knowledge of geophysics and geology to process the raw data gathered in the field. This report presents the observations and data gathered in Chaffee County by and the interpretation of that data.
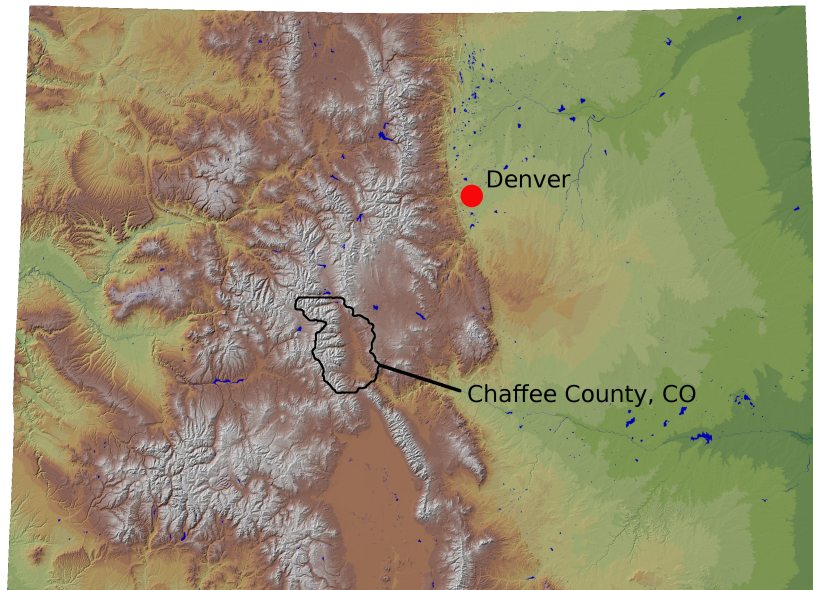
Figure 1.1: Map of Colorado showing the location of Chaffee County. [3]

1.2 Objectives

The main objective of the field session is education. Each student gained invaluable knowledge about field procedures, including field safety. Geophysical equipment transport, set up and operation was a large factor in field education. Many students also had the opportunity

to learn survey management and organization. The latter half of the field session included students learning about data processing and interpretation as well as report and presentation preparation.

The geophysical objective of this field session is to gain an understanding of and build upon the previously known structure of the Upper Arkansas River Basin, specifically, the water and heat flow within the basin structure. Within the chalk creek valley the investigations were done with the primary objective of characterizing the shear zone that offsets the Sawatch fault. A comprehensive understanding of the fault structure in this particular valley will allow an interpretation of fluid movement within the fault/shear system. Determining the depth from surface to basement rock in the Upper Arkansas River Valley was another primary objective of the investigations. Accomplishment of this goal will give an idea of the feasibility of a geothermal power generation plant within the valley.

1.3 Survey Locations

Geophysical data was collected in Chaffee County from primarily three locations. These three locations can be seen in the below figure (Figure 1.2). The northern most location was along County Road 325. There were gravity and magnetic surveys collected along this road as well as two deep seismic lines. The east-west seismic line runs approximately 10km while the north-south seismic line is approximately 5km. Gravity and magnetic data was collected along the east-west line. This survey location will be referred to throughout the report as either the deep seismic line or CR 325 (Figure 1.3). This north-south deep seismic crosses the east-west line and a line of deep seismic data collected in 2005.

Within the Chalk Creek Valley there were multiple surveys conducted. Based on the recommendations of the Colorado School of Mines 2008 field session, there was a dense survey grid set up on Steve Longs property [4]. Mr. Longs property contained an abundance of high desert vegetation including cacti and yucca, yielding students to name the grid the Field of Pain (FOP). Within this survey grid the students conducted a shallow 3D seismic investigation. Students also collected gravity and magnetic data within the grid. A total of fourteen lines of direct current resistivity (DC) data and self-potential (SP) data were collected within the grid. There were also five longer DC and SP lines of data collected to the west of the grid. Around the Chalk Creek Valley the students had access to two wells from which there were a variety of vertical seismic profile (VSP) data collected. The students, with assistance from the USGS, set up 13 passive seismic stations. This survey location will be referred to throughout the report as either the north site, chalk creek or the FOP (Figure 1.4).

The Southern end of the Upper Arkansas River Basin and the northern end of the San Luis Valley are separated by Poncha Pass. On the north side of the pass sits the town of Poncha Springs. Poncha Springs gets its namesake from the hot spring located in this area. This survey location will be referred to throughout the report as either Poncha Springs or the south site. Gravity, magnetic, electromagnetic (EM), DC and SP data were all collected
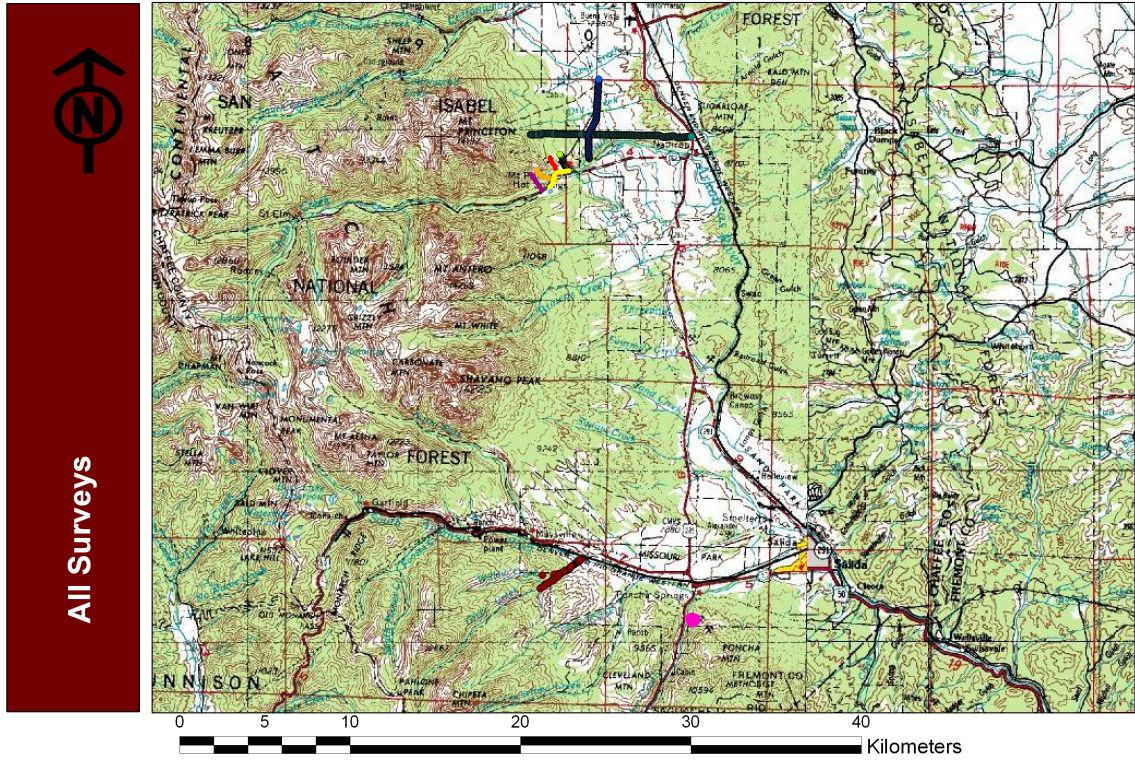
Figure 1.2: Reference map of all survey locations

at the south site (Figure 1.5). The purpose for this survey location is to better characterize geothermal fluid flow in the area. The town of Poncha Springs is hoping to locate another near surface source of hot water that will not structurally interfere with the known source, for which the town of Salida owns the water rights.
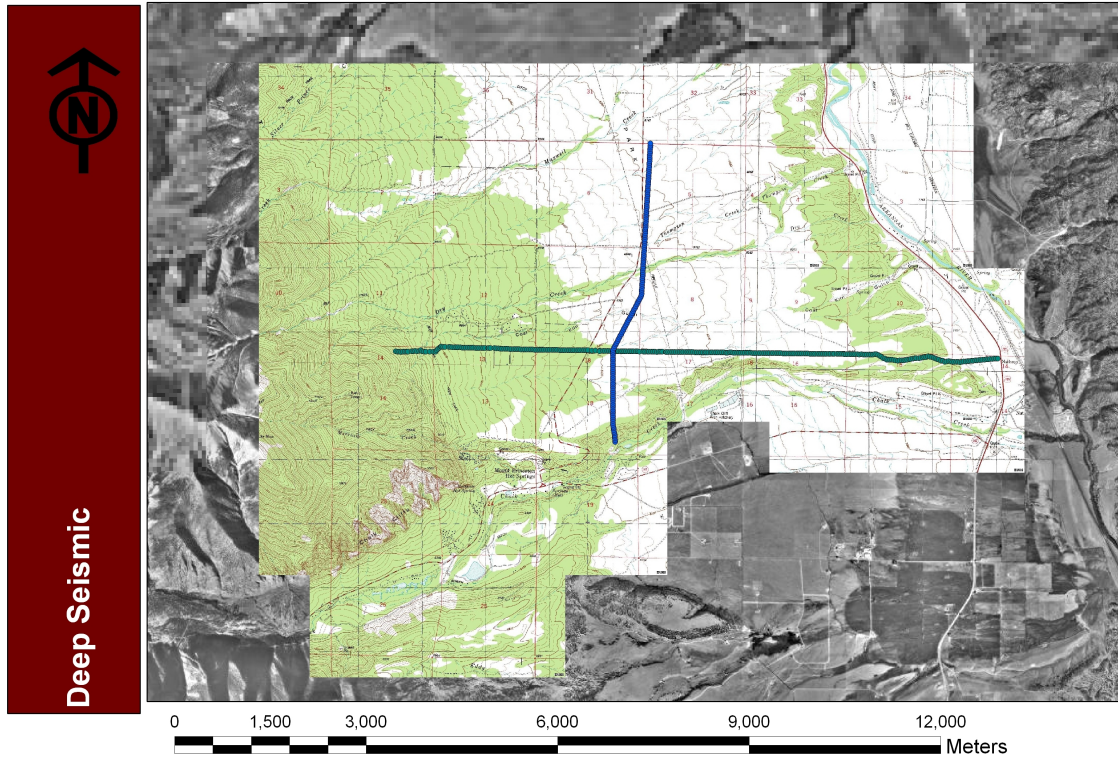
Figure 1.3: Survey Location: Deep Seismic Line / County Road 325
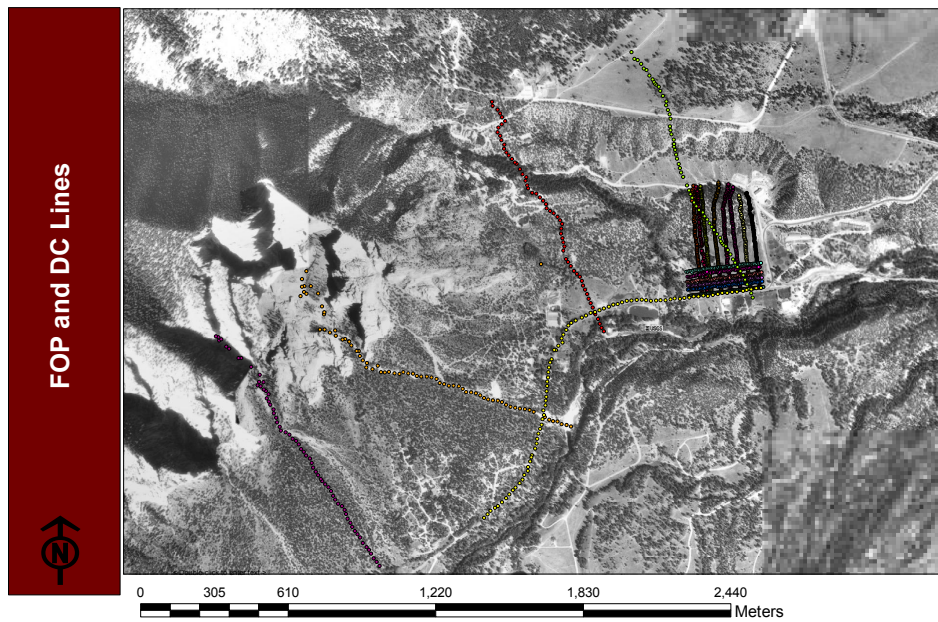
Figure 1.4: North Site / Chalk Creek / Mr. Long's Field
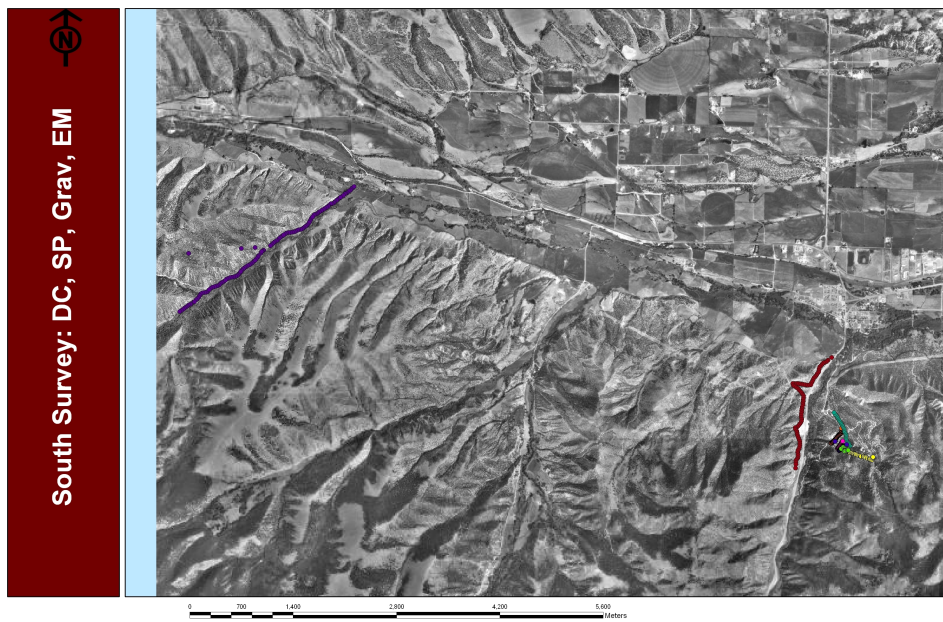
Figure 1.5: South Site / Poncha Springs

Chapter 2

Geologic Background

2.1 Introduction

The state of Colorado contains a unique, though in some areas unexplored, geology. It is important to study the geology of a region in order to better understand its surface, which can be used to deduce what might be held within the subsurface. This can help researchers narrow down the region of exploration and find locations for the application of geophysical methods. Geology is a useful tool, but often challenging because it only provides information that can lead to educated guesses as to what is present in the subsurface. In spite of this obstacle, by combining the geophysical data with geological interpretation, it can help support the gathered data and solidify the geophysical overall interpretation.

Colorado is a state that has seen many periods of uplifting and erosion. Approximately 300 million years ago (Ma) there was a set of mountains present in the region different from the Rocky Mountains of today. These mountains are dubbed the Ancestral Rocky Mountains. They were uplifted, and then consequently eroded away. Their sediments can still be seen today in the present Rocky Mountains, and are seen in the Upper Arkansas Basin. The Rocky Mountains present today were created during a period of uplift that occurred approximately 65-70 Ma, changing the landscape once again.

Within the Upper Arkansas Basin, there is a large presence of a rare type of metamorphic rock in the area. This metamorphosed granite basement rock has been created over years by massive amounts of sediment accumulation. As the Ancestral Rocky Mountains were eroded away, the sediments were deposited in layers on top of one another. As there were more and more sediment deposited, the bottom most layers became exposed to large amounts of heat and pressure, compressing the sediments, creating metamorphic rock. These compacted layers of sediments resulted in what is referred to as the Precambrian basement rock. This basement granite, because of the metamorphic process, is very dense and highly impermeable; fluids traveling in the rock travel mainly through the fractures and faults present in the unit. During the continuous sediment deposition on the surface, the sediments even-

tually became sorted by size due to mass movement processes such as river flow. These processes deposited the larger sediments at the bottom due to the high amount of energy present in the system, with the finer sediments deposited on top as the energy of the system decreased. Following this was a period of glaciers and on top of the fine sediments you can see glacial deposits. Glacial deposits display poor sorting of sediments, with their sizes ranging from fine grained sands to boulders. The sediments from glaciers are smooth and round due to the movement of the ice against the Earths surface. Along with glaciers and erosion, the topography of the area was also changed by tectonics as well as volcanic activity.

2.2   Geology of the Upper Arkanasas Valley

The Upper Arkansas River Valley is a complicated geological area. The land has morphed much over time from what it was in the past. Going back millions of years, the Upper Arkansas River Valley was a relatively flat region with valleys incised in the landscape running in an east-west direction. This is evident due to a narrow flow of lava that runs from Mt. Princeton and travels to near Castle Rock, CO. There is also an igneous extrusive batholith in the Southern Mosquito Range, which is composed of a substrate of obsidian, a volcanic rock. This same type of rock is also seen along the Front Range and in Castle Rock, CO. This obsidian is known as the Castle Rock Rhyolite. As these volcanic deposits are flowing, it can be inferred that there were likely valleys there to channel the lava flow in a west-east direction. These lava flows are dated to be approximately 36.7 Ma. These lava flows occurred after the uplifting of the present-day Rocky Mountains. Due to the large uplifting that occurred in the area, the volcano that created these igneous extrusive rocks is no longer present.

The basin that is seen today in the northern end of the Rio Grande Rift Valley, was formed by a major north-south oriented fault. The Sawatch Range which contains the Collegiate Peaks, was then uplifted, and the ancient valley that was present began to subside. This subsidence created the graben that is seen today, which now comprises the Upper Arkansas Valley. This occurred around 15-20 Ma, and allowed entry for the Western Interior Seaway. The Western Interior Seaway crossed much of the North American Continent, and covered most of Colorado throughout the Cretaceous period. During this time, there were many marine sediments deposited, which can still be seen today (such as the shale present in the valley.) The basin that was created by the subsidence is asymmetric, with the primary faulting located on the west side. These were the faults that uplifted the Sawatch Range and created the Upper Arkansas Valley. As a result of the faulting and uplift, you can see the ancient volcanic and basement rock on the west side of the fault (where Mount Princeton is located) due to the upheaval of the rock units. On the east side of the fault, the basement rock is covered in layers of sediments. This is observable in the Southern Mosquito Range at Trout Creek Canyon, where the stratigraphic progression of the basement rocks and overlying sedimentary rock is exposed. At this site, above the Precambrian basement rock is the Manitou Dolomite (Ordovician in age, 488-443 Ma). Located stratigraphically

above this unit is a beach quartzite (Paleozoic sandstone) and located on top of the beach quartzite is a more resistive rock unit of limestone. The limestone is called the Leadville Limestone, which makes up much of the horizon of Trout Creek Canyon. Above the Leadville Limestone sits the Belden Shale. This shale is not very prevalent in the area due to much erosion. Sediments of all of these rock units are found inside the Upper Arkansas Valley. The sediments from Trout Creek and the Southern Mosquito Range ended up in the Upper Arkansas Valley due to erosion. As the Arkansas River began flowing through the valley, it carved the valley deeper and exposed older sediments, even the very deeply located basement rock. There were also glaciers present in the area, and the outwash materials from their movement pushed the river to the east as they encroached on the valley, as seen by the prevalent fluvial deposits extending far to the west, sometimes reaching the base of the mountains.

The Upper Arkansas Valley is a rift valley. A rifted valley is, generally, an extensional environment that is experienceing a local thinning of the Earth's crust. The process of rifting produces much heat from deep within the subsurface, which results in the hot springs found in the Upper Arkansas Basin. The Chalk Cliffs show great evidence to support the presence of hydrothermal energy. Once basement rock comprise primarily of feldspar, the Chalk Cliffs have been hydrothermally altered and transformed into kaolinite. The cliffs have been exposed due faulting and uplifting in the area.

The major fault of the western side of the valley runs along Chalk Creek. Between Mount Princeton and Mount Antero, the major western fault has been somewhat displaced. The cause of this displacement is unknown, but it is believed to be due to a younger east-west running fault.

The entire area of the Upper Arkansas Valley and surrounding mountain ranges are believed to possibly be a consequence of what is known as negative inversion. Negative inversion is a geologic process in which a thrust fault/compression system changes into a normal fault/extension system. This is believed to have occurred because the Collegiate Range was created due to compression uplift, but the present day Upper Arkansas Basin was created by extension.

It is important to acknowledge and understand the local geology of the region for the understanding of the groundwater as well as local geothermal systems. Much of the water that is introduced into the area is due to snow melt run off and rain. This water consequently flows downwards, entering the basin. A portion of this water can enter the subsurface and circulate very deep below the basement rock where it can become heated and expands, traveling back up to the surface to form the hot springs found within the rift valley. By looking at the chemical composition of the hot spring water, it is possible to partially determine the depth that the water had traveled within the subsurface. The water that is found in the hot springs must travel beneath the Precambrian basement rock, which is a difficult task as the basement rock is highly impermeable. The water must therefore travel through faults and

cracks found within the basement rock unit, which is why it is very important to gain an understanding of the numerous faults found near the mountains and surrounding area.

Most of the water that enters the basin system from rain and snow melt will not travel beneath the basement rock, and will continue to flow in the basin, collecting in the local shallow aquifers. This water accumulation most likely occurs in the sedimentary rock units, as they are more permeable than the other units found in the area. The water will flow down-gradient, traveling into the low areas of the sedimentary rocks, and will eventually drain into the Arkansas River. The amount of groundwater present is not constant and varies drastically due to factors such as water redirection for drainage ditches or irrigation, annual rainfall, and upstream human consumption.

The following paragraphs will describe some of the specific rocks and minerals found in the Upper Arkansas Valley. The descriptions will go from the west to the east unless otherwise noted. The west side of the basin is composed of a Tertiary batholith, as mentioned above, that is about 36.6 Million years old. That would place its formation in the late Eocene. This batholith contains some quartz monzonite. This rock is dark gray in color and is often thought to be basement granite at first glance. The quartz monzonite contains medium sized grains and has equal amounts of potassium and plagioclase feldspar. It is mainly comprised of quartz grains, hence the name. Quartz monzonite is often found in mountain belts and since it is resistive to weathering it often can form dramatic landforms. The area near the quartz monzonite also contains a few zeolites. Zeolites make up a group of about fifty different minerals that are similar to both clays and feldspars. They usually form when minerals in the cavities of volcanics are altered by either heat or pressure. As well as zeolites and quartz monzonite being present there is naturally some plain quartz present as well. Quartz is the most common mineral in the Earths crust. Quartz is trigonal in its crystal structure and comes in a variety of colors. It is a very resistive mineral with a hardness of seven on the Mohr scale and can be found in igneous, metamorphic, and sedimentary rock. Also in the Tertiary batholith are units of Rhyolite, quartz porphyry, and dacite. The dacite is still Eocene in age but the rhyolite and quartz porphyry are Oligocene to Miocene in age respectively. All three of these rocks are volcanic in origin, silica rich, and are light in color. Rhyolite is a fine grained rock that is often contains bands of darker minerals. The colors range from light pink to tan and can include white or gray. Rhyolite usually contains quartz, both potassium and magnesium feldspar, and biotite mica. Due to the high quartz content rhyolite lavas are generally cooler than oceanic volcanic lavas and are much more viscous. Rhyolite can also form from solidified ash and pyroclasts. Quartz porphyry is a rock that is similar to both granite and rhyolite but contains white quartz inclusions. The grain size can vary for this type of rock, and its color range is light red to light brown. Dacite is a fine grained rock and can even have a glassy appearance. Banded layers are common in the light red to light brown rock. Dacite contains quartz, potassium feldspar, plagioclase feldspar, biotite, and hornblende. Dacite is often used for road chippings.

Moving out from the Tertiary batholith toward the center of the valley there is evidence of an unconformity that contains possible basement rock, comprised of granite. Granite is a plutonic rock, which means that it formed deep underground. It is coarse grained with large crystal inclusions in it. Granite is usually white, gray, or pink in color with black specks. Granite contains quartz, feldspars, mica and hornblende. It is extremely resistive to weathering and is found under nearly all mountain ranges in the form of huge batholiths. Along with this granite is a metamorphic rock called quartzite. Quartzite is a non-foliated unit and can be formed by either contact or regional metamorphism. It is medium grained, angular in grain shape, and well sorted. Colors for quartzite are white and gray with a red tint. It is composed of tightly locked grains of quartz with some feldspar and mica. Quartzite is similar in appearance to marble at first glance but is much harder and browner. It should also be noted that the center of the valley contains many alluvial (river deposited), colluvial (mass transport deposition), and glacial till deposits from the late Pleistocene through the Holocene. These deposits came in relatively rapid succession. Also located in the center of the Upper Arkansas Valley, usually under the alluvial deposits, is the Dry Union Formation which will be discussed later on.

The east side of the basin contains a variety of different formations. One of them is the Manitou Dolomite. Dolomite is a biogenic sedimentary rock that, unlike other limestone rocks, is composed of magnesium carbonate instead of calcite. Grain sizes are very fine to fine, and it has a sugary texture. Colors range from white and gray to a weathered brown. Dolomite can form from direct precipitation from oceans if the magnesium carbonate concentration is high enough but most dolomite is thought to form from the recrystallization of limestone. Along with the Manitou Dolomite is the Leadville Limestone. The Leadville Limestone is a fossiliferous (crinoidal) limestone. That means that this type of limestone contains many pieces of fossilized sea creatures. These creatures flourished in the Carboniferous period when many of the worlds limestones were being deposited. This limestone is fine grained with crinoid pieces, rarely intact specimens. It is composed of calcite and is white, gray, or brown in color. This layer is named after Leadville, Colorado where it is very abundant. The Belden Shale is the next featured layer. Shales are at least 50% clay sized grains, well sorted and can contain fossils. Shale has high fossility which means it can be pulled into thin, flaky layers. The color is usually gray or white but can be red if iron oxides are present or black if organics are in it. Other components in the shale include quartz, feldspar, and mica. Oil is often trapped in shale, but it is currently not economic to extract and produce. It should be noted that along the cross section these units have been eroded away and have been extrapolated from other locations nearby. The area also contains a small amount of bedded chert. Chert forms from the ooze left on the seafloor by the remains of plankton and other sea creatures. It is very fine grained, so much in fact that the crystals cannot be seen by the naked eye. The texture is glassy, and fractures with a conchoidal pattern when hit by a hammer. Chert is composed of nearly pure quartz and the colors are variable depending on impurities within the sample, grays and browns being the most common. Since chert is a very hard rock it was often used for tools by ancient peoples.

All of these organic types of rock can lead to the formation of karst terrain when erosion

occurs. Even though these rocks often form in water they are easily eroded by slightly acidic water. Rain and groundwater can become acidic enough from the carbon dioxide the water absorbs, to disolve limestone. When these rocks, especially limestone, are located near the surface, acidic water can seep into cracks and begin to dissolve the rock. After thousands of years vast caverns are formed. If the caverns collapse they can form gorges. Given enough time only large pillars of rock will remain once all of the other rock is dissolved away.

The basement rock on the east side is capped by a lava flow that contains obsidian. Obsidian is basically a volcanic glass. The color is dark black but can have some tinting depending on if there are any inclusions in the rock. The composition of obsidian is similar to rhyolite. Obsidian was often used for knives by ancient cultures and can easily be dated because it absorbs water easily and stores it. The basement rock on the east side of the valley is composed of gneiss and granodiorite. These two rocks are 1.66 billion years old making them Precambrian in age. The gneiss, specifically augen gneiss, is foliated and forms by either regional or dynamothermal metamorphism. It is medium to coarse grained and contains large crystals called augen. Augen gneiss is gray to pink in color with dark banding, usually containing either alkali feldspar or garnet. Light bands are quartz or feldspar and dark bands are biotite. Gneiss forms at the most extreme temperatures and pressures and usually comprises some of the oldest rocks on Earth. Granodiorite is an intrusive plutonic rock and is a granitoid meaning it is like granite. Its grain size is coarse with a uniform structure and texture. Its color is black and white with pink potassium feldspar inclusions, giving it a salt and pepper look. Other components of Granodiorite include quartz, plagioclase feldspar, biotite, and hornblende.

Directly underneath the alluvial and glacial deposits, and sometimes on the surface in the center of the valley is the Dry Union Formation, which is the only sedimentary rock feature in the valley. All other rocks units are either igneous or metamorphic in origin. At its deepest, the Dry Union Formation is over 5,000 feet, or 1,500 meters, thick. The Dry Union Formation is composed of four different types of materials; silstones, sandstones, conglomerates, and volcanic ash. The sandstone formation is of a well sorted light brown sandy composition, which is over 50% silt sized particles. Siltstone is often laminated and contains crossbedding, ripple marks, and fossils. The composition of siltstone is a mix of quartz, feldspar, and mica, with colors including shades of gray and other browns. Siltstones often have a gritty feel to them because of the quartz content. The sandstone of the Dry Union is an interbedded, friable sandstone, emaning that the sandstone layer lies between other layers within the formation. Friable means that this sandstone has been highly weathered. Sandstone, as its name suggests, is composed of over 95% sand sized grains, having a gritty feel and because it is usually well sorted and rounded. The cement that makes up the rest of a sandstone can be a variety of different materials but it is usually quartz or calcite. Its composition is mostly quartz with other rock fragments, feldspar, mica, organics, clays, and other minerals. Colors for sandstone can be variable with reds and browns being the most predominant. A third substantial component of the Dry Union Formation was a conglomerate. Conglomerates are rocks that are composed of pieces of other rocks that

have been cemented together and consist of coarse grained pebbles, cobbles, and boulder sized materials. Conglomerates are poorly sorted and contain no bedding marks with colors covering a wide range, depending on the material. The composition of conglomerates is also a wide range of materials, but is usually include quartz, feldspar, rhyolite, quartzite, or slate. The cement that holds conglomerates together is typically a silicate, calcite or iron oxide. The final material found in the Dry Union Formation is a volcanic ash ignimbrite, deposited during the eruptions in the late Miocene to the late Pliocene. Ignimbrites usually have medium sized grains and are usually composed of Rhyolite.

Our South site survey location had many of the same types of rocks found in the Buena Vista area, however there were three other materials that were unique to the South study, namely Fluorite. Fluorite has an isometric crystal shape and twinning is common for this mineral with a chemical formula of Ca_2. Fluorite has the greatest range of colors for any mineral, with the ones in this area being white with a tint of brown. On the Mohr hardness scale fluorite is a 4 and fractures in a conchoidal pattern. In the area that we surveyed there is an abandoned fluorite mine so we know the concentration here was good enough for economic production.

Poncha Springs is located near a geothermally active site, explaining the high content of travertine being present. Travertine is a rock that forms from the precipitation of calcium rich water around hot springs or caves, composed of calcite and occasional aragonite. Travertine is fine grained, almost powdery, friable, and is banded with colors ranging from reds to browns. The final mineral found in this area on the survey was epidote. Epidote has a monoclinic shape and can have striations, with a chemical formula of $Ca_2Al_2(Fe^{3+}; Al)(SiO_4)(Si_2O_7)O(OH)$. Its hardness is six to seven on the Mohr scale, cleaves in one direction, and fractures unevenly. The color of epidote is almost always pistachio green but it can have other shades of green, yellow, or brown. Epidote usually forms when plagioclase feldspar or other rocks are altered by contact metamorphism. Large deposits of this exist in Chaffee County, being formed when the limestone was metamorphosed.

2.3   Stratigraphic Column

Please see the stratigraphic column in the appendix for further information and details.

Chapter 3

Seismology

3.1 Introduction

Seismic analysis is a branch of geophysics that studies the propagation of sound waves through the Earth (seismic energy). It is generated either naturally by earthquakes or artificially using sound wave sources to send energy into the subsurface such as a vibroseis truck, dynamite, a sledge hummer, or airgun (in case of marine data.) The physical propagation of the seismic energy through the earth is mainly compressional waves (longitudinal moving plane waves), shear waves (transversely moving plane waves) or Rayleigh (surface) waves depending on the direction of propagation of the wave relative to that of the particles. These waves are reflected and refracted when there is a contrast in the acoustic impedance (i.e. the product of velocity and density) between any two different media. The waves are recorded at the surface by either geophones, hydrophones or seismometers.

3.2 Wave Theory

3.2.1 Reflection

This method utilizes the waves that propagate downwards and reflect upwards at an interface between two layers. The reflected energy is received by geophones, marshphones, or hydrophones Figure 3.1. Different energy sources and receivers could be used to acquire this type of data depending on the location whether it is marine or land data. It provides information and understanding of the subsurface geological structure as well as lateral continuation and estimation of layers thicknesses.

3.2.2 Refraction

The subsurface can get complicated when there are many layers, indicating a change in the geology of the rocks. Some waves from the source do not immediately bounce back to the surface but instead are refracted through the surface. The refraction of the wavefronts occur
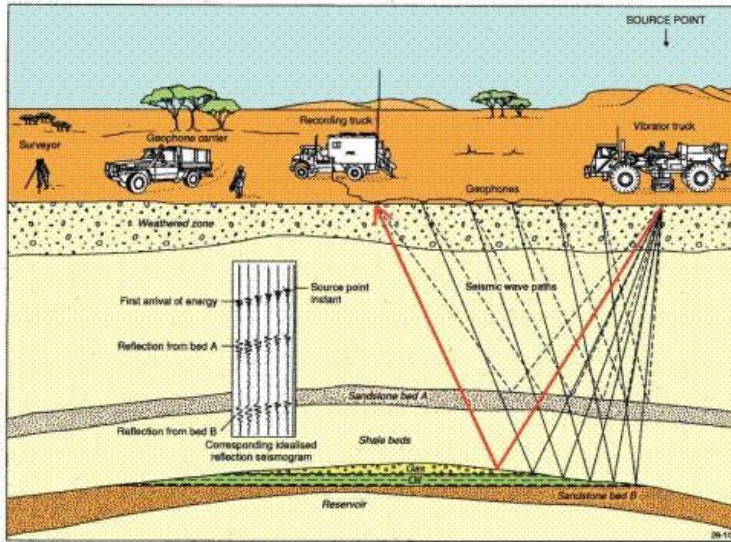
Figure 3.1: Waves propagating in the subsurface from a source
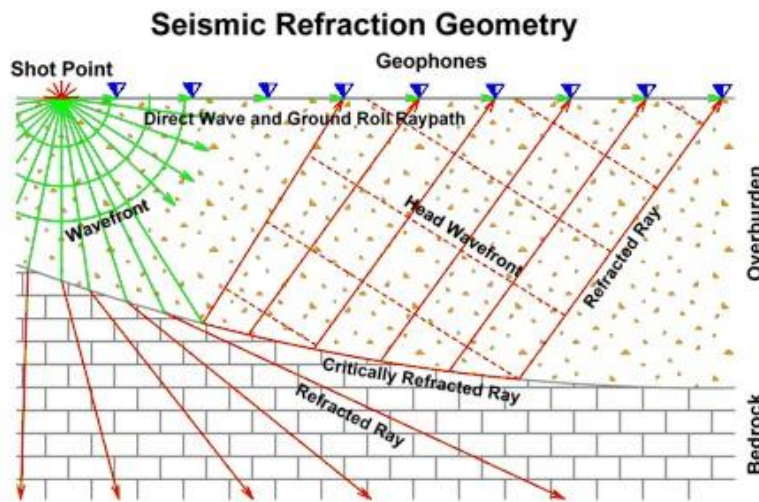
Figure 3.2: Geometry of waves reflecting and refracting in subsurface off of boundaries

when the incident angle is equal to the critical angle Figure 3.2. The energy travels along the interface and refracts back to the surface at each point along the interface. The seismic energy sources and receivers are similar to the ones of reflection. This method is analyzed to estimate the velocities of the weathered and bedrock layers. It also can be extended to analyze more refracted energy in case of long receiver lines that can receive deep refracted energy. Another use of the refraction data is to correct for the topographic variations that change the travel times (i.e. static correction). The analysis is done by picking the first breaks of the direct arrivals and the head wavefronts indicating different slopes. The differ-

ences in slopes are due to different velocities of the interfaces.

These main two phenomena of wavefront propagation occur when acquiring seismic data whether it is 2D or 3D, land or marine data. Because the energy propagation paths are different along different media, their characteristics and forms in the shot records are different and can be separated for different analysis.

3.3 2D Deep Seismic

3.3.1 Introduction

A 2D Deep Seismic survey is a single line collecting data in only two dimensions. It is considered a deep survey because the data acquired provides an overall image of what is occurring very deep within the subsurface over a considerably large topographical region. Deep seismic data was collected to help determine subsurface geology, stratigraphy and specifically the faults that exist within the surveyed region. Seismic data is often most usefully used to help interpret deep geological information. This is because other geophysical methods tend to struggle with deep data acquisition based on the variation of the physical properties of the earth in contrast with other geophysical methods.

3.3.2 How the Seismic Method Works

Figure 3.3: Seismic data acquisition in the field [5]

2D Deep Seismic data acquisition is done through laying out a single long line of geophones extending multiple kilometers in length across the region. Two sources (vibroseis trucks) were then used to induce low frequency velocity waves into the earth. It is through this low frequency and long wave length correlation that the waves are able to travel into the deep subsurface and provide an image that is over 1.5 kilometers in depth. The image itself

25

is collected through the reflecting wave velocity signature picked up from the geophones that are coupled with the ground. After the data is collected, further interpretation is carried out to create a polished image of the deep subsurface. Once this image is developed, analysis and interpretation of the deep geologic subsurface is carried out so that an overall census of what is occurring in the region can be achieved.

3.3.3 Equipment

Figure 3.4: Veibroseis Trucks [6]

- P-Wave Geophone

- Geophone Cables

- CGG Veritas Vibroseis Trucks (2)

- Doghoues: Unix System for Data aquisition

- Pickup Trucks (2)

- Tape Measure

- Survey Flags

- Differential GPS

3.3.4 Location and Survey Design

Within this survey, two separate survey lines were collected. The two separate deep seismic lines were near County Road 322 which is about parallel to Highway 285. The easting deep seismic line extended from County Road 322 on the west side all the way east to Highway 285 for approximately $10.2km$. The North-South line was perpendicular to the East-West line and crossed just east of County Road 322 and extended for about $7.4km$. The geophone spacing was $5m$ in both lines with flag spacing every $30m$ giving 6 geophone locations for every $30m$.

The two vibroseis trucks that were used had separate rolls along the survey. One truck was the far truck, providing shots at a set distance from the grid, and another truck was the near truck which provided information of the subsurface for a near shot source. Both vibroseis shots did 10 sweeps per location. Each sweep within the data was carried out for 5 seconds, and then an additional 6 second space was left for geophone data acquisition. Providing a total data acquisition length of 11 seconds. The sampling interval was every $2ms$ at a frequency of $200Hz$.

The nyquist frequency of $200Hz$ was also determined for the data set. The nyquist frequency helps interpret what frequency levels need to be avoided so that the wave signal shot into the subsurface can be reconstructed into an image upon data acquisition. If this parameter is ignored, the collected data can deem to be worthless due to the noise levels of the collected information. See appendix for more information on Nyquist Frequencies.
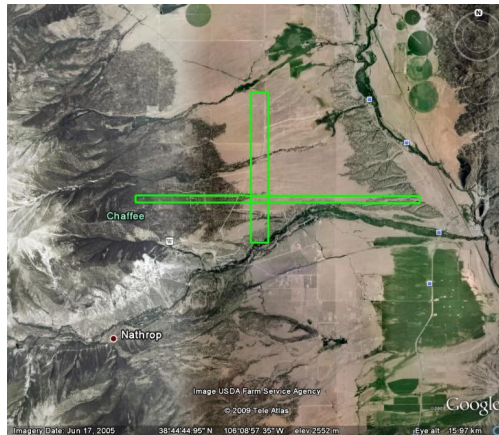
Figure 3.5: Regional aerial photo of surveyed region

GPS data was acquired separately for each geophone location so the surface locations of the subsurface information would be easy to interpret later on. The GPS data was collected using the differential GPS for higher accuracy on locations; plus or minus a meter.

Shown below are two aerial photos of the surveyed region. The Zoom Out figure shows a rough image of where the survey lines were. The Zoom In photo is a closer look at the survey lines which also shows that the survey was not two directly perpendicular straight lines, due to terrain and property issues.
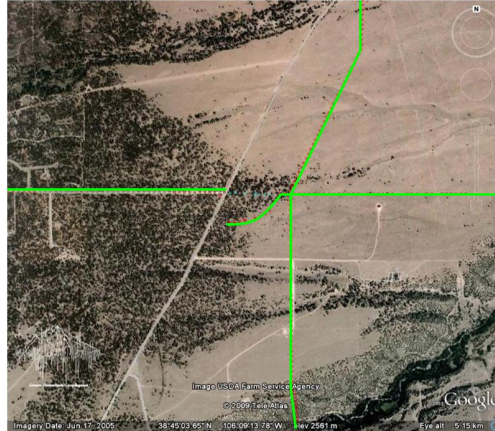
Figure 3.6: Zoomed in aerial photo of surveyed region,(N.B.-not exact GPS locations)

3.3.5 Processing

The raw data acquired at the field requires processing in order to create a fully formed image of the sub-surface. The two lines acquired were processed under the supervision of ION GX Technologies using the Landmark ProMAX software package.

As the energy waves generated by the vibrosies travel through the sub-surface they get scattered and refracted as a result of the variation of the physical properties of different rock layers. The waves returning to the receivers are contaminated by random noise, air blast and ground roll noise. The main aim of the processing is to get rid of all noise in order to create a clear image of the sub-surface using the P-wave energy (the simplest possible reflected paths to the receiver arrays). All other energy that is not a primary reflection is considered noise and needs to be removed or attenuated during processing.

A single processing flow was developed and used to process the two seismic lines (Figure 3.7). The processing sequence is applied at stages in order to ensure that at each interval of the processing flow the desired result is obtained and no errors or problems are encountered.

Geometry

The very initial step was to create a geometry setup for the row data acquired at the survey to allow the processing algorithms to make consistent and proper applications to the data

according to the true layout of the survey. This involved computing the source and receiver locations in terms of their UTM coordinates and this was aided using the observer logs which give detailed descriptions of how the survey took place on daily basis. A few geophones had reversed polarity but this issue was resolved early in the field. This stage also involved killing and getting rid of bad traces that were generated by bad geophones and wiring problems. To obtain this, each shot gather (containing all the traces recorded from a single vibroseis shot) was analyzed and thus the quality of the data is improved. Figure 3.8 shows the geometry of the two seismic lines.
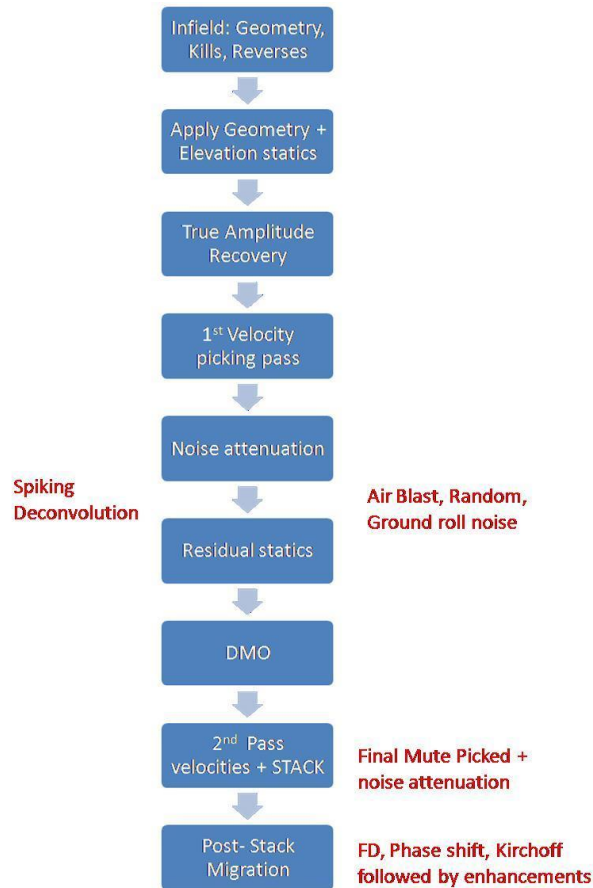
Figure 3.7: general processing sequence applied to the two seismic lines.

Elevation Statics

Due to the variation in elevation across the area of the survey, the sources and receivers had different elevations. To correct for this effect, a residual static application was applied to the data set. The term statics implies that the changes are constant with time and so the corrections are fixed across the data.
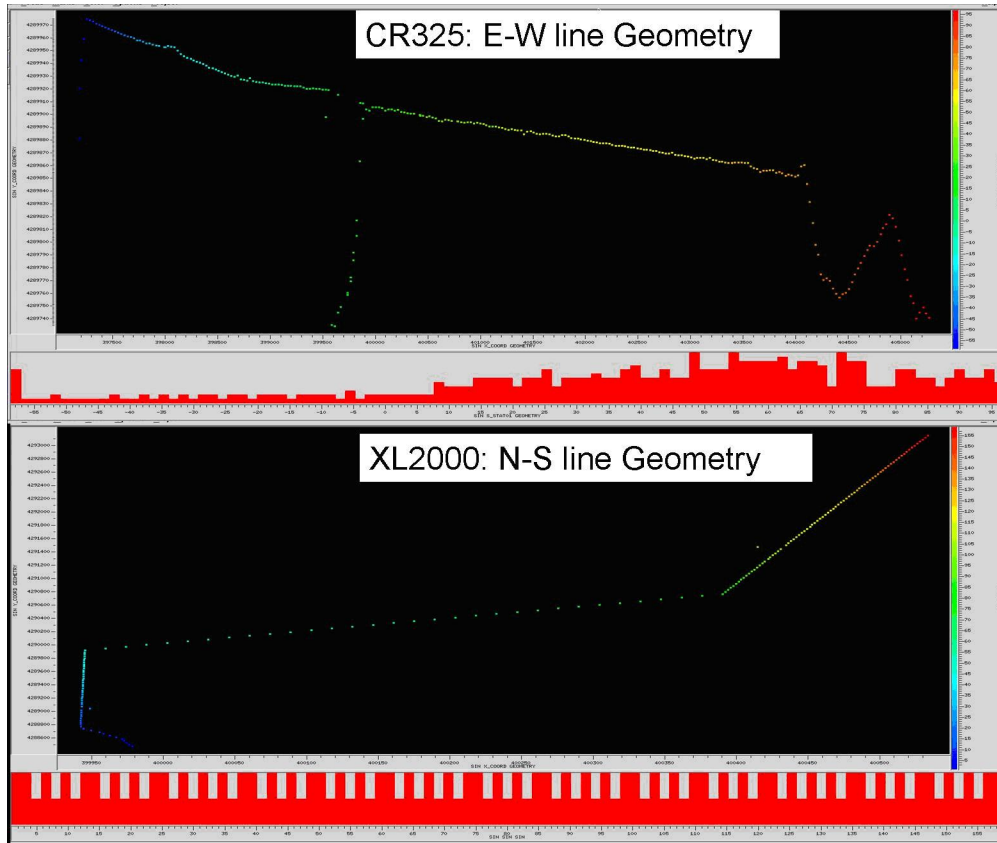
Figure 3.8: The geomoetries of the 2D seismic lines acquired

Prior to the application of elevation statics, a brute stack was created using some rough velocities obtained from the seismic line acquired in summer 2008. These velocities are used to flatten the hyperbolic events using a process called Normal Moveout (NMO) correction. NMO is the difference between the two-way time at a given offset and the two-way zero offset time. The NMO velocities are then used to correct the travel times and remove the influence of offset. The NMO correction is applied prior to stacking. Stacking data is the process of summing all the traces recorded at the same common mid point and it increases the signal-to-noise ratio and also attenuates multiples (repeated reflectors from the same interface). The term brute here implies that the velocities used for the NMO correction are rough or estimated and so a brute stack can provide a general baseline judgment of the processing sequence developed so far. Figure 3.9 Shows a brute stack created for the E-W line.

The main aim of creating a brute stack is to get a preliminary image of the sub-surface at earlier stage of the processing sequence which would help on deciding which processing algorithms to be applied. Once the brute stack was generated, the elevation statics application was applied and Figure 3.10 shows the effect of the application.
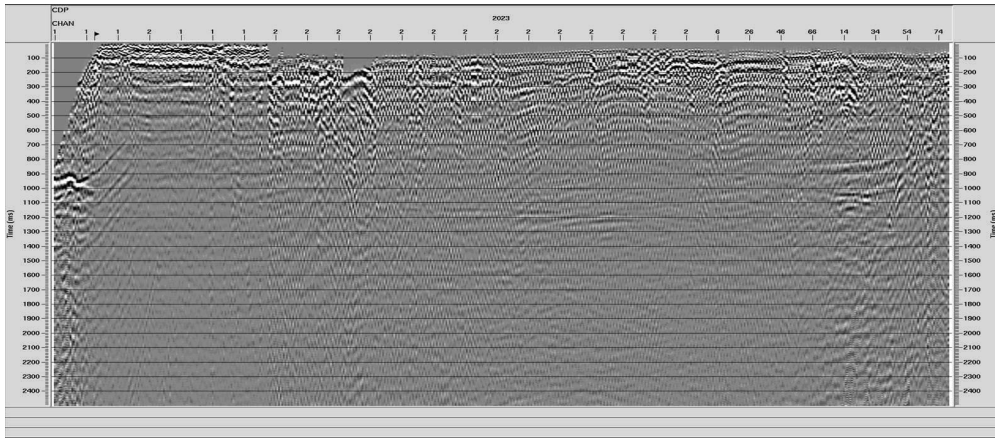
Figure 3.9: A brute stack for the E-W seismic line
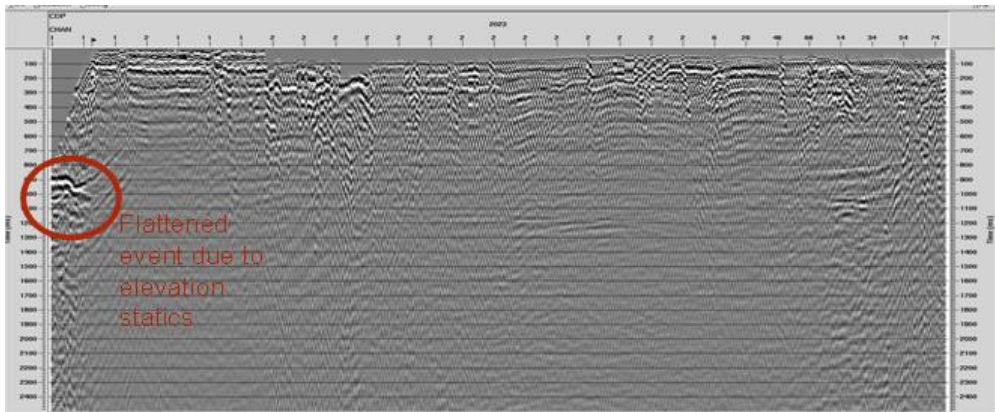
Figure 3.10: A brute stack for the E-W seismic line with elevation statics applied

Muting

The NMO process causes the data to stretch out at far offsets and the mute application can be used to cut off or mute these sections out to produce a better image.

True Amplitude Recovery

As the wave energy travels through the sub-surface, it loses its energy due to absorption, transmission/reflection and its spherical spreading. This energy loss is compensated for by applying an Amplitude Recovery algorithm which attempts to recover the energy from the top to the bottom of the seismic section.
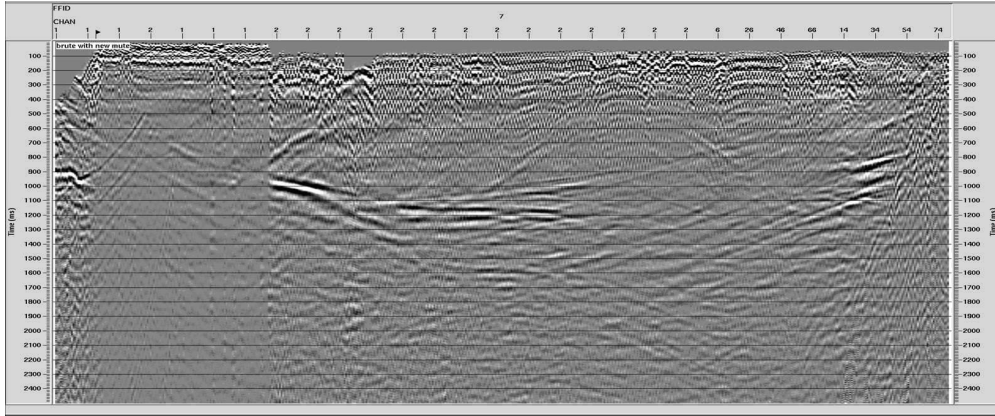
Figure 3.11: A brute stack for the E-W seismic line mute applied

First pass velocity picking

Velocities were picked at fixed increments of 30 CDP (common depth point) which is equivalent to 450 meters. The velocities picked are checked by looking at the corrected NMO gathers and the produced velocity field. The correct velocity should flatten the hyperbolic event in the CDP gather. In order to improve the velocities used to stack the data, semblance spectrum were created on which rough velocities were picked. Each spectrum is color coded with warmer colors representing stacking velocity values at a given TWT (Two-Way Time) that would produce a flat event in an NMO corrected gather. Some of these warm colors could correspond to multiples and diffractions and it is therefore important to be careful when picking the primary energy peaks. Figure 1.12 shows the semblance spectrum and velocity picking for the E-W seismic line.

In general, the stacking velocity usually increases with depth and therefore the general velocity trend is clear. At each CDP location, stacking velocities are picked as functions that vary with TWTs which are then used to define the NMO correction at each point where a velocity has been picked. The times at any offset are then converted to that at zero-offset and these velocity control points are then interpolated across the whole data.

Figure 1.13 shows the velocity field profile produced for the E-W seismic line. The smoothed velocity profile was then used to generate the stack shown in Figure 3.14. This stack, generated using a first velocities pass, already shows some structure visible but yet additional processing and noise attenuation is required to improve the quality of the image.

The first velocities pass stack can also be depth converted to produce the image shown in Figure 3.15.

Noise attenuation

Seismic data acquired on land usually contains random noise (e.g. traffic) air blasts and ground roll noise. Air wave noise includes the noise caused by the vibrator sound traveling through the air and being recorded by the geophones. Examples of filters applied to the data
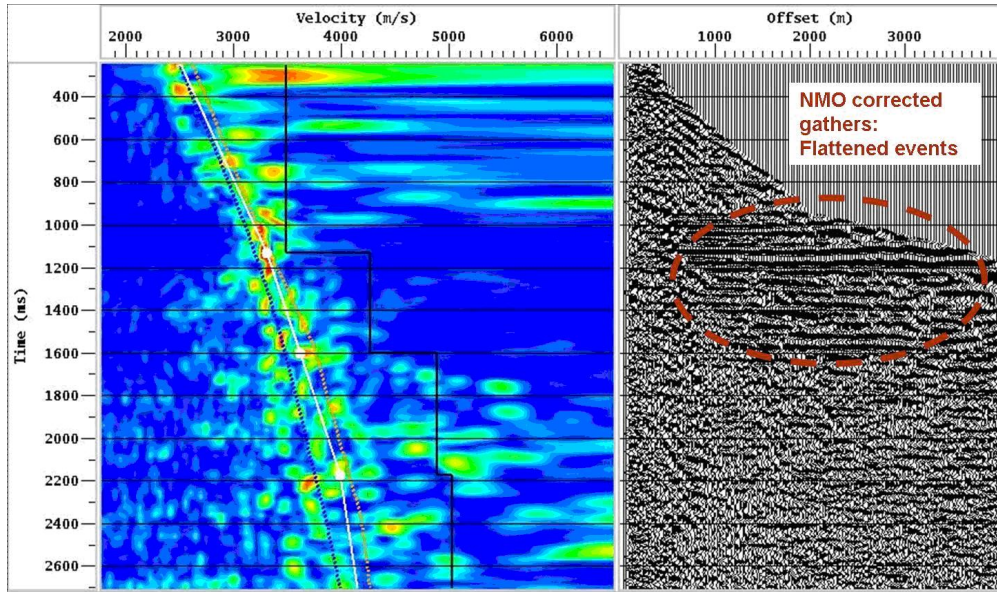
Figure 3.12: Semblance spectrum for a selected CDP gather with warmer colors indicating the velocity picks used for NMO correction

include band pass filters and notch filters. Since the dominant noise is of high frequency, a low band pass filter is applied to get rid of this noise.

In order to improve the clearness of the image spiking deconvolution was applied. This attempts to correct for the effect of the source wavelet as each wavelet is represented by one amplitude.

Residual Statics

The application of elevation statics is imperfect and this is improved by the application of residual statics that is usually applied to correct for the remaining static errors. It is generally based on correlating prestack data and stacked traces in an attempt to solve for source and receiver statics.

DMO

The CMP or CDP processing methodology works and holds well for horizontal multilayer and not for dipping interfaces. Therefore an account for dipping reflectors must be taken into account. It is therefore essential to apply a Dip Moveout (DMO) correction to compensate for the dipping interface effect. The application of DMO correction is also useful since it attempts to collapse diffractions in order to remove false high velocity events and it can also remove some steeply dipping noise.

33
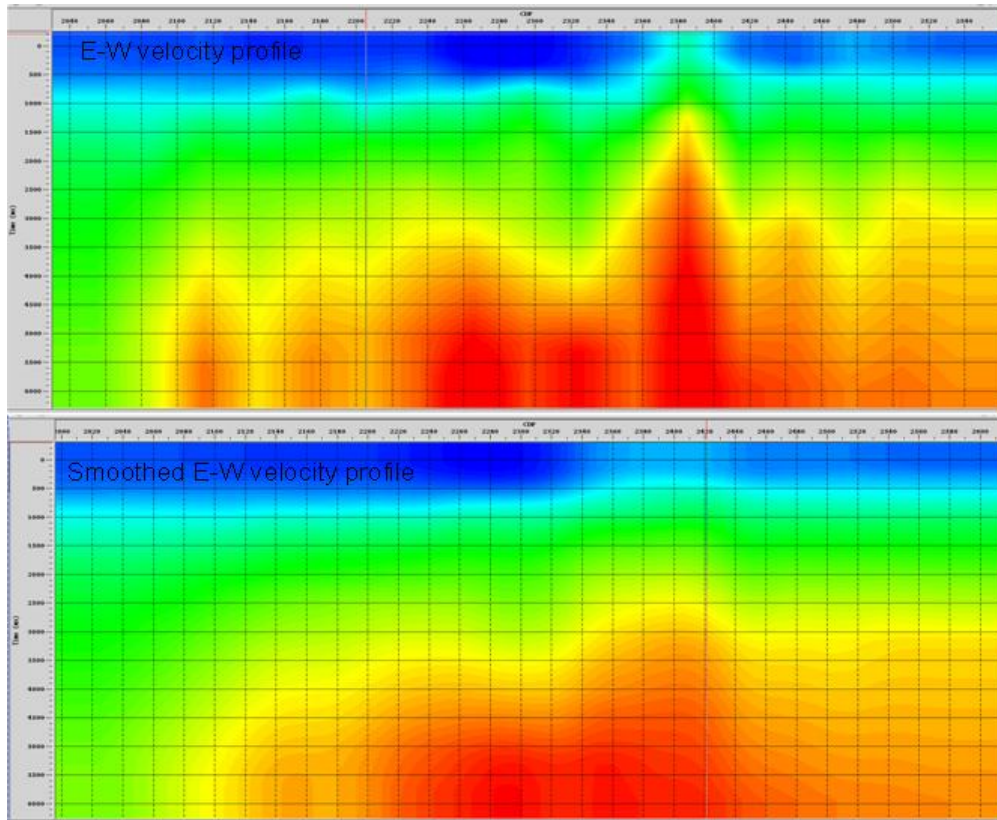
Figure 3.13: (a)A velocity profile field created for the E-W seismic line. (b) A smoothed E-W velocity profile
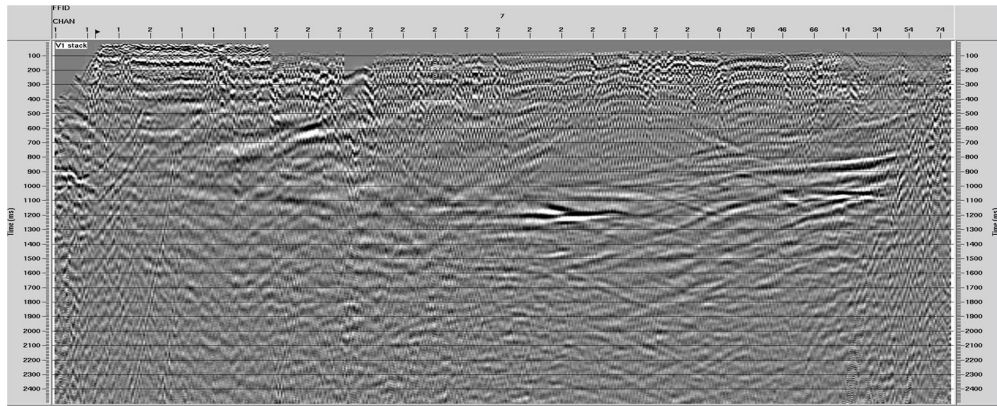
Figure 3.14: A stack for the E-W line created using the first pass of velocity picks.

Second pass velocity picking and final mute

In order to improve the quality of the stack and to increase the signal-to-noise ratio, a second pass of velocity picking was performed. These velocities were then used to improve the NMO

Figure 3.15: Depth conversion of the E-W line stack

Figure 3.16: The E-W seismic line with residual statics applied

corrections and thus allowing the creation of an effective stack. At this stage, a final mute was applied to the data to get rid of the distortion at far offsets caused by NMO stretching (Figure 3.18).

Post-stack migration and final enhancements

The stacked sections illustrated earlier assume a wave field that would have been recorded if the source and receiver were in the same place and thus represent a zero-offset wave field at the surface. However, the seismic energy is being scattered and diffracted back off the sub surface and in order to produce a correct image, migration is applied to the data to collapse the diffractions and produce a focused image of the subsurface structure. Migration converts

Figure 3.17: (a) A DMO stack with low frequency noise. (b) A band-pass filter applied to the DMO stack to get rid of the low frequency noise.

zero-offset reflections into reflectors. It does nothing to horizontal reflections but it steepens dipping reflections, shortens them and moves them up-dip.

In this case, three types of migration algorithms were applied to the data; Finite Difference (FD), Phase Shift (PS) and Kirchoff migration. Figure 3.19 shows the result obtained using the Finite Difference migration algorithm. As can be seen, some noise still appears in the migrated stack and thus final enhancements on the data were performed. These included bandpass filters, TV spectral whitening, and GXT Rogain.

Despite the fact that the FD method produced a decent section, the final image with best
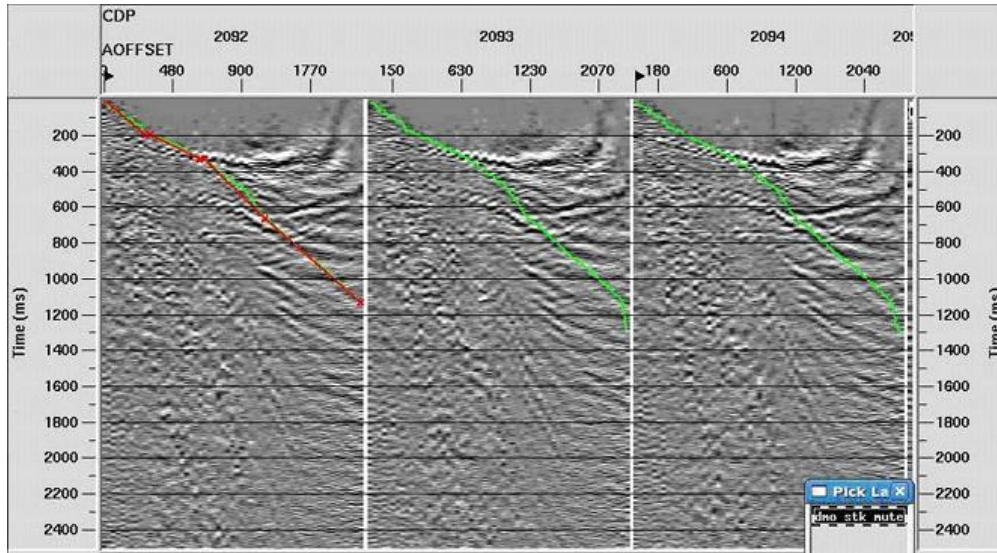
Figure 3.18: The process of muting out distorted data at far offsets caused by NMO stretch using the second pass of velocities

quality was created using the Phase Shift algorithm and this is illustrated in the following Figure 3.20.

The same processing sequence was applied to the N-S line with the final image produced using phase shift migration. The final seismic image of the N-S line is illustrated in the following section.

3.3.6   Interpretation

One of most important aspects in imaging the earth's subsurface is the velocity of the bedrock. On the final stack, Figure 3.21 gives the Precambrian basement at the depth of 2000m, 1100ms. It is clear to distinguish the basement because of simplicity of its composition, normally very dense and crystalline rock. This composition, due to its homogeneity we get a very consistent seismic signature.

On the west side of the line, we see a roughly 70 degrees east dipping fault which correlates not only with the geology of the area, but also with gravity and magnetic interpretation. The angle of this fault decreases with depth, yet continuous which suggests being much deeper than it appears. The fault separates the fill material from the mid section of the basin. Moreover, moving towards East along the fault its observed the faced spurs located on the mountains. It is typical of rift valleys to fill with sediments as the extension occurs; in our case we recognize the fills to be the Dry Union formation, glacial and alluvial on top of the basement.

Another very important reflector on the east ending suggests to be a lava flow due to the increase in velocity by the end of the Dry Union formation. Furthermore, the interpretation
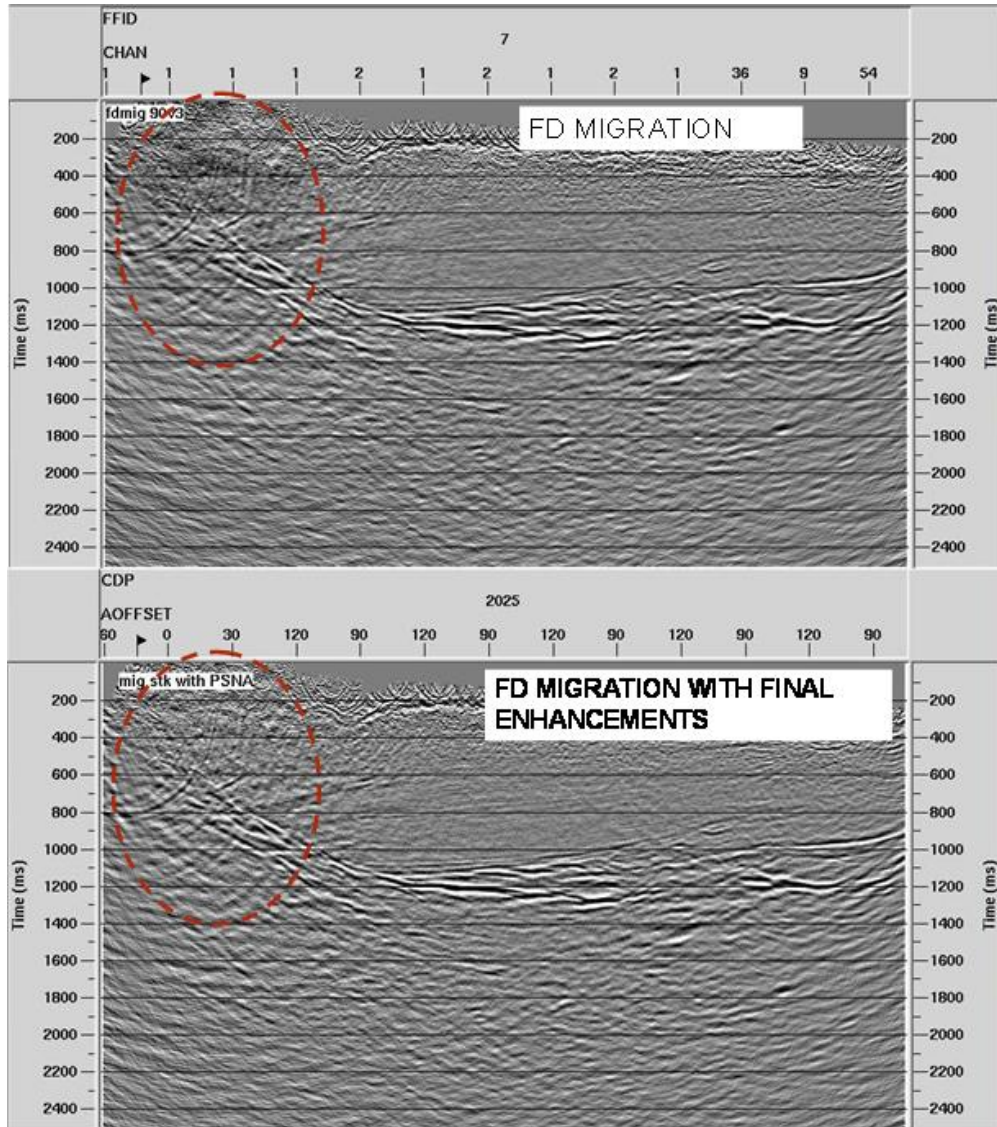
Figure 3.19: (a) A post-stack migrated data for the E-W line using Finite Difference migration algorithm

of the lava flow can be reinforced by the fact that some lava flows are exposed along the eastern side of the Upper Arkansas Valley. Due to the lava flow we can predict the presence of an unconformity along the boundaries.

At the circled area a zone of high density can be seen which can be explaind by the presence of large boulders, ranging from 0,3 m to 2.5 m in thickness found on the Dry Union Formation. [7] Another parallel explanation is the presence of fractures and small faults.

Two smaller faults striking N-S and dipping west are the type of structure capable of accommodating the displacement shown on the seismic profile.
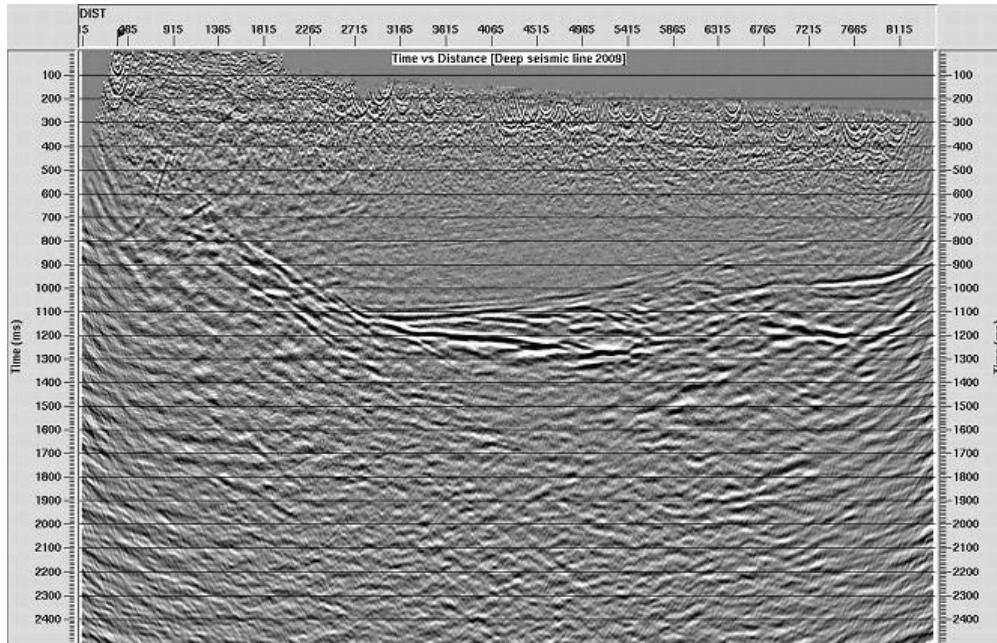
Figure 3.20: A final "time versus distance" image of the E-W seismic line. Phase shifted post-stack migrated with final enhancements applied
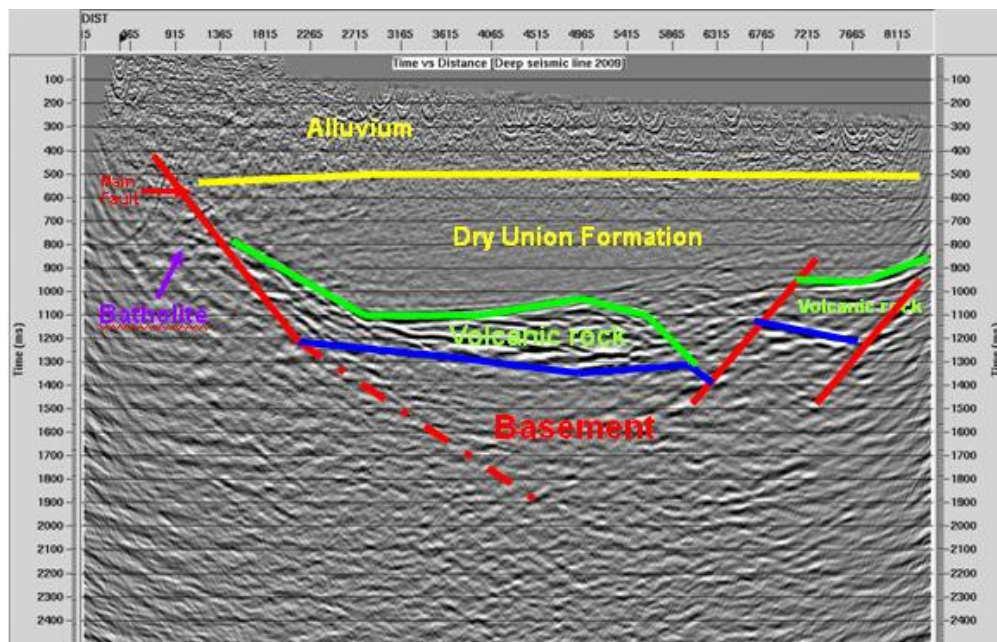
Figure 3.21: W-E line Interpretation of the boundaries and main structure contacts

39
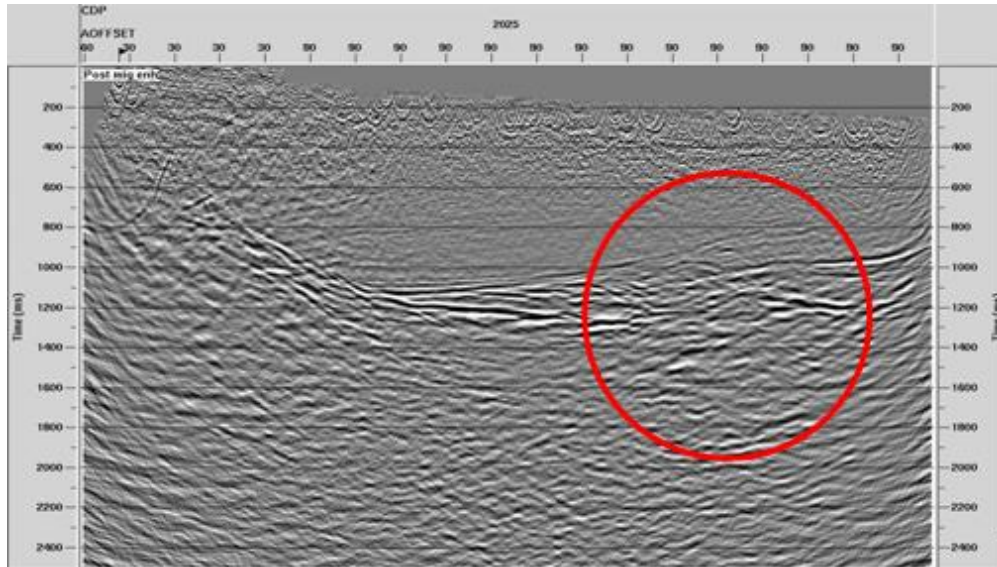
Figure 3.22: Post migration stack with enhancement

S-N seismic line was surveyed across to the W-E line and extends parallel to the main road approximately 5 km from the South to the North. All seismic acquisition parameters were selected the same as for the W-E line.
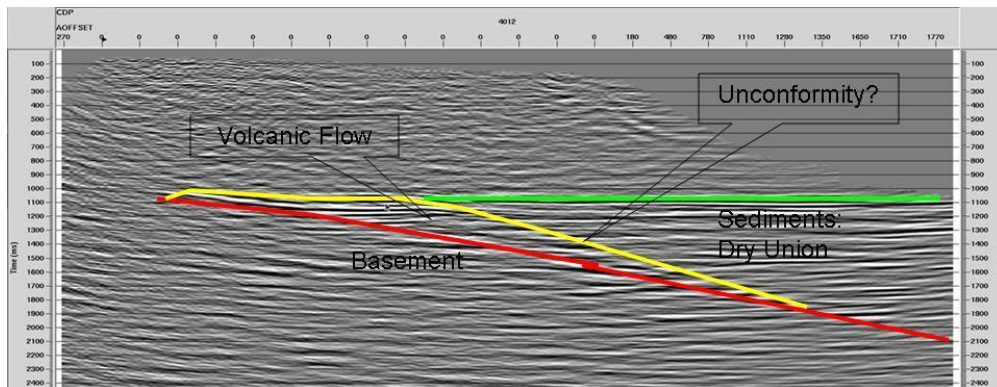
Figure 3.23: S-N line interpretation of the boundaries

The final stack data shows that the strong reflector of the Precambrian basement occurs at 1400ms and it ties with the interpretation of the W-E line. The volcanic rock occurs just about 1100-1200ms that were selected as the strong reflector above the basement. Overlying sedimentary rocks have weak amplitudes and were divided roughly according to W-E line where their amplitudes were shown improved. The main fault which occurs in the W-E line could not be clearly identified in the S-N line as the survey was done parallel to the fault.

A correlation between the E-W and N-S seismic lines was also performed roughly to give

a general idea of how the 3D image would look. The procedure involved figuring out the CDPs at which the two seismic lines intersect and plotting the two sections roughly at 90 degrees to each other as shown in the following Figure 1.24.
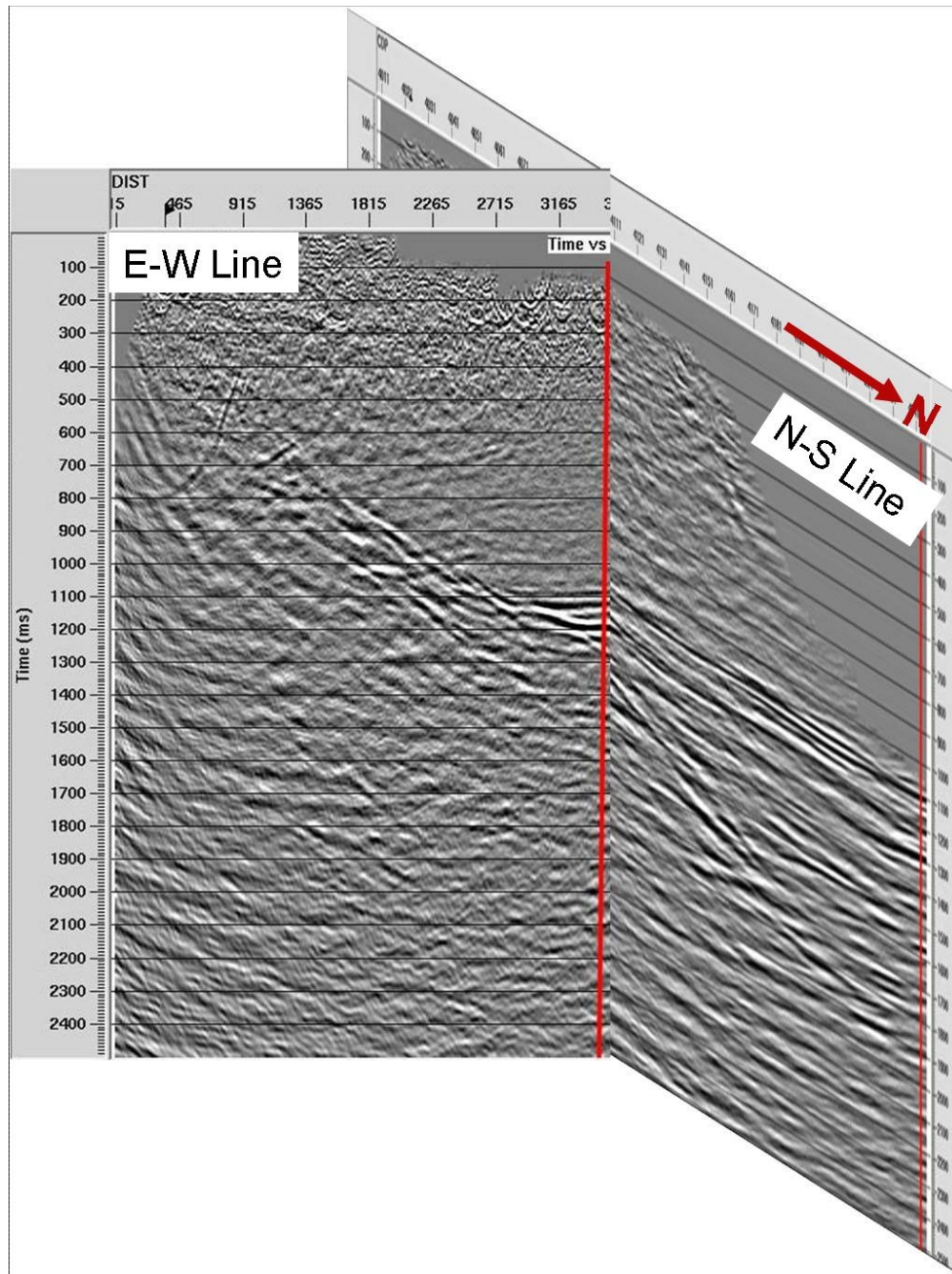
Figure 3.24: Correlation between the E-W and N-S seismic lines. The red line represents the line of intersection

As can be seen from the figure, a good correlation appears between the high amplitude

volcanics occurring in both lines.

2006, 2008 and 2009 Deep Seismic Lines
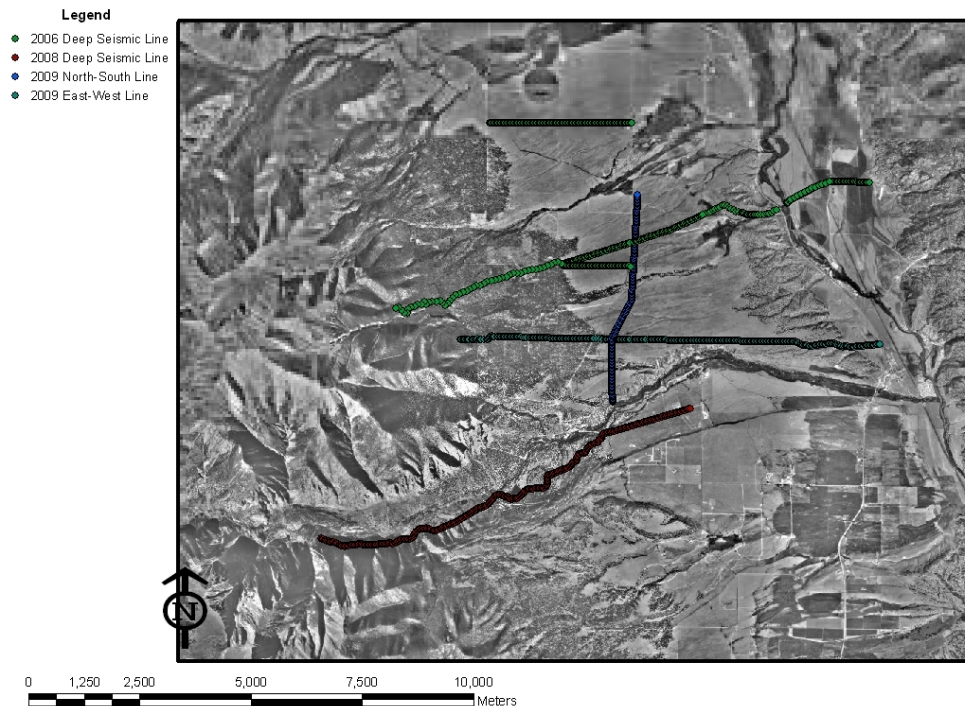
Figure 3.25: 2006, 2008, and 2009 compelation of deep seismic lines

In 2006 a team from Colorado School of Mines ran two deep seismic lines in the Upper Arkansas River Basin in Chaffee County Denver. The first of the two lines is of special interest to the 2009 team because it runs from West to East and intersects with the South to North deep seismic line from 2009. In the figures below the red lines are the points where the deep seismic lines intersect each other. Below is line one from 2006 and it shows where it intersects the North/South line from 2009.

Figure 3.27 is the deep seismic line from 2009 that runs from West to East and where it intersects the North/South line from 2009.

Figure 3.28 is the deep seismic line from 2009 that runs from South to North and where the West to East lines of 2009 and 2006 cross it respectively.

When all three figures are integrated, one can see from the images that the time to basement occurs at right about the same time which is about 1200 milliseconds or 1.2 seconds. From the 2006 findings one can see that the depth to basement is just a little over 2 km and that is also true for our 2009 findings as shown in the Figure 3.29. In the second part of the 2006 report it puts the basement at the point of intersection with our 2009 South to North line at about 2.26 km and this seems to be a fair estimate according to our 2009 data.

In 2008 another team from Colorado School of Mines traveled to the Upper Arkansas
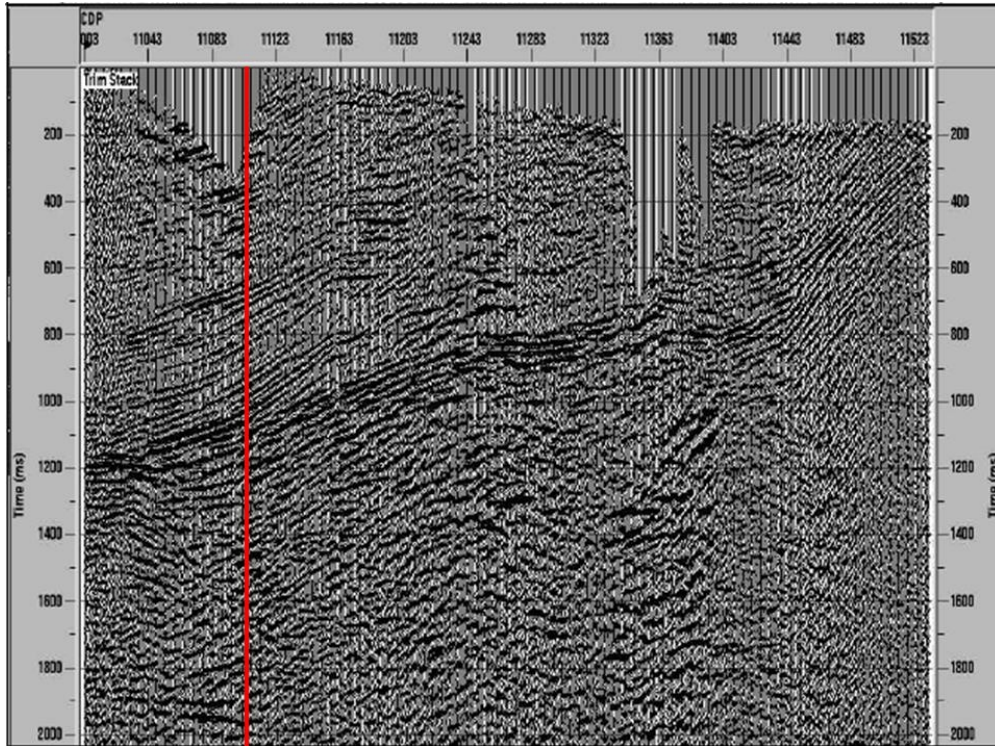
Figure 3.26: Data from 2006 West to East deep seismic line 1
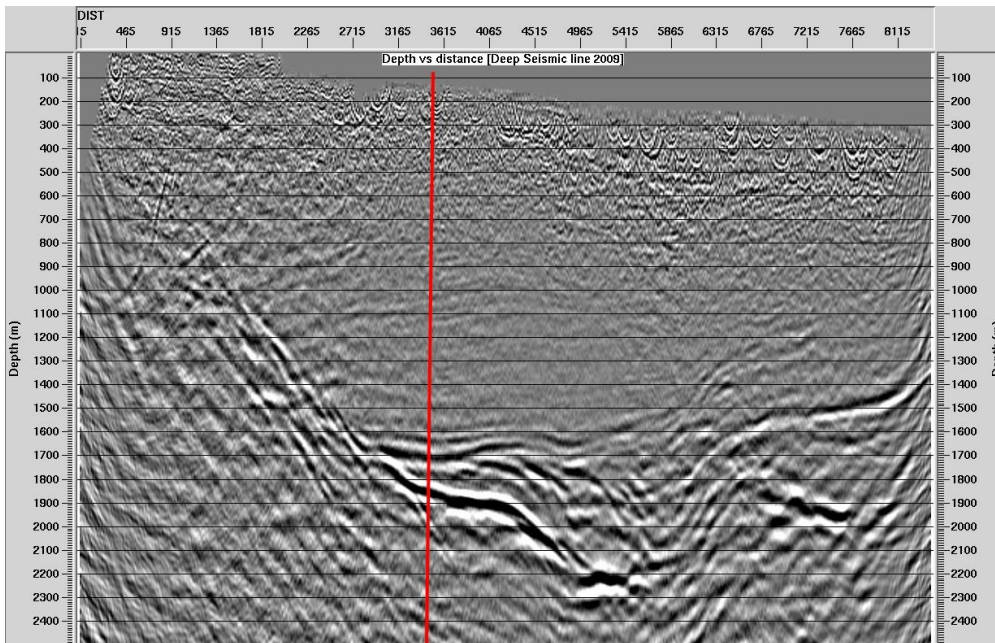
Figure 3.27: Data from 2006 West to East deep seismic line 1
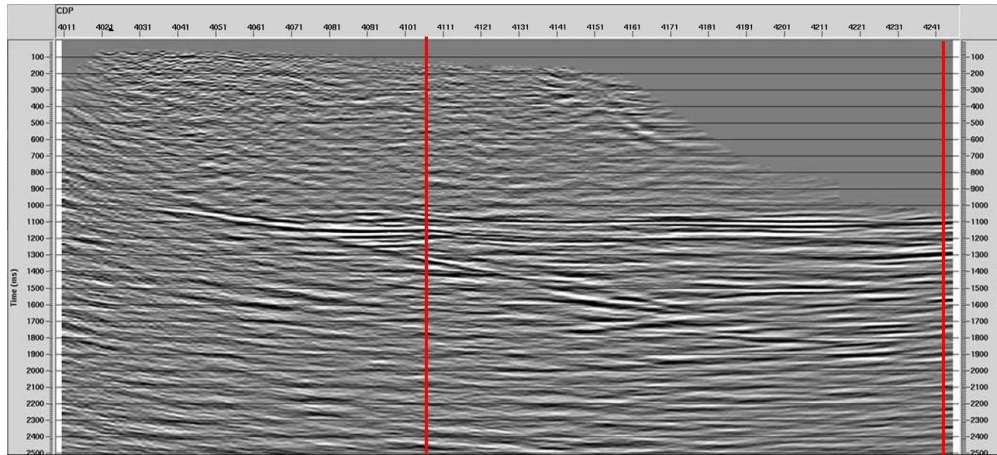
Figure 3.28: Data from the 2009 South to the North deep siesmic line. The West to East from 2009 crosses on the left (South) and the West to East fromj 2006 crosses on the right (North)
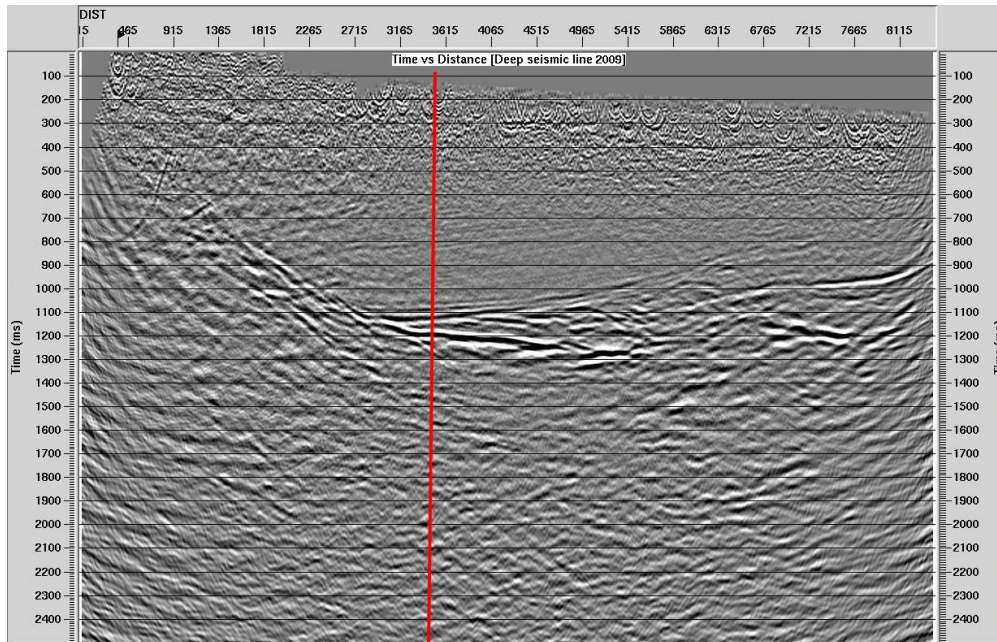
Figure 3.29: Depth vs. Distance, West to East deep seismic line 2009

River Basin and ran another West to East deep seismic line which did not intersect any of the lines ran before or since. If however, the South to North line from 2009 continued straight Southward and intersected the 2008 line it would have crossed the seismic line at the red line shown in the figure below. The estimated depth to basement determined by the image below looks to be about 1 km. This means that from the 2008 line to the 2009 line the depth to basement increases by about 1 km because of terrain and elevation differences

and also possibly a shallower basement at the 2008 seismic line site.
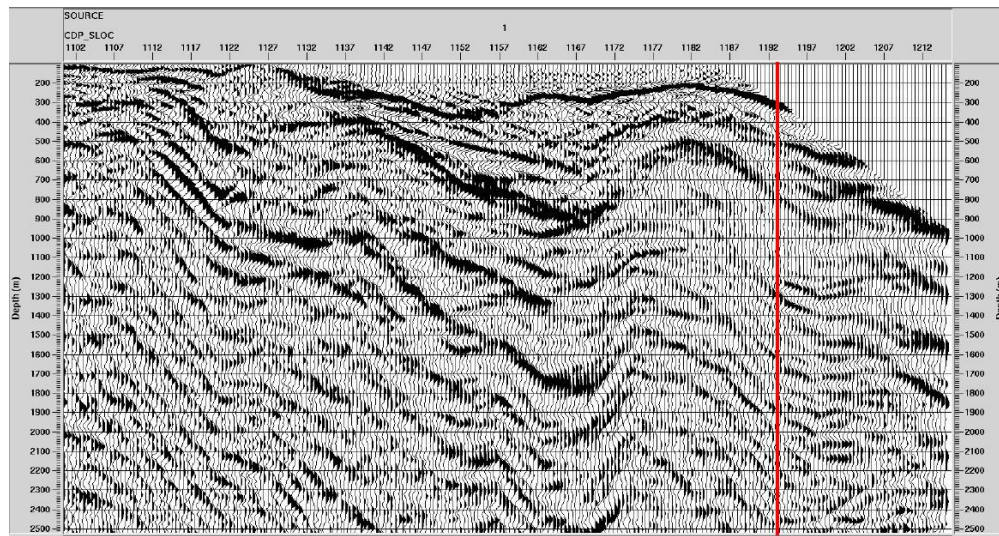
Figure 3.30: Data from 2008 West to East deep seismic line

Through correlation of the data from 2006, 2008, and 2009 the teams found evidence of faulting near valley edges, shear zones, multiple layers of sediment deposited within the valley, and also possible evidence of volcanic rock overlying basement at the bottom of the valley.

3.3.7   Error Analysis

Seismic interpretation is not an exact science. Many different geophysicists may examine the exact same data and come up with many different answers. After interpreting the data acquired throughout the survey it proved to closely resemble the geological model of the area. There were however some areas that werent as easy to interpret as others and those areas required more processing attention than the others.

The biggest problem encountered by the team processing and interpreting acquired seismic data was reducing the noise. Even in the final processed image there is still noise present that could not be filtered out without also losing data. There are only a couple types of noise in seismic processing, coherent and incoherent noise. Coherent noise comes from a source that may or may not be known and it always displays itself in a pattern that can be easily recognized. Concerning seismic noise, coherent noise may include the following: ground roll, artificial noise (man or animal made), noise from a separate event, and electromagnetic interference. Coherent noise can generally be reduced using a variety of signal processing filters and mutes because it typically is present only in certain frequency ranges. In this survey, there is noise present from power lines at around 60 Hz. This noise was filtered and

45

since there was useful information at around 60 Hz a small bandpass filter called a notch filter was used by the processing team to cut out frequencies between 58 and $62Hz$ only Figure 1.31.
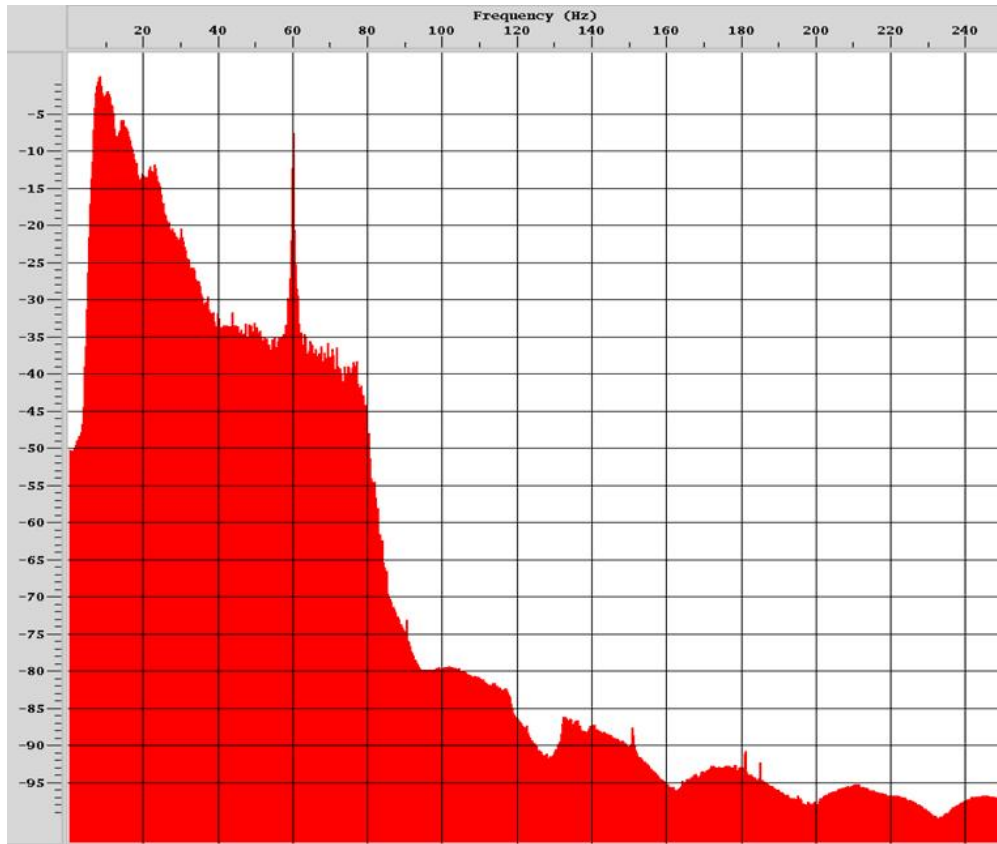
Figure 3.31: Spectral Analysis before notch filter was applied

Incoherent noise on the other hand is completely random and cannot typically be accounted for using signal processing techniques. However, common depth point or CDP stacking as it is called does a great job of attenuating incoherent noise. In fact, the signal to noise ratio increases as the square root of the number of samples in the CDP.
A second source of error encountered during processing came during velocity analysis. The processing team hand picked velocities in increments of 30 CDPs and then smoothed these velocities to attain a velocity profile which was to be used in later processing. Velocities were chosen to the best of the teams ability however, there most certainly is some interpretive error from pick to pick.

Another possible source of error in processing these seismic data is those that are caused a result of mute picking. Like velocity picking, mute picking is done by hand and at the discretion of the team. Several mutes were chosen and the best of them were used to process the final image.
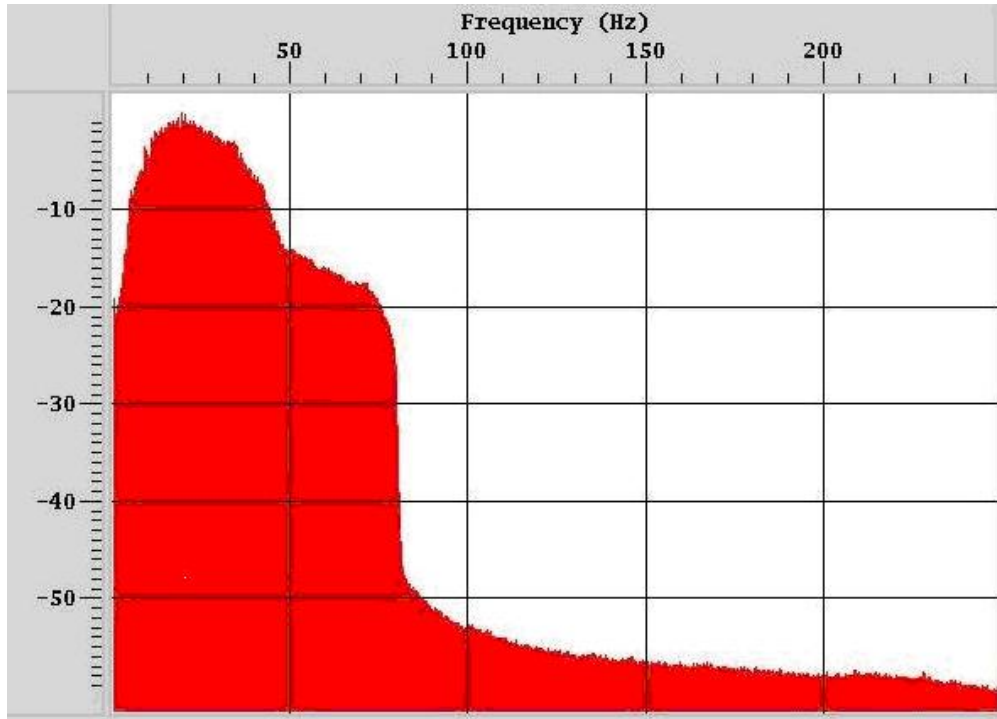
Figure 3.32: Spectral Analysis after notch filter was applied to cut noise from power lines. Other noise fitlers were also applied
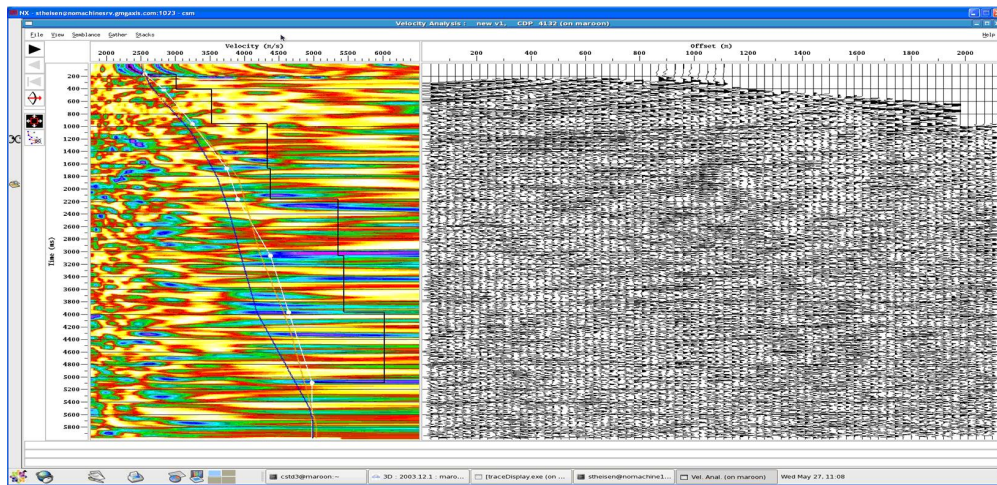
Figure 3.33: First pass velocity picking

Other sources of error that should also be mentioned include slight geometry errors, most of which were corrected during processing, however slight offsets most likely still remain. Noise that is caused by the survey itself or events happening during the same timeline as the survey may also result as sources of errors. Multiples returning back from the reflection off another layer should theoretically be attenuated during CDP stacking, however they may

47
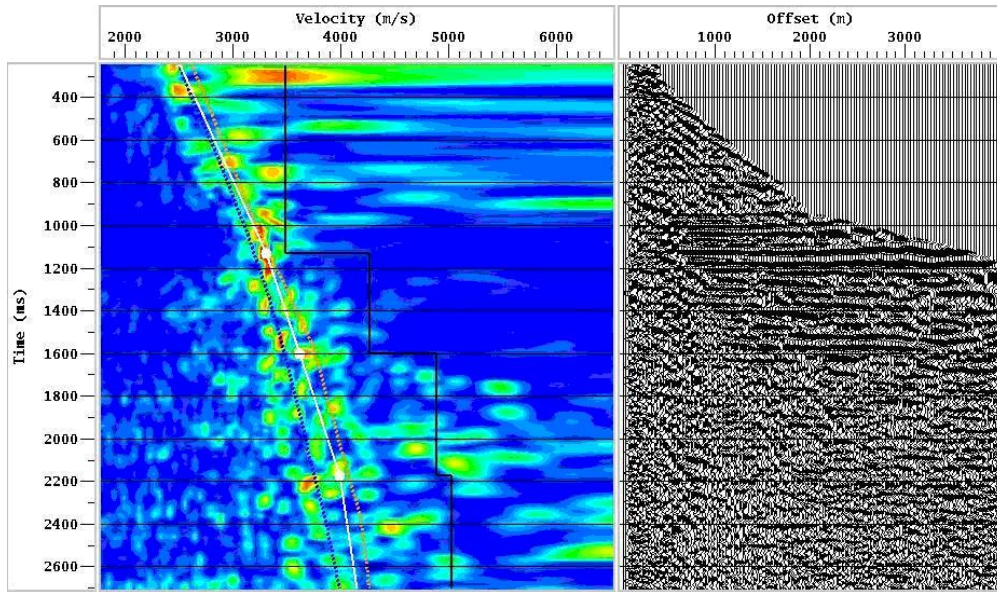
Figure 3.34: Second pass velocity picking
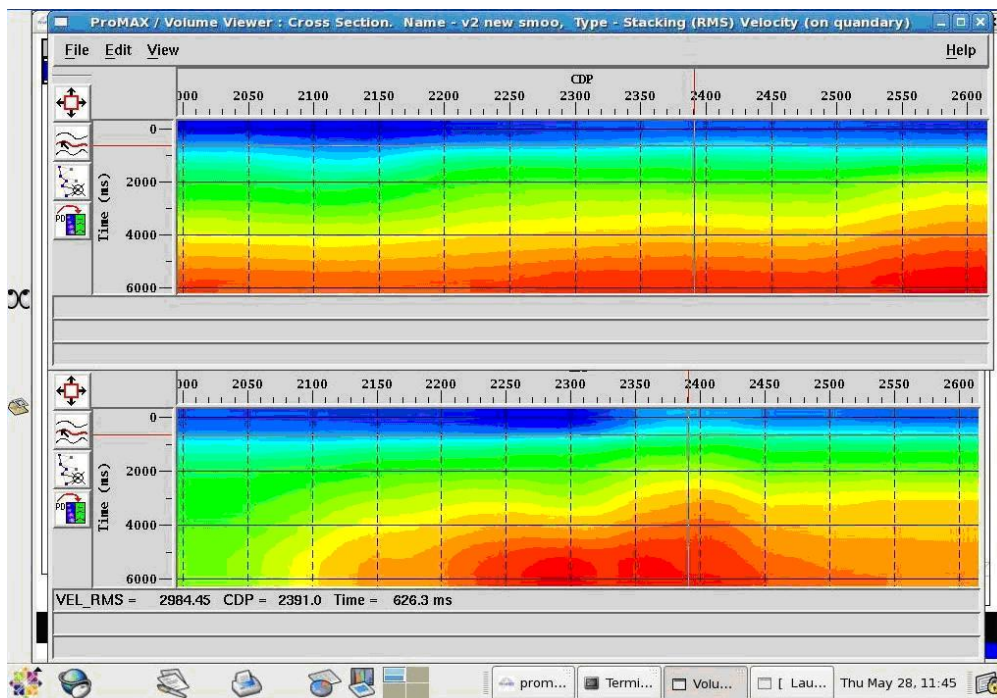
Figure 3.35: Velocities after smoothing, 2nd velocity over 1st velocity

still appear depending on their characteristics, and therefore care should be taken not to interpret multiples as layers as they are not a physical surface.

In conclusion, the actual amount of error is hard to calculate and even harder to assign an
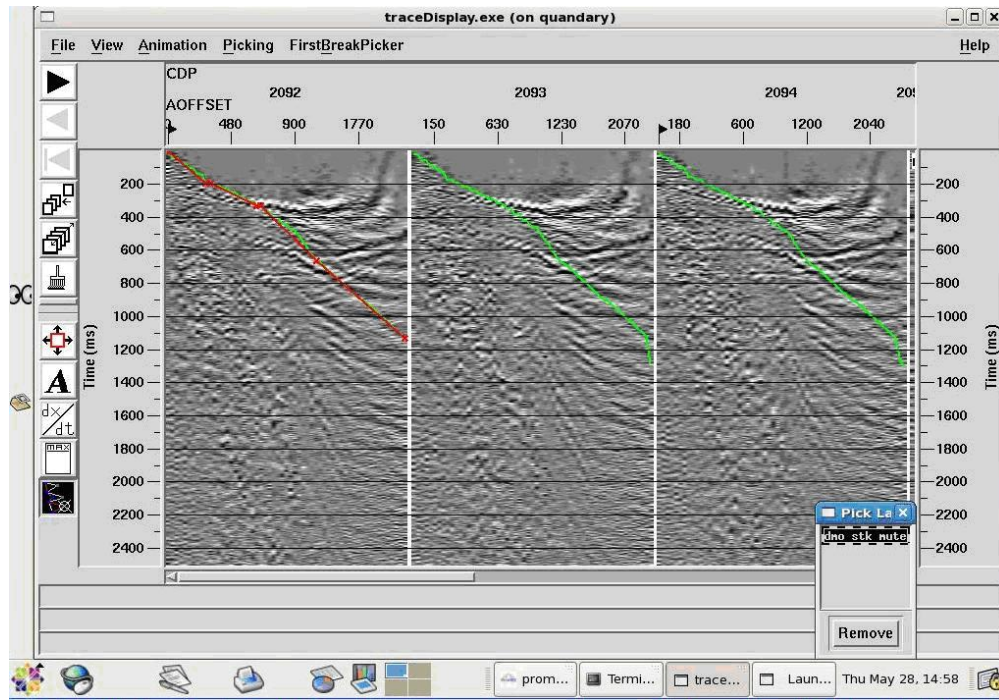
Figure 3.36: Some examples of mutes that were selected

actual value to. Due to the amount of values that are handpicked there is no way to measure what the human error may be, but instead one must just know it is there and accept it.

3.3.8 Conclusions

The deep seismic method as the name implies allows us to image very deep into the earths subsurface, more so than any other geophysical method employed in the region. Our findings this year tie in very well with existing geological models as well as past seismic surveys done in the Upper Arkansas Valley.

The processing of 2D Land Seismic data is a very long process. Seismic data processing involves the application of several corrections to the raw data set. There are many sources of noise that must be removed so that we just see the signal from the layers in the subsurface. The earth is very complex and a number of assumptions are made in order to process the data and produce a usable image for interpretation. The data collected at Field Camp 2009 was processed in four days and so it must be noted that with more time and further processing of this data set better images could be produced. Our data near the surface was very noisy and because of time constraints we were unable to clean it up.

We were able to map the normal fault on the west side of the valley. The Precambrian basement was seen at about 2000m. We were also able to interpret a volcanic lava flow above the basement that we know occur around 36.7 million years ago. There were faults interpreted on the East side of the valley, this may be due to the weight of millions of years

49

of sediments being deposited on the basement. Figure 3.36 shows our interpretation of the Upper Arkansas and our findings are reflected in the Geologic cross section.
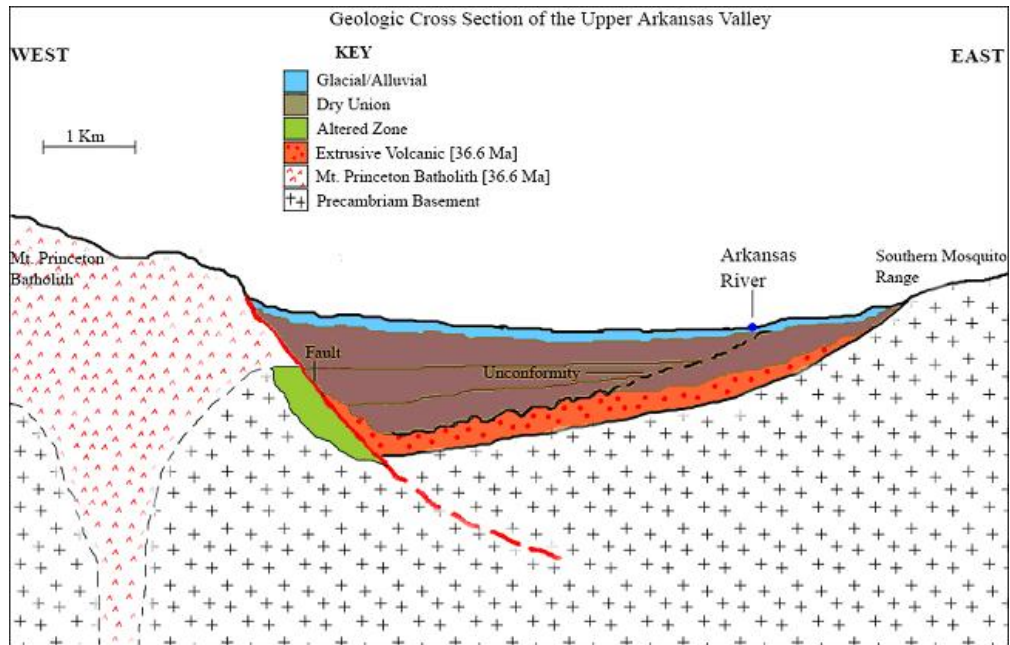
Figure 3.37: Geology of Upper Arkansas Valley

Chapter 4

3-D Seismic

4.1   Introduction

A 3-D seismic grid was established at the base of the Chalk Cliffs in order to characterize the shallow subsurface geology. The specific location was chosen based on the self-potential data collected in the 2008 field camp (see Section 11, 2008 Report). The 2008 self-potential survey located a high, positive anomaly that was reproduced in the 2009 survey. The high resolution 3-D seismic survey was designed to address the recommendation for a more detailed investigation of the area. Geological field observations indicate that a dominant North-South trending normal fault and an East-West trending shear zone are present in this area. The purpose of the investigation was to determine the depth to bedrock and characterize the faulting associated with the rifting of the Upper Arkansas basin. The collected seismic data can also be used to determine the thickness of the sedimentary section and bedrock topography. There is limited information concerning the true subsurface structure, therefore the shallow seismic survey was intended to further explain the hydrothermal activity and faulting in the area.

The geometry of the survey is shown in Figure 4.1. Although a large data set was collected, only one 2D seismic line was processed due to time constraints. For line 4600, the data was recorded using a Vibroseis truck and a hammer-drop source. The P-wave data from the hammer source was utilized in the seismic refraction study. The final profile can also be correlated with DC, SP, gravity, and magnetic information to yield a more comprehensive understanding of the subsurface. Since the hydrothermal activity is likely constrained by fault geometry, characterization of the basin faulting and basement will aid well drilling efforts in the future.
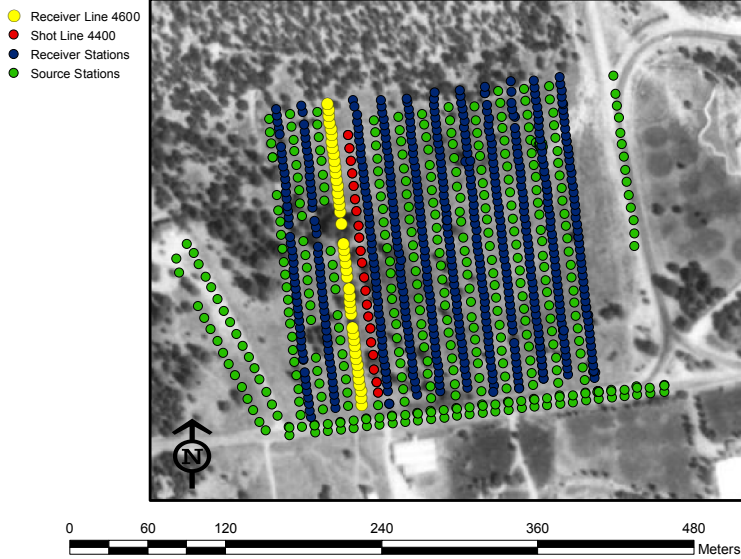
Figure 4.1: Aerial view of acquisition area. The field is located near the intersection of the dominant N-S trending, east-dipping normal fault and the E-W trending shear zone.

4.2 Acquisition Parameters

The acquisition parameter design is dependent on many factors including the subsurface target depth, geological structure, and sufficient aperture width for data migration. The shot and receiver intervals are relatively smaller than the deep 2D seismic profile because the target is much shallower.

Two different source types were used in the Field of Pain (see Table 4.1). The Thumper Vibroseis was utilized to acquire compression and shear wave data. Since the hydrothermal potential occurs at relatively shallow depths, relatively high frequencies were chosen for the Vibroseis sweep. The sweep was repeated twice for each source location for vertical stacking to enhance the signal to noise ratio (SNR). The second source was a weight drop (hammer). Compression wave (P-wave) data were acquired across the entire grid, but the shear wave and hammer-drop data are limited to the lines indicated in Table 4.1. The results from the seismic refraction studies for each source can eventually be compared to determine differences in image quality.

For the purpose of this project, a single shot line (4400) and adjacent receiver line (4600) in the inline direction were extracted from the 3D seismic data for geophysical analysis and interpretation. This particular 2D line was chosen because the three different sources (compression, shear, and weight drop) were acquired at the same source line. Unfortunately, there was insufficient time to complete the processing for the three sources.

4.3 Processing

The survey area has non-uniform topography, as well as obstacles such as trees and many yucca plants. As previously discussed the survey was designed specifically for the terrain and region it covered in order to ensure good data quality and optimize turnaround time. Aliasing was minimized through careful consideration of receiver spacing. The survey was desigened to be non-intrusive to the environment as well and ensure the safety of the seismic operation crew plus local inhabitants.

1. Tape

   The first step in processing the data was reformatting the data. In the field the data comes from the receivers was sorted into trace order and the data was written to tape. All the raw records were retained to allow for possible reprocessing at a later stage. The output for any hammer drop survey is always a minimum-phase wavelet. A minimum-phase wavelet is one that starts at time zero and has as much energy near the start as physically possible. However, it should be noted that the earth attenuates higher frequencies as the wavelet passes through it, and this alters the phase of the wavelet. Even if the wavelet going into the ground were to be zero-phase, it would not remain so at depth.

2. Remove Shots

   Using the observer notes (recorded in the field) it was necessary to edit and kill all the shots that were falsely triggered, allowing only good shot records to be retained for further processing. The traces were also checked for excessive noise, caused by anything including equipment failure but no traces needed to be removed.

3. Apply Geometry

   The next step was to apply the location geometry of the survey, which is an important process that assigns the correct positioning information to the source and receivers so that the Common Mid Point (CMP) locations can be determined accurately.

4. Elevation Statics

   The entire survey needed to be corrected for the arrival time changes due to topography and although it is also possible to correct for variations in the thickness of the near-surface layer, time constraints meant that this correction was not applied to the data set.
   First arrival times from field records were used to estimate static corrections because it is impossible and uneconomical to drill holes at every shot and geophone location. When calculating the statics to be applied it was important to ensure consistency across the survey area. The large redundancy in 3-D data means that there is often conflicting information about the statics required at any one location and special software can be

used to generate the corrections but this was not necessary in this case. Instead only a basic elevation statics correction needed to be applied to the data set.

5. AGC

Once the data could be viewed as CMP gathers an Automatic Gain Control (AGC) was applied to improve the detail available in the image. The AGC maintains the average absolute amplitude at a constant value within a specified time window. A window of $300ms$ was chosen allowing weaker reflections and refractions in the data to be viewed at higher two way times.

6. Band-pass filter

A band-pass filter was then applied; tests were conducted that removed the highest and lowest frequencies from the data and a 10;20;80;120 frequency range was adopted because it best preserved the highest and the lowest frequencies. The lowest frequencies are often heavily contaminated by noise (e.g. ground roll), which may swamp any underlying signal. As waves passing through the earth are reduced in frequency, frequencies over a certain amount are removed as they represent only noise. The band-pass filter attenuates the linear noise from ground role and after the filter was applied a brute stack was generated in order to see the results of all the pre-processing stages (see Figure 4.2).
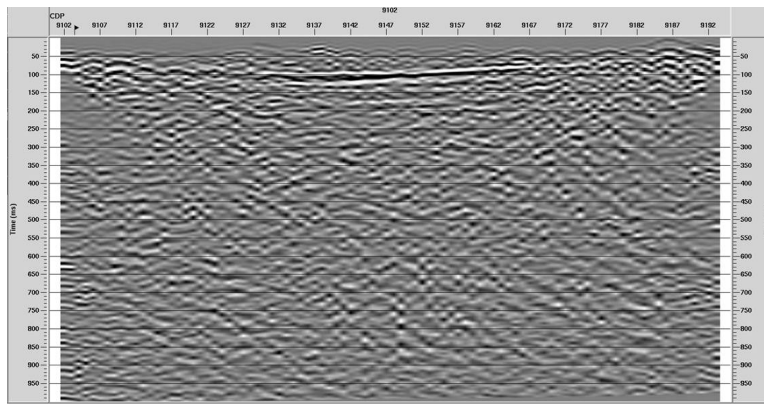
Figure 4.2: Brute stack generated after steps 1-6 had been completed.

7. Spiking Deconvolution

Deconvolution improves the temporal resolution of the seismic data by compressing the basic seismic wavelet. This process helps remove ringing effects often found within the data. It can also remove a significant portion of multiple energy found in the data. The recorded seismogram can be modeled as a convolution of the Earth's impulse response with the seismic wavelet. This seismic wavelet has many components including the source signature, recording filter, surface reflections and geophone response. If the

54

Earth's impulse response could be recorded then the wavelet would just be a spike. Ideally, this is what we desire through carrying out deconvolution. Deconvolution should compress the wavelet components and eliminate the multiples, leaving only the Earth's reflectivity in the seismic trace.

Autocorrelation was also carried out on the data in order to distinguish the wavelet. Since autocorrelation of the data is equal to the autocorrelation of the wavelet, then all noise and multiple data can be extracted from the seismic data. We are making the assumption that the geology is uncorrelated and noise in the data is also uncorrelated leaving only periodic events, representative of the wavelet. An understanding for the characterization of the wavelet can then be known i.e. an estimation of its length and period. In this case, the length of the wavelet hammer source was $40ms$ (See Figure 4.3).
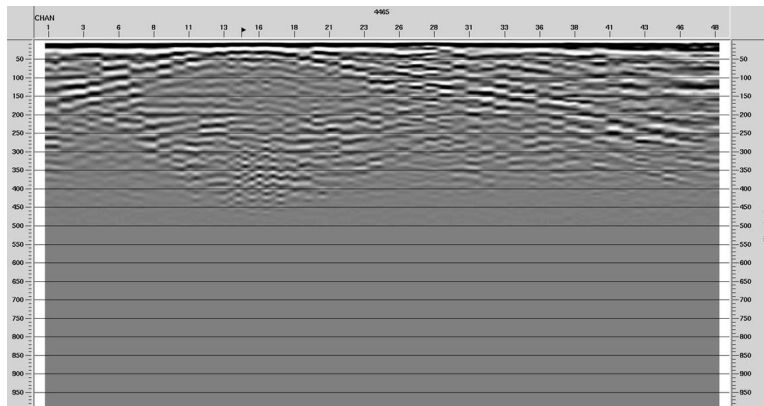
Figure 4.3: Autocorrelation of the initial brute stack.

The other assumption that can be made is that the wavelet of the hammer source is minimum phase since the energy of the wavelet is front ended. Spiking Deconvolution was applied to the seismic data trace by trace within the shot record. Spiking Deconvolution gives maximal wavelet compression, where a gap of 1ms was used and the operator length was adjusted accordingly. Spiking deconvolution was used since theoretically it assumes minimum-phase input data. Initially, an operator length equal to the wavelet length (40ms) was used. Using a 40ms operator length was too short since the multiples are not cut out and are still visibly apparent within the window. See Figure 4.4.

By increasing this operator length, more of the multiples should be able to be taken out of the data. By using an operator length of $150ms$, the desired result was achieved. If the operator length is increased beyond what is required, then this can act as an eliminator of valuable data; killing the primaries instead of the multiples. Using an operator length of $200ms$ and above will be too long and may destroy valuable primary reflection data. See figures 4.5 and 4.6.
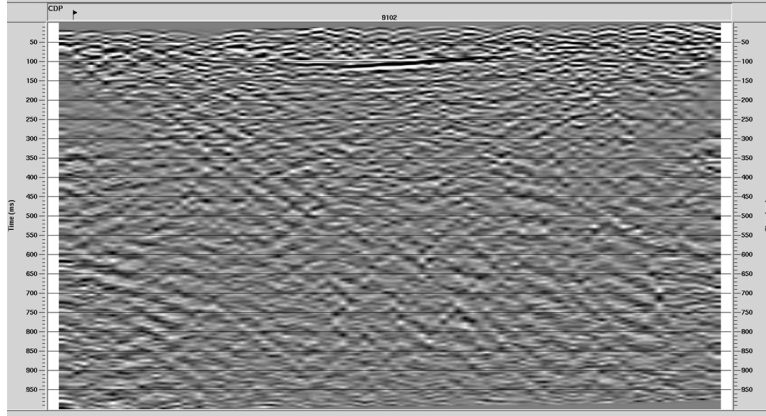
Figure 4.4: Stacked Deconvolution using an operator length of $40ms$ and a gap of $1ms$.
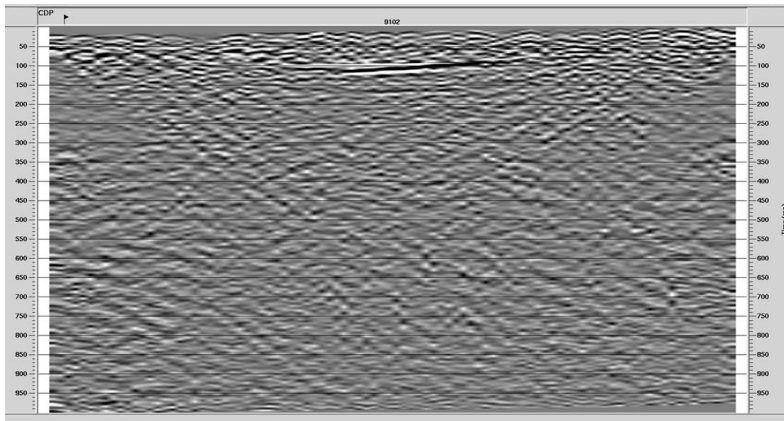
Figure 4.5: Stacked Deconvolution using an operator length of $150ms$ and a gap of $1ms$.
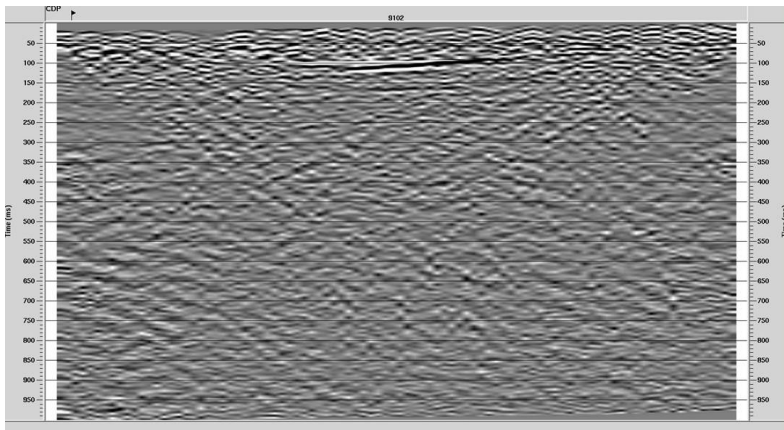
Figure 4.6: Stacked Deconvolution using an operator length of $200ms$ and a gap of $1ms$.

An operator of 150ms was chosen as the optimum length since this length is short enough that valuable primary data is not eliminated, but long enough to ensure most multiple energy is attenuated. See Figure 4.7.
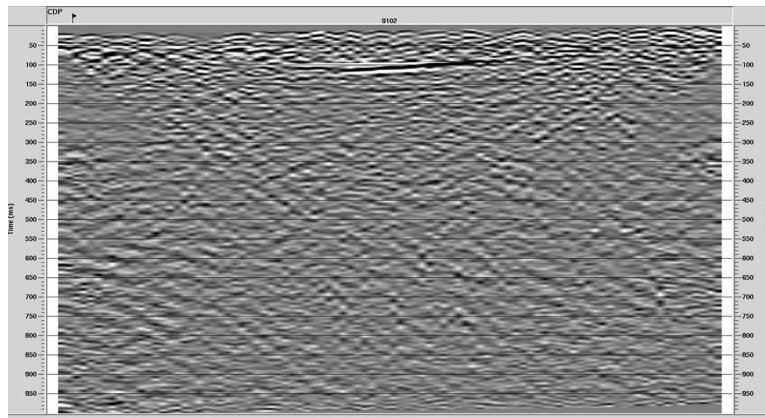
Figure 4.7: Stacked Deconvolution using final parameters that were chosen. An operator length of 150ms with a gap length of 1ms.

Looking at the frequency spectrums before and after deconvolution, it is evident that the high frequencies have been restored through the deconvolution process. Figure 4.8 Clearly shows this effect. The top image the figure shows the frequency spectrum of the brute stack before deconvolution (see previous brute stack figure 4.2) and the lower image shows the effect that deconvolution has had on the final stacked image (figure 4.7 of final stacked image). Deconvolution has removed much of the ringing effects, while it has compressed the waveform at each of the prominent reflections. The seismic data after deconvolution is more dominated by higher frequency data due to the extraction of low frequency reverberations and short period multiple energy.
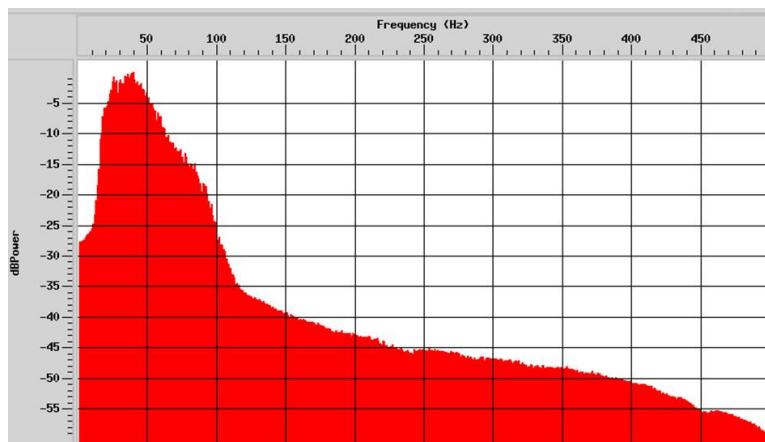
Figure 4.8: Frequency spectrums before and after deconvolution from previous brute stacked sections.

8. Refraction Velocity

There was an insufficient number of shot gathers to enable adequate coverage for a full velocity analysis. However, as shown in Figure 4.9(a) and 4.9(b), by analyzing the seismic data and looking at first breaks, it was possible to establish a subsurface velocity that could be inputted into the ProMax model.

It was assumed that the subsurface was homogenous and isotropic (e.g. with constant lateral velocity) and a simple two layer model was adopted. The first velocity was determined to be 900 $\frac{m}{s}$ and the second layer velocity was found to be 4300 $\frac{m}{s}$. In order to establish these values a number of shot gathers were extracted from different points along the line because the velocities changed due to the dipping reflector. From Figure 4.9(b) it is also clear that the shot gathers were asymmetrical.
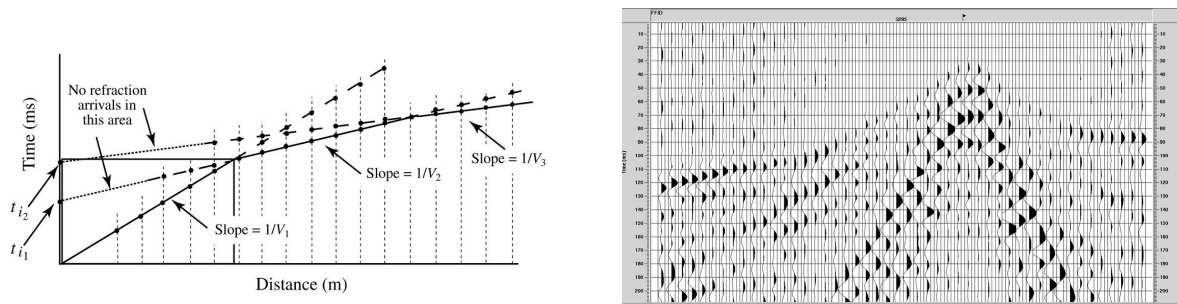
(a) **Diagram explaing the theory behind refraction velocity analysis.**

(b) **Example of a shot gather displayed in ProMax illustrating how V_1 and V_2 were calculated.**

Figure 4.9: Refraction velocity

9. Residual Statics

A static correction is a time shift that is applied uniformly across a particular trace. For example, the affect might be to shift an entire trace downwards by $8ms$. A neighboring trace might have a different time shift applied to it. Such shifts are typically needed when processing land data, to remove near-surface time delays particular to each shot and receiver location, as a result of changes in elevation and thickness changes in the near-surface low-velocity layer. Residual statics are applied to the data after deconvolution to adjust and fine tune any last statics that may need to be applied.

Three iterations were conducted using three different time shifts 12, 7 and 4 ms. The final results are displayed in Figure 4.10(a) and 4.10(b). It is possible to see clear enhancements in Figure 4.10(b). The image is sharper, indicating that the model is good even though it is not as accurate as desired. The shallow reflection in Figure 4.10(b) is also much clearer compared to Figure 4.10(a) where the peak is not as well resolved. In Figure 4.10(b) it is clear to see a strong progression of black, white, black, white reflections.
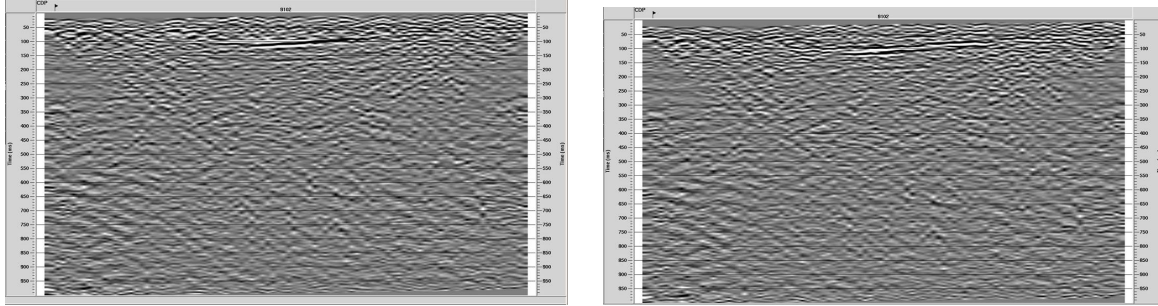
(a) **Stack before residual static correction.**   (b) **Stack after residual static correction.**

Figure 4.10: Residual static correction.

10. NMO

   Normal Move Out (NMO) is the case where the source-receiver spacing expands sys-
   tematically about a common midpoint, and refers to the increase in travel-time from
   the zero-offset case. Correcting for NMO is essential before traces can be stacked to-
   gether. This NMO correction will shift the individual samples of a finite-offset trace
   upwards by an amount that decreases with increasing travel-time. Consequencially,
   far-offset traces will be stretched (NMO stretch) and therefore shifted towards lower
   frequencies. At shallow depth and long offset, the effect may distort traces so badly
   that they are unusable and have to be removed (muted out) before stack [8].

11. Stack

   Adding a number of traces together improves signal to noise ratio. After the traces
   were corrected for the increased travel-time at the longer offsets (NMO), the traces
   with different source-receiver offsets but with a common midpoint were added in this
   case.

   Mute: Reflection traces recorded at long offset and short travel-time will be strongly contaminated by
various types of unwanted signal, such as refractions, and will be distorted by the application of NMO
correction which stretches the individual loops. They are usually removed before stack by setting to zero
all trace values for offset beyond a specified offset-TWT curve (the mute) but in this data set it was not
necessary to apply a mute.

4.4 Interpretation

The seismic data from line 4600 shows a distinct reflector in the center of the profile. A consistent overburden velocity of 900-1100 $\frac{m}{s}$ was obtained from the shot gathers, and the time/depth conversion yields a reflector depth of approximately 40-50 meters. Since the shot gathers show a relatively high velocity of 4000-4500 $\frac{m}{s}$ for the first break, the reflector is interpreted to be the boundary between the overburden and fractured/altered granitic basement. The observed velocities are too high to be associated with the sedimentary layers of the Dry Union Formation. An alternative explanation for the reflector is the location of the water table.
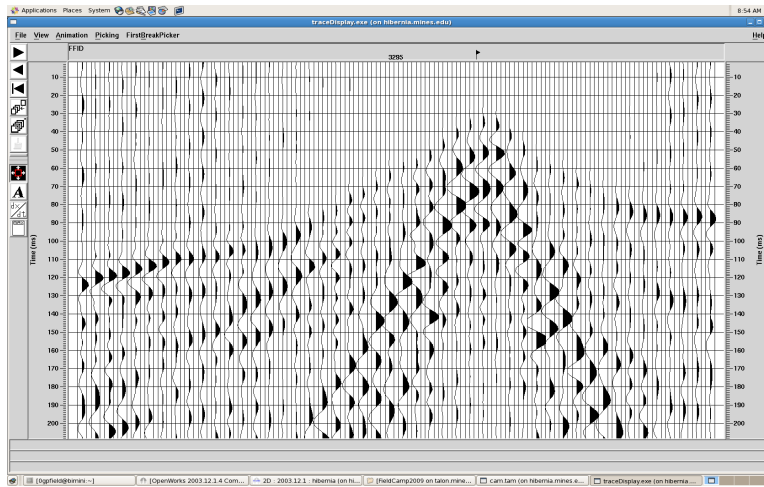
Figure 4.11: Shot gather (3295)
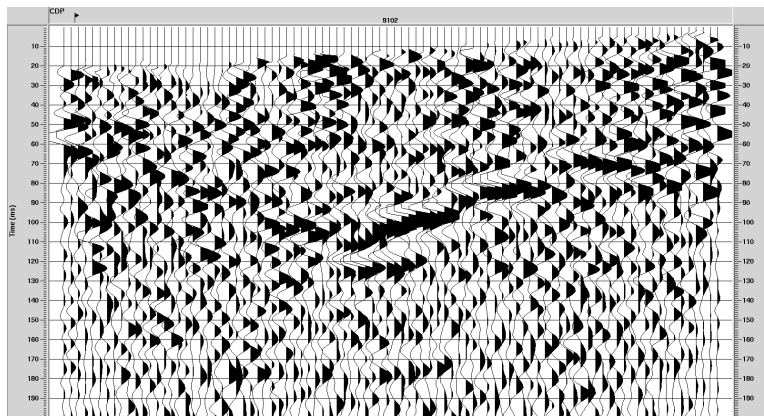
Figure 4.12: Seismic profile of Line 4600

4.5   Conclusions

It is imperative to note that the interpretation is very limited by the one-dimensional seismic profile available. The loss of resolution at the edges of the profile precludes a definitive explanation of the geology for the entire 240 meter section. The short duration for data processing is also problematic because certain assumptions are made to expedite the investigation. The two-layer velocity model is certainly reasonable, but deviations in seismic velocities due to lateral heterogeneity are likely. Therefore, a refined refraction analysis would also be beneficial for the study. Further processing of the remaining 3D data will likely provide a more confident interpretation of the local geology. The characterization of the basement is important because other independent geophysical techniques indicate that geothermal activity is not completely confined to faults. In this case, water may preferentially flow away from a shear zone toward highly fractured bedrock.

Source type	IVI T-15000 Vibroseis
Source interval	10 m
Shotline interval	20 m
Number of source points per shotline	25
Sweep frequency	30 - 300 Hz
Sweep length	12 s
Listening time	14 s
Number of sweeps per source station	2
Source array	none
Receiver type	40 Hz geophone
Receiver interval	5 m
Receiver line interval	20 m
Number of in-lines	12
Number of cross-lines	48
Number of receivers per line	48
Inline fold	12
Source line orientation	N - S
Receiver line orientation	N - S
Group array	none
Shear Waves Acquisition Parameters	
Sweep frequency	20-200 Hz
Sweep length	12 s
Geophone type	shear geophones (2 Horizontal Components)
Shot Lines	4000-4600
Receiver lines	4600-5400
Hammer Acquisition Parameters	
Source type	EWG-H
Shot line	4400
Receiver lines	4200-5400

Table 4.1: 3D Acquisition Parameters

Chapter 5

Vertical Seismic Profile

5.1 Introduction

Vertical seismic profile (VSP) surveys are seismic measurements made in a well, usually with a source at the surface and receivers at known depths within a well that are relatively close to each other. Both the down-going and up-going energy is recorded to generate an image of the subsurface. VSP surveys help to provide a more reliable correlation of well horizons to seismic data than sonic logs.

During the field camp five VSP surveys were acquired in two wells drilled in 2009, and located in:

1. Dead Horse Lake

2. Frontier Ranch
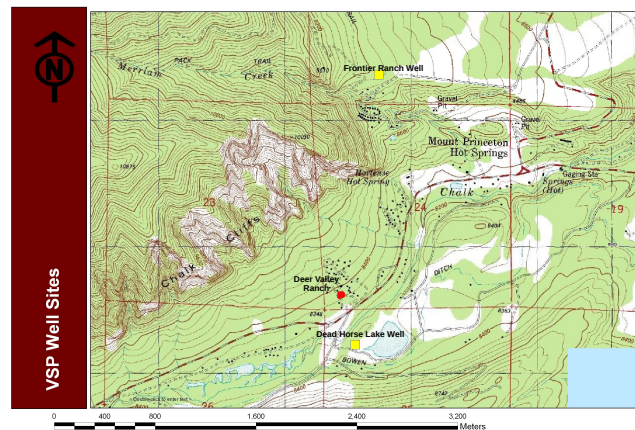
Figure 5.1: Locations of VSP surveys, Yellow: VSP Wells; Red: Deer Valley Ranch

5.2   Survey Design

The VSP surveys were acquired using a hammer as the seismic source and a string of thirty seven hydrophones placed in the borehole as the receivers. Three different surveys were acquired for the well at Dead Horse Lake:

1. Zero offset survey The hydrophones were lowered to the bottom of the wellbore while the source was located at the well head (Figure 5.2.) The hammer was then swung three times to acquire data at a single location. The hydrophone was shifted in ten centimeter increments up the wellbore and the procedure was repeated until the highest hydrophone was at the top of the well.
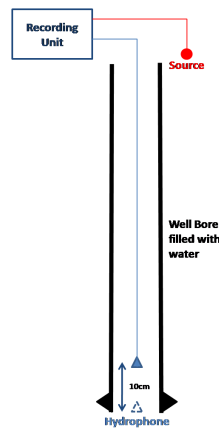
Figure 5.2: Design showing the zero offset geometry for Dead Horse Lake

2. Walk-away VSP The hydrophones were lowered to the bottom of the borehole, and the source was positioned ten meters away from the surface of the hole. The hammer was swung three times and data were acquired at this position. For the same hydrophone position the source was offset in ten meter increments for a maximum offset of one hundred meters from the borehole. This process was repeated using a hydrophone increment of ten meters up the borehole. This process can be seen in Figure 5.3.

3. Radial Offset VSP the hydrophones were placed at the bottom of the well and using a source distance of ten meters the source position was shifted along the circumference of a semicircle (radius ten meters) from zero degrees to one hundred and eighty degrees. Data were acquired for each 30 degree increment. For the same hydrophone position, the source distance was increased to twenty meters and data were acquired for different angles around the borehole, from zero too one hundred and eighty degrees. This procedure was repeated for each hydrophone location using a hydrophone spacing of five meters (Figure 5.4.) A second radial survey was conducted decreasing the angle between flag locations.

64
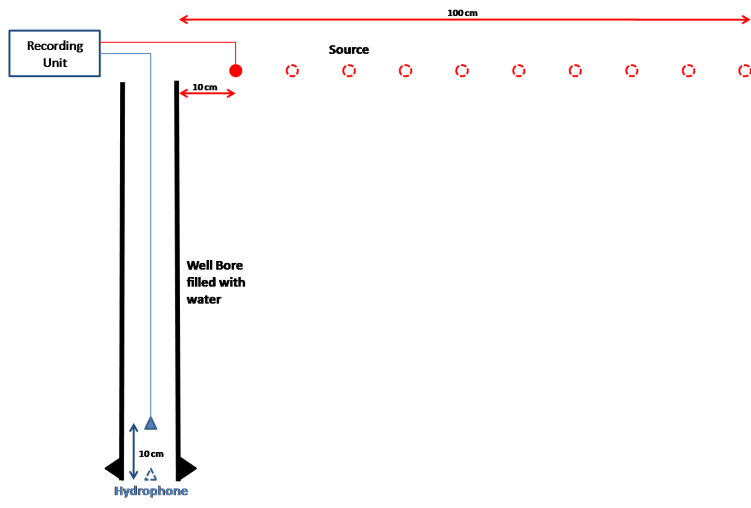
Figure 5.3: Geometry of a VSP walk-away survey at Dead Horse Lake
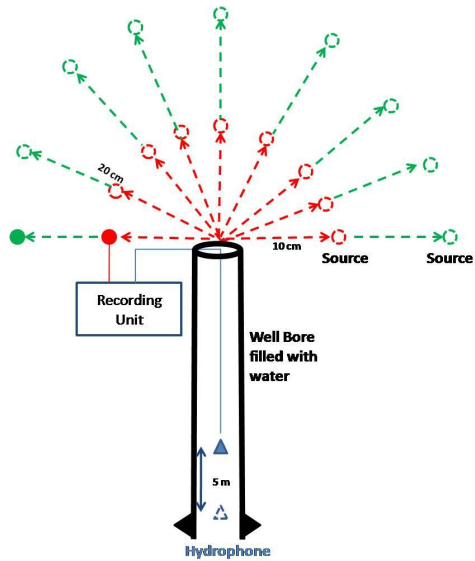
Figure 5.4: Geometry of a VSP radial offset at Dead Horse Lake

A zero offset survey was conducted at Frontier Ranch, the main difference was that the hydrophone string was moved in two meter increments.

5.3 Processing

5.3.1 Frontier Ranch Zero Offset VSP

The frontier ranch zero offset VSP was the simplest to process since the source position did not change, and the increments of hydrophone change were relatively constant. This was done by sorting the data into common receiver positions and if there was any redundancy then these positions were stacked in order to decrease any random noise.

This initial image can be seen in Figure 5.5. At early arrival times two arrivals of different slopes (velocity) are visible, and these were interpreted to represent two different velocity layers. Initially the steeper (slower) arrival was thought to be the airwave, but after a first pass velocity analysis the velocity appeared to be slightly too high, so this interpretation was discarded. It can also be seen that there are some arrivals that dip in one direction and others in the opposite direction, these represent waves that travel straight to the receiver (downgoing energy) and waves that reflect off a boundary first (upgoing energy.) These direct arrivals give information about the subsurface velocities, and these reflected arrivals give information on the subsurface geology; since the main purpose of this investigation was to try and constrain some of the subsurface velocities it was decided to focus on these direct arrivals.
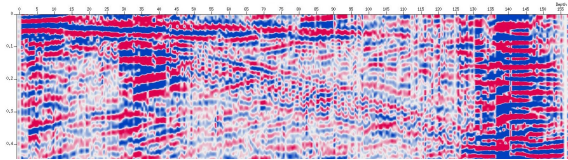
Figure 5.5: VSP profile throughout Frontier Ranch survey.

These two types of data were separated by a filter designed according to dip, and any data with a positive dip (upgoing energy) was removed. Some data with negative dips also required removing, due to the nature of the acquisition the data was 'spatially aliased' meaning at some points the data points were too separated to observe the actual dip of these arrivals, and so data above and beyond dips corresponding to what were believed to be our velocity limits were removed.

Figure 5.6 shows the section after this dip filtering, and the recordings after trace 250 were removed as these were particularly noisy and no coherent data could be observed throughout here. This section still contains some unphysical high frequency events that occur throughout the entire dataset. In order to clean up this image a second filter was used to remove any frequencies that were either too high or too low to be seismic reflections, and this section can be seen in Figure 5.7, with two different velocities interpreted. The arrival in red can now be seen to intercept the origin however the arrival in yellow is still ambiguous shallower than about 40m. The slow velocity wave reflection/transmission at trace 240 (depth of 120m) possibly shows the air wave reflection off the water table contact.

66

FK-Filtered Frontier Ranch VSP
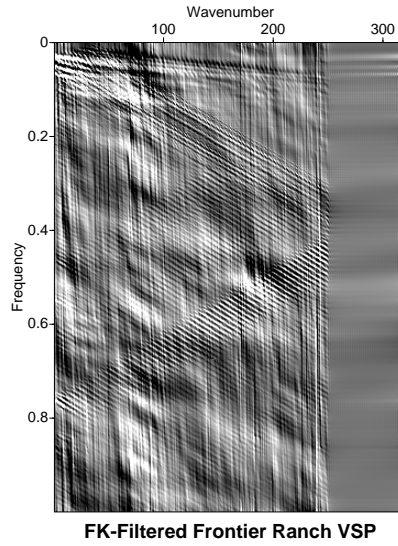
Figure 5.6: FK filtered Frontier Ranch VSP data.

FK and Band-Pass Filtered Frontier Ranch VSP
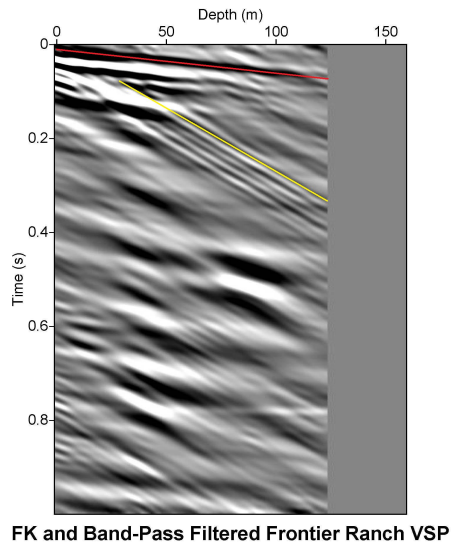
Figure 5.7: Frontier Ranch processed and filtered data displaying arrival picks. Yellow line shows Airwave and loose sediments. Red line shows a distinct arrival, possibly the well casing.

5.3.2 Dead Horse Lake Zero Offset VSP

The Dead Horse Lake zero offset survey was simple to process similarly to the Frontier Ranch zero offset survey. However the survey did take some extra processing due to the fact that the survey was conducted over three days by three separate survey crews. In the Dead Horse

survey the hydrophone string was pulled up the borehole in ten centimeter increments. With the three separate files, the initial data preparation had to be done to each file individually and then the three files had to be incorporated into one before stacking could be done. With the small hydrophone string increment, this produced more common hydrophone points reducing data noise that was more pronounced in the Frontier Ranch data.

The initial stacked data can be seen in Figure 5.8. The data shows that the down-going energy reflections (negative dip) have very similar dip, the up-going energy (positive dip) follows the same trend. Also the up and down-going energy have similar dips to one another, just with opposite signs in dip. The break in the data can be explained to the fact that the survey is taken over different days and that there may have been differing receiver locations. The next step was the same as Frontier Ranch, and that was to separate out the differing en-
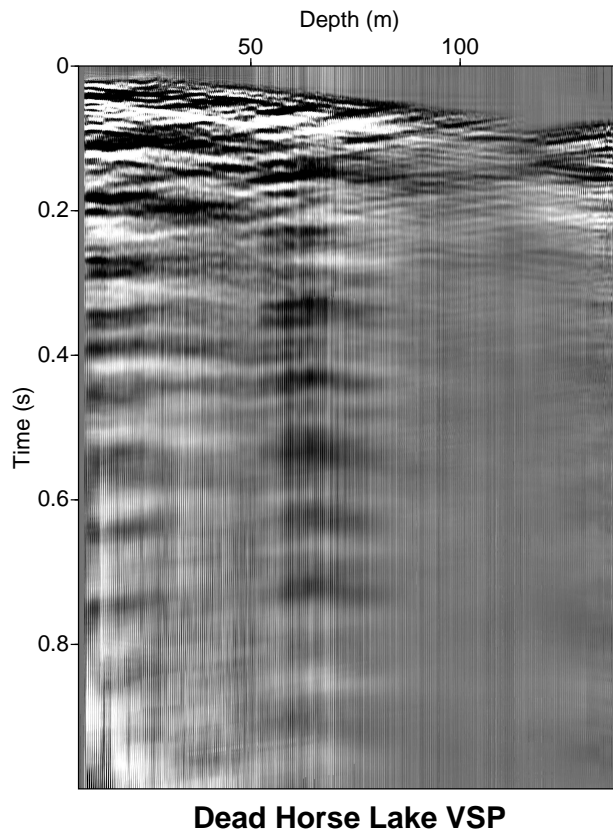
Figure 5.8: Stacked VSP data from zero offset survey at Dead Horse Lake well.

ergy components, wanting to keep the down-going energy. Luckily the spacing in this survey, unlike the Frontier Ranch survey, did not produce 'spatial aliasing' since the hydrophones

were moved in ten centimeter increments not two meter increments. This also helped in keeping basically all down-going energy reflections. Next a band-cut filter was applied to the data to filter out frequencies that are too high or low to be seismic data, the final filtered data can be seen in Figure 5.9.
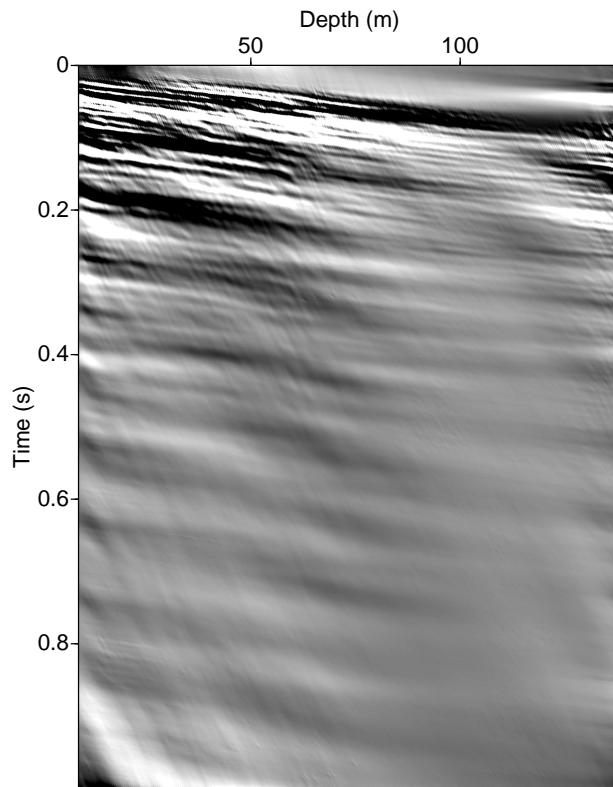
Band Cut Dead Horse Lake VSP

Figure 5.9: Band-cut and FK filtered VSP data from zero offset survey at Dead Horse Lake well.

5.3.3 Dead Horse Lake Radial VSP survey

After analysis of the zero offset it was decided to move onto the radial survey and to try and see if any conclusions could be made. The format of the acquisition is discussed earlier in the section, and the idea of this survey was to try and see how the velocities varied with depth and angular offset in order to see if there is a direction where the velocity is preferentially faster. If this is case it means that the velocity will vary with direction, a phenomenon

known as anisotropy, and is common in fractured rocks. If any anisotropy is discovered it gives an idea of rock type and a better constraint on the errors of any other velocity analyses. Another possible interpretation of any velocity variations with angular offset could be that the field is either dipping or there is a lateral velocity variation.

This data required more rigorous processing than the zero offset data, since the source position varied with both angle and with radial distance from the well, in addition to the hydrophone changing periodically. This meant to order the data several shell scripts were required, and these are detailed in the VSP appendix. It was decided the most efficient way of analyzing these data was to look at a certain depth in the well for a certain radial offset, to stack on these common attributes and analyze this trace across the seven angular offsets available. This method could then be done for different depth points in the well and for different radial distances.

Using these stacked traces the first breaks were picked, meaning that the first arrivals on each trace corresponding to each angle were picked on arrival time, and any differences between these for constant angle would indicate velocity variation with angle.

Since the data was acquired on land each source point was at a slightly different height so an additional processing step known as statics was required next. Using the recorded elevations for each shot point a weathering layer velocity from the zero offset data was estimated and then these statics were applied as a pure time shift for each trace. The velocity used was 400 m/s since the static differences were of the order of less than one meter, and so the velocity here will probably be near the slowest possible since the ground was loose dirt. In this instance the static shifts were almost an order of magnitude less than the observed time shifts, however they were applied anyway to help to reduce uncertainty and convince the interpreter that any arrival time inconsistencies were due to velocity variations and not any other external influences. The elevation shifts of shot points and the positions of shots and the well can be seen in figure 5.11.

Once the processing was complete to look at the data three depths were picked, at 49m, 80m and 100m. These were chosen since the data here was relatively clear and they gave a good sampling in depth. There were only two different radial offsets, so these were separated and compared. The data was plotted and viewed in both time-angle plots and velocity-angle plots, and the results displayed here are velocity-angle plots.

If true anisotropy is observed then one would expect to see a similar velocity profile with angle across all depths and radial offsets, however due to the nature of the position picking it is likely that the errors in picking may approach the shifts due to anisotropy. An error analysis will follow this section. Another effect that would be expected is to observe a gradual increase in average velocity with depth since the velocity observed is the average velocity of the first arrival to that depth.
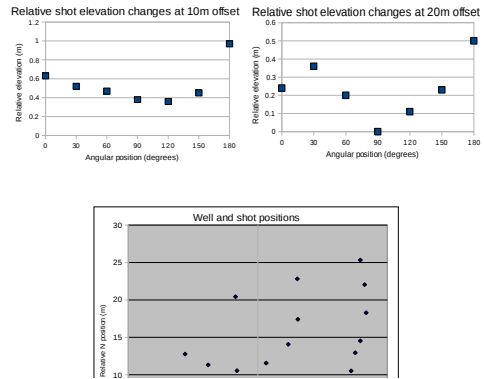
Figure 5.10: Elevation (static) shifts for each offset and positions of shots and the well. For the outer positions only every third point was shot on, but the positions have been interpolated for viewing ease.
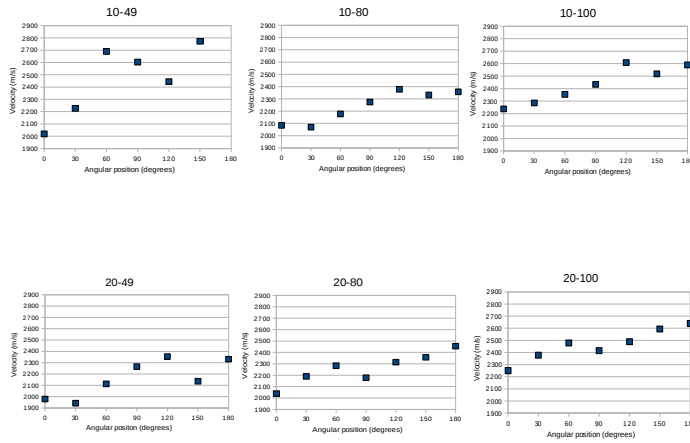

Figure 5.11: Plot 10-49 denotes a radial offset of 10m and a depth of 49m etc.

71

It is clear to see a general increase in velocity with increasing angular position throughout all six presented plots. Before static corrections there was a fairly consistent velocity peak at 120 degrees, however after further careful processing this was substantially suppressed. From these plots there are several conclusions that can be made, each with varying degrees of confidence. There are several plots that seem to conform to the fact that there is a velocity peak at 60 or 120 degrees, however since all depths and offsets do not agree to one angular position it is hard to be confident about drawing these sorts of conclusions. One issue with these data is that for true anisotropy the plots should resemble a half sine curve however several of the presented diagrams do not show the same velocity at 0 and 180 degrees, which would be expected. From looking at figure 1 it is clear the angular increments are not 100% correct since they do not form a full semi-circle, so this problem at 0 and 180 degrees could be considered as an artifact of the acquisition.

The trend of increasing velocity with angular position could be put down to lateral velocity variations through the area surrounding the well, and these indicate a fairly strong transition since the velocity shifts are fairly large in magnitude. This is the most likely conclusion that can be drawn from this analysis, to be more confident of this then more depths should be looked at to check, however with the current time constraints this is not possible before the time of print.

There were several key problems in this method that has introduced several uncertainties. The data itself was fairly rough and required several DC, dip and band pass filters in order to observe the first breaks. Even after these processes often the peaks were ambiguous and the time shifts were small, meaning there may be a large error inherent in these data. However after calculating the velocities the standard deviations on these differences were between 6 and 15%, the standard deviation for the error in the zero offset survey was certainly no larger than 5% and the same is true for this survey. This quick pass check helps us to be confident that the variations observed are not due to data errors but due to some form of angular velocity variation; however to be sure of exactly what sort of variation this is then more depths need to be observed and more offsets should have been originally acquired.

5.4   Error Analysis

The nature of the acquisition of the VSP data meant that the measurements were inevitably going to be full of different types of error. The manner in which the receivers were deployed (pressure reading hydrophones in a water filled well) caused errors since it was often not known how full the well was and whether all the hydrophones were submerged or not dry phones against the well wall would also have picked up a signal however this means the exact amplitudes of the various signals could not be entirely trusted. This point is furthermore assured since a variety of different people of varying strengths used the plate and hammer to induce the seismic signal meaning that the amount of energy going into the ground for each hit also varied substantially. Also even for the strongest hitters the amount of energy

transferred into the ground in the correct direction was small, which is why it was decided to vertically stack three shots at each shot point in order to try and reduce the error due to these random errors.

There were also problems with certain hydrophones being dead and not recording any signal this means that in stacking the fold at each point was more variable than otherwise, and hence the signal to noise was increased.

There were also errors that were unavoidably induced in the processing. The utmost care was taken in pre-processing in order to be confident the correct headers were assigned for each trace to avoid any errors in the naming and sorting of the files. In light of this the main processing errors came from picking the first arrivals in an attempt to try and estimate the velocity model for the area surrounding the well. Various fillters discussed above were used to reduce the uncertainty in the location of these picks, but nonetheless the standard deviations of the derived velocities were approximately 5% of the value, which with regard to the acquistion and processing is a reasonable error to expect.

To reduce the errors in processing more rigorous methods such as a spiking deconvolution could have been applied in order to reduce the differences due to the varying source signature, and with a close analysis of the dead hydrophones a linear program could have been applied in order to remove all these traces between sorting and stacking. In terms of the acquisition being assured all phones are submerged and a more consistent source would be desirable.

5.5   Interpretation

5.5.1   Frontier Ranch

The responses seen from the Frontier Ranch processed data (Figure 5.7) were picked and put into time-depth charts, which could then be plotted to observe what the velocities were and how they varied with depth. The arrival mapped in yellow on figure 1.7 is referred to as arrival 1, and the red as arrival 2, and these charts can both be seen in Figure B.4. Arrival 1 had an average velocity of $400\frac{m}{s}$ and a standard deviation of $26\frac{m}{s}$, and from Figure B.4 it is apparent this does not change greatly with depth. This is slightly too fast for the speed of sound in air $(340\frac{m}{s})$ and so was considered a very loose weathering layer velocity. Arrival 2 had an average velocity of $2120\frac{m}{s}$ and a standard deviation of $110\frac{m}{s}$ and it can be seen that the velocity increases with depth, which is what was expected.

As a brute velocity check some shot gathers from the nearby 3D seismic data field were analysed, and first breaks were picked and velocities for three distinct layers were estimated. This was a rough method as only one shot at a time was looked at, the velocities were estimated by eye, and this would also help to augment the work done in the 3D velocity analysis. Their nearsurface model consisted of three layers, with rough velocities of 750, 900 and 1500 $\frac{m}{s}$, from the first break brute check three layers of roughly 500, 1250 and 2000 $\frac{m}{s}$ were found. This method is inherently full of errors and was employed a first pass QC check to see if the VSP velocities compared to other methods. These layers produce a model as

can be seen in Figure 5.12, while these depths will not be the same at our well site, the material and hence velocities should be comparable.
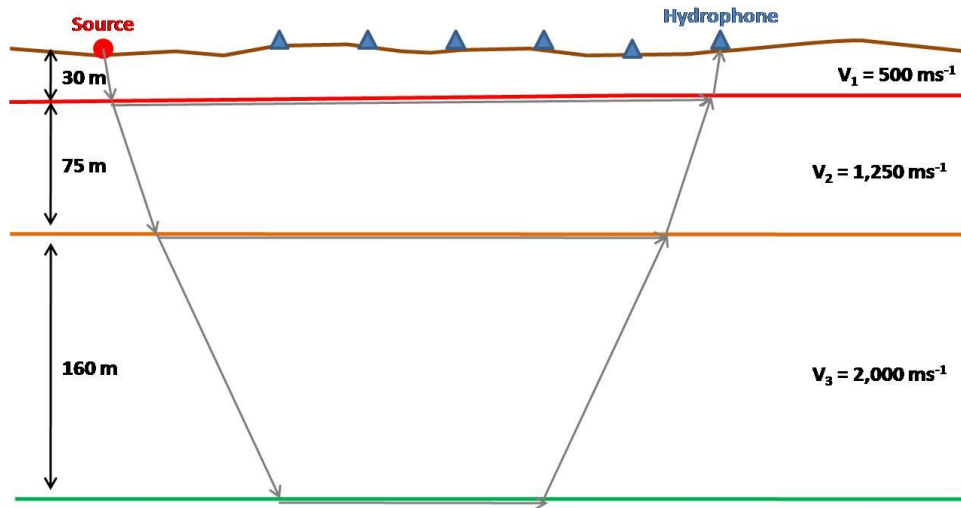

Figure 5.12: Velocity model from picked velocities from shallow seismic shot.

5.5.2 Dead Horse Lake

With the Dead Horse Lake data, two reflections were picked, this was due to the fact that the dips in the data shown in Figure 5.13, dips at very similar dip throughout the well section, however the direct wave can be seen. The direct arrival was picked to be put into a time-depth chart to calculate the velocity for the reflection. The velocity of the sediment was determined to be 1470 $\frac{m}{s}$. The velocity then changed as depth increased from 3500 $fracms$ to 4700 $\frac{m}{s}$ as the wave entered the basement granite. The velocity curve produced can be seen in Figures B.5 and B.6. This profile makes sense, due to the fact that the wave traveling through both sediments and granite will have a slower velocity than just granite alone.

In Figure 5.13 there is evidence of a Stoneley wave that travels down the borehole and reflects off the bottom. With this wave the velocity was picked to be 2700 $\frac{m}{s}$ with the velocity curve seen in Figure B.6. Overall the zero offset survey at Dead Horse Lake gave examples of the velocity profile in the area and helped further understand the geology in the area.
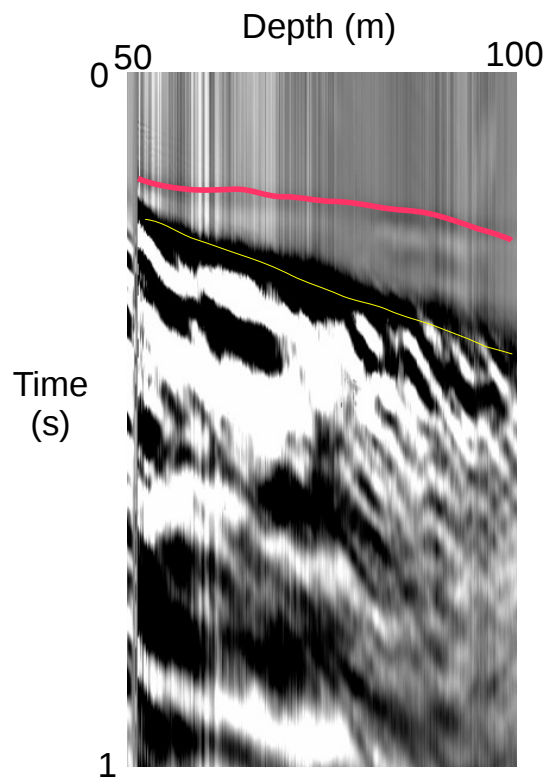
Figure 5.13: VSP stacked data of Dead Horse Lake Zero Offset, second run through

Chapter 6

Electromagnetic

6.1 Introduction

Electromagnetic (EM) methods measure the apparent conductivity of the subsurface. There are many instruments that measure in the frequency or time domain and can be used for differing geophysical applications. Electromagnetic methods are used for mineral exploration, groundwater surveys, geologic mapping, permafrost mapping, geologic faulting, and geothermal resource investigation. These are merely a few of the numerous applications EM can be used for. However, for the area under investigation, groundwater surveying, faulting and geothermal activity are especially important because Poncha Springs has active faulting with geothermal pockets and groundwater flow.

The instruments used in the Upper Arkansas Basin measured the apparent conductivity in the frequency domain. The purpose of having a device that measures in the frequency domain is to collect data at varying frequencies. The frequency domain devices measure both the primary and secondary magnetic field. Current is applied in pulses and is switched off in order to measure the secondary field. This process is similar to that of a spring and dashpot where current is turned on and the decay is measured once the current is turned off. Figure 6.1 shows how the subsurface current decays when the source current is turned on and turned off.
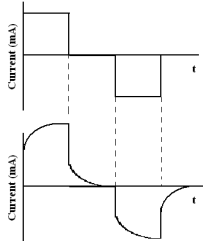

Figure 6.1: Top: Source current graph. Bottom: Subsurface current.

Generally, the transmitter coil generates a current which induces the primary electromagnetic field that propagates through the subsurface. If there is a conductive body in the subsurface, alternating currents flow within the body creating a secondary electromagnetic field. Figure 6.2 shows how a secondary magnetic field is produced by a conductive body in the subsurface. The primary magnetic field (blue) is produced by the transmitter, and once it interacts with the conductive body the secondary magnetic field is produced (red).
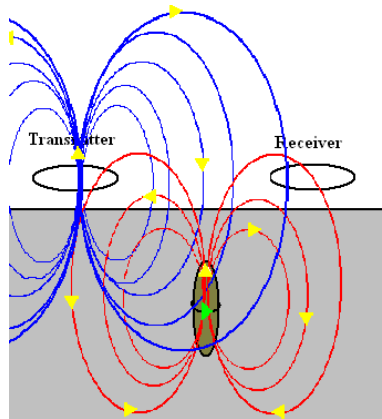

Figure 6.2: Three loop system, source (Tx), receiver (Rx) and anomalous loop.

The secondary and primary fields are detected by the receiver and are measured concurrently. This is one of the downfalls of frequency domain electromagnetics because generally, only the secondary field is the important field in acquired data.

6.2 Istrumentation

6.2.1 EM-31

The Geonics EM31-MK2 (Figure 6.3) measures near surface apparent conductivity at a maximum depth of six meters. This is ideal for subsurface conductive anomalies that could potentially indicate geothermal activity from faulting and groundwater flow. The EM-31 measures the current in the frequency domain with two sensors on either end of the device. It is important to walk at a constant velocity to ensure a consistent electromagnetic current distribution. It is also important to keep the device at the same angle to the ground the entire time (usually for simplicity parallel orientation is chosen). More detailed instruction on how to program and operate the EM-31 is seen in the Equipment Appendix.

Figure 6.3: Colorado School of Mines student Orion Sandoval carrying EM-31

6.2.2 EM-34

The EM-34 (Figure 6.4) is very similar to the EM-31 except that the coils are much larger and are transported individually as opposed to being contained inside a pole as a system. The distance between the coils is not fixed in the EM-34 system since the coils are at an approximated distance apart. This is important to note because the greater the coil separation, the greater the depth of investigation. The EM-31 is limited in depth of invesitgation due to the fixed distance between coils, but the EM-34 can penetrate much deeper into the ground. The orientation of the EM coils is horizontal (laying flat on the ground as seen in Figure 6.4) so that the primary magnetic field is vertical.

Figure 6.4: Colorado School of Mines students working with EM-34 loops

6.3 Data Reduction

Figure 6.5: Map of Poncha Springs area indicating location of EM-31 surveys.
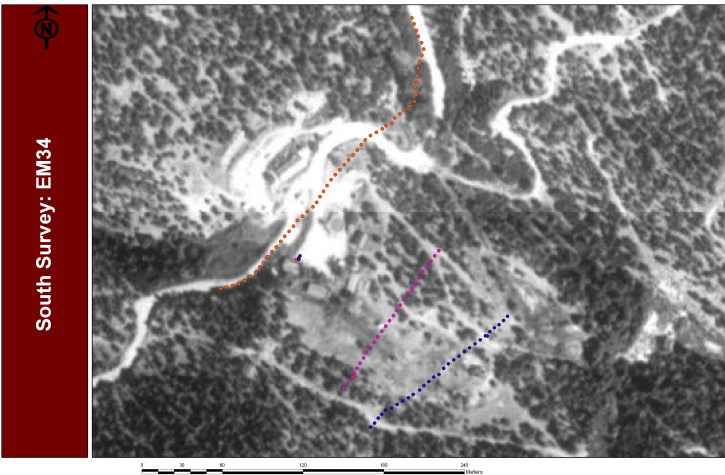
Figure 6.6: Map of Poncha Springs area indicating location of EM-34 surveys.

As already discussed, the EM method determines the conductivity of the subsurface down to a few meters. This method was used in the Poncha Springs area to determine where there may be an alternate source of hot springs, other than the above-ground shows already discovered. This is possible with EM for a few reasons, first of all, hot water has a higher conductivity than cold water and second that conductivity changes can be used to find faults which hot water will likely travel through.

6.4 Data-Observations

6.4.1 EM-31

Plots

EM-31 data was acquired in the field near Poncha Springs along DC resistivity lines. The data was collected using the EM31-MK2 and processed using a program called Dat31W. The program was able to open the files created in the field which were saved as FILE.G31. These files are unique in that they cannot be viewed easily by another program. Therefore, the files were then written into a .xyz file and manipulated in Excel for easier plotting and manipulation.
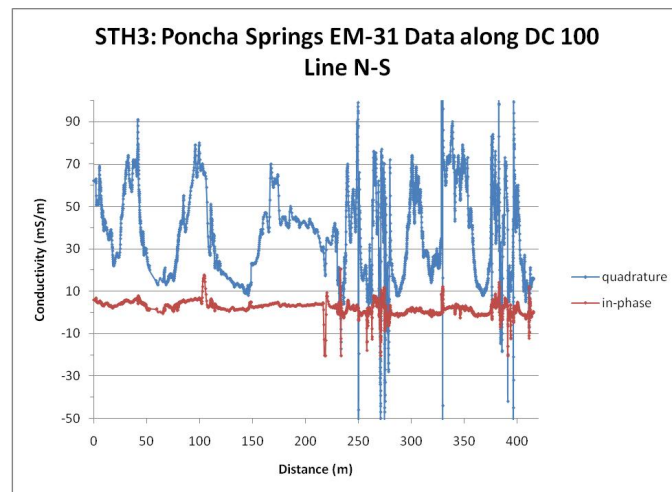

Figure 6.7: EM-31 data collected along DC 100 line in Poncha Springs

Figure 6.7 above shows the EM-31 data collected along DC Line 100 in Poncha Springs. There is not a lot of noise (compared to line 200), and the quadrature and in-phase lines are relatively close together. Both lines follow the same trend of highs and lows.

Figure 6.8 is the data collected along DC Line 200 in Poncha Springs. The range at which data was collected is much larger than the previous plot. This is due to the variability of the device when collecting data because the operator has to walk at a constant velocity, keeping the device level. If at any time this does not occur, spikes can be seen in the data. This is apparent in this data where there is huge jump in conductivity. Overall, the plot is noisier and has a lot more unexplainable spikes. The data collection for this line was a problem because of weather interruptions and a steep slope. DC resistivity only collected data for half of the line whereas EM-31 data was collected on the entire line. This creates a problem in correlating the data because it is not clearly defined where the lines began and ended for both data sets since they are in relation to distance and not specific flag numbers or coordinates in space.
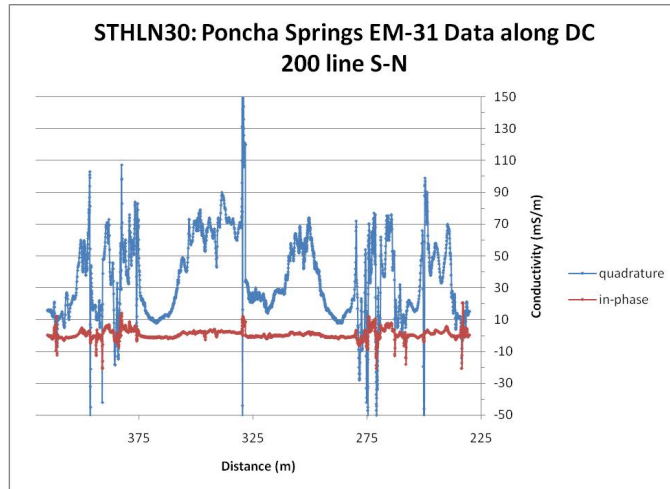
Figure 6.8: EM-31 data collected along DC 200 line in Poncha Springs

Figure 6.9: EM-31 data collected along CO-221

The EM-31 is a great device because it can be easily transported and is fairly easy to operate for long distances. Data in Figure 6.9 was collected about ten miles west of the previous data, along County Road 221 (where magnetic data was also acquired). This data will be incorporated with the processed magnetic data for further interpretation and discussion.

Correlation with DC Data

The EM-31 data collected along County Road 221 was compared with magnetic data collected with the cesium vapor magnetometer. These two data sets correlate quite nicely, indicating a change in conduc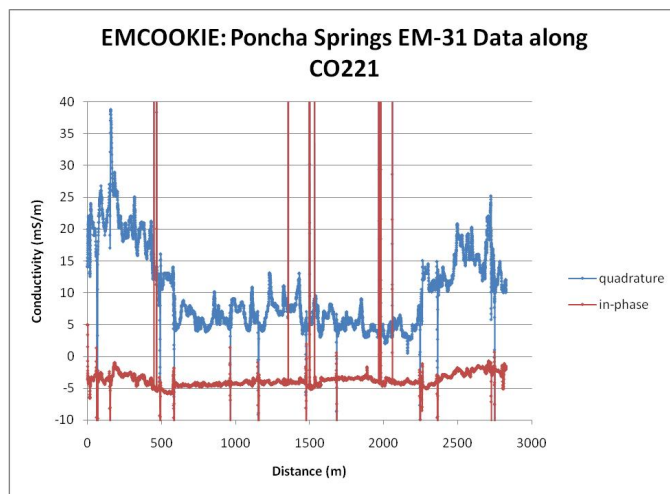tivity and susceptibility of the subsurface. Electromagnetics measures a change in conductivity whereas magnetics measures a change in magnetic susceptibility. Magnetic susceptibility is the physical property of how easily a material can be magnetized. The current induces a magnetic field into the subsurface anomaly, creating a change in magnetic susceptibility. The plots shown together are connected with a dotted green line indicating a rough interpretation of where the data points correlate.

Both plots in Figure 6.10 follow the same trend of increase and decrease curvature over the long distance of 2500 meters. The far left of the plots indicates a possible fault in the area. This is especially seen in the magnetic data where there is a large change in susceptibility. The same trend is noted in conductivity where there is a large, sudden spike in the electromagnetic data. Looking at a geological map of the area, there is some indication that County Road 221 runs along the boundary between two units. One unit appears to be the Dry Union, which has been found across the basin and the other unit seems to be localized to that area of Chaffee County but is not clearly defined on the geological map. This change in boundary between the units is seen on the plots where there is an increase and decrease, indicated by the dotted green line. The change in susceptibility and conductivity shows when data collected crossed the boundary, especially since the data followed a road that was not linear.
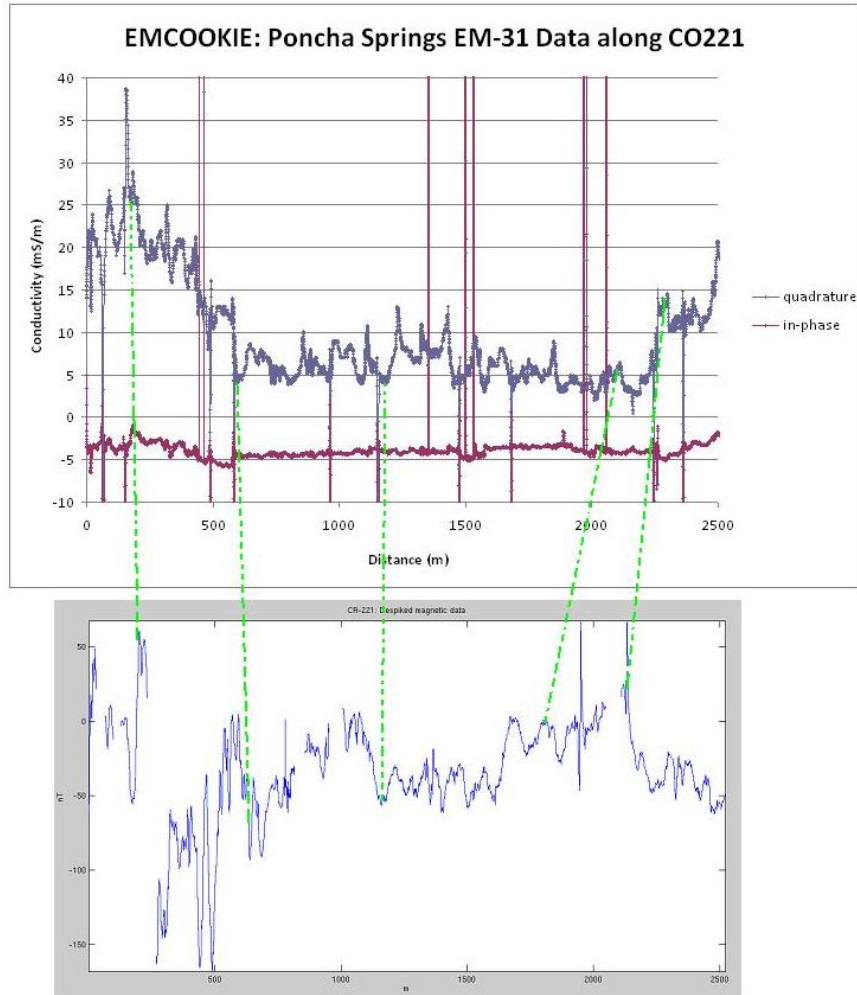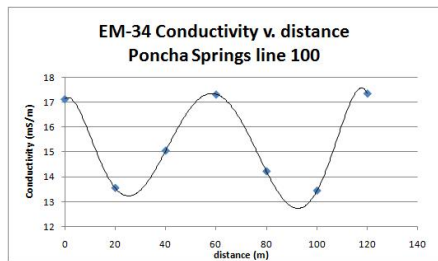
Figure 6.10: Correlation of data along CO-221

Acquisition Notes

The data collected along CR 221 was in two data files (EMCOOKIE and EMCOOKIE2), which were combined to form the EMCOOKIE plot above. The other data set is also in two files (STH3 and STHLN30) but they were not combined since after the first line the next was shifted and data was then collected in the opposite direction. The EMCOOKIE files both contain a 5pt linear smooth to QV1 because bad tuning of the instrument caused a loss of significant figures which required the data to round and thus resulted in jumps in the graph. The STH files also contained these jumps but since the overall anomaly trends were much larger the smoothing wasnt needed in those files. Additionally, there seemed to be a magnetic body around flag 106 on the DC line that could affect the STH data. On this same grid the 200 line was on a steep gradient, and a few times weather became inclement so the survey was stopped. One line here was lost completely due to user error.

6.4.2 EM-34

Plots

Unlike the EM-31 data, the EM-34 data was not saved as a .G34 file, but was entered by hand into an Excel spreadsheet and plotted there. This was because all the data points taken in the field were manually recorded. This was fairly easy to model because the EM-34 does not constantly record data, unlike the EM-31.

(a) **EM-34 survey of line 100.**   (b) **EM-34 survey of line 200.**
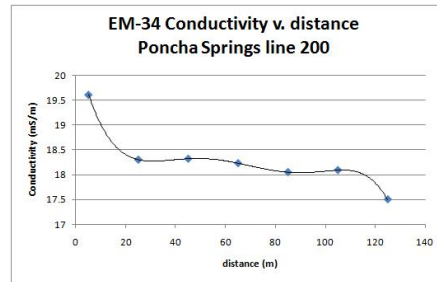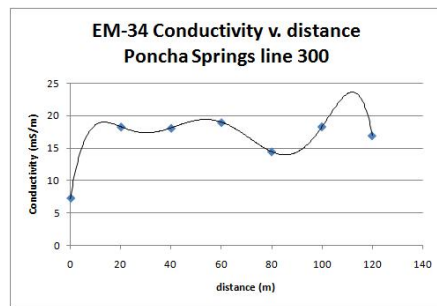
(c) **Em-34 survey of line 300.**

Figure 6.11: **EM-34 Surveys of Poncha Springs.**

Correlation with DC Data

Figure 6.12: Correlation of EM-34 and DC data along the 100 line.

Figure 6.13: Correlation of EM-34 and DC data along the 200 line.

Figure 6.14: Correlation of EM-34 and DC data along the 300 line.

Correlation of DC data with EM-34 data started with scaling both so that the distances matched up. When this was done trends within each data set matched up. As a note, the DC plots are in resistivity where the EM plots are in conductivity, so h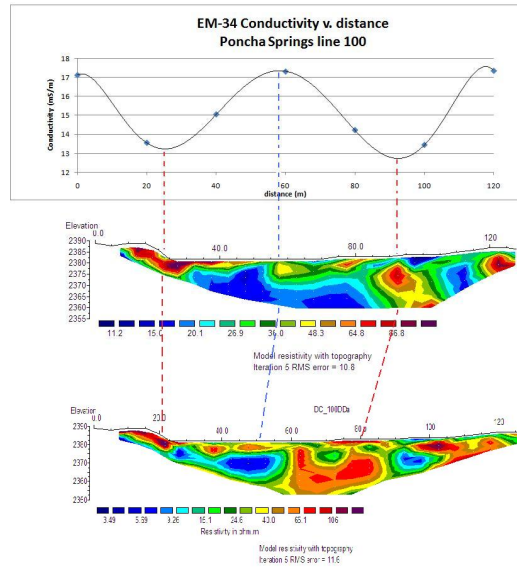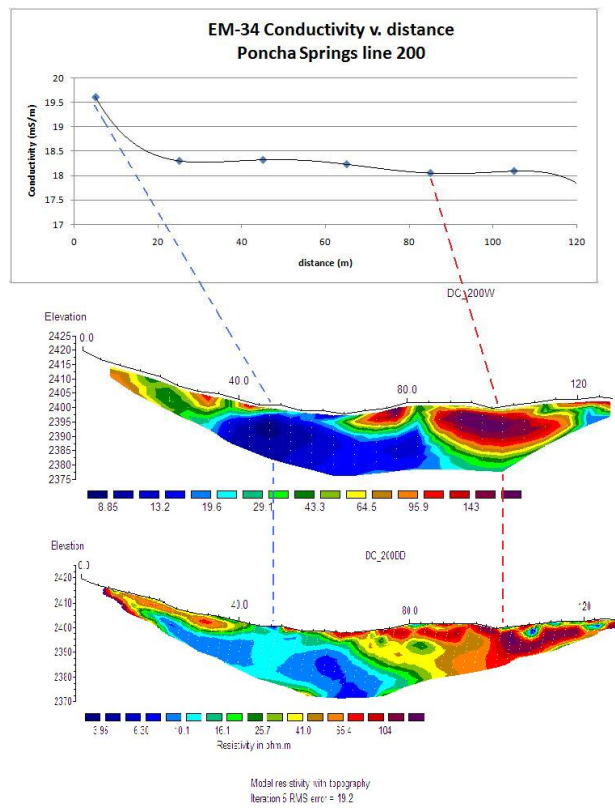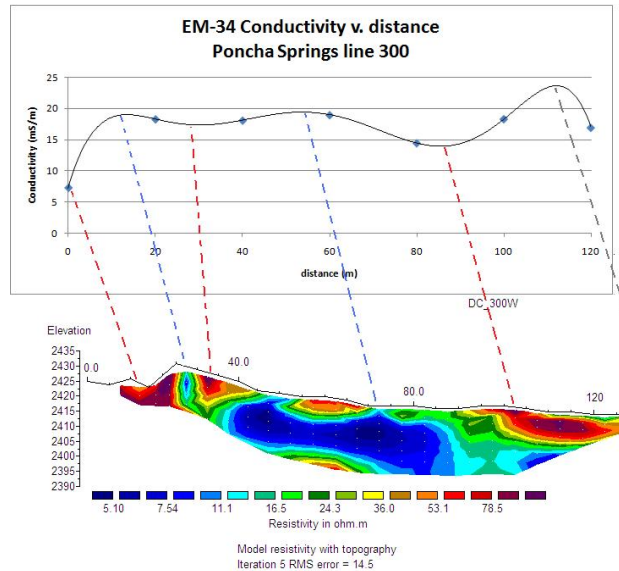ighs in one were correlated with lows in the other. Since red stood for high resistivity and blue for low resistivity, those colors were chosen to represent the correlations in the form of dotted lines connecting the plots. In line 100, theres an obvious low, high, low pattern to the EM data, which correlates to a red, blue, red pattern in the DC data. This matches up over the Wenner and dipole-dipole arrays, but is more obvious in the Wenner. In line 200 theres a high to low constantly down-sloping trend to the EM data, which correlates to a large blue to large red trend in the DC data. In this case the correlation is more obvious in the dipole-dipole over the Wenner array, because the highs and lows are spread out more towards the outer edges of the data set, just as the EM data is. Lastly, for the 300 line, there was only a Wenner array taken, so the correlation is just with that data. However, the match is very close with more correlation points than there were for the rest of the plots.

The trend in the EM data starts low, high, low, wide high, low, and then very tall high. This matches the DC data with only a slight offset to the left, with a red, blue, red, large blue, red. The last EM peak is believed to be off the end of the DC data set since there is a blue just visible off the bottom right corner of the plot (this was correlated with a gray line to show the ambiguity). In looking at the conductivity scales for the EM plots, line 300 has by far the largest and smallest extremes. Because the potential difference across this line is so large there is a good possibility for flowing water here. At the largest peak (around 115m at conductivity of around 24 mS/meter) there is likely a hot water source which is why the general trend of the conductivity of that area is fairly high. Also, looking at the EM data

86

plot for line 100, there is great potential difference again so theres a possibility that the flowing water is present under this line as well.

Acquisition Notes

First of all, the loops can either be laid horizontally on the ground or they can be rotated so as to be sitting on their sides (so an object through the loop would be parallel the ground). In this instance the loops were laid horizontally on the ground, so a vertical magnetic field is produced. Also, in looking at the plots the distances plotted are distances in meters from the 00 flag (i.e. 100, 200, and 300).

6.5   Conclusion

On CR-221 there is a fault toward the beginning of the line (furthest North), as was seen from the huge spike in conductivity (from th EM-31) and susceptibility (from the Cs-magnetometer). The drastic slope after that huge spike indicates a change in rock unit typically associated with faulting. The geology of the area also supports this conclusion. Other rises and falls in the data represent changes in rock unit, but are not as drastic as the change at the beginning of the line so are not assumed to be faults. When looking at the data taken along three lines near the Boy Scout camp (EM-31, EM-34, and DC), it is appropriate to interpret the change in conductivity toward the east end of the line as a potential hot water source. This is especially visible on line 300 of the EM-34 data, where theres a huge spike in conductivity.

One error that came into light during this survey was user error, particularly the user forgetting to hit enter after an EM-31 line and thus losing all that data. Some other errors that may have affected the readings were environmental, primarily inclement weather and steep hills. The weather stopped data collection for safety reasons and as a result, starting again resulted in differences that are not apparent at first glance. The steep hills may have affected the EM-31 data since the instrument must be kept parallel to the ground, proving to be difficult due to the terrain. The biggest source of error may be due to magnetic items around the instruments, which are very sensitive to both instruments but primarily the EM-31 because it is constantly recording data. As noted above, there was a magnetic body on the DC line that the EM-31 surveyed, so that may have affected the data. Also if metal flagging, cars (parked or moving), metal fences, etc. were in the area of the instruments and were not accounted for in the survey notes, those could create false anomalies in the data. This is particularly important for the EM-31 data taken along CR221.

Chapter 7

Magnetics

7.1 Method

The magnetic method is a very powerful tool in the geophysical world. The Earth generates a magnetic field caused by circulating currents in the hot metalic core. Any object or geologic mass that has a magnetic susceptibility will have a secondary magnetic field induced by the Earth's primary field. The response that a magnetometer will read from the secondary field can be representative of a number of objects (geology, faults, cars, electrical lines, houses, UXO, etc.).

A magnetometer will read the total magnetic field present at a given time. That includes both the primary magnetic field and any secondary response due to geology or cultural influence. In order to separate the primary and secondary resonses, a base station magnetometer will be set up during a survey so the Earth's magnetic field and the magnetic drift can be subtracted from the mangetic survey data. The magnetic drift is caused by solar flares and the Earth's changing position with respect to the sun. This will eliminate the Earth's overwhelming magnetic field($\approx 52,000nT$).

The equipment used to take magnetic readings in Chaffee County included the cesium vapor magnetometer and the proton free-precession magnetometer, which are both forms of resonance magnetometers (they measure the precession of particles in the Earth's ambient magnetic field to determine total magnetic field). The proton free-precession magnetometer consists of a protein-rich liquid in a container surrounded by a coil of wire connected to the measuring apparatus. The protons initially align mainly parallel to the Earth's magnetic field, and so the liquid obtains a net magnetic moment in the direction of that ambient field. At this point, the current in the loop is turned on briefly so that the protons realign with the newly generated field. Once the current is turned off, the protons precess around the ambient field and the frequency of that precession (Larmor frequency, which is proportional to the strength of the field) is measured. Please see Figure 7.3 for a visual description. There are two of the containers in the instrument, but in this particular survey we
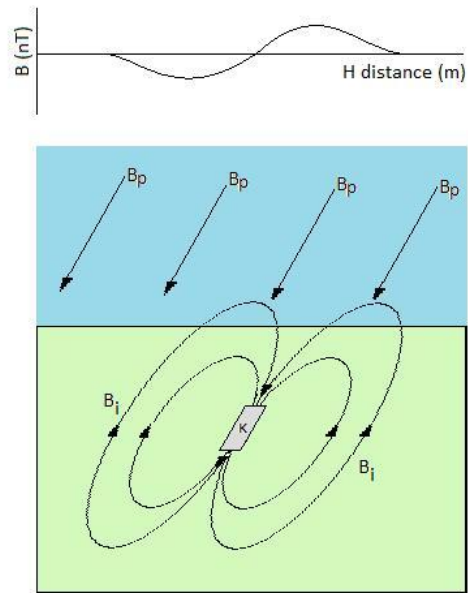
Figure 7.1: A metallic body in the Earth's primary magnetic field then induces its own magnetic field which produces the signature shown in the plot.

only paid attention to the top sensor because the noise would be too great in looking at both.

Figure 7.2: Setup of the base-station proton free-precession magnetometer

The cesium vapor magnetometer operates on a principle of optical pumping. A light bulb

with a cesium filament produces incident light that travels through a container of cesium vapor at a correct wavelength so the incident photons are absorbed by the vapor and so excite low energy level (A) electrons in the vapor to a higher energy level (B).
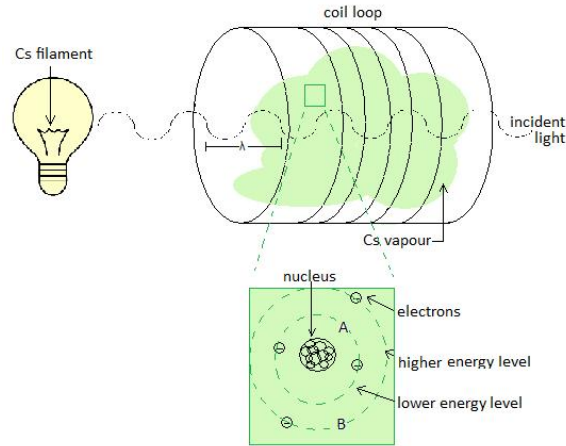

Figure 7.3: Inner workings of a cesium magnetometer

Since the light is circularly polarized, only certain low-energy electrons get excited, and then the unused photons travel through the vapor and are detected by a photocell at the other end as a higher intensity of light. The container that the vapor is in is wrapped in a wire coil through which a small AC current is passed. The frequency is then adjusted until the Larmor frequency of the vapor is reached, at which time the generated magnetic field takes some of the excited electrons back to their low-energy level A. Light intensity measurements here will decrease until the saturation level of the vapor is reached. The cesium vapor magnetometer can take almost-continuous measurements (around 10 per second) to an accuracy of $0.1nT$. [9]

Usually to correct for effects of topography upward or downward continuation would be applied (allowing for comparison to airborne surveys), but in this case a static shift correction was applied instead to do the same thing but in a more timely manner. A drift correction was also applied using the base station information and returns to the base station to take into account diurnal variation (change in the Earth's magnetic field over the course of the day).

7.2   Survey Design & Data Collection

In general, the two types of magnetometers were set up to record over the same time period. The proton free-precession magnetometer was employed as a stationary base-station and the

Figure 7.4: The cesium magnetometer used in the field by CSM student David Manthei

cesium vapor magnetometer was employed as a roving magnetometer. The base station took continuous readings throughout the survey so that the drift correction could be applied to remove the effects of diurnal variation from the data.

7.2.1 North Site – East West Deep Investigation Group

Magnetic data was taken adjacent to the East-West trending deep investigation line just north of Mount Princeton Hot Springs. The purpose of using magnetics is to aid gravity and seismic surveys in investigation of large-scale geologic features in the Upper Arkansas River Basin. The magnetics will primarily aid in finding faults. The magnetic data was aquired using the cesium magnetometer at a rate of $1Hz$ while walking at a constant pace. Because a GPS did not accompany the magnetometer, every $30m$ was marked, and readings were interpolated between the marks to account for change in walking pace.

7.2.2 North Site – Mr. Long's Field

Magnetic data was taken along the seismic lines that had a $10m$ spacing in Mr. Long's Field. The spacing of lines were $10m$ and a differential GPS was used to mark the position of each reading. This is shown in Figure 4 The data was taken over the course of two days and had three different data acquirers. The unit was placed on a backpack for ease of walking.

7.2.3 South Site – Poncha Springs Boy Scout Camp

Magnetic data along three lines (shown on map) were recorded and processed and then used in conjunction with known geological, fault, aeromagnetic, and topographic maps to help in the understanding of the Poncha Springs area. The first line ran North-South for $1.3km$

(with $50m$ spacing) starting on highway 285 directly south of Poncha Springs, approximately $100m$ North of the South Arkansas River bridge, crossed the bridge, and then went uphill on the dirt track towards the Boy Scout Camp. A second 550m line (with 50m spacing) was recorded starting at the camp and moving down the South side of the hill. The third line taken was a detailed $5m$ spacing line running $135m$ over the actual hot springs area on the hills directly above the camp. The two longer lines were taken to probe the overall geology and faulting of the area, whilst the detailed $5m$ spacing survey was taken to attempt to construct a subsurface model of how and why the hot springs are where they actually are.

7.3   Data Reduction

After the data has been collected in the field, it needs to be downloaded from the instruments. Downloading from the proton magnetometer and the cesium magnetometer is very easy and does not take a lot of time. The base station data (from the proton magnetometer) is downloaded in a format which is easily read but the downloaded data from the cesium magnetometer needs a little processing before it can be accessed easily. Processing magnetic data requires only a few steps. The first is to correct the data for magnetic drift. Because of the Earth's changing position with respect to the sun and the moon, the magnetic field changes throughout the day, the month, and the year. After drift correction, the data is plotted. From here, a number of steps can be applied, depending on each case. The next sections explain the processing done on each dataset.

7.3.1   Processing the Deep Magnetic Line Data

The deep magnetic line data was taken by three people during three separate days with a total of four datasets and three base station datasets. The first two datasets (taken in one day) were opened in MagMap2000 software, along with the base station data for that day. MagMap2000 easily corrects for drift using the base station data. The only step is to export the data while having the base station data open in the program as well. Exporting the data is also the easiest way to change the data format from binary, which is not easily accessed, to a *.dat file, which can be opened with a number of editing programs (such as Gvim, Excel, etc). When the data is exporting, MagMap2000 also gives the user the option of choosing what data is exported, including diurnal calculation, time stamps, the date, and GPS information (if there is any). In the case of the County Road 325 line magnetic data, MagMap2000 exported x and y position and the corrected magnetic reading. The same process was done to all datasets.
The next step is to view the different datasets all at once. For this, Matlab was used and code was written to perform the task. Each corrected dataset was loaded into Matlab and plotted. Because there were flags along the entire line, the data already contained the correct x positions in meters, starting at zero and ending close to 9500 m. Three different people took this data. Because of the different heights of these people, the sensors were at different

heights. Thus, the signal that was measured is larger for a shorter person or smaller for a taller person. The ideal method to resolve this issue is to use upward (or downward) continuation, a process that attenuates the signal. However, this is very time-consuming and mathematically complex. As an alternative, two of the datasets were statically shifted up or down. Recall that the first 2 datasets were taken by the same person. By shifting the datasets, the transition from one to another was smooth and thus the data did not have any major jumps.
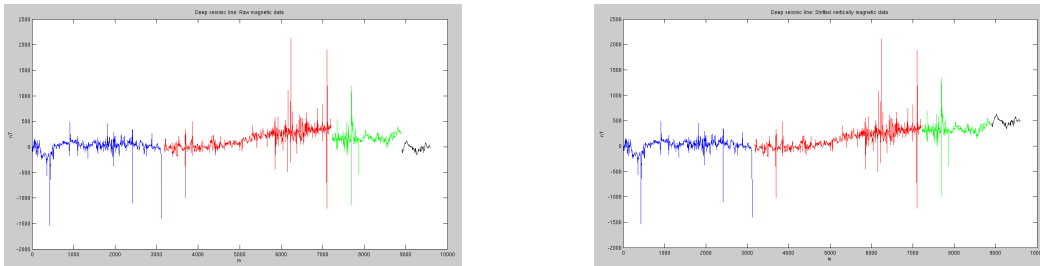
(a) Four raw, very noisy, magnetic datasets taken along the W-E deep line

(b) Four datasets statistically shifted to account for noise and height of the magnetometer.

Figure 7.5: Magnetic datasets along the W-E deep line

At this point, a wavelet filter was applied to the data. The wavelet filter needs certain parameters and the following were determined to be the best using a trial-and-error method:

- Symmlet

- 16

- 6

- Manual

- Soft

- 344.37

The program used for this was dnsgui.exe, written by a past graduate student at Colorado School of Mines. The wavelet filter follows the general trend of the data and ignores many of the large noise spikes. However, the filter does try to fit some of the noise, like that caused by the road around 3000 m and the house around 500 m. These spikes need to be removed manually before more processing can be done.

Removing the noise is done in Matlab. The field notes help to locate sources of human culture that have affected the data. By knowing the flag numbers as locations for the noise
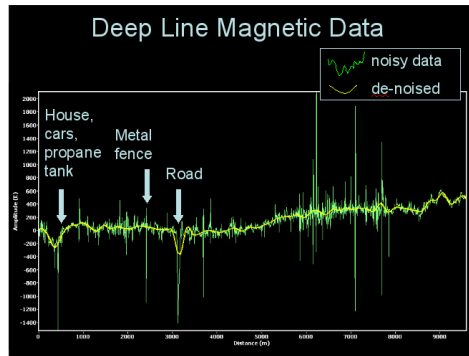
Figure 7.6: shifted mangetic data(green) and filtered data(yellow). The wavelet filter reduces noise.

and the flag spacing along the line, it is easy to calculate the distance at which the noise occurs. This distance can then be found on a plot of the data and a decision can be made whether or not the spike should be removed. This highly depends on whether the wavelet filter ignored the spike or tried to fit the noise. Using this method, four spikes were chosen to remove from the data. Removing the noise was simply done by cutting those sections of data. After the noise has been cut, the four different datasets were merged into one dataset, and thus, one data file, which allows for easier access and plotting.

The next step is to redo the wavelet filter, now on the merged dataset. The wavelet filter should now just interpolate between the deleted noisy data. The parameters found to be the best fitting are the following:

- Symmlet

- 18

- 6

- Manual

- Soft

- 355.68

Again, the program used was dnsgui.exe. These parameters allows for the wavelet filter to follow the general trends in the data but not fit the noise. The filtered data can now be used for inversion.

The next step is to prepare the data for inversion. For Fred Burkman's inversion program, the data can have a maximum of 100 points and the points need to be equally gridded, meaning that the distance between two points has to be constant. Currently, the points are not equally gridded because data was taken at a certain time interval. To equally
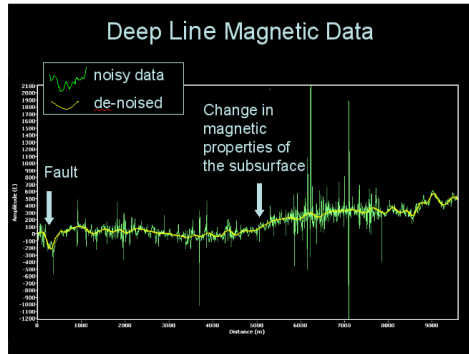
Figure 7.7: Shifted magnetic data (green) with noise spikes removed. The yellow line represents data following the general trend, while ignoring noisy spikes.

grid the data, interpolation was done in Matlab. By using interpolation, exactly a 100 equally-spaced data points could be extracted. After this was done, it was easy to import the GPS information from the deep line. The elevation measurements also needed to be interpolated so that the 100 equally-spaced data points each had an accurate elevation value. The final data file for Burkman's inversion program contained position information, elevation information, and the magnetic data. Because Burkman's inversion program proved to be tricky to work with, GM-SYS was attempted as an alternative. This program can take up to 16,000 points but because of simplicity, the 100 equally-spaced data points were also used with this program. The next section will talk about the inversion process.

7.3.2 Inversion of the Deep Magnetic Line Data

The program used to create a 2D geologic model beneath the line was GM-SYS. The first step in order to invert the magnetic data from the deep line was to create a geologic model. To make this easier, the depth-migrated seismic profile from the deep line was imported into the program. Using the reflectors from the image, contacts between the major geologic units were drawn. The next step was to assign magnetic susceptibility values. At this point, the observed magnetic data and gravity data were imported into the program. Magnetic susceptibility values and density values were assigned to the different blocks in the geologic model. These values were chosen from published studies of the local geology, as well as published tables of density and susceptibility value ranges for common geologic units. [9] After that point, it was possible to see how well the response of the geologic model compared to the actual data. In order to increase the fit between the model response and the actual data, the model's geometry and its susceptibility and density values were adjusted to move the model response closer to the observed data. This process required continual adjustment and was very time-consuming. The final resulting geologic model shows the major fault in the west, the Dry Union formation, volcanic layers, basin fill, a fault near the east, the Mount Princeton batholith, and the basement.
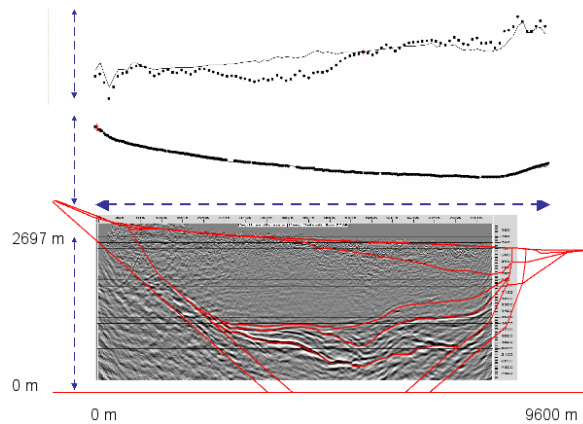
95

Figure 7.8: Overlay of deep-magnetic data and deep-seismic data, showing correlation between different methods.

The response from the geologic model is close to the actual gravity data, but the magnetic data was harder to fit and the response and the actual data are not so close. If more time was available, the model could be made to fit the magnetic data. The software can perform inversions based on physical properties and unit geometry. Inversion will only produce realistic results for a well-defined geologic model. The creation of the model to fit the observed data and known geologic and physical constraints did not leave enough time to perform more than a few brief attempts at inversion. Unfortunately none of these attempts produced realistic results.

7.3.3 Processing Mr. Long's Field Data

Only three lines from the Mr. Long's Field data were processed. These lines match the lines done with the gravimeter. This was done because inversion can be done simultaneously using gravity and magnetic data.
MagMap2000 was used to open the base station data file and the first dataset from May 20, 2009. The other two datasets include magnetic data from Bill's property to the west and the 1.2 km line on which DC data was also taken. These data files were not processed due to time constraints. In Magmap2000, the first dataset, which includes data on lines 1000 to 4200 from the Mr. Long's Field, was plotted. The 2D contour map contained a lot of heading errors, which was another reason to just pick a few lines instead of processing the entire field. Using MagMap2000, all lines were deleted except lines 3000, 3400, and 3800. These lines were exported as a *.dat file. Parameters that were chosen to export in this file include GPS information and corrected magnetic measurements.
From here, Matlab was used to further process the data. To start, the data file was loaded
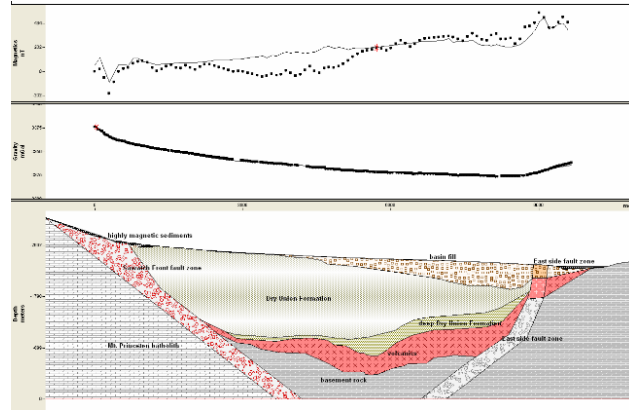
Figure 7.9: Inversion of deep-magnetic data showing how the basin has been filled in by various types of sediments.

Geologic unit	Density [g/cc]	Susceptibility [SI]
Highly magnetic sediments	1.80	0.019
Basin fill	1.55	0.017
Mt. Princeton batholith	2.55	0.020
Sawatch Front fault zone	1.80	0.001
Dry Union Formation	2.10	0.005
Deep Dry Union Formation	2.30	0.010
Volcanics	2.60	0.080
Basement rock	2.70	0.022
East side fault zone [basin fill]	1.50	0.017
East side fault zone [volcanics]	2.40	0.060
East side fault zone [deep]	2.10	0.020

Table 7.1: Density and magnetic susceptibility values assigned to each geologic unit in the model.

97

Figure 7.10: Aerial view of deep-magnetic line in the Upper Arkansas Basin.

Figure 7.11: Inversion of deep-magnetic data showing how the basin has been filled in by various types of sediments after density and susceptibility changes.

Geologic unit	Density [g/cc]	Susceptibility [SI]
Highly magnetic sediments	1.90	0.0190
Basin fill	1.55	0.0180
Mt. Princeton batholith	2.55	0.0200
Sawatch Front fault zone	1.80	0.0010
Dry Union Formation	2.10	0.0050
Deep Dry Union Formation	2.30	0.0100
Volcanics	2.60	0.0800
Basement rock	2.70	0.0220
East side fault zone [basin fill]	1.50	0.0140
East side fault zone [volcanics]	2.40	0.0700
East side fault zone [deep]	2.10	0.0185

Table 7.2: Density and magnetic susceptibility values assigned to each geologic unit in the model.

and the three lines were plotted and the data file was separated into three different sections, based on each line. This allows for distinguishing between lines in Matlab such that each line can be treated differently. For each line, interpolation was used to calculate 100 equally-spaced data points with GPS information. This was done in the same way as for the deep magnetic line. The information for each line was then written to a file. For each magnetic measurement, there was also GPS information in these files. These three files were then ready to be used in Fred Burkman's inversion program.
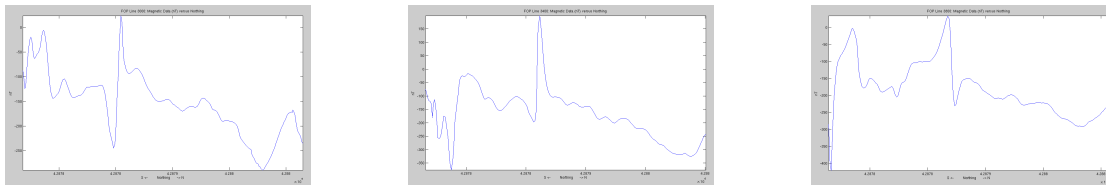
(a) Magnetic data from line 3000 in the Mr. Long's Field. The large dipole in the center is the response of a pipe near the surface.

(b) Magnetic data from line 3400 in the Mr. Long's Field. The large dipole in the center is the response of a pipe near the surface

(c) Magnetic data from line 3800 in the Mr. Long's Field. The large dipole in the center is the response of a pipe near the surface.

Figure 7.12: Magnetic Data from Mr. Long's Field

Because Burkman's inversion program can be slow and tricky to use, the data from the three lines was also prepared to be used in the GM-SYS inversion program. This program only takes distance and does not need GPS information. Because the three lines from Mr. Long's Field basically run north-south, the northing information was used. The smallest value was set to 0 and the other values were determined by subtracting the smallest value

from each point. Another issue noticed were "loops" in the data. The data, when connected as a line, would sometimes form a loop. This may be due to walking around a tree or other obstacle in the field. However, these loops give errors when entering the data into the inversion program. They were cut in the same manner noisy spikes were cut. The code was also used to pick 35 equally-spaced points from the data using interpolation. These points can be used in the lab version of the GM-SYS software. The three data files include distance, elevation, data, and elevation plus the height of the magnetometer. These data files can now be used in the GM-SYS inversion program. This will be discussed in the next section.

7.3.4   Inversion of Mr. Long's Field Data

Inversion was first done on line 3000 from Mr. Long's Field. A quick look at a seismic line from the same field yielded an initial idea for the geologic model. Ideas from the interpretation from the DC data also provided input for the geologic model. The geologic model used consists of a top layer of sedimentary deposits with a high magnetic susceptibility. Below that is the basement rock with a fairly low magnetic susceptibility. The contact between the sedimentary deposits and the basement undulates along the line. This is a more realistic geologic setting than a straight contact. To the north of the section is a eroded moraine, which consists of glacial till deposits.// The lab version of GM-SYS was used to do the inversion. The data was imported, along with the elevation profile. The geologic model was tweaked to allow for the greatest fit of the data. Although the fit is not perfect, the general trends in the data are followed and the model is geologically feasible as well as simple. The proposed fault near the glacial till deposit makes sense when thinking about the overall geologic setting. The susceptibility values assigned to the different units in the geologic model were found in the Reynolds book [9]. The book gave ranges for the susceptibility values and an initial value within the range was chosen. These values were altered as was needed to make the model fit the data. The susceptibility values (SI units) are the following:

- Sedimentary layer: 0.00098

- Basement: 0.02698

- Glacial Till: 0.000013

The next step was to invert the magnetic data from line 3400. Because there is also gravity data collected along this line, a dual inversion was attempted. Again, GM-SYS was used to import both the gravity and the magnetic data. Because the magnetic data used its own GPS information that was collected simultaneously with the magnetic data and the gravity data used the DGPS information, the elevation had a significant discrepancy. Fortunately, the discrepancy was constant along the entire line and the elevations of the gravity stations could be vertically shifted up.
The next step was to create a geologic model. To start, the same idea was used as for the inversion of the magnetic data from line 3000. This proved to be very close to fit the gravity
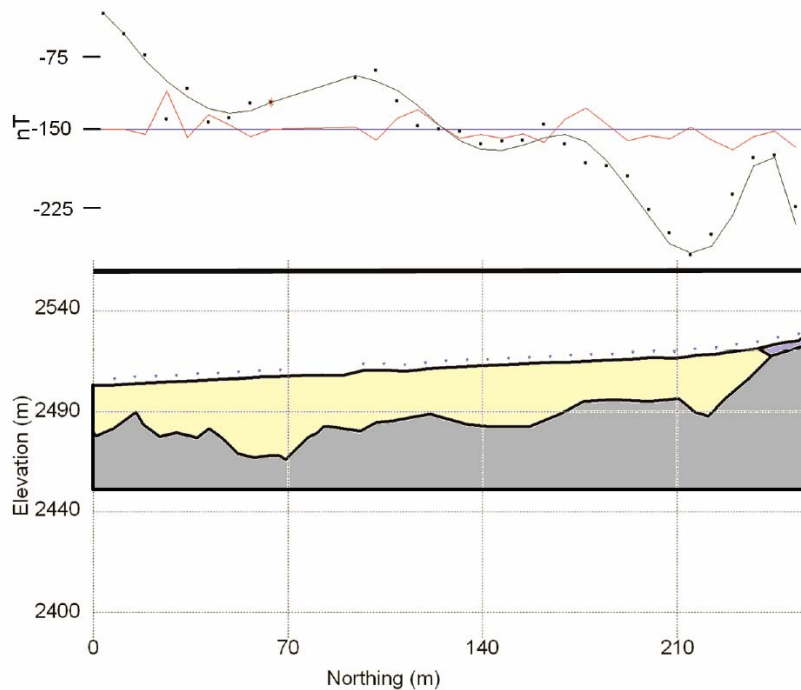
Figure 7.13: (a)Magnetic data and the fit created by the model. Shows error between actual data and response to geologic model. (b) Geology that models the data

and magnetic data from line 3400. The susceptibility values differ somewhat but this may be due to differing sediments and changing fracturing within the subsurface. The geologic model consists of a sedimentary top layer that extends about 45 meters below the surface. Below that is a highly fractured basement rock. To the north of the model is a zone of glacial till.

7.3.5   Processing CR-221 Data

Near Poncha Springs, only one magnetic survey was processed by students. This was along CR-221, from flag 1 to 121. This survey was done on May 16, 2009 but the base station data was not desirable. Also, the proton magnetometer and the cesium magnetometer were not synchronized for time. This could have been corrected for but it was unknown at what time the survey was started or ended. Thus, this dataset could not be used. Luckily, because the base station data was not good, the survey was redone on May 17, 2009.

MagMap2000 was used to open the base station file and datasets 4 and 5. When first looking at the base station, there are several huge spikes that were obviously not caused by the Earth's drifting magnetic field. These were cut out using MagMap2000's range despike function. This function is easy to use: a section that needs to be removed is highlighted
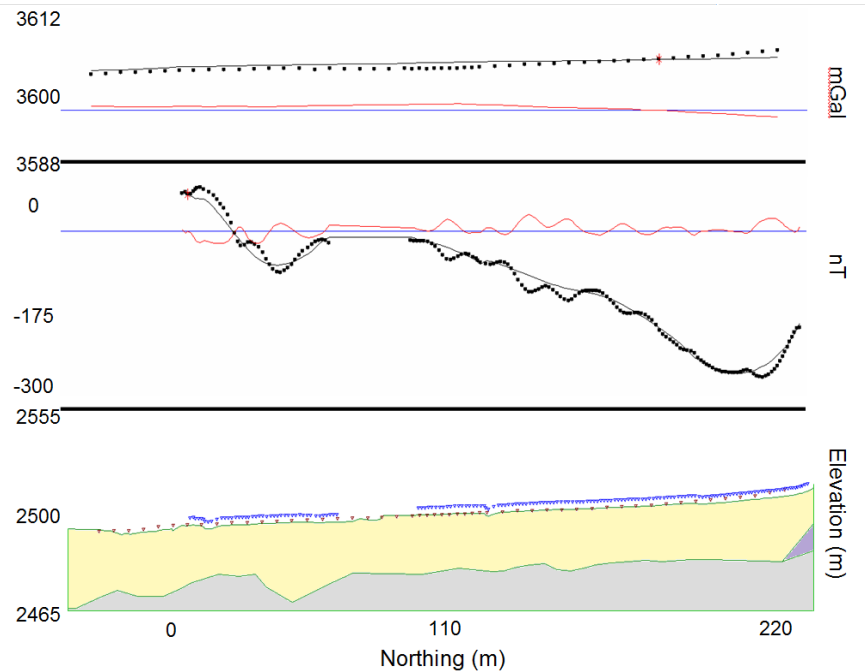
Figure 7.14: (a)Gravity data, calculated resonse, and the error. (b) Magnetic data, the calculated resonse, and the error. (c) Geologic model, which is very similar to the model from the line 3000.

and the function is applied. After this, the two datasets were exported, which automatically corrected for magnetic drift.

After the datasets were exported, Matlab was used to further process the data. The first step was to view the data and determine which sections needed to be cut due to high spikes of noise. This could also have been done in MagMap2000 but it was found that MagMap2000 did not remove enough of the outer sides of the spikes to be considered usable in inversion. It is best to remove all of the spike, even if some of the actual data is removed as well. After noise was removed from both datasets, the two datasets were combined into one. No static shifts were needed in this case because the data was taken by the same person, and thus the height was constant.

The next step was to integrate GPS information with the magnetic data. A few GPS points were deleted because they were outliers. Because there may not be an actual point of magnetic data at each flag, the GPS information was interpolated to match the locations of the magnetic data. The data, now with northing, easting, and elevation was written to a data file. The file could now be used for inversion. It was later discovered that the file for inversion needs to have distance and not GPS information. Matlab was again used to interpolate distance points for the magnetic data, as well as elevation. This file, in the

102
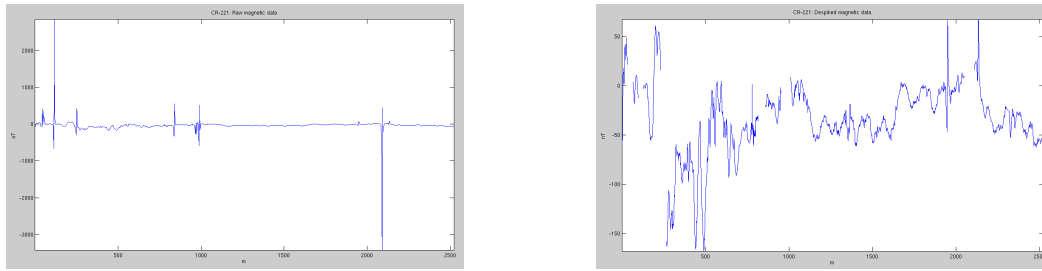
(a) Magnetic data from CR-221. Large spikes are from cultural artifacts

(b) Magnetic data from CR-221 despiked

Figure 7.15: Magnetic data from CR-221

correct format for inversion, includes distance, elevation, magnetic data, and elevation plus the height of the magnetometer. The inversion will be discussed in the next section.

7.3.6 Inversion of the CR-221 Data

Inversion of the magnetic data was attempted along with the gravity data for CR-221. However, due to time constraints and issues with the susceptibility values, the geologic model did not fit the magnetic data very well. It is known that there is a ridge close to the magnetic data line which will influence the data. Other geologic features will also influence the data, making this a 3D problem. It would be very difficult to model a 3D geologic problem as a 2D line. The gravity response of the geologic model fits the actual gravity very well.

7.4 Error Analysis

7.4.1 Deep Magnetic Line Error Analysis

There may be multiple sources of error in the magnetic data collected along the deep line. Because data was first taken on the mountain to the west, it was difficult to keep the sensor at the same height from the ground. This would cause the signal to be amplified or attenuated and would show unrealistic highs or lows in the data. Another issue can be caused by soils at the surface that have a high magnetic susceptibility. These soils cause high spikes in the data, which can overwhelm a signal from the deeper geology. Another source of error was the abundance of human infrastructure encountered along the line. Because the seismic crew was also there while magnetic data was being collected, noise was collected as data from geophones, cables, and electric boxes. Noise was also collected from metal fences, drainage pipes, electrical wires, and more. The noise created spikes in the data and many of them were ignored when the wavelet filter was applied. However, the filtering program may have

somewhat fitted the noisy data, which would give make it harder for a geologic model to fit the data. The data was taken by three different individuals, which allows for a difference in how the data was taken. The height of each individual matters the most as this changes the strength of the signal measured. The data had to be statically shifted to compensate for this but it is unsure whether the data was shifted correctly. This may be another reason why the response from the geologic model and the actual data are off in certain areas. The error from the inversion shows the difference between the response of the geologic model and the actual data. The response will never be exactly like the actual data because noise should be accounted for and should not be fitted. However, in some areas, the error is fairly high. One answer that explains the error is that there is a low magnetic anomaly to the north of the line. Because of this anomaly, the 2D assumption is violated and may become impossible to create a 2D geologic model that will fit that low magnetic response.

7.4.2   Mr. Long's Field Error Analysis

There are various potential sources of error while collecting the magnetic data on the Mr. Long's Field. First, there were many natural obstacles in the field, such as trees and large areas with yucca plants. These had to be walked around with the magnetometer, causing the line to no longer be straight. This could have very well caused heading errors in the data. Another source of error may be due to other geophysical methods taking data in the field. There may have been cables, geophones, and electrodes along the lines that magnetic data was taken on. It is very likely that there were GPS errors, especially since it is known that the elevations between the gravity and the magnetic had a discrepancy. The discrepancy was constant along the line so it could be easily fixed. However, the result was not perfect, meaning that there were errors in either the magnetic data's GPS information or the DGPS information. Inversion of the two lines from the Mr. Long's Field definitely includes some error. It is almost impossible to fit the data exactly. To go even further, it is unwise to fit the data exactly because the noise would also have been fitted. The red line on Figure 7.13 and 7.14 shows the error from the inversion.

7.4.3   Poncha Springs Error Analysis

There are many possible sources of error in the magnetic data collected along CR-221. There were distinct noise spikes in the initial data due to human infrastructure. Also, there were noise spikes in the base station data. This alone could cause numerous errors in the data because the data depends on the base station for drift corrections. Other human artifacts, such as pipes, electrical lines, and drainage ditches, will create noise in the data. It was very likely that there are effects of this in the data because the data was taken along a road. There were also many issues with the GPS information, especially the elevation. The GPS information was taken with a handheld, which automatically has a great amount of error. Because the elevation had too much error in it, a digital elevation model was used instead.

7.5   Interpretation

7.5.1   Deep Magnetic Line Interpretation

The geologic model created in GM-SYS for the deep magnetic line largely agrees with the geologic cross section for the area. The geologic model consists of eleven different blocks: highly magnetic sediments, basin fill, Mount Princeton batholith, Sawatch Front fault zone, Dry Union formation, deep Dry Union formation, volcanics, basement rock, east side fault zone with basin fill, east side fault zone with volcanics, and the east side deep fault zone.

An initial model used major reflectors within the seismic profile as boundaries for the major geologic units, and while this provided an excellent fit to the observed gravity data, it was not possible to create a reasonable model that also fit the magnetic data. There are several factors that are believed to be responsible for this discrepancy. Observation of the raw magnetic data indicate highly susceptible deposits at the surface, which can mask the magnetic signature of deeper features. An aeromagnetic survey of the area show a significant low adjacent to the line, and it is not possible to account for this anomaly within a 2D model. Another consideration taken into account is that it is highly likely that the depth migration performed on the seismic profile produced a vertically exaggerated image. The final model attempted to account for this by decreasing depth to deeper contacts, which resulted in thinner units at increased depth and a simplified geometry. As this vertically shifted model created a better fit to the observed magnetic data, it was felt that the assumption of vertical exaggeration in the seismic profile is correct. The final 2D model represents a reasonable integrated interpretation of the subsurface geology, although it is relatively simple and other interpretations are possible.

7.5.2   Mr. Long's Field Interpretation

The geologic models created in GM-SYS for the Mr. Long's Field show a fairly simple subsurface. There are three main bodies for each line. The susceptibility values for the layers differ between line 3000 and line 3400 but this can easily be due flow of water, different fracturing patterns, and different fluvial deposits. The geologic models show a sedimentary layer on top of a shallow basement. The basement is proposed to be between 45 m to 60 m below the surface. There may be several different layers within the sedimentary deposits. The calculated magnetic data for both lines does not fit every trend in the data. More detail within the sedimentary layers and possibly fracturing within the basement can result in better fitting of the data. Overall, there are three different bodies that allow for the magnetic and the gravity data.

7.5.3   Poncha Springs Interpretation

Poncha Springs Magnetic Data from CR-221

Because the inversion could not be finished for the magnetic data along CR-221, an indepth interpretation can not be made. It is known that there is a fault in the north-east and the

basement is fairly shallow. There is also a response from a nearby ridge in the center of data which could not be modeled but can clearly be seen in the data. The basin on either side of the high response due to the ridge is presumed to be of the same material.

Poncha Springs Magnetic Data from Fred Burkman

Magnetic data along three lines (shown on map) were recorded and processed and then used in conjunction with known geological, fault, aeromagnetic and topographic maps to help in the understanding of the Poncha Springs area.

The first line ran North-South for 1.3km (with 50m spacing) starting on highway 285 directly south of Poncha Springs approximately 100m North of the South Arkansas River bridge, crossed the bridge, and then went uphill on the dirt track towards the Boy Scout Camp. A second 550m line (with 50m spacing) was recorded starting at the camp and moving down the South side of the hill. The third line taken was a detailed 5m spacing line running 135m over the actual hot springs area on the hills directly above the camp. The two longer lines were taken to probe the overall geology and faulting of the area, whilst the detailed 5m spacing survey was taken to attempt to construct a subsurface model of how and why the hot Springs are where they actually are.

Figure 7.16: Magnetic data for Hwy285 & Poncha Hot Springs Road

Line one shows a general increase in the magnetic field from North to South, which corresponds to the general increase in terrain elevation, and also correlates to the data trends

shown in the USGS aeromagnetic survey, although the actual numerical values are different. Data are not recorded at points 50 and $100m$ because of crossing the bridge. At $250m$ and at $500m$ along the line, there are clear anomalies in the data. These anomalies in the magnetic field could correspond to either a fault or a change in rock lithology. If all the data are considered, and nearby faulting shown on the 1956 USGS survey map is extended to the survey region, two possible fault lines can be drawn onto the maps at the locations where the anomalies are seen. This indicates the presence of at least two faults in the area. The possible faulting in the area is not shown on the aeromagnetic data map, as it is taken from relatively high above the ground, leading to low resolution data showing only general trends, and the $50nT$ anomalies at the possible fault boundaries are too small to show on the survey.

The second line shows a generally decreasing magnetic field from North to South. This anomaly again follows the general trend shown by the aeromagnetic survey data, indicating accuracy within the data taken and previously recorded measurements.

The closely-spaced line was taken directly over the area where the hot springs are on the surface in the hope of finding anomalies to help indicate the positioning and directions of faults in the subsurface through which the water maybe reaching the surface.
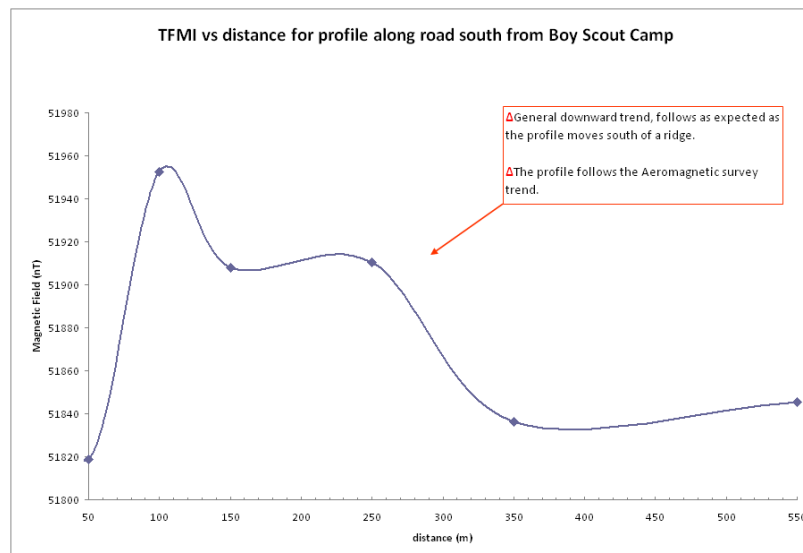
Figure 7.17: Magnetic data for road south of the Boy Scout Camp - Poncha Springs

The detailed magnetic line running for 135m directly across the Poncha Hot Spring is featureless except for a large 30m wide anomaly from 45-75m. Two possible interpretations
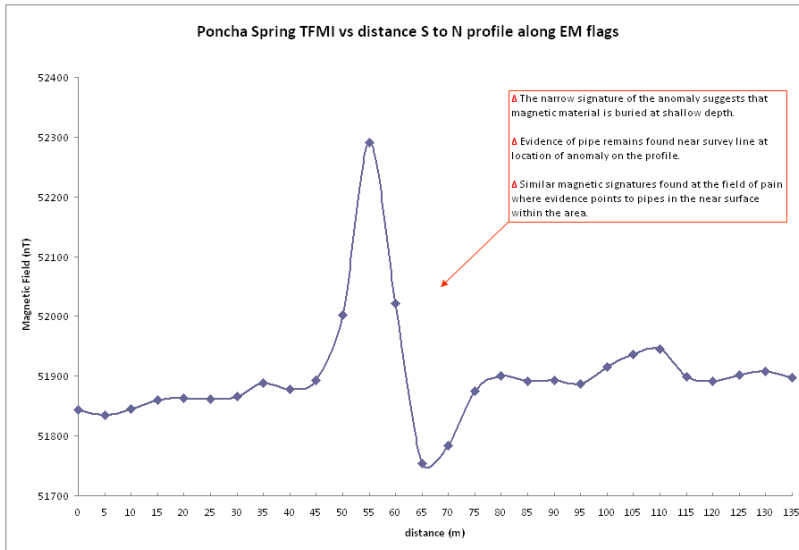
Figure 7.18: Poncha Springs magnetic data along EM flags

for this anomaly are faulting or a pipe running across the survey line. Both of these were modeled, and it was found that the pipe model gave an anomaly of approximately the correct width although the modeled anomaly was symmetric whilst the data is not. The fault anomaly, although it matched the anomaly shape, had a width of over 150m, over five times the actual anomaly shown in the data. This initial evidence suggests that the anomaly is more likely to be a pipe than a fault. Further evidence indicating that the anomaly is likely to be a pipe are fragments of rusted pipe found along the survey line, and similarities in the shape and width of the magnetic response at Poncha Springs compared with the response from a known pipe location in the Mr. Long's Field in the North site. A final piece of evidence against the anomaly relating to a fault is the fact that, in order to achieve a narrow anomaly, the fault would have to be sitting at the surface of the ground, and there was no evidence for this observed visually in the field at the time of surveying.

7.6   Conclusion

Concerning the line along CR-325, as the final 2D model is based upon the assumption that the depth migrated seismic profile is vertically exaggerated, and this model produces a better fit to the observed data, it is recommended that the seismic profile be reprocessed with the model parameters taken into account. An improved seismic profile could then be used to

further constrain geologic unit geometry, which could then in turn be integrated to produce a more refined model. The Field of Pain magnetic data resulted in 2 geologic models, one for line 3000 and one for line 3400. These geologic model both show a shallow basement with glacial till deposits to the north and a sedimentary layer above the basement. The Poncha Springs magnetic data does not have a clear interpretation but is known that there is at least one fault and possibly more. There seemed to be a lot of noise in the data which made it more difficult to model. Overall, the magnetic data provided additional information about the Upper Arkansas Basin. Combined with the data sets from other methods, the magnetic data will provide more confidence in the final interpretation

Chapter 8

DC

8.1   Introduction

The electrical conductivity of the rock corresponds to the ease with which it conducts electrical currents. Resistivity is the inverse of the electrical conductivity. The DC resistivity method is a geophysical technique aimed at providing an image of the distribution of the electrical conductivity of the ground. DC Resistivity surveys have a wide variety of geophysical applications. They are used in:

1. Locating ground water sources

2. Monitoring contamination of ground water

3. Locating subsurface cavities, faults, fissures, mineshafts and permafrost.

4. Down hole logging of wells

(Reynolds, 1997)

   The objective of conducting DC Resistivity surveys at Mt Princeton and Poncha Springs was to:

1. Image the shear zone and map its extent- especially in the Mt Princeton- Chalk Creek Valley area. This shear zone consists of fractured basement granitic rock which acts as a conduit for hot water to move towards the surface.

2. Identify areas where the geothermal water in the subsurface is flowing upwards.

   The DC resistivity method measures the apparent resistivity of the subsurface rocks. The method works by injecting a known current into the ground via two electrodes and the resultant voltage drop between two potential electrodes is measured. From this, an estimate of the apparent resistivity (an average of the resistivities in subsurface layers) of the rocks can be derived.

Resistivity, ρ is an intrinsic property of the rock. It can be defined by:

$$R = \frac{\rho * L}{A} \tag{8.1}$$

Where R is the resistance of the material/rock, L is the length of the material and A is the cross sectional area of the material. By Ohms law,

$$V = IRg \tag{8.2}$$

Where V is the potential difference, I is the current, g is a geometrical factor depending on the position of the electrodes, and R is the resistance of the rock. It is the resistance, R that is measured in the field and depending on the electrode configuration, resistivity can be derived.

Resistivity, ρ measured in ohm m = $\frac{1}{\sigma}$ where σ is the conductivity of a material. The conductivity of a rock depends on the porosity, water saturation, water salinity, clay content and temperature of the rock. With increasing water content, salinity, clay content and temperature, the resistivity of the rock decreases. Sedimentary rocks can have a wide range of resistivities but where they are porous or filled with water, their resistivities are low (¡100 ohm m). Granite has a high resistivity of around 10 000 ohm m, while fractured granite and altered granite can have a resistivity of 100 ohm m. It is for this reason DC Resistivity is extremely useful in identification of upwelling geothermal waters and shear zones of fractured granite because these will have anomalously low resistivities compared to the surrounding granitic basement rock in this area.

8.2 Field Procedure and Survey Design

The equipment needed to do a DC resistivity survey are electrodes, cables, reels, a power source as well as a meter to measure the current and voltage. The cable used in this survey consists of an array of 64 steel electrodes with takeouts of 5 and 20 meters. These electrodes (stainless steel) were hammered into the soil ensuring good electrical contact with the ground. Once the electrodes were hammered in, water was poured around and near the electrodes so as to improve current flow and reduce electrode's contact resistance.

For the surveys done at Mount Princeton, a handheld GPS system with an altimeter was also carried along to record the elevations at each point. The same was done for surveys at Poncha Springs except for line 1000, 100, 200 and 300 where a DGPS system was used.

There are different types of electrode configurations or spreads that can be used for a DC survey but for this survey only Wenner and Dipole-Dipole arrays have been used in the present study.

DC surveys were done at two locations:

1. Mount Princeton

   - Mainly Wenner arrays
   - ABEM system
   - Battery: Autolite 84
   - Power frequency: 60Hz
   - Cable: Schill IT 380.Rm
   - Connector from electrode: Copper Wire
   - Acquisition delay: 0.3sec, acquisition time: 0.3sec, total cycle time: 3sec
   - 64 electrodes (with 5m electrode spacing)
   - Five 2D lines (FOP30, ULT01, P1, ULT02 and YBR)
   - One 3D survey (250 x 300m)

2. Poncha Springs

   - Super-sting system
   - Wenner and Dipole-dipole
   - 7 lines:
     - Line 0 (20m electrode spacing)
     - Line 0E (20m electrode spacing)
     - Line 100A (5m electrode spacing)
     - Line 100B (5m electrode spacing
     - Line 200 (5m electrode spacing)
     - Line 300 (5m electrode spacing)
     - Line 1000 (20m electrode spacing)
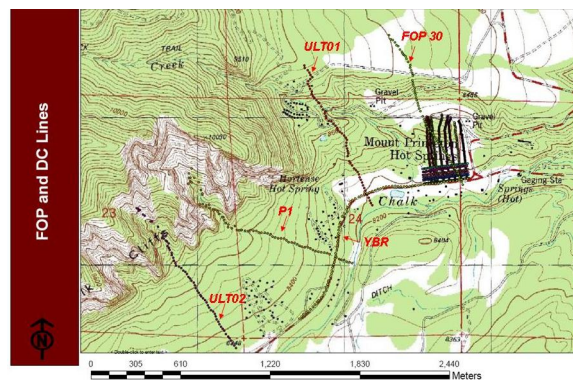
Figure 8.1: Map of survey at Mount Princeton
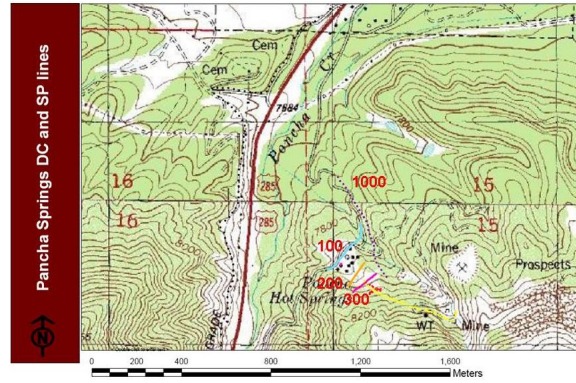
Figure 8.2: Map of survey at Poncha Springs

Figure 8.3 below show the configurations for Wenner and Dipole-dipole arrays.

In the Wenner array, the electrodes have uniform spacing. For dipole-dipole array, a distance is chosen between the two current electrodes and the two potential electrodes. Wenner array has a good signal-to-noise ratio compared to the dipole-dipole array. It would be ideal to combine Wenner and Dipole-dipole array because Wenner array is sensitive to horizontal structures while the dipole-dipole array is sensitive to vertical structures.
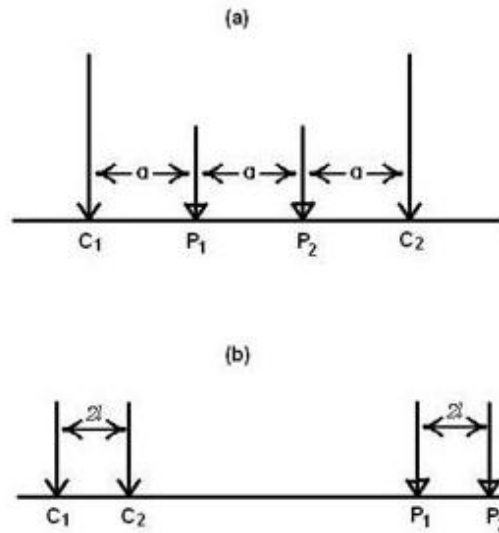
Figure 8.3: a) Wenner array b) Dipole-dipole

R is measured in the field and apparent resistivities are calculated by the formula below:

$$\rho * a = 2\pi * aR \tag{8.3}$$

8.3 Processing

8.3.1 2D Resistivity Inversion using RES2DINV

Inverted resistivity profiles of all the acquired lines were produced using the RES2DINV software. During data acquisition in the North at Mt Princeton, the ABEM equipment stored the number of readings, electrode position, electrode spacing and apparent resistivity values. The first step for data processing involved transferring the raw data from *.s4k format to *.dat format so that the RES2DINV software could read in the raw data. However, it was first required to add the GPS elevation data that were manually recorded by a hand held GPS (accuracy of 10 ft) to the .dat file in order to create a true, inverted resistivity profile that had topography included. Inversion procedure in RES2DINV was as follows:

1. Raw data were read in as .dat files

2. Bad data points were removed when necessary, such as anomalously high or low values in the dataset. This was a key step in processing line YBR which was very noisy because it was acquired along the road with an underground gas pipe and cable wires around it.

3. Combined Marquadt and Occam inversion method was used to invert the data, via smoothness constrained least squares approach.

4. Five iterations of the inversion were done until the RMS fit (a measure of the error) was reasonable for the given dataset. For example, for good data, the final inverted data had an RMS fit of less than 6, while for the noisier data, RMS fit was from 15 to 45. The higher the RMS value, the less reliable the inversion result.

5. Sometimes further editing of the data was done in order to improve the inverted result. This included increasing the level of damping especially for noisy datasets to stabilize the inversion result and produce a lower RMS fit.

The raw data from the South at Poncha Springs were recorded using the SUPERSTING equipment, which were in a different format to the ABEM recorded data. Processing for this data required:

1. Conversion from *.stg format to a *.dat file.

2. Re-ordering the data in the *.dat file into electrode position, electrode spacing and apparent resistivity value as required by the RES2DINV software for the given array: Wenner and Dipole-Dipole.

3. Addition of topography elevation information to the .dat file.

4. Repeating the inversion procedure in RES2DINV i.e. steps 1- 5 above for this new data set.

Inverted resistivity profiles were created for the:

- Five 2D lines in the North at Mt Princeton: ULTO2, P1, ULT01, FOP30, YBR.

- Fourteen lines of the 3D survey in the North at Mt Princeton.

- Seven lines in the South at Poncha Springs: Lines 1000, 100A, 100B, 200, 300, 0, 0E

There were several lines that did not undergo processing due to errors in reading the file. The Dipole-Dipole and Wenner surveys for line 100B were not processed, and neither was the Dipole-Dipole survey for line 300.

The resistivity profiles will be presented in Section R.3 of the report, together with the geophysical interpretation of the results.

8.4   Error Analysis

The greatest uncertainties associated with the DC Resistivity survey are related to:

1. Positioning

2. Quality of data acquired due to the influence of external sources

3. Inversion

Most of the DC Resistivity data points' positions were acquired using the hand-held GPS. This had an accuracy that ranged from ± 3 ft to 100 ft depending on the number of satellites that were available at the time and obstacles such as trees being at the electrode locations. However, the average error was 10 ft in most cases. In the south at Poncha Springs, for lines 1000, 300, 200 and 100, the data points' positions were acquired using the DGPS which had an accuracy of 10 cm on average.

The quality of the resistivity data acquired depended on the location and timing of acquisition. The line YBR is the noisiest data set because it was acquired along the county road. It had telephone line running parallel to the road, buried gas pipe underneath, it rained during the second half of the acquisition of the line and hence it had a lot of bad data points. As a result, the inversion could only produce a resistivity profile that had a RMS fit of 45, which is high. Thus the validity of the inverted product is questionable but the profile was validated against the perpendicular lines P1, ULT01 and FOP 30 that intersected it.

The inversion result is non-unique, data dependent and has inherent uncertainties in it. The objective was to produce the simplest model that fits the data reasonably well. Hence no more than five iterations were done to avoid perturbing the data too much in an effort to minimize the RMS error. The RMS error is indicative of the degree of error in the inverted result and hence gives an indication of the validity of the result. Most of the final products had RMS that was under 15, which indicates that the results are reasonable.

Due to the corruption of data from the Differential GPS, the topographical information for lines 0 and 0E are not as accurate as the other lines in the south (100,200,300,1000). A hand held GPS was used when SP data was taken along line 0, but not to the full extent of the line, so four points had to be extrapolated at the west end. The beginnings of both lines start on the west, than the lines converge to be the same line at the twelfth electrode of line 0. Since SP was not taken along line 0E, the first eleven points had to be extrapolated.

There was an issue in the south data associated with the re-ordering of the *.dat files from the SUPERSTING. The columns were labeled as follows: Ax, Ay, Bx, By, Mx, My, Nx, Ny, V/I, Current, Rho, and Error Percentage. After analyzing the positions of the electrodes in a Wenner survey, it was discovered that columns Ax and Mx were switched. The necessary information for the re-ordering of the files was extracted, but it is unknown if there are any other discrepancies within the files.

8.5   Data Interpretation

8.5.1   North- Mt Princeton

2D Inverted Profiles

Inverted Resistivity profiles were produced for the five 2D lines: FOP 30, ULT01, P1, ULT02 and YBR and all fourteen lines in the 3D survey area. Only FOP 30, ULT01, P1, ULT02, YBR, FOP3, FOP9, FOP15, FOP21 will be presented in this section. See appendix X for additional images.

1. FOP30 Inverted Resistivity Profile

   The resistivity ranges from about 10 ohm m to about 500 ohm m on this profile with a maximum depth of penetration of around 150 m. The low resistivities on this profile suggest that mainly sedimentary rocks or fractured granite are within this first 150 m of section. The anomalously low resistivity areas seen in blue of 10 to 35 ohm m, can be interpreted to be areas of upwelling geothermal water. A shear zone can be imaged on this line with a resistivity of 10 to 90 ohm m and width of approximately 240 m. It is possible that this is the shear zone that laterally offsets the main east dipping fault that truncates the faceted spurs along the eastern edge of the Collegiate Mountains-western side of the Upper Arkansas Valley. This shear zone causes this
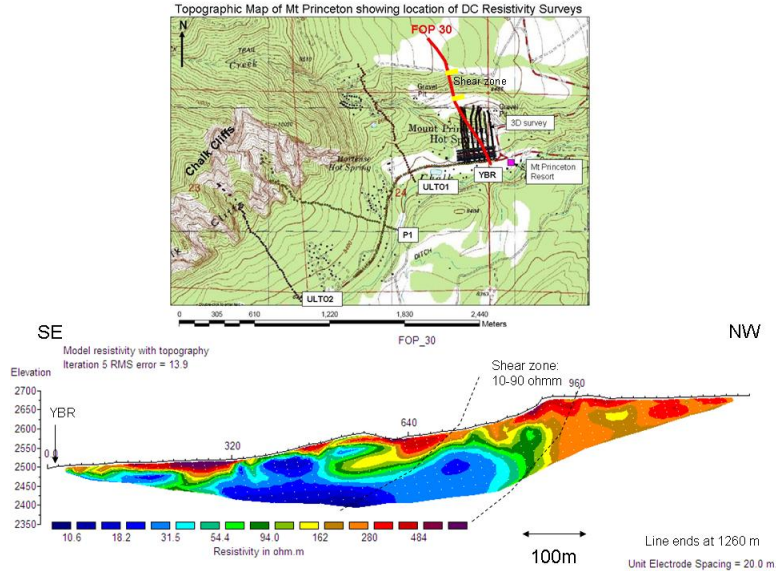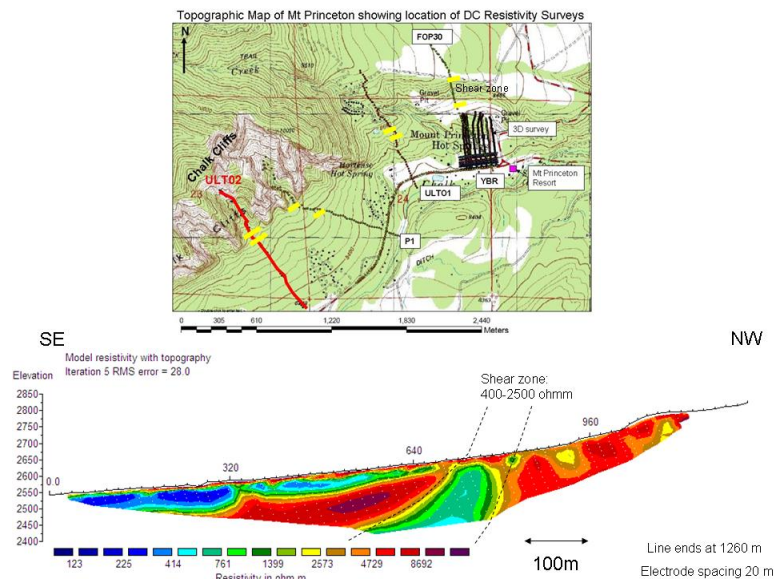
Figure 8.4: Above illustrates the inverted resistivity profile for FOP30 along with a topographic map showing the location of the interpreted shear zone from the profile.

main North-South trending fault to terminate in this Chalk Creek Valley area. This shear zone of fractured granite acts as a conduit for the hot water to rise to the surface. On this particular line however, there is no surface manifestation of this hot, upwelling water.

2. ULT01 Inverted Resistivity Profile

ULT01 is taken approximately 750 m west of FOP30 as seen in Figure 8.5 above. The resistivity ranges from about 5 ohm m to about 250 ohm m on this profile with a maximum depth of penetration of around 150 m. This profile has imaged even lower resistivity rocks and and the low resistivities on this profile again suggest that mainly sedimentary rocks or fractured granite are within this first 150 m of section. The anomalously low resistivity areas seen in blue of 10 to 20 ohm m, can be interpreted to be areas of upwelling geothermal water. A shear zone can be imaged on this line with a resistivity of 6 to 80 ohm m and width of approximately 70 m. It is possible that this is the same shear zone of fractured granite seen on FOP30, that acts as a conduit for the hot water to rise to the surface. On this particular line however, there is no surface manifestation of this hot, upwelling water.

3. P1 Inverted Resistivity Profile

P1 is taken approximately 500 m west of ULT01 as seen in Figure 8.5 above. The resistivity ranges from about 100 ohm m to about 4500 ohm m on this profile with a

117
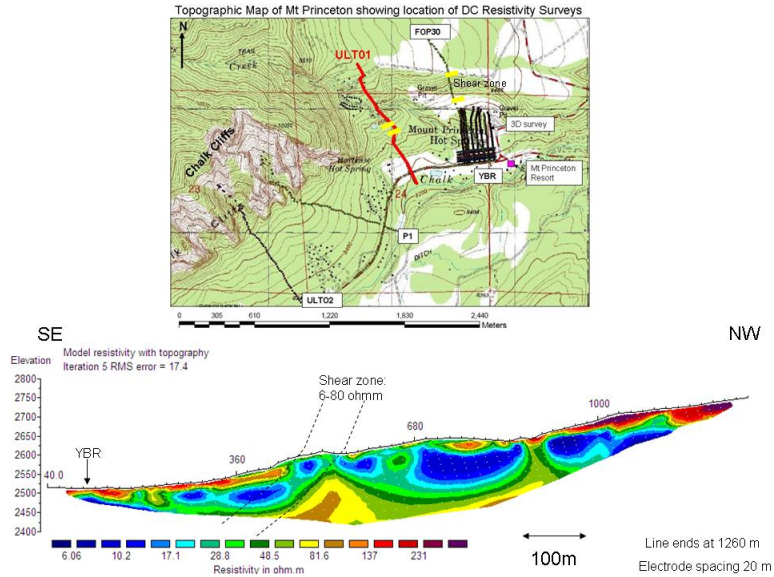
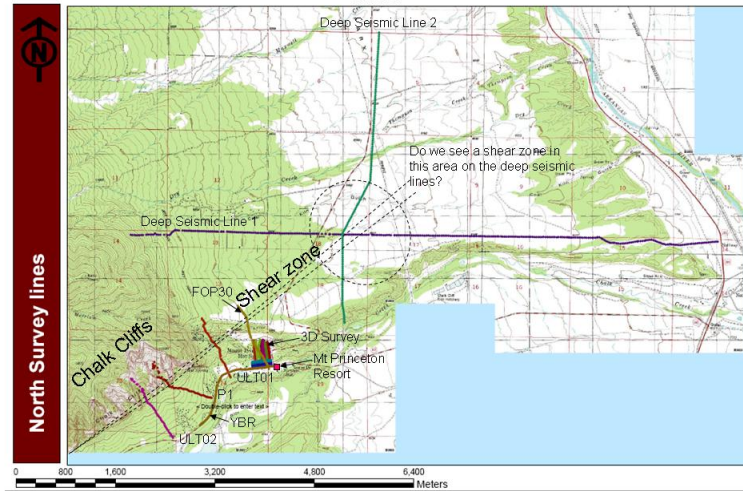Figure 8.5: Above illustrates the inverted resistivity profile for ULT01 along with a topographic map showing the location of the interpreted shear zone from the profile.
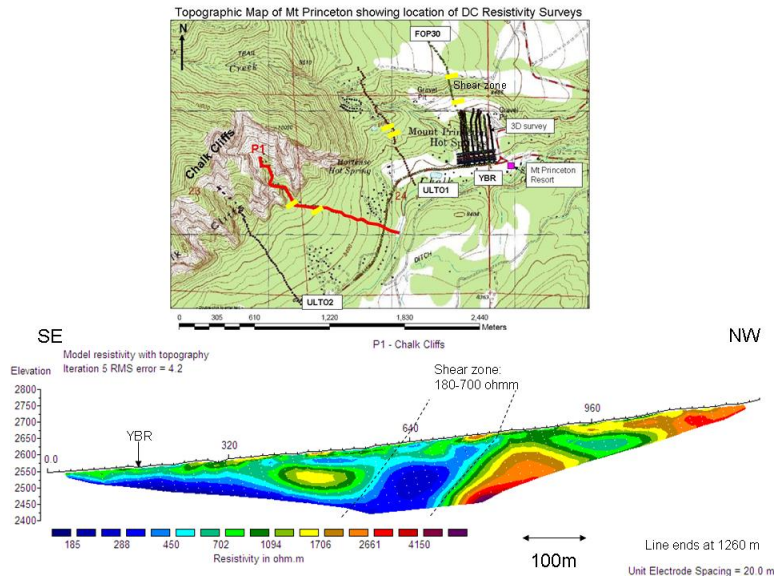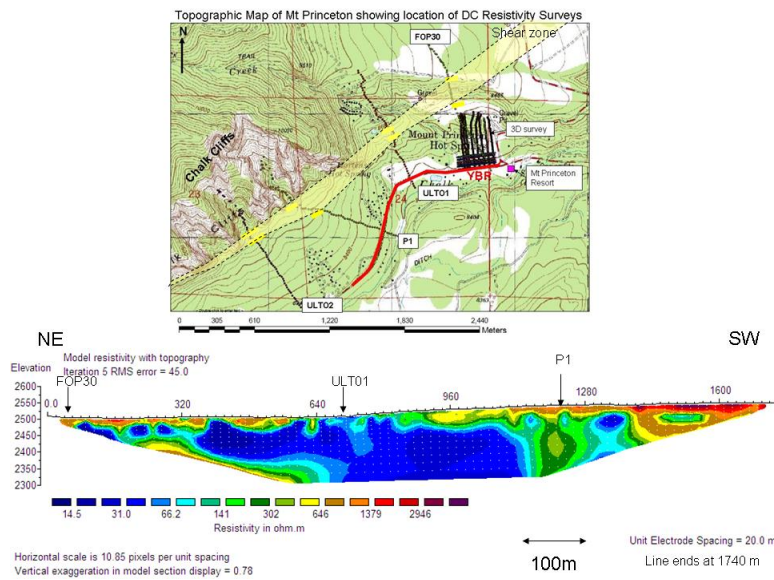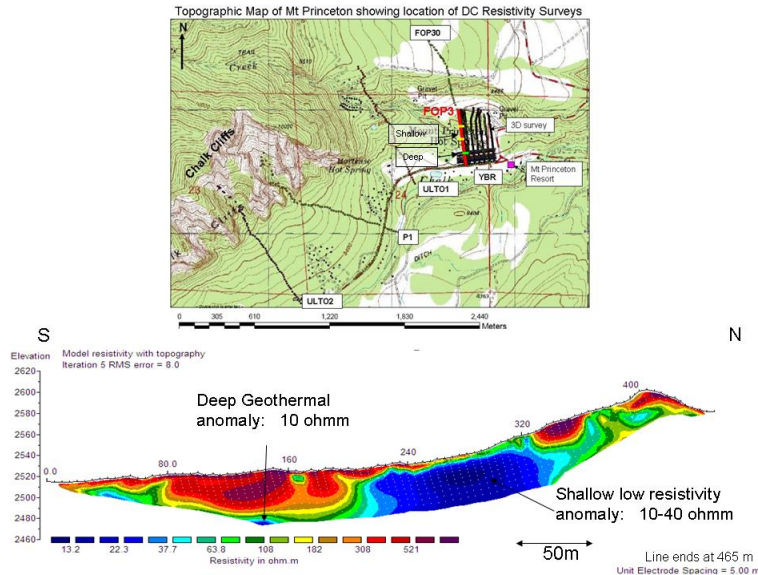

Figure 8.6: Above illustrates the inverted resistivity profile for P1 along with a topographic map showing the location of the interpreted shear zone from the profile.

maximum depth of penetration of around 150 m. This profile has imaged much higher resistivity rocks than the first two lines that has been previously discussed. These high resistivities suggest that more granitic rocks are being imaged on this section. The anomalously low resistivity areas seen in blue of 100 to 450 ohm m, can be interpreted to be areas of upwelling geothermal water. A shear zone can be imaged on this line with

a resistivity of 180 to 700 ohm m and width of approximately 175 m. It is possible that this is the same shear zone of fractured granite seen on FOP30 and ULT01, which acts as a conduit for the hot water to rise to the surface. On this particular line however, there is surface manifestation of this hot, upwelling water seen by the Chalk Cliffs. The Chalk Cliffs are hydrothermally altered granitic rocks that are now kaolinite, which is a white clay mineral. This provides evidence of the fact that hot water is rising in this shear zone and hence altering the granite rocks in this area. The location of the shear zone has been plotted as yellow lines on the topographic map. On this line, the shear zone is located immediately south of the Chalk Cliffs, also confirming that hot water is rising through this zone and hence altering the rocks.

4. ULT02 Inverted Resistivity Profile
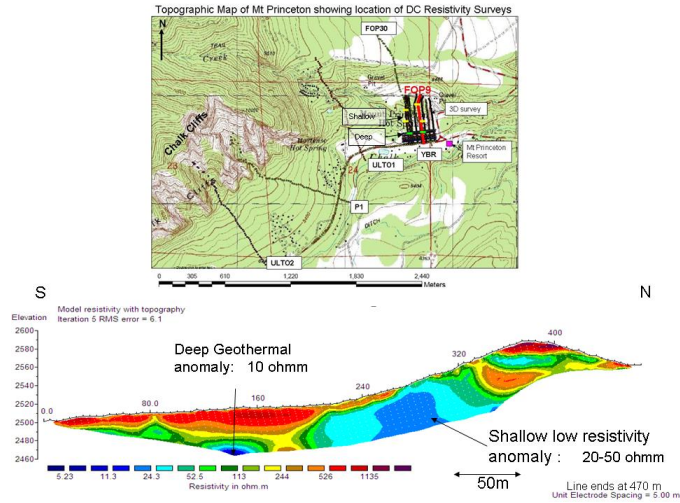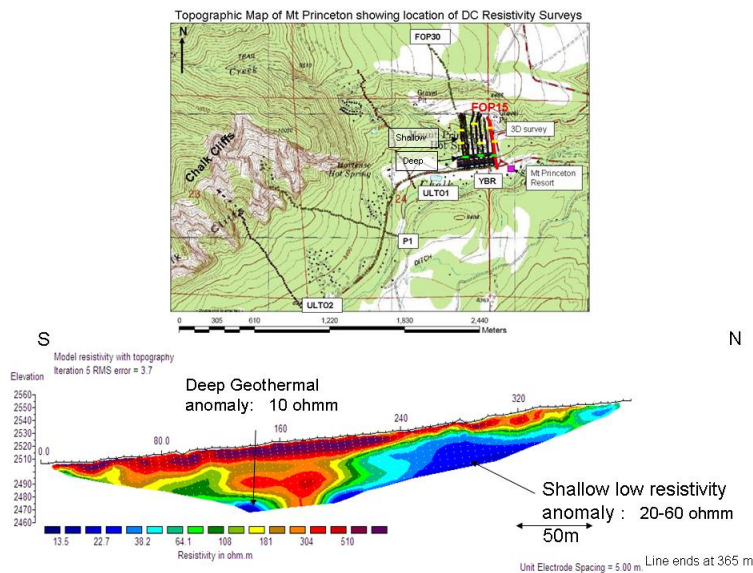

Figure 8.7: Above illustrates the inverted resistivity profile for ULT02 along with a topographic map showing the location of the interpreted shear zone from the profile.

ULT02 is taken approximately 975 m south west of P1 as seen in Figure 8.7 above. The resistivity ranges from about 100 ohm m to about 9000 ohm m on this profile with a maximum depth of penetration of around 150 m. This profile has imaged even higher resistivity rocks than the first three lines that have been previously discussed. It is observed that the resistivities of the subsurface rocks are increasing westwards. These high resistivities suggest that mainly granitic rocks are being imaged on this section as seen in the red and orange areas. The anomalously low resistivity areas seen in blue of 100 to 450 ohm m, can be interpreted to be areas of upwelling geothermal water. A shear zone can be imaged on this line with a resistivity of 400-2500 ohm m and width of approximately 100 m. It is possible that this is the same shear zone of fractured

granite seen on FOP30, ULT01 and P1, which acts as a conduit for the hot water to rise to the surface. The shear zone resistivity also is increasing westwards and this line the shear zone has a particularly high resistivity- not completely consistent with the resistivity of fractured granite. As such, it can be interpreted that the shear zone is dying going south and eastwards. On this particular line there is still surface manifestation of this hot, upwelling water seen by the Chalk Cliffs. This provides evidence of the fact that hot water is rising in this shear zone and hence altering the granite rocks in this area. The location of the shear zone has been plotted as yellow lines on the topographic map. On this line, the shear zone is located immediately south of the Chalk Cliffs, also confirming that hot water is rising through this zone and hence altering the rocks.
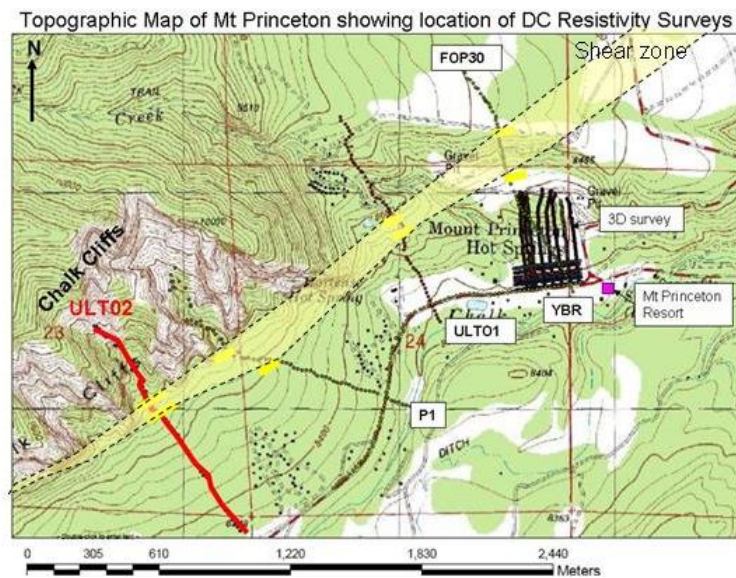
Figure 8.8: Above is a topographic map showing the location of the interpreted shear zone from the four NW-SE 2D profiles.

The shear zone has been interpreted in this Mt Princeton Chalk Creek Valley area, based on the resistivity profiles. It has been interpreted to be dying out to the south west and has been extrapolated further to the north-east as seen in Figures 8.8 and 8.9. Figure 8.9 shows where the shear zone could possibly intersect the two 2D deep seismic lines. These 2D seismic lines were investigated to see if the shear zone can be identified. The results will be discussed in Chapter X.

5. YBR Inverted Resistivity Profile

YBR is 1.7 km long taken along the county road in front of Mt Princeton Resort. This line is intersected by FOP30, ULT01 and P1. The resistivity ranges from about 10 ohm
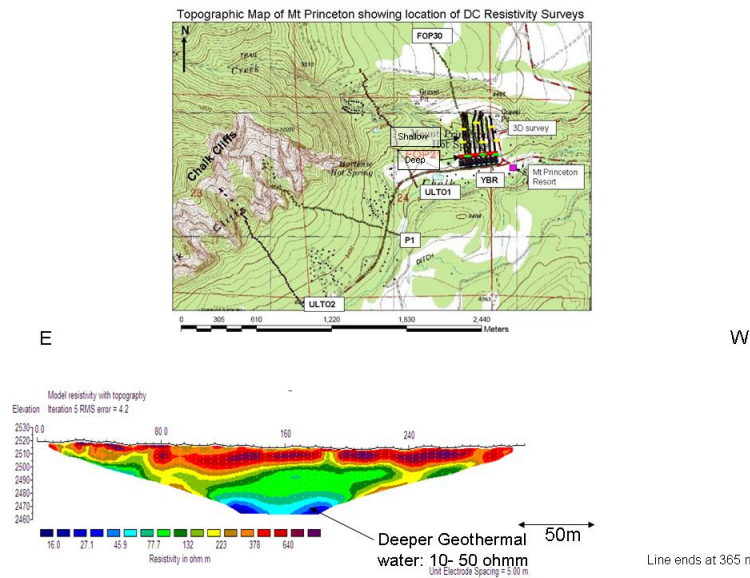
Figure 8.9: Mt Princeton Shear Zone

Figure 8.10: Above illustrates the inverted resistivity profile for YBR along with a topographic map showing the location of the interpreted shear zone from the previous four 2D profiles.

m to about 3000 ohm m on this profile with a maximum depth of penetration of around 200 m. This profile has confirmed that there are higher resistivity rocks being imaged to the south west of the Mt Princeton area. The anomalously low resistivity areas seen in blue of 10 to 70 ohm m, can be interpreted to be areas of upwelling geothermal water. There are surface manifestations of this hot, upwelling water as seen by the Mt

121

Princeton hot springs towards the start of the line in the North east. Although this was the noisiest line to process, and hence the highest RMS error, the section has been validated by the intersection points with P1 and ULTO1. The resistivities seen on this profile is consistent at the point of intersections.

5. FOP3 Inverted Resistivity Profile

Figure 8.11: Above illustrates the inverted resistivity profile for FOP3 along with a topographic map showing the location of the low resistivity anomalies identified from the profile.

The resistivity ranges from about 10 ohm m to about 550 ohm m on this profile with a maximum depth of penetration of around 50 m. The low resistivities and low depth of penetration on this profile suggest that mainly sedimentary rocks or fractured granite are being imaged on this section. The anomalously low resistivity areas seen in blue of 10 to 40 ohm m, can be interpreted to be areas of upwelling geothermal water or clay rich areas. A shallow anomaly not more than 5m below the surface can be identified, as well as an anomaly at around 2470m elevation.

6. FOP9 Inverted Resistivity Profile

The resistivity ranges from about 5 ohm m to about 1200 ohm m on this profile with a maximum depth of penetration of around 50 m. On this profile, higher resistivity rocks have been identified on the northern end of the section, suggesting more of the basement granite is being imaged on this section. The anomalously low resistivity areas seen in blue of 20 to 50 ohm m, can be interpreted to be areas of upwelling geothermal water or clay rich areas. A shallow anomaly not more than 5m below the surface can also be identified on this section, as well as an anomaly at around 2470m elevation.

Figure 8.12: Above illustrates the inverted resistivity profile for FOP9 along with a topographic map showing the location of the low resistivity anomalies identified from the profile.

7. FOP15 Inverted Resistivity Profile

Figure 8.13: Above illustrates the inverted resistivity profile for FOP15 along with a topographic map showing the location of the low resistivity anomalies identified from the profile.

The resistivity ranges from about 10 ohm m to about 550 ohm m on this profile with a maximum depth of penetration of around 50 m. The low resistivities and low depth of penetration on this profile suggest that mainly sedimentary rocks or fractured granite are being imaged on this section. The anomalously low resistivity areas seen in blue of 20 to 60 ohm m, can be interpreted to be areas of upwelling geothermal water or clay

123

rich areas. A shallow anomaly not more than 5m below the surface can be identified, as well as an anomaly at around 2470m elevation. The resistivity of this shallow anomaly has increased eastward.

8. FOP21 Inverted Resistivity Profile

Figure 8.14: Above illustrates the inverted resistivity profile for FOP21 along with a topographic map showing the location of the deep low resistivity anomaly identified from the profile.

The resistivity ranges from about 10 ohm m to about 700 ohm m on this profile with a maximum depth of penetration of around 50 m. On this profile, a 10-20m layer of higher resistivity rocks have been identified across the profile. This suggests more resistive sedimentary or unfractured granitic rocks imaged on this section. The anomalously low resistivity areas seen in blue of 10 to 50 ohm m, can be interpreted to be areas of upwelling geothermal water associated with the deeper anomaly seen on the southern part of the sections of FOP 3, 9, 15.

Therefore in this 3D Survey, two geothermal anomalies can be identified. A deep anomaly at around 2470m elevation at the southern part of the field and a shallow anomaly from 0- 10m below the surface extending in the northern areas of the field. This can be seen in Figure 8.15.

8.5.2   South-Poncha Springs

The goal for conducting surveys in the Poncha Springs area was to characterize the known geothermal reservoir, and perhaps find new ones. On the east end of line 0, a hot well was
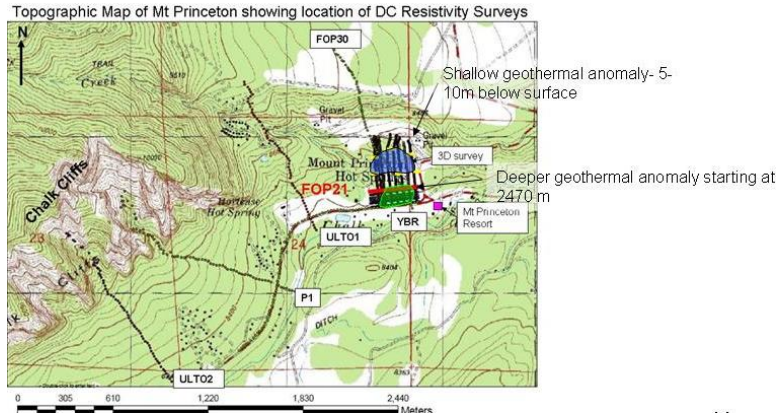
Figure 8.15: Above showing the extent of the two low resistivity anomalies identified on the 3D DC resistivity survey.

drilled by the request of the owner of the property where the old fluorite mine sits. Therefore it is known that there is hot water in southeastern area of the following map.
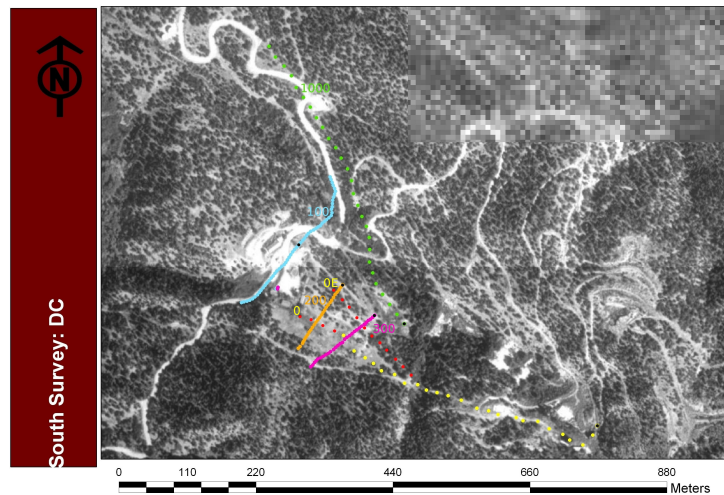
Figure 8.16: Map of the DC survey lines in the Poncha Springs area, with lines labeled appropriately. The extrapolated points mentioned in the Error Analysis section are in red, and their locations on the map were completely approximated since there was no GPS data associated with it. The black dots represent the beginning of each line.

The area to the southeast of the Boyscout Camp is a known area with geothermal activity. In the figure above, it is the barren area in which the 200 and 300 lines intersect the 0 and 0E lines.

All of the processed images for Poncha Springs were scaled to the same color scale that

was produced by the Wenner array for line 200. This color scale was chosen because it had an average range among the images, and for consistency. The colder the color, the more conductive the material.

The beginning of both lines 0 and 0E are on the east end of the line, where the lines share the same electrode positions. There are two conductive zones, in blue, along these lines. The zone of conductivity on the left hand side is in the area where a hot water well was drilled. Further study would have to be conducted in order to determine if this is part of the geothermal reservoir to the west. It could possibly be a result of a mine shaft being filled in, but it is unknown the complete extent of the mine. However, the hot water suggests geothermal influences. The confined conductive zone in the middle could be an extension of the conductive area previously mentioned, the Wenner survey for line 0E would suggest this. The conductive areas on the right hand side are associated with the known geothermal zone to the southeast of the Boyscout Camp. The Wenner survey for line 0E shows a stronger conductive zone that represents the geothermal reservoir. Lines 200 and 300 intersect these lines, and it is quite obvious there is geothermal activity from the images produced from the data.

This beginning of the line 100a starts in the middle of line 100 and continues in a westward direction. The large conductive zone starting at the beginning of the line appears to be associated with the geothermal area found on lines 0 and 0E. The extent of this geothermal zone is also confirmed in the intersecting lines 200 and 300, as can be seen in the figures below.

The beginning of both lines 200 and 300 is on the east end and continues west. The large conductive zones seen in the above figures show the extents of what is probably a geothermal reservoir. The smaller, confined, zones of conductivity seen on the right hand side of the Dipole-Dipole survey of line 200, are most likely associated with pipes. There are many pipes in the area, since the city of Salida is pumping water for their hot springs.

The beginning of line 1000 is on the south end, close the Boyscout Camp, and continues north. A large conductive zone is seen on the north end. It is unclear if this is a continuation of the previously mentioned geothermal zone due to the missing data from line 100b (please refer to the Error Analysis section of this chapter for further information on this). Further investigation is needed to determine if this is a separate geothermal reservoir.

8.6   Conclusion

The goal of conducting DC Resistivity surveys was to image the shear zone and map its extent- especially in the Mt Princeton- Chalk Creek Valley area. This shear zone consists of fractured basement granitic rock which acts as a conduit for hot water to move towards the surface. A low resistivity shear zone was identified parallel to the Chalk Cliffs on the four NW-SE resistivity profiles in the Mt Princeton are. Its extent mapped and also extrapolated
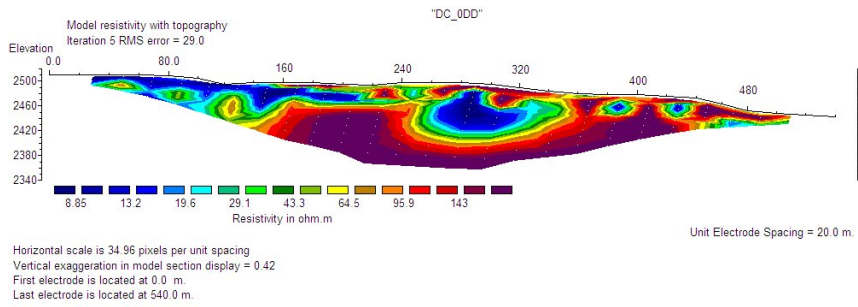
(a) **Dipole-dipole survey taken along line 0.**
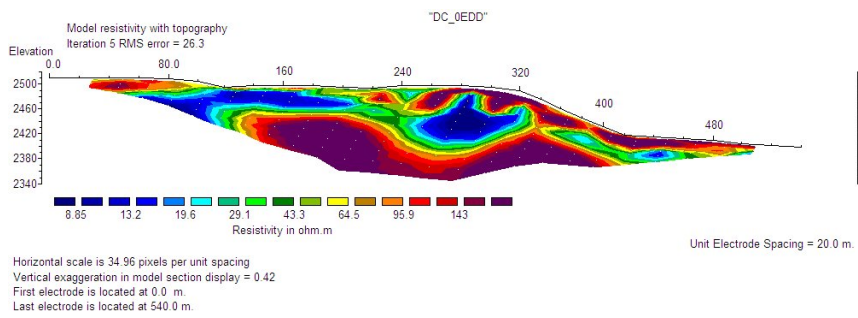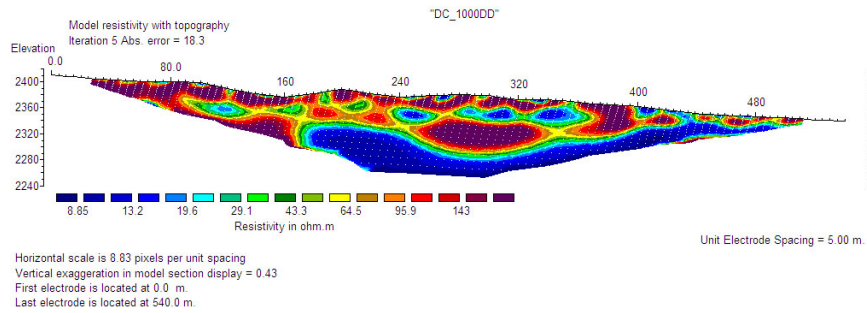

(b) **Dipole-dipole survey taken along line 0E**
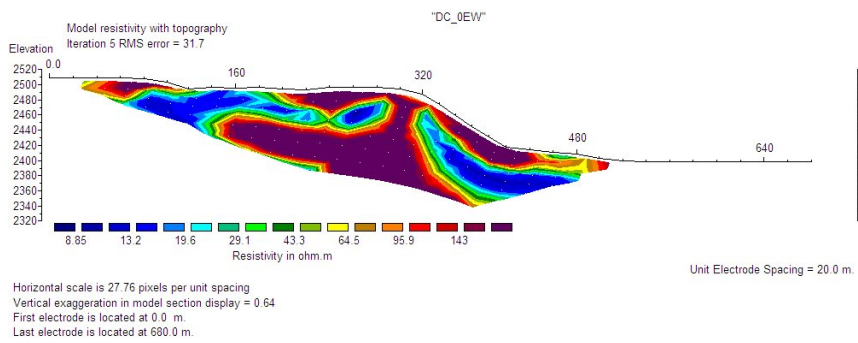
(c) **Wenner survey taken along line 0E.**

Figure 8.17: **Poncha Springs surveys.**

127
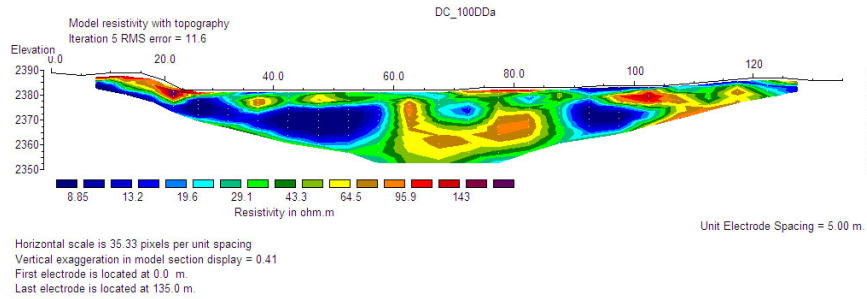
(a) **Dipole-dipole survey taken along line 100a.**

(b) **Wenner survey taken along line 100a.**

Figure 8.18: **Poncha Springs surveys along line 100a.**

to the deep seismic lines to see if it is present further north. The shear zone is the conduit that allows subsurface geothermal water to rise and alter the basement rocks hence forming the Chalk Cliffs. The shear zone appears to die out south westerly as its resistivity increases in that direction.

The second goal of acquiring DC data was to identify areas where the geothermal water in the subsurface is flowing upwards in the subsurface. Two geothermal anomalies were identified in the 3D survey area: a shallow anomaly at around 5-10m below the surface that was more prevalent towards the northern end of the survey and a deeper anomaly at around 2470m in elevation towards the south of the field. On line YBR along the county road, a low resistivity zone assumed to be associated with geothermal water was identified. This was at least 1.2 km in extent. The DC survey has also seen that the resistivity of the rocks increase south easterly. This may suggest that the thickness of the sedimentary section may

128
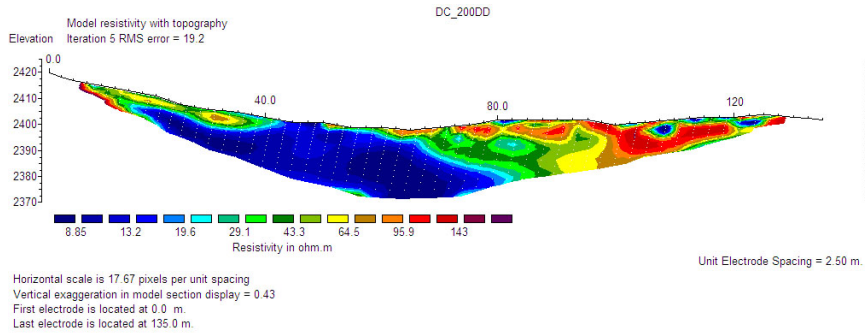
(a) **Dipole-dipole survey taken along line 200.**
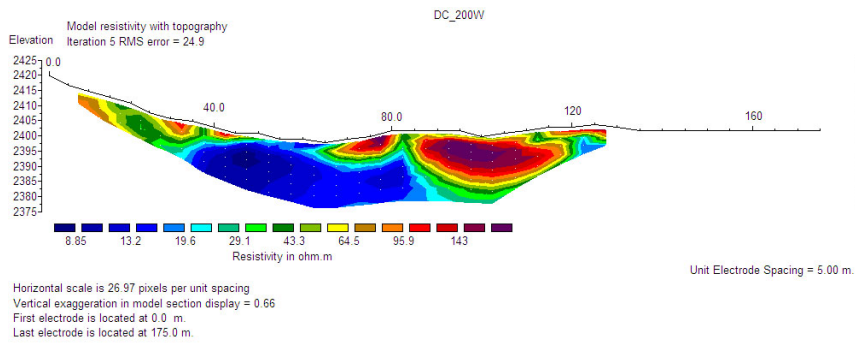
(b) **Wenner survey taken along line 200W**
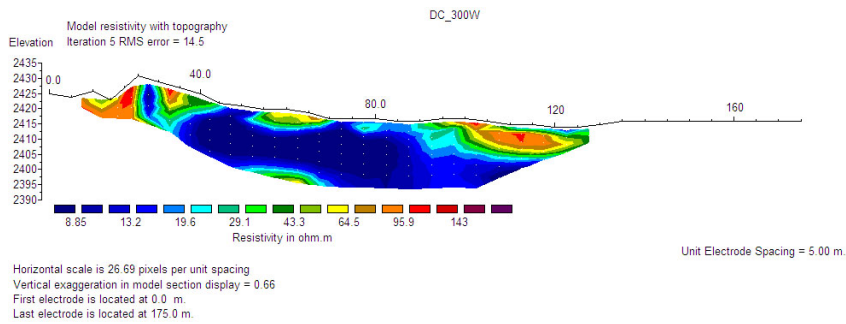
(c) **Wenner survey taken along line 300.**

Figure 8.19: **Poncha Springs surveys.**

(a) **Dipole-dipole survey taken along line 1000.**
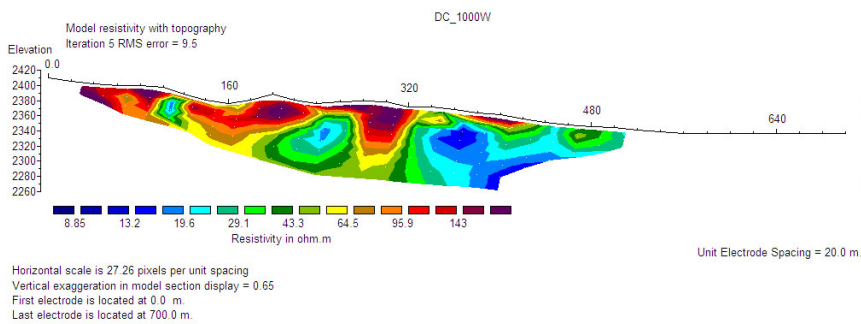
(b) **Wenner survey taken along line 1000**

Figure 8.20: **Poncha Springs surveys.**

be thinning south easterly and more granitic basement rocks are present in that direction. In future surveys, perhaps more 2D lines can be acquired south of the river to possible identify the fault that has been laterally offset by the shear zone.

Chapter 9

Self-Potential

9.1 Introduction

The self potential method is an inexpensive, near surface geophysical method that is amongst the easiest to operate. It is widely used in metal exploration, ground water and geothermal exploration. [9] This method was used in this geophysical investigation at Mount Princeton and Poncha Springs to image and map ground water flow, specifically the extent of the up-welling, and geothermal waters at shear zones and faults.

SP, like DC resistivity, measures the potential difference across two electrodes. But unlike resistivity, no current is injected into the ground. Natural potential differences are measured and hence it is considered to be a passive electrical method. The potentials measured can vary from millivolts to 1 volt but the sign of the potential difference is important in interpreting anomalies i.e. whether the measured SP is positive or negative with respect to a reference electrode generally placed at the beginning of the profile. The electrodes are usually non-polarizing electrodes. For the measurements, we used $Pb/PbCl_2$ electrodes known as Petiau electrodes. The voltmeter should have a high sensitivity ($0.1mV$) and high internal input impedance ($100M\Omega$).

SP method is very sensitive to groundwater flow. In porous media, the pore water has an excess of electrical charge that is generally positive. Therefore, the drag of the excess of electrical charges by the flow of the pore water generates a current density in the ground. This current is a source term in the continuity equation for the conservation of electrical charge and generates an electrical field. Only the distribution of this electrical field is recorded at the ground surface of the Earth. [10] The potentials tend to increase in positiveness with the direction of water flow as electric charge flows in the opposite direction.

In the case for Mount Princeton and Poncha Springs, positive anomalies are expected to be associated with the rising geothermal waters; and no anomalies represents the background ground water flow.
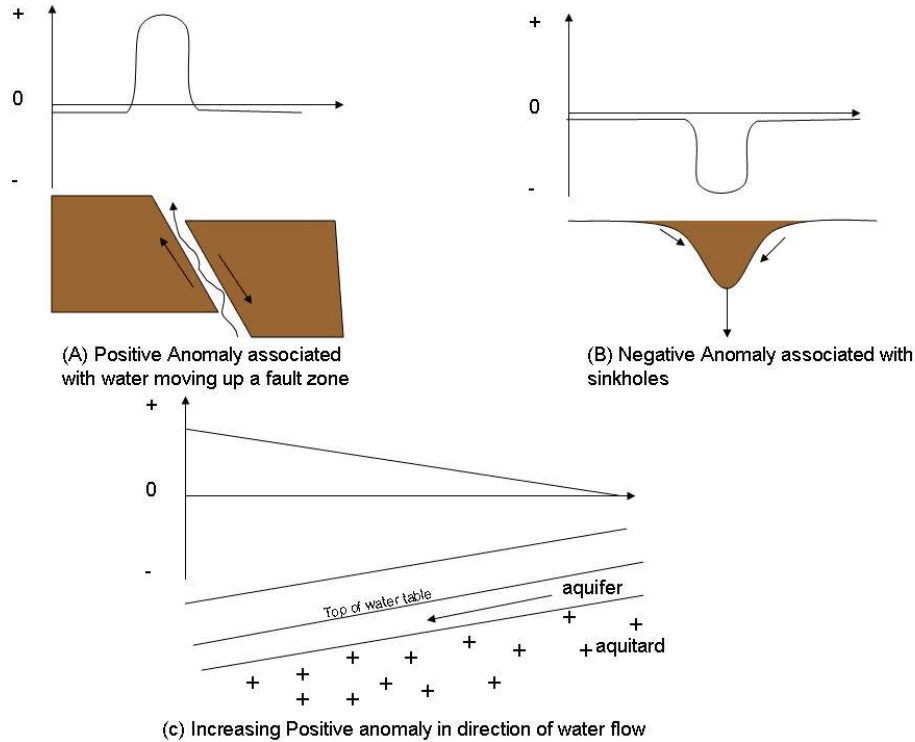
Figure 9.1: typical geologic situations and the associated SP anomalies. (Adapted from diagrams by A. Revil, 2009)

9.2   Field Procedure and Survey Design

The field equipments for Self-Potential (SP) survey consist of a voltmeter to which a pair of $Pb/PbCl_2$ electrodes (Petiau electrodes) are connected and a reel with a long cable. One electrode is fixed at a reference point and the other is a travelling electrode. The SP measurement is taken by scrapping off a bit of earth at each point and taking the average SP value in millivolts (mV). The "travelling" electrode moves forward to a new station after each measurement and the voltmeter is always with the travelling electrode. The advantage of this layout is that the voltage or potential is measured consistently with respect to a point that is fixed (i.e. the reference point).

For the surveys done at Mount Princeton, a handheld GPS system with an altimeter were carried along to record the elevations at each point. The same was done for surveys at Poncha Springs except for lines 1000, 100, 200 and 300 where a DGPS system was used.

SP measurements were taken along all the DC Resistivity lines at Mount Princeton and

along some of the DC lines at Poncha Springs. The interval between each SP measurement is 5m at Mount Princeton and 10m at Poncha Springs.

At Mount Princeton, the SP lines were orientated such that they would cross a known positive anomaly and a shear zone.
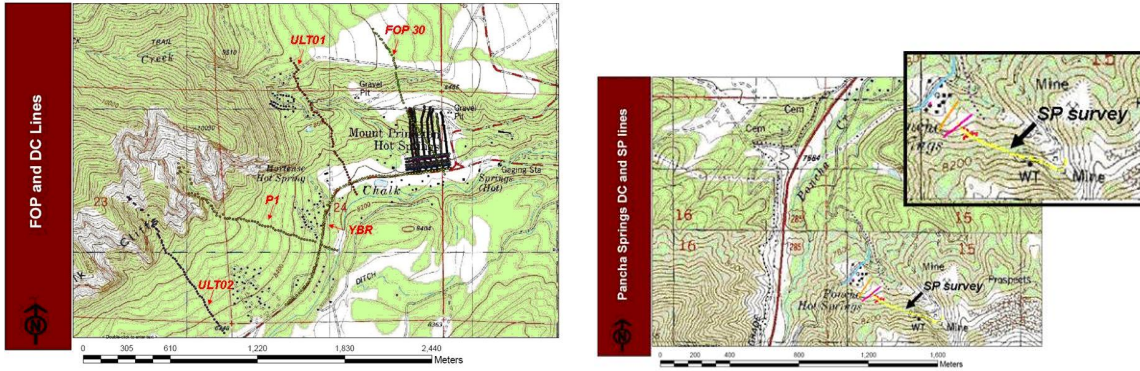
(a) Map of SP survey at Mount Princeton Springs

(b) Map of SP survey at Ponchas Springs

Figure 9.2: SP Survey sites

9.3 Data Processing

Self-Potential (SP) data is processed to get a set of profiles and a contour map of points with the same potentials (i.e. equipotentials). Processing SP data involves inputting sets of SP, elevation, GPS as well as error values written on the field onto an excel spreadsheet. Each SP line has its own reference point so when processing these data, re-referencing needs to be done.

Re-referencing changes all the reference points of all lines to a common point. In this case, the first electrode on the Yellow Brick Road (YBR) line is set to be the common reference point.

For example, re-referencing is done by finding the difference between the anomaly on YBR line and the anomaly of line P1 at their point of intersection. This difference is then subtracted from P1 anomaly to get a "new" anomaly for P1 with reference to the common point. This process is repeated for lines FOP30, ULT01 and ULT02. This is illustrated in the example given in Figure 9.4.

After re-referencing is done for all the lines, a contour map is then generated by using software called Surfer. Surfer can also plot the data in X, Y and Z directions creating a 3D
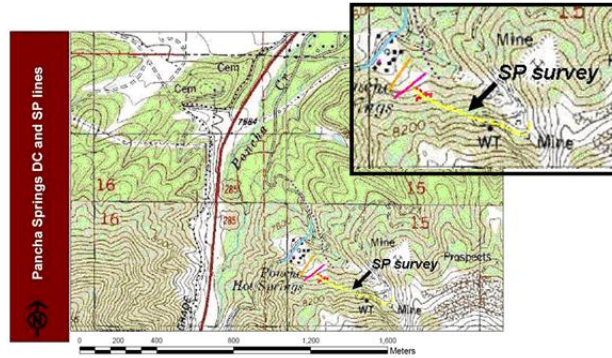
Figure 9.3: Schematic map which shows SP line surveys (in red) and the common reference point on YBR
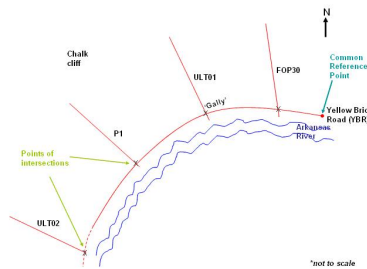
Figure 9.4: (a)Example of how to change reference point line 2 to reference point of line 1 (b) Re-referenced line 2

display of the data.

A topography correction needs to be done before plotting the SP values to remove the topographic effects on the readings. This is done by fitting a regression line through the SP plot. This will give an equation of the form:

$$SP_{topocorrection} = az + b$$

where z is the elevation, a is the gradient and b is the coefficient. The new corrected SP will be SP value minus $SP_{topocorr}$.

9.4 Error Analysis

The greatest uncertainties associated with the SP survey are related to positioning, and quality of data acquired which may be affected by external sources as well as the saturation of the ground.

Most of the SP data points positions are acquired using the hand-held GPS. This has an accuracy that ranges from $\pm 3ft$ to $100ft$ depending on the number of satellites that are available at the time and obstacles such as trees being at the electrode locations. However, the average error is $\pm 10ft$ in most cases. In the south at Poncha Springs, for lines 1000, 300, 200 and 100, the data points positions are acquired using the DGPS which has an accuracy of $\pm 10cm$ on average. When the ground is too dry, the hole is dug a bit deeper for moisture and an average of several measurements in the hole is taken to reduce error.

9.5   Data Interpretation
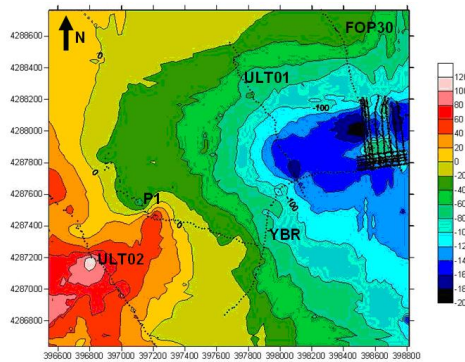
Figure 9.5: SP Map showing all survey positions referenced to YBR

The SP map in the figure above shows that there is generally an increasing SP value trend from North-East to South-West. However, this map is not reliable because the survey lines are sparse and the interpolations between the lines are system-generated. There is SP data from previous years for different areas of this map region however there is no elevation data available for them so topography corrections could not be applied and therefore the old and new data sets could not be integrated.
Figure 9.6 shows the SP profiles for lines FOP30, ULT01, P1, ULT02 and YBR.

The SP plots from survey lines P1 and ULT02 show positive anomalies which indicate that there may be upwelling of water at the area. On the other hand, survey lines YBR, FOP 30 and ULT01 do not show any anomaly. ULT01 is believed to be on one of the faults itself and therefore it is missing the anomaly.

Anomalies are seen in DC resistivity profiles and not in SP plots for lines YBR, FOP30 and ULT-01. This may be because there is an overcorrection of SP/topography trend for these lines.

Figure 9.7 shows the SP map for FOP. It clearly shows a high anomaly in the middle of the field which indicates an upflow of water in the area.
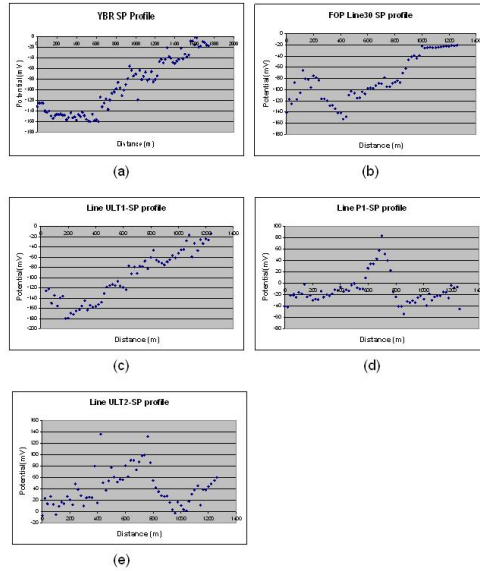
Figure 9.6: SP profiles of YBR, FOP30, ULT1, P1, and ULT2
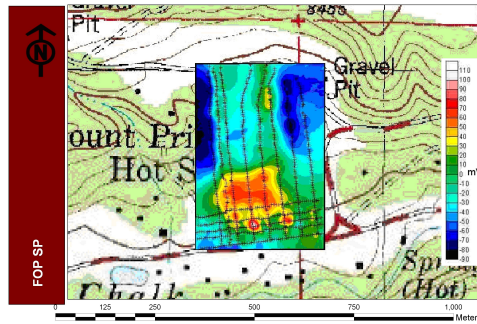
Figure 9.7: SP profile for Mr. Long's Field

The SP profile in Figure 9.8 shows that there may be two positive anomalies present although this may not be the case as it could just be random plots of SP data. On its own, this SP profile doesnt show much. It makes more sense once it is analyzed together with DC resistivity results as shown later in the integration chapter.

9.6 Conclusions

The SP data in the North has low resolution because there is not enough data to get a good interpolation of SP data of the area. The data from the previous year could not be used because they do not have elevation profiles which are needed to do topographic correction and therefore could not be integrated with the data from this year. Further suggestions would include having more survey lines between ULT02 and P1, P1 and ULT01, and ULT01
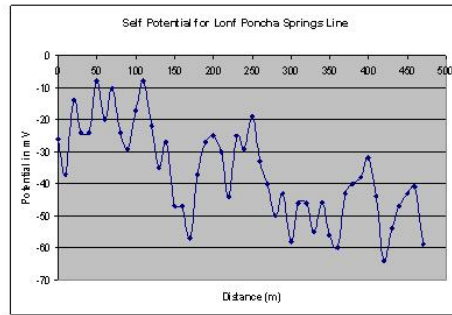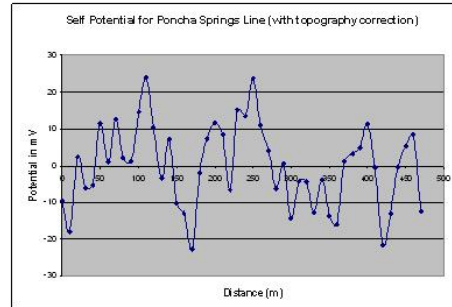
Figure 9.8: (a) SP profile for the south side without topography correction (b) Sp profile with topography correction

and FOP30. This would ensure that the SP map interpolation results are more reliable for interpretation. This area could be one of the main focuses because it seems to show an interesting SP trend from North-East to South-West.

The SP data on the Field of Pain (FOP) is of a higher resolution because the survey lines are closer to each other. From the SP data it is concluded that there is an upwelling of water at the south side of FOP.

The SP data in the South (Poncha Springs) cant really be interpreted on its own. There is only one survey line done here and looking at the SP profile of this one line there could be two anomalies present. This could only be confirmed by integrating it with the DC resistivity profile or by doing further investigations or more surveys around this area.

Chapter 10

Gravity

10.1 Introduction

10.1.1 Theory

Gravity is the attraction force between any two objects with mass. Because the near surface geology is heterogeneous, there are variations in density, which cause fluctuations in the gravity field. These variations can be measured by a gravimeter. From these gravity field variations, one can reconstruct the subsurface model, which identifies the density distributions and constrains the locations of any anomalies. These density-based subsurface models allow researchers to differentiate geological materials. Figure 10.1 (p39 of [9]) shows some of the possible differences in density for various rock types. While volcanic and metamorphic rocks typically have a higher density than sedimentary rocks, the sedimentary rocks have a large range of possible density values. Common factors that affect the density of the sedimentary rocks include "composition, cementation, age and depth of burial, tectonic processes, porosity and pore fluid type" [p39 of [9]]. Therefore, gravity surveys are widely used in the mineral exploration. Some of the minerals are typically associated with geothermal alteration zones. Gravity surveys are also popularly used in petroleum explorations, seismology, regional geological studies, void detections, volcano monitoring and geodesy. Gravity surveys can also compliment or aid in the interpretation of magnetic and seismic data.

10.1.2 Equipment

For the gravity surveys outlined in this report, two different types of gravimeters were used to acquire the data. They are the LaCoste and Romberg G-491 Geodetic Gravity Meter (LNR) and the CG-5. The CG-5 has much higher accuracy and less instrument drift than the LNR. The CG-5 has the ability to measure variations on the order of few micro-Gals, while LNR is only accurate to a few mili-Gals. One Gal = 1 cm/s^2 (this is technically a measure of the acceleration due to gravity at the survey location). The CG-5 was used to collect the datasets from the Field of Pain (FOP) and the Deep Gravity Line. The LNR was

Material type	Density range (Mg/m³)	Approximate average density (Mg/m³)
Sedimentary rocks		
Alluvium	1.96–2.00	1.98
Clay	1.63–2.60	2.21
Gravel	1.70–2.40	2.00
Loess	1.40–1.93	1.64
Silt	1.80–2.20	1.93
Soil	1.20–2.40	1.92
Sand	1.70–2.30	2.00
Sandstone	1.61–2.76	2.35
Shale	1.77–3.20	2.40
Limestone	1.93–2.90	2.55
Dolomite	2.28–2.90	2.70
Chalk	1.53–2.60	2.01
Halite	2.10–2.60	2.22
Glacier ice	0.88–0.92	0.90
Igneous rocks		
Rhyolite	2.35–2.70	2.52
Granite	2.50–2.81	2.64
Andesite	2.40–2.80	2.61
Syenite	2.60–2.95	2.77
Basalt	2.70–3.30	2.99
Gabbro	2.70–3.50	3.03
Metamorphic rocks		
Schist	2.39–2.90	2.64
Gneiss	2.59–3.00	2.80
Phylite	2.68–2.80	2.74
Slate	2.70–2.90	2.79
Granulite	2.52–2.73	2.65
Amphibolite	2.90–3.04	2.96
Eclogite	3.20–3.54	3.37

Figure 10.1: Densities of common geologic materials
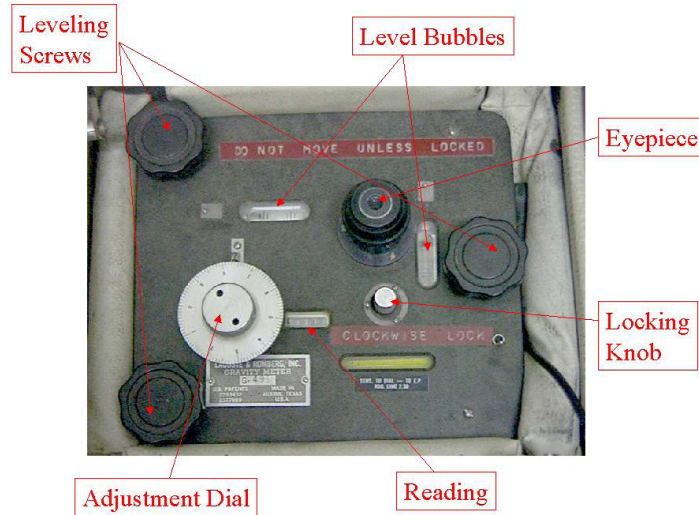
Figure 10.2: Diagram of the LNR instrument.

used on the two southern lines, which run along county road 206 and 221, just outside of Poncha Springs.

10.1.3 Acquisition procedures

For the CG-5:

1. Level the stand on a roughly horizontal surface. Then place the CG-5 onto the stand.

2. Create a new file name for the dataset you are going to collect.

3. Set the correct station ID and other parameters on the STATION DESIGNATION screen.

4. Then go to leveling screen by pushing F5. Level the instrument according to the icons shown on the screen.

5. Push F5 to the data acquisition screen. You have 10 seconds to get 15 to 20 feet away from the sensor. Stay still and avoid any moving objects coming close to the instrument (like a passing truck). Blue line on the font indicates data acquisition in process.

6. After the blue light goes off, recorde the data in a notebook and press F5 to record it in the instrument. The detail of how to do each steps correctly is shown in the appendix of this chapter.

For LNR:

The LNR instrument is shown in figure 10.2

1. Level the meter using the three leveling screws.

2. Unlock the meter by tuning the locking knob counterclockwise all the way.

3. Tune on the light by the small switch to the right of the locking knob.

4. Look through the eye piece and turn the adjustment dial until the cross hair in the eye piece is at 2.4.

5. Record the reading. The detail of how to read the reading is shown in the appendix of

this chapter.

10.1.4   Importance of the survey

Gravity data can be integrated with other geophysical methods in order to give the most accurate and precise interpretation of the area. As discussed before, the gravimeter measures the Earth's gravitational field with a small spring inside the device. The change in gravity readings from location to location is indicative of a change in density from varying porosity, rock composition, and even faulting. This is especially important for the area because geothermal activity is under investigation and therefore having accurate interpretation of faults would reveal any possibility of heat flow in the subsurface. Density changes in the subsurface could be from a change in permeability of the rocks. An increase in permeability indicates possible water flow in the subsurface. The presence of water in the area is known however potential locations of hot water and geothermal activity is the goal. Gravity data would be able to reveal any subsurface anomalies that reflect a change in density of the geology.

10.1.5   Survey sites

Gravity readings were taken in three locations within Chaffee County. The Northern side of the survey was done between Mount Princeton Hot Springs and Buena Vista perpendicular and West of Highway 285. The 10.2 kilometer line started on a private road West from County Road 325 and extended East, crossing County Road 322, and ending at Highway 285. Data was collected over a few days with the CG-5 Gravimeter with a spacing for data points of 30m. The results of this survey will be paired with 2D deep seismic and magnetic data along the same survey line.

Just North of Mount Princeton Hot Springs at the intersection of County Road 321 and County Road 322 was another field under investigation. This field, referred to as the Field of Pain (FOP), is about 400x400 meters at a fairly level elevation. Investigation on this field was previously done with DC Resistivity and Self Potential. The purpose of performing a gravity survey, using the CG-5, is to further understand the region for geothermal activity. Many geophysical methods were done on the FOP so the results from the gravity survey will be tied into shallow seismic, magnetics, DC resistivity, self potential, passive seismic and vertical seismic profiling.

Another survey area was under investigation near Poncha Springs where two lines of gravity data were collected using the LNR. One line was nearly parallel to Highway 285 running North to South along the railroad. The other line was approximately 10 miles to the west off of Highway 50. Data was collected every 30 meters along the road, ensuring that a base station or looped station reading was taken every 10 stations or 300 meters. The survey line along the railroad only had gravity data so it is important to incorporate it with other data collected in the area so that a regional idea of the geothermal activity can be determined. The results of the extended line along the road will be combined with magnetics and electromagnetic surveys performed along the same line.

10.2   Data Reduction and Corrections

10.2.1   Unit conversion of the LaCoste and Romberg (LNR) gravimeter data

To obtain a gravity reading, g, in mGal, the meter reading on the LNR G-491 has to be converted using Equation 10.1

$$g = C + F(A - B) \ mGal, \qquad (10.1)$$

where A is the instrument reading, B is the integer to nearest hundred smaller than the reading, C is corrected gravity value (mGal) and F is interval factor. Values for C and F were determined using B and Table (Appendix D.1).

10.2.2   Correcting for the effects of latitude

The combination of Newton's law of universal gravitation and Newton's Second Law enables us to write the gravitation acceleration, g, as a function of the Earth's radius (Equation 10.2).

$$g = GM/R2 \ m.s^{-2}, \qquad (10.2)$$

where, G is universal gravitational constant (S.I), M is the mass of the Earth (kg) and R is the radius of the Earth (m). Thus, g becomes larger towards the equator (as R decreases) and gravity decreases towards the poles.

When carrying out relative gravity surveys, data needs to be corrected relative to the location (latitude) of the base station. In the Northern hemisphere, the correction will be positive when taking measurements to the South of the base station and negative when measurements are done to the North.

The latitude correction Δg_L follows Equation 10.3

$$\Delta g_L = \pm 0.001626 sin\phi cos\phi \Delta y \ mGal, \qquad (10.3)$$

where, ϕ is the latitude of the station number (degrees), and Δy is local northing (m)

Note that the latitude correction also accounts for the differences in angular acceleration which are due to the earth's rotation as well as tidal drift.

10.2.3   Tidal and instrument drift corrections

Two measurements taken at Δt at the same location with the same gravimeter will almost always differ. This variation caused by two factors: instrument drift, which is due to small changes in the physical constants of gravimeter components (spring relaxation), and tidal effects, which are dependent on the positions of the sun and moon relative to the Earth ([11]). Instrument drift affects reading to such a point that it is necessary to tie in initial base station measurements every few hours. This process is called looping and it indicates whether or not drift has occurred and, if so, its magnitude.

Tidal variations are not linear on a timescale of one day, but they can be considered to be linear from one to three hours segments. Because instrument drift is linear on the same scale length, a drift curve may be constructed in order to remove both tidal and instrument effects, if base station measurements are repeated every few hours. The Equation 10.4 describing such a drift correction is given below.

$$\Delta g_D = g_b + (t - t_b) * [(g_e - g_b)/(t_e - t_b)] - g_1 \ mGal, \tag{10.4}$$

where t is reading time of a measurement (hours), g_b and g_e are gravity readings at the beginning and end of survey loop, at times t_b and t_e, respectively ($mGal$), and g_1 is the first base station reading ($mGal$)

10.2.4 Free-air correction

The free-air correction accounts for the difference between gravity measured at sea level and at elevation, h, where the measurement is taken, assuming there is no rock mass in between. The elevation was obtained at each station using a differential global positioning system (DGPS). This technique is of very high resolution as elevations can be measured to the nearest centimeter. The accepted value for free-air correction is given in Equation 10.5

$$\Delta g_{FA} = \pm 0.3086 h \ mGal, \tag{10.5}$$

where h is the station elevation above sea level (m). Effectively, the free-air correction removes the elevation difference from one station to the next. This reduces the data to a constant elevation datum.

10.2.5 Bouguer correction

Unlike the free-air correction, the Bouguer correction accounts for the rock mass between the reference datum (sea level) and each gravity station. It computes the attraction of an infinite slab of density and thickness z when correcting for excess material. Bouguer corrections should be subtracted from the observed gravity values for stations above sea level. The Bouguer correction is given by Equation 10.6

$$\Delta g_S = 0.1119 h \ mGal, \tag{10.6}$$

where h is the station elevation above sea level (m). N.B: A Bouguer density of 2.67 kg.m-3 was used in processing.

10.2.6 Terrain correction

In areas where there are considerable variations in elevation, a special terrain correction must be applied, as the Bouguer assumptions make no allowance for hills (excess mass) and valleys (mass deficit), locally. Figure 10.3 illustrates the Bouguer slab model for a gravity
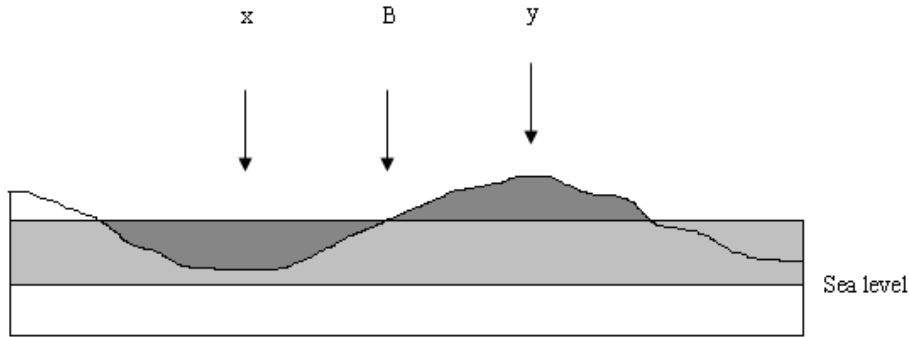
Figure 10.3: Illustration of terrain corrections required at localities x and y due to the oversimplified nature of the Bouguer correction applied at B (adapted from [11])

observation station at B. To adjust observed gravity at B to the reference datum, the effect of the mass in the slab should simply be subtracted as the topography coincides with the slab. However, at x, no rock or sediment is present as the shaded area is above the land surface. The Bouguer assumption over corrected gravity at this point as it subtracted a mass effect where no mass existed in the first place. At y, the excess mass exerts an attraction on the gravimeter mass at B. The vertical component of this attraction reduces observed gravity at B. Thus, in both x and y cases, the gravity correction factor must be added to the observed values (if stations above sea level). ([11])

The terrain corrections were computed using the Oasis Montaj software, by Geosoft. Note that the values of excess/deficit mass are calculated by using a regional correction grid of the terrain at two scales. This grid is generated from digital elevation models of the area.

10.3 Data processing

Each gravity line was processed separately, the same techniques and corrections were applied to each line using Microsoft Excel.

Three lines were fully processed:

- Gravity along the deep seismic line,

- County Road 221 in the southern area, near Poncha Springs,

- Field of Pain, line 3400.

The data from the Southern area were acquired using the LaCoste and Romberg Gravimeter. These data needed converting, the counter reading into mGal values. The CG5 Gravimeter, used on the other lines, gives the counter readings as mGal values. Once the raw data is in mGal, the first step is to apply the drift correction. This is done by subtracting the drift values from the raw data at each station. Next, the data is statically shifted, so that relative readings taken on different days are made equivalent. Then for any station where repeat

144

readings were made, an average of these is taken forward to give one value at each station. Or in the case of an anomalous reading, the repeat values are discarded. The remaining corrections can now be applied in Excel (Latitude, Free Air and Bouguer). There values are also subtracted from the observed gravity reading. Finally, the terrain corrections must be applied. These are complex and are calculated externally using the Oasis Montaj application within Geo Soft. The calculated values are exported into Excel and added to the observed gravity to give the final gravity anomaly in mGals.

10.4 Inversion results and interpretation

After all the data processing, we obtain the gravitational field. From this gravitational field, the subsurface density model can be inferred. This process is called inversion. A software called GMSYS is used to invert the gravity data. First, a geological model is built by the software and the gravitational field from this model is calculated. Second, the modeling gravitational field is compared with our processed gravitational field. Based on the comparison, the geological model is modified to fit our data better. The gravitational field from the updated model is compared with field data again to get a better geological model. The process is repeated until the modeling gravitational field satisfactorily fits the measured gravitational field.

- **Gravity on the deep seismic line**

Using the topography of the line, a layered model is produced in order to deduce the geology of the subsurface with a known range of density values assigned to each layer. The final model (fig. 10.4) fits the gravity anomaly well as the main trend towards a gravity low (eastwards) can be related to the sedimentary basin and the positive anomaly to the far East corresponds to the uplifted denser basement. Note that the model also shows a major normal fault to the West of the profile, dipping East, and this can be associated to the steeper dip on the gravity profile at the same position.

To the East of the fault the basement rock is first overlain by a thin layer of volcanic rocks and then approximately 2000m of Dry Union sediments fill the basin. To the far East of the basin there is a thickening package of Quaternary sediments, which pinches out onto the basement. These Quaternary sediments overlie a smaller, antithetic normal fault at the Eastern edge of the basin, where some shallow volcanic rocks and Dry Union sediments are seen. At the Eastern end of the profile the basement rock outcrops. The deep seismic profile showed clear fault surface and basement reflectors, which were used as the main reference surfaces for the gravity and magnetic modeling. Gravity and Magnetic data here are shown to fit the same geological model.

- **Gravity on the FOP**

The Field of Pain shows a slight increase in gravity northwards, about 3 mGal from the start to the end of the profile. This anomaly was modelled alongside the magnetic data.
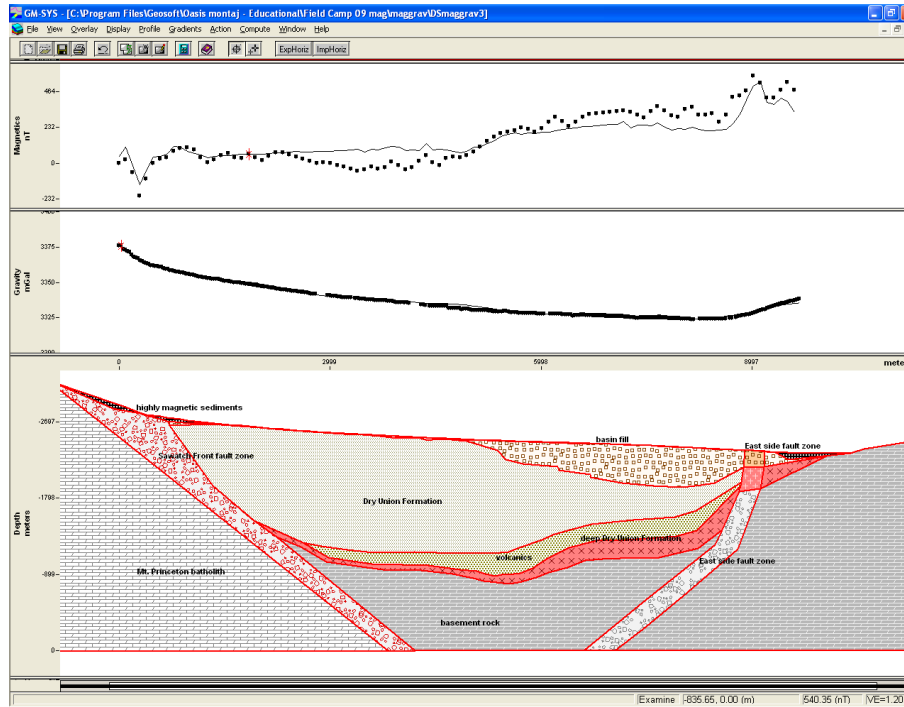
Figure 10.4: The geological model (bottom panel) from the gravity (top) and magnetic (middle) joint inversion of the deep seismic line.

The GRAVMAG model depicts a thin layer of Quaternary sediment (max. 40m) overlaying the Pre-Cambrian basement. There is also a small interpreted package of glacial till to the Northern end of the profile.

- **Gravity on the South 221**

Gravity data was taken along County Road 221 using the LNR. The data shows that there is a fault in the northeast portion of the line outcropping around 300m from the start of the line. The basement shallows towards the southwest. The line started as a joint inversion with the magnetic data, however because of time restraints, the magnetic data was not integrated. The final product only shows the geological interpretation of County Road 221 based on the gravity data collected. See Figure 10.6 for the geologic interpretation. The brown layer was interpreted to be basement rock. The bright yellow layer could be part of the Dry Union Formation, and the top layer at the surface could be Quaternary fluvial/alluvial deposits. This geological interpretation was determined with help from geological maps of the area and the expertise of Fred Burkman.

10.5 Error analysis

- **Instrument errors:**
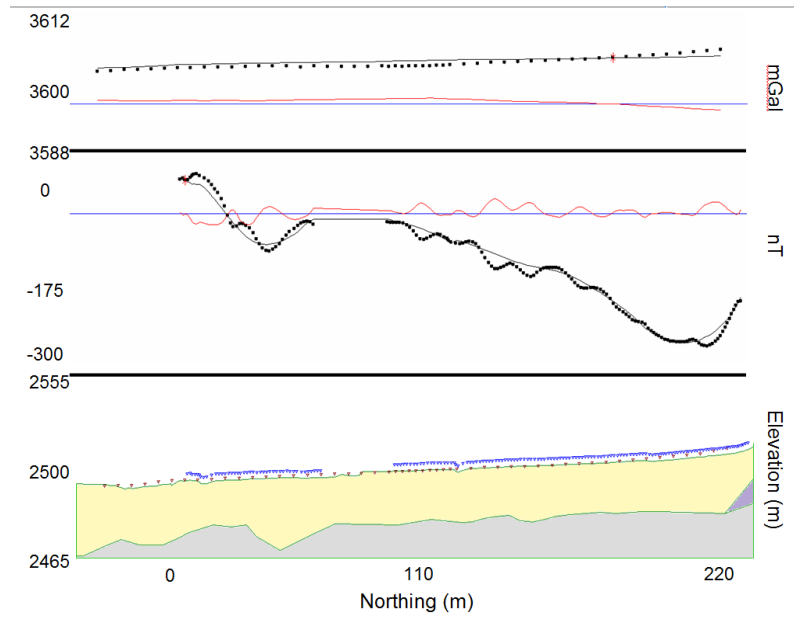
Figure 10.5: The geological model (bottom panel) from the gravity (top) and magnetic (middle) joint inversion of the line 3400 in the FOP.
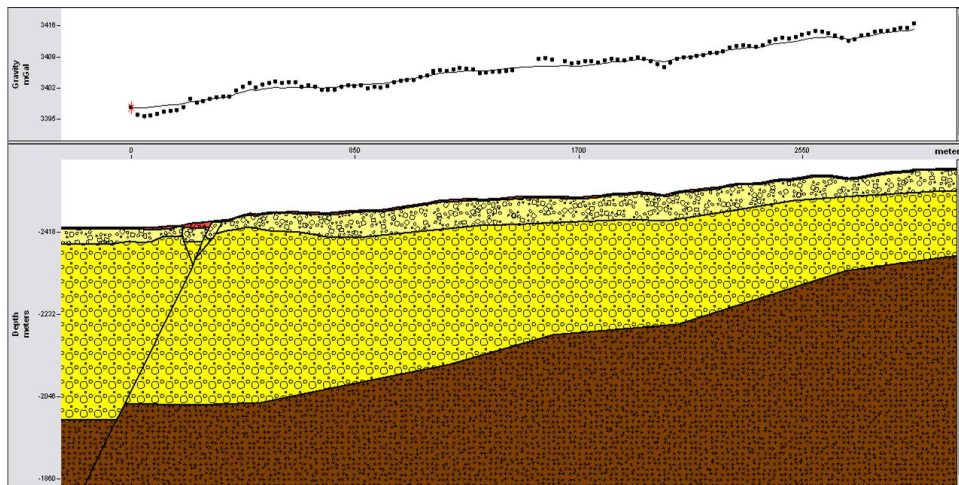
Figure 10.6: Gravity interpretation in Poncha Springs CR 221

Instrument errors are caused by varying spring relaxation times between measurements. This is compensated for through the drift correction. However this assumes a linear drift, which may not be the case. Instrument measurements may also be affected by battery life and temperature, which cannot be corrected for. Acquisition errors are mostly due to human error. These erros include leveling inaccuracies, movement during occupation time, traffic,

and looping method, and may have a major effect on the data. For example, the gravity line acquired along County Road 221 had to be specially processed in terms of drift correction because of an error in looping during acquisition. The drift correction was based on one large loop from the start to the end of the survey, which lasted 8 hours. Positioning errors are generally caused by poor GPS resolution, as a result of bad weather or insufficient satellite coverage. Resolution is poorer when using the hand held GPS rather than Differential GPS. Inaccuracies are also introduced when converting from lat/long to UTM coordinates for the hand held GPS. The coordinate conversion was made in the Oasis Montaj application within Geo Soft.

- **Processing errors:**

Latitude corrections are affected by positioning and conversion errors. However, the gravity deep seismic line runs roughly E-W so the variation in latitude may be considered as negligible. Free air and Bouguer corrections rely on elevation data at each station, which are again affected by GPS resolution. In addition, the Bouguer correction relies on an estimation of density, which was taken as constant across all the surveys, and this might not be consistent with geological observations. Terrain corrections are only as accurate as digital elevation map resolutions will allow.

- **Inversion errors:**

The quality of the data may have strong effects on the models obtained from inversion. All models are non unique but incomplete or poor datasets are more likely to lead to less accurate inversions. All layers in the models were assigned an average density from geological and well data and this does not account for anisotropy, therefore introducing more uncertainties. The fact that the geology is poorly constrained in the area, especially on the 'Field of the Pain' and the Southern area, makes modeling more difficult.

10.6   Conclusion and recommendation

The models that were derived from the previous data are not unique. However, it is believed that they are the simplest and most consistent models between the different datasets. Based on problems encountered in this years' fieldcamp, future surveys should focus on deciding upon a base station for each gravity line with a fixed looping interval in order to give a more reliable drift correction. Also, the hand held GPS should not be used if possible.

Chapter 11

Passive

11.1 Introduction

Passive seismic data refers to the recording of seismic energy generated by natural sources such as earthquakes, fluid movement, and geothermal activities. Passive seismic is also associated with the analysis of low energy waves generated by human activities in order to identify damages in pipes, or to monitor hydraulic fracturing operations. In our study, passive seismic refers to "listening" to microseismicity induced by stress changes caused by the movement of geothermal fluids. [12–16].

The Mount Princeton geothermal system is recognized as a good candidate in Colorado for an enhanced geothermal system to produce heat and electric power in the future (MIT report on Enhanced Geothermal Systems, 2006). Prior to starting and during the production process, it is necessary to have adequate knowledge of the properties of this geothermal system such as the lateral and depth extension of the heat source, fracture density and orientation and the fluid flow path. Therefore, our goal in this project is to understand the properties of the Mt. Princeton geothermal system and monitor the subsurface changes in terms of hydraulic fractures expansion and fluid flow paths. This information helps ascertain locations for water injection and steam production in future.

11.1.1 Advantages

Active seismic surveys are expensive to use in some areas, especially in terms of time-lapse acquisitions for monitoring the changes in reservoirs or geothermal systems. Also, with regards to accessibility and environmental or community concerns, using active seismic sources is not always possible. On the other hand, microseismic monitoring creates very little local surface damage and is safer to use [13]. Another advantage of using passive seismic data during the injection or extraction process is its potential to characterize the reservoir within several kilometers of the injection well [17, 18]. Therefore, it is sufficient to install receivers and listen to natural seismic activity.

11.1.2 Passive Seismic Applications

Passive seismic techniques have been used in many different types of surveys. For example, they have been used in mining to detect the impending mine collapse [19]. Passive seismic monitoring of the hydraulic fracturing process for enhanced recovery of oil and gas is also becoming more popular [12, 16, 20–28]. Shapiro et al. (2004) used the kinematic and dynamic signature of induced microseismicity to characterize the hydraulic fracture properties in Cotton Valley Field, East Texas. Shell corporation has conducted a monitoring project in the Peace River heavy oil production zone, Northwest Alberta, Canada using microseismic data [22] Their study has provided valuable understanding of the movement of steam and bitumen in the reservoir. Eisner et al. (2006) used microseismic data to monitor hydraulic fractures in Canyon Sand formation, West Texas, which is a study that is similar to the one taking place in the Upper Arkansas Valley, CO.

The passive seismic methods can be useful in reservoir characterization and monitoring. Eisner et al. (2006) suggest that microseismic events with similar mechanisms can be used to identify fracture characteristics. During injection, the high pressure fluid injected into the reservoir, opens fractures and increases the permeability. Monitoring the permeability changes can be useful in production management for determining the proper location and depth of production wells [24]. In addition, microseismicity resulting from fracture extension can be used to understand fracture orientation and depth, and ascertain the presence of fluids.

Geothermal Field

Basil, Switzerland has one of the biggest potential sources for geothermal energy in Europe [29]. This geothermal system is used for heating and generating electric power. Kumano et al. (2007) analyzed the microseismic data acquired during hydraulic stimulation and they recognized that the extension of the microseismic distribution was consistent with hydraulic injection. Kedar and Kanamori (1998) used the bubble collapse as a source of passive seismic in Old Faithful Geyser, Yellowstone. They concluded that the number of bubble collapse signals depends on the heat and hot water pressure and is controlled by the geometry of the conduit. Romero et al. (1994) evaluated the micro-earthquake data in the Geysers geothermal field, California for monitoring fluid flow during injection within the reservoir. They concluded that continuous monitoring of passive seismic can be a useful reservoir management tool. Feng and Lees (1998) studied the microseismic data in the Coso geothermal field, Eastern California. They found a direct correlation between the microseismicity and fluid circulation in the geothermal system.

11.2 Data Acquisition

11.2.1 Station Locations

Acquiring the data for the passive seismic experiment required installing several passive seismic instruments through out Dear Valley, CO. The first step in acquiring the data was to determine what the best locations for the stations would be. It was important to find locations that would be low in anthropogenic interference, for example, moving vehicles, foot traffic, household noises, and vandalism. It was also important to consider the natural environmental factors that may affect the seismic instruments, such as noise created by surface water flow and animals moving near the stations. The ability to keep the instruments dry was also of upmost importance, due to the fact that the instruments would not record data properly when wet. In order to ensure the instruments would remain dry, they were packed in large plastic bags and placed at locations that were away from natural water drainages. Additionally, it was important to find a location that would receive an adequate amount of direct sunlight for the solar panels in order to provide power to the data acquisition system.
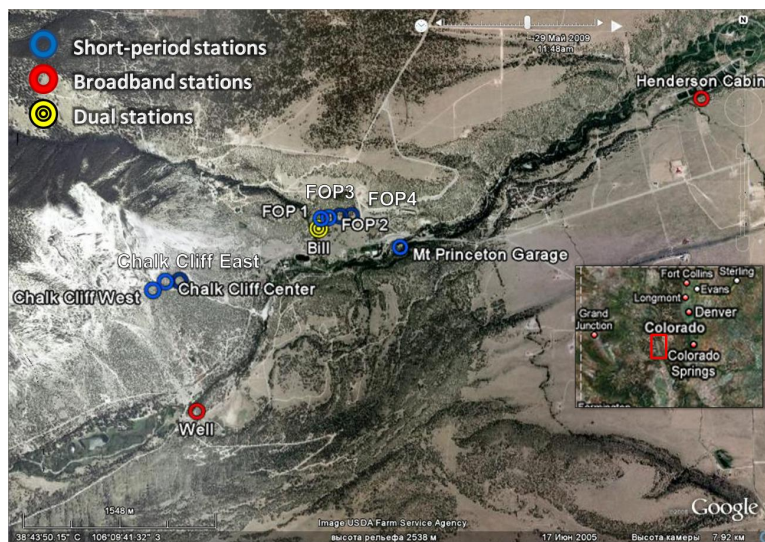
Figure 11.1: Map of the seismic stations used in the passive seismic survey, Deer Valley, CO.

Geological features were also considered when replacing the stations. For example, the Chalk Cliffs area was selected because it considered to be above the shear zone created by the fault system. Lastly, all locations were selected considering the property permits or permission and the safety of the equipment. Ultimately, the locations of thirteen stations were chosen based on these criteria. Please refer to Figure 11.1 for a map of the station locations selected for this passive seismic experiment.

11.2.2 Equipment Used

The equipment used to acquire the passive seismic data was provided by the Incorporated Research Institutions for Seismology (IRIS) PASSCAL Instrument Center. The primary equipment used to acquire the data included two types of seismometers, a Gurlan CMG-3T broadband instrument(see Figure 11.2(a)) and a Mark Products L22 short period instrument (Figure 11.2(b)).

(a) **Image of the Gurlan CMG-3T broadband instrument. Three of these instruments were used for the passive seismic survey.**

(b) **Image of the Mark Products L22 short period instrument. Nine of these instruments were used for the passive seismic survey.**

The main difference between the two types of sensors, broadband and short period, is the range of frequencies that each one can record. Broadband recorders are much more sensitive and exhibit a higher response to small perturbations. Thus, broadband sensors record lower frequencies than short period sensors. This is particularly important in that microseismic events generally represent low frequencies. Also used in this experiment were Reftek RT130 data acquisition systems (DAS), solar panels, batteries, power boxes, global positioning systems and a hand-held personal digital assistant (PDA).

The solar panel and batteries were attached to the power boxes which allowed the Reftek to be powered consistently by one of the two sources. The Reftek RT130s were instruments with 3-channel digitizers that were used to physically record the data acquired by the seismometers. Each Reftek held two removable and replaceable 2GB memory disks where the data was stored until retrieved by a person involved in the experiment. The PDA was used to communicate with the DAS by sending the desired data acquisition configurations. The global positioning systems were used to determine the exact time that the stations were recording. Ensuring the stations were consistent in the time they displayed would allow the recorded events to be examined across all the stations, a step that would be of great importance later in our data processing procedures.

11.2.3   Installation Procedures

Before beginning formal installation of the passive seismic stations, the broadband instruments were put in a huddle test in order to do a preliminary examination of the data they would record. The huddle test included setting up all three instruments in the basement of a building where there was little foot traffic, especially during the evening and early morning hours. It was soon found that the broadband instruments were far too sensitive for a huddle test environment. The data they recorded showed strong signs of the mass within the instrument drifting. This was determined because of the temperature fluctuations above the surface of the Earth, where the broadband instruments are too sensitive to adjust to. According to the IRIS PASSCAL Instrument Center, the broadband instruments were most steady when the experienced less than one degree Celsius of temperature fluctuation throughout a 24 hour period. It was then decided that the huddle test was an inadequate test for the broadband instruments and that they would be best tested below the surface.

The first step in the installation process was to dig a hole deep enough to allow the top of the seismometer to be about one foot below the surface of the ground and narrow enough to keep the sensor stable once buried, which was generally a little more than one foot in diameter. Before burying the sensor, it was important to level the sensor and align it to magnetic north. Once the sensor was placed in the appropriate position, the serial number was recorded for future reference and the cables between the power box, the DAS, the solar panel, and the sensor were connected. The sensor was then ready to be carefully buried.

The next phase of installation included configuring the DAS to follow specified parameters of acquisition, which was done using the PDA. Through use of the PDA, the sample rate could be selected. Though there was some experimenting with determining the sample rate that would be used for acquiring the passive seismic data, it was ultimately decided that a sample rate of 100Hz would allow the instrument to acquire data for 30 days without being serviced. An image of a fully installed passive seismic station can be seen in Figure 11.2.

One of the primary differences in the installation procedures for the 3T and L22 was that the 3T records data using a mass that must be locked when the station is not acquiring data in order to avoid damage. Before beginning data acquisition, the mass was unlocked and centered to ensure accurate data retrieval. The L22 does not require the step of unlocking its mass. Once the stations were oriented, buried, connected, and configured they were ready to begin data acquisition. Refer to Figure 11.3 for times of data acquisition for the passive seismic stations.

11.2.4   Servicing/Retrieving Data

For the first two weeks of data acquisition the stations were serviced at least once in order to to ensure the data was acceptable. In order to service the stations data acquisition was stopped and the disks that the data had been recorded on within the DAS were switched

Figure 11.2: Image of a fully installed passive seismic instrument. This station is located at the Henderson Cabin in Deer Valley, CO

with new disks. The parameters of the stations were rechecked to make sure the station was once again ready for data retrieval. Then, data acquisition was restarted. The disks with data stored on them were then ready to be downloaded onto a computer with the necessary software and converted into the most appropriate formats. Once the stations have retrieved enough data to fulfill the goal of the experiment they are disassembled and returned to the IRIS PASSCALL Instrument Center. Currently, the plan is to continue recording passive seismic data in Dear Valley, CO until September, 2009.
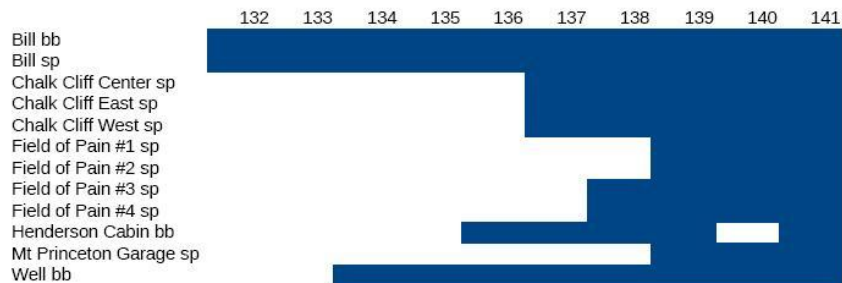
Figure 11.3: This table shows the days that the passive seismic instrument were recording data while the field camp team was at Deer Valley, CO. All of the stations ran through June 3, 2009 and all of the stations but the FOP stations will run until September 2009.

11.3   Data Analysis

11.3.1   Introduction

Similar to conventional geophones, the passive seismic sensors used in this study measured particle velocity. The seismometers were multicomponent devices and measured particle velocity in three different directions. Energy induced by the source travels in the form of waves which that excite particles in different directions. This results in the movement of the magnet relative to the coil and generates a voltage value proportional to the velocity of the particle. Figure 11.4 shows one minute of recorded data at the Chalk Cliff West station.
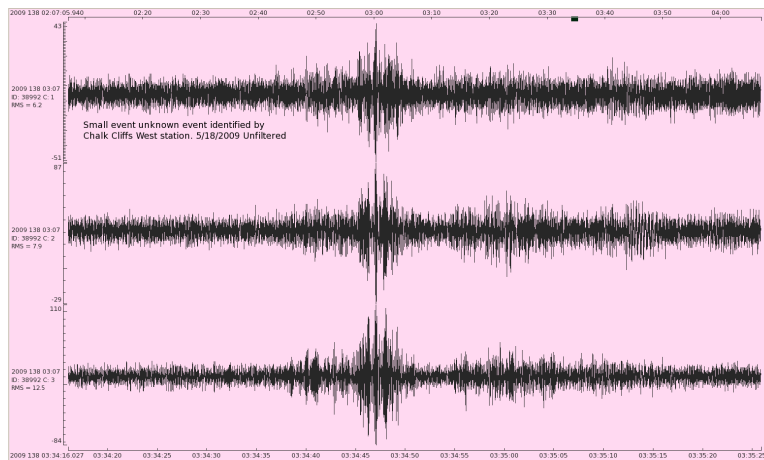
Figure 11.4: Sample of the data retrieved by the Chalk Cliff Center short period instrument. Channel 1 indicates the vertical component, Channel 2 indicates the North-South component and Channel 3 indicates the East-West component.

Each direction is showed as an individual trace; channel 1 measures the particle velocity in the vertical direction, channel 2 in the north   south direction and channel 3 in the east   west direction. The difference on the strength of some events relative to others is an indication of different types of sources and is one of the parameters used to interpret the data.

As mentioned above, the broadband and short period sensors are designed to record different frequency ranges. Figure 11.5 shows the difference in the data recorded by a short period sensor and a broadband sensor, at the same location and time.

From the figure it is clear that the short period sensor does not show any response for the low frequency event. Moreover, looking at the amplitude scale of broadband sensor versus the short period sensor, it is evident that the sensors record data very differently. For instance, the broadband recording shown in Figure 11.5 is an entire magnitude greater than the short period recording.
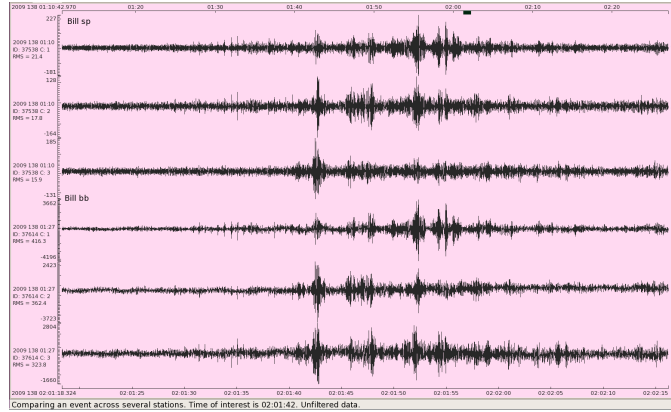
Figure 11.5: Sample of the differences in data retrieved by the broadband and short period instruments. Note the difference in the scale of the amplitude between the two instruments.

From the seismic data we can also plot the amplitude spectra. The amplitude spectrum shows the frequency content at each amplitude value and is a useful way to see the frequency content of specific events. As mentioned above, in broadband sensors most of the energy is confined at low frequencies compared to the short period sensor. By examining the frequency spectra it is possible to determine the type of filter that may be helpful in analyzing the data. An example of an amplitude spectra can be seen in Figure 11.6.
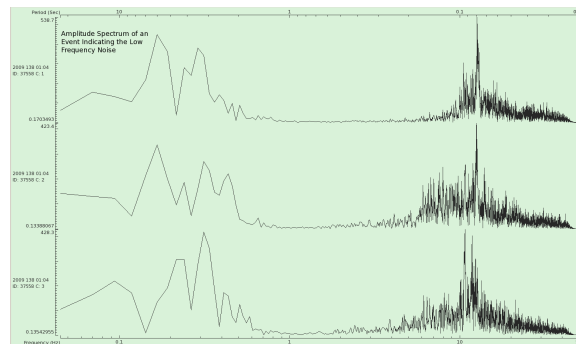
Figure 11.6: Sample of the amplitude spectra of the three components of the passive seismic recordings. Examining these amplitude spectra may lead to the determination of a suitable filter.

11.3.2   Software Used

The software used to process and analyze the data was PASSCAL Quick Look (PQL II) provided by IRIS. The data is analyzed as a function of time. All the recorded data was separated in files of one hour. The best characteristic of PQL is its display options. Different channels at different locations and times can be displayed in the same screen, which offers

the possibility to correlate events for different locations in a fast and easy way. Moreover, PQL zoom options allow the visualization of the data on ranges of time from one hour length to 0.1 seconds length. It also produces the amplitude spectra of any specific time range. On the other hand, PQL offers the possibility to generate and apply bandpass, high pass and low pass filters.

11.3.3   Validating the Data

As the aim of data acquisition was to detect microseismic activity of hydrothermal flow, the processing workflow was targeted to try to identify any microseismic events, if possible. A first look at the data showed a significant quantity of events. In order to determine the reliability of the recordings some earthquakes were tracked at each station. This is helpful in that the time of occurrence and location of the earthquake are known. It is possible to approximate the arrival times of the P and S waves generated by the earthquake at the stations. Figure 11.7 shows a recorded earthquake of magnitude 4.7 that occurred in the Greater Los Angeles area, CA, on May 18, 2009 at 03:39 GMT, according to the United States Geological Survey [30].
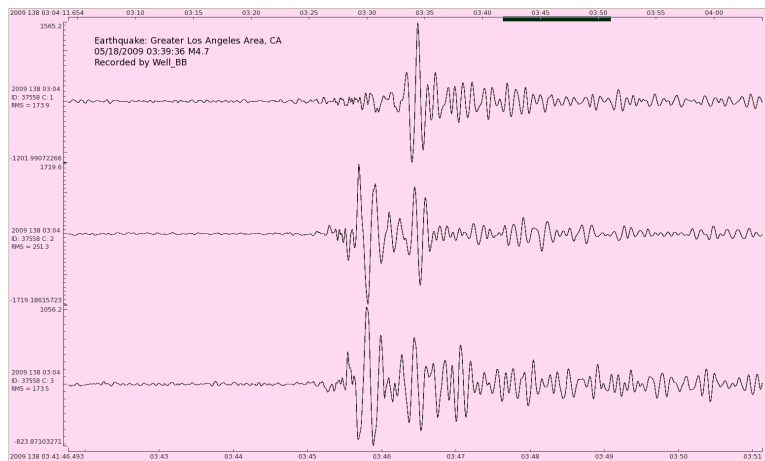
Figure 11.7: Sample of a recorded earthquake. This earthquake was of magnitude 4.7 and occured in the Greater Los Angeles area, CA, on May 18, 2009 at 03:39 GMT.

The California earthquake was identified on all 13 stations at similar times. Different filtering was applied to the data in order to recognize the earthquake arrivals at the stations. By using the Jeffrey-Bullen travel time tables [31], the assumed P and S wave arrival difference can be estimated in order to determine if the signals are infact the earthquake in interest. In addition, different amplitudes of P and S wave arrivals in three components can give an idea of the directions of the arrived waves.

This earthquake example illustrates the frequency response difference between broadband and short period sensors. Using the spectra of the California earthquake, filters were

designed in order to better image the broadband and short-period responses. Examples of the spectra for the California earthquake at Bill's broadband station can be seen in Figure 11.8.
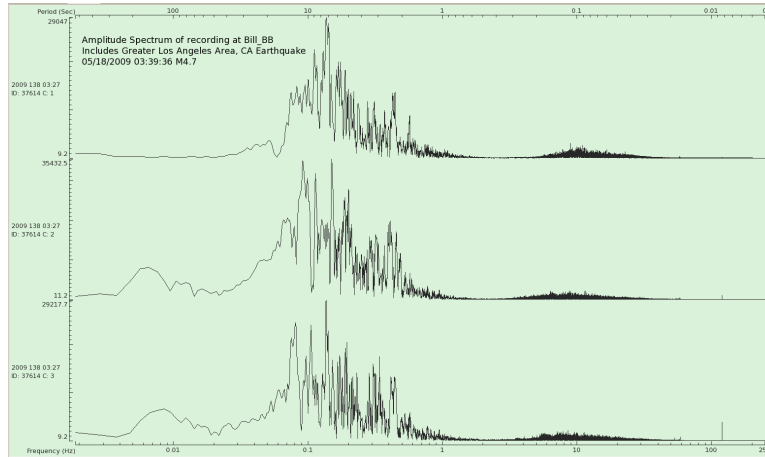
Figure 11.8: Sample of the amplitude spectrum of the recorded California earthquake that occured on May 18, 2009

11.3.4   Identifying Unknown Events

The primary purpose of this experiment was to identify unknown events. In order to do this, it was important to first eliminate known events such as signals from the active seismic surveys and noise from anthropogenic and animal interference. These surveys occurred throughout the duration of the field camp. For example, Figure 11.9 illustrates the vibroseis sweeps being conducted on the Field of Pain while Figure 11.10 illustrates the hammer blows conducted by the VSP group.

Looking at the night data, we can refer to unknown events as possible microseismic activities. Because these event occurred during the night they could not be sweeps and do not correspond to any of the significant earthquakes identified by the USGS.

The frequency contents of some of these unknown events are recognized to be in the range of 1-10Hz which corresponds to the frequency content of most microseismic events. For example, Figure 11.11. These events have lower amplitude and higher frequency content relative to those for earthquakes and vibrosies sweeps.

However, any assumption may result in the loss of valuable data. Thus, initially the data was analyzed and interpreted unprocessed and included two main points. First, the data was analyzed at different times to get the idea of noise content in the traces. Data acquired during daytime, particularly 9am-6pm, contained vibroseis sweeps, VSP hammer blows and other types of anthropogenic interference. Data acquired during the night hours
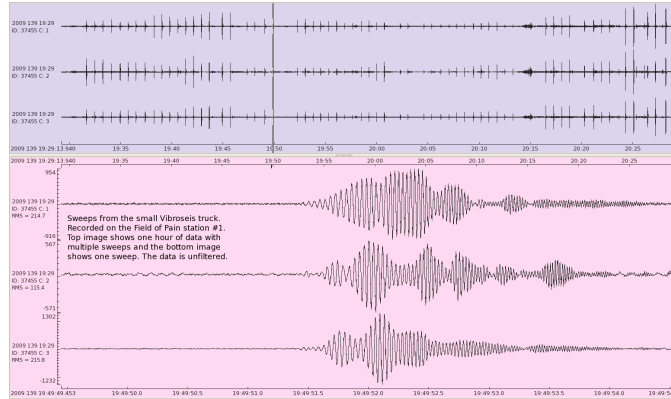
Figure 11.9: Sample of the vibroseis sweep signals collected by the passive seismic instruments
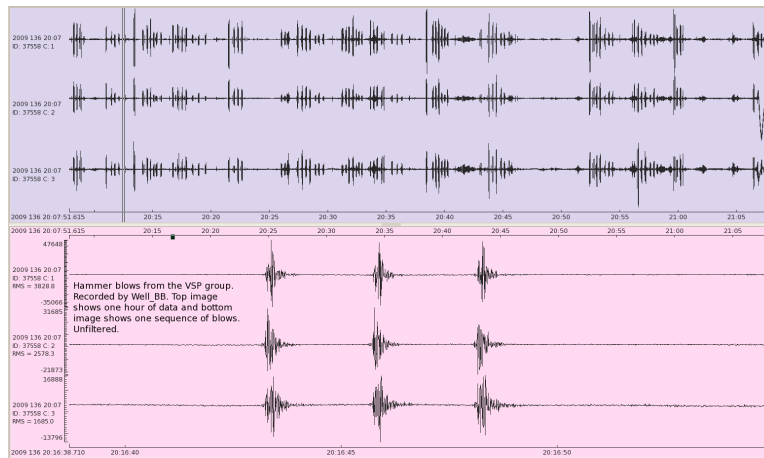
Figure 11.10: Sample of the VSP hammer blows signals collected by the passive seismic instruments.

have the least amount of surface noise. Second, events were identified, when possible, by tracking them through different stations and looking at their frequency spectra. An event was considered of interest if it were seen clearly in all the stations at the same recording time. This included the creation of an events database. This method reduced the possibility of picking noise as valuable data, considering that in certain cases some of the noise was random and not correlated in all the stations.

Once it was clear that the stations were collecting similar events at similar times, the next step included attempting to identify events that could not be classified as documented earthquakes, VSP hammer blows, vibroseis sweeps, anthropogenic noise, or animal noise. Identifying these unknown events would allow the passive seismic research team to better understand whether or not there were microseismic events related to the geothermal system present in the area. An example of the unknown events that were identified can be seen in
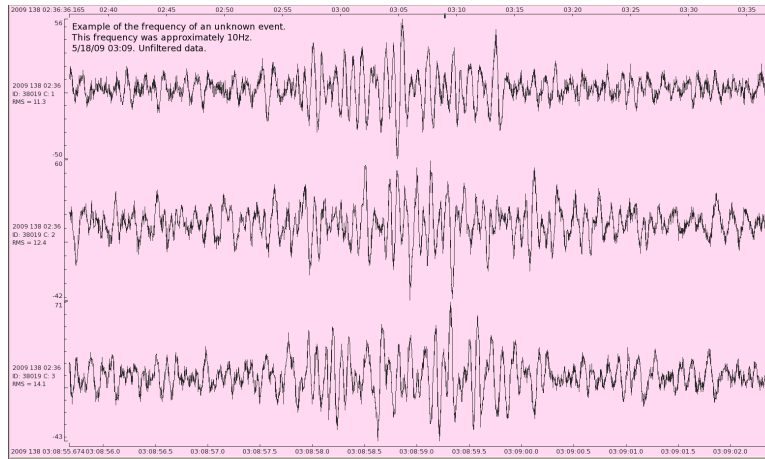
Figure 11.11: Sample of the frequency of one of the unknown events that was identified. The frequency was approximately 10Hz

Figure 11.12.
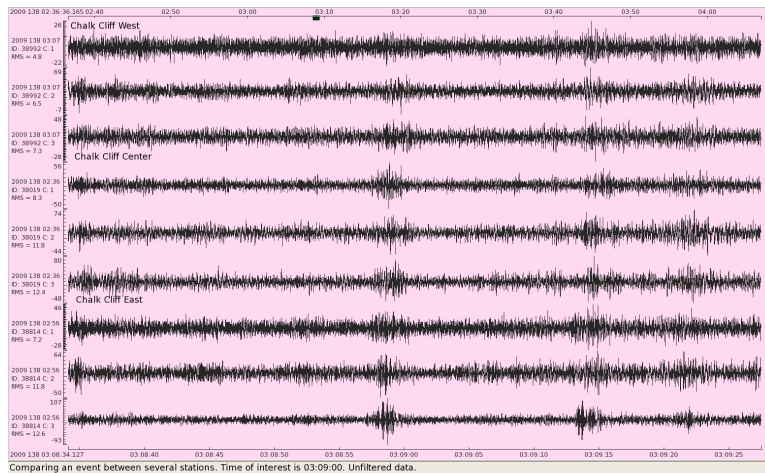
Figure 11.12: Sample of an unknown event. The event was recorded by all seven stations that were closely analyzed. This leads to the possibility of this event being microseismic and related to the geothermal system.

In particular, one evening of data recorded by seven stations was closely analyzed and ten different events were identified in most the passive seismic stations. More specifically, two events were detected by all the passive stations, five events were detected by five stations, and three events were detected by four stations. This shows that there are unknown events that are identifiable throughout many or all of the stations, which may indicate local, low magnitude events. Table 11.1 shows which unknown events were identified at each stations and their approximated arrival times.

160

Estimated Time (GMT)	Number of Sensors	Chalk Cliff West	Chalk Cliff Center	Chalk Cliff East	Bill SP	Bill BB	Well BB	Henderson BB
02:01:42	6	02:01:55	02:01:55	02:01:55	unclear	unclear	02:01:56	-
03:04:45	6	03:04:45	03:04:45	03:04:45	03:04:45	03:04:45	03:04:44	03:04:44
03:07:30	7	03:07:33	03:07:33	03:07:33	03:07:30	03:07:30	03:07:30	-
03:09:00	6	03:08:59	03:08:59	03:08:59	03:09:00	03:09:00	03:08:59	03:08:59
05:28:40	7	05:28:42	05:28:42	05:28:42	-	-	05:28:42	-
06:13:55	7	06:13:57	06:13:57	06:13:57	06:13:59	06:13:59	06:13:59	-
12:29:05	6	12:29:06	12:29:06	12:29:06	-	-	12:29:05	-
12:36:45	7	12:36:46	12:36:47	12:36:27	12:36:46	12:36:46	12:36:46	-
12:40:18	7	12:40:17	12:40:17	12:40:17	12:40:15	12:40:15	12:40:15	-
12:43:28	6	12:43:27	12:43:27	12:43:27	12:43:28	12:43:28	12:43:27	-

Table 11.1: Identified unknown events for day 138 by time and station. Two unknwon events were identified across all seven stations that were analyzed

Though it cannot be determined that these identified events are microseismic, it is a possibility and future research may indicate a passive source for these events.

11.4 Conclusions and Further Suggested Studies

Although the purpose for including the passive seismic project in the field camp 2009 for the first time was mostly to test the feasibility of acquiring data, the preliminary results confirm that passive seismic methods may be promising to detect the geothermal activities. As shown in the data analysis, there are several unknown events which are correlated between most of the stations. We still do not know about the nature of these unknown events. But what we know is that they are not the possible noises that are recorded at the stations or any human activities around the study area. Also, their frequency content potentially corresponds to the frequency content of some microseismic events [32]. Determining the frequency of microseismic events near Mt. Princeton, CO will require further research.

For future studies, it is worthwhile to apply accurate processing methods in order to identify the characteristics of microseismic events related to geothermal activities. For example, there are a few softwares, such as HYPOINVERSE, to identify the locations of the microseismic events. Some recent methods for identifying the microseismic events and locating them are time reversal inversion methods [33]. Identifying the arrival times and locations of the microseismic events is critical for answering the important questions such as:

- Does Mt. Princeton geothermal system create microseismicity?

- Can the microseismicity be used to find the properties of induced fractures?

- Can microseismicity help us understand the fault structures?

The proper answers to above questions can be very important step toward characterizing the Mount Princeton geothermal system.

Chapter 12

Method Integration

12.1 Introduction

Several surveys were conducted at three main locations across the Upper Arkansas Valley and the Chalk Creek Valley. Individually they provide useful information about the different geological features and processes present in the area. However, each technique is subjected to uncertainties and errors related to the measurements and equipments. Moreover, some surveys such as DC resistivity, magnetics and gravity, exhibit anomalies across considerable areas and, in the qualitative analysis, are difficult to interpret.

On the other hand, seismic techniques offer an approximate image of the subsurface and may reach significant depths. Issues related to the acquisition and processing of the data may result in a poor image and the information that this may provide depends on the knowledge and the geo-imagination of the interpreter.

Each technique relies on different parameters, which can be related, and frequently are affected by the same geological phenomena. Thus, anomalies present in one survey can be interpreted alongside anomalies present in other surveys. Alone, a survey may not represent an anomaly but when compared with another could show similar features.

In order to obtain a more accurate interpretation of the geological features and processes at the three different locations, different surveys were analyzed together.

12.2 Deep Seismic Line

Two deep seismic lines were shot in the North-South and West-East directions across and along the Arkansas Valley to the north of Chalk Creek. Gravity and magnetic surveys conducted on W-E deep seismic line were aimed to complement the seismic data to concise interpretation of the target Figure 12.1.
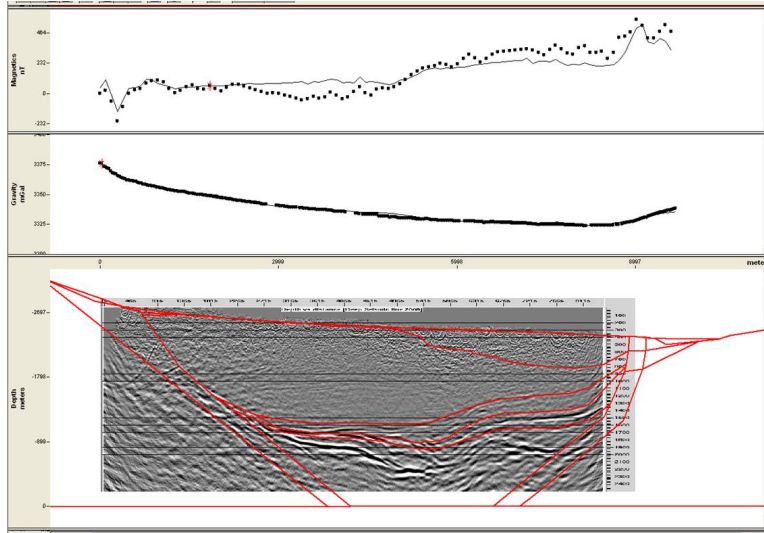
Figure 12.1: Integrated model derived from seismic, gravity and magnetic surveys along W-E Deep Seismic line.

Gravity and magnetics picked up a strong signal from the Sawatch fault, which is a major fault at the west side of the basin, which is corroborated by the geological maps of the area [34]. This create a western margin of the basin and are the controlling faults of the basin rift system.

Deep seismic, magnetics and gravity agree on having a response from a high density and magnetic susceptibility zone, where there is presence of Precambrian basement, lava flow and the Dry Union Formation. The geologic cross-section parallel to the W-E line 12.1 shows a nearly vertical fault zone leading to a prediction of shearing and faulting with no evidence at the surface.
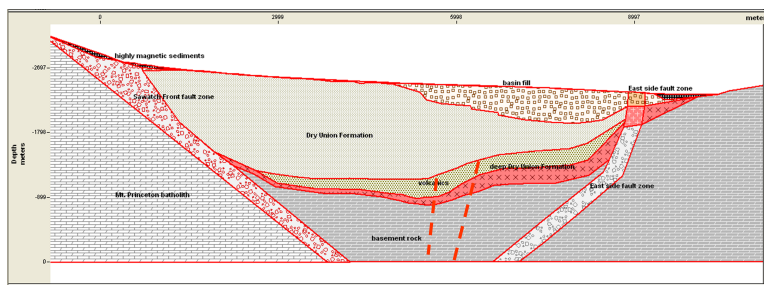
Figure 12.2: Final geological cross-section of the W-E Deep Seismic line

The shear zone, the dashed lines on Figure 12.2, is possibly one of the Precambrian fault systems of the northeast trend, suggested by Ogden Tweto, rather than part of the opposite side of the rift system. These shear zones are nearly vertical and the fold axes associated with them suggest predominant strike-slip movements, which in this case were the result of

163

both Laramide compression and Neogene extension periods which formed the basin [35]. The trajectories of these shear zone faults can be derived by connecting the northeast-trending valleys within the west Sawatch range with those in the east (e.g. Chalk Creek and Trout Creek).

However, Direct Current resistivity measurements, made southwest of the intersection point between S-N and W-E deep seismic lines, extrapolate a Chalk Cliff shear zone that could be extended all the way to the point of intersection Figure 12.3.
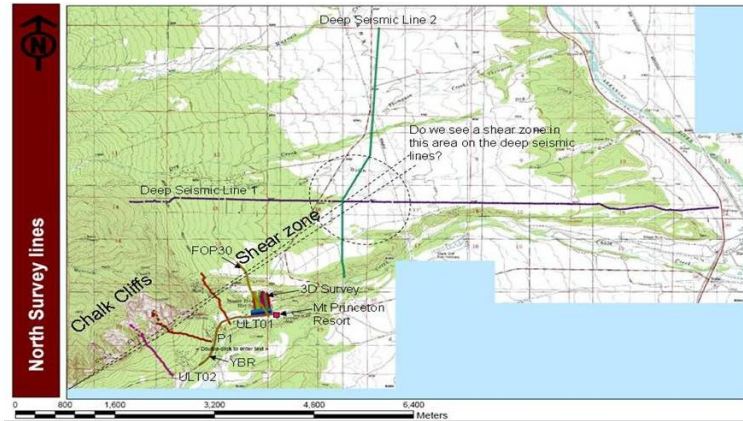
Figure 12.3: Topographic Map showing the shear zone identified at Mt Princeton/Chalk Cliff extrapolated to the Deep Seismic line

A little further East there is a nearly perfect correlation of the boundaries between different layers, where the volcanic lava is lined up, and for the boundary between the lava and the Dry Union. However, there is no correlation between the boundary of the Dry Union and the alluvium, which may be the result of large boulders falling from the mountains and being burried near the surface with the composition of basement rocks, thus giving a high amplitude magnetic signal. Two smaller faults at the East end of the seismic profile are identified and the correlation is nearly perfect, matching the surrounding geology.

12.3   Field of Pain

The techniques used at the Field of Pain were 3D seismic, gravity, magnetics, VSP, DC resistivity, SP and passive seismic. The latter three techniques extend to other areas of the Chalk Cliff Valley. The seismic line shows an unconsolidated overburden section approximately 40 to 50 meters thick with a velocity ranging from 900 to 1100 $\frac{m}{s}$, and an underlying fractured, altered granitic basement section with a velocity ranging from 4000 to 4500 $\frac{m}{s}$. This correlates with the gravity and magnetic data which also shows a two layer model with an overburden density of 1800 $\frac{kg}{m^3}$, and an underlying basement density of 2970 $\frac{kg}{m^3}$.

The VSP data from the Frontier Ranch shows a three layer model with the unconsolidated sediment approximately 30m thick overlying a 75m thick layer of velocity $1,250\frac{m}{s}$, and 160m of a layer of velocity $2000\frac{m}{s}$. Frontier ranch is approximately 245m higher than the Field of Pain which possibly accounts for the extra 235m of sediment present in the VSP model. Also the VSP survey is at a considerable distance from the seismic, gravity and magnetic surveys. Thus basement rock is expected below the third layer identified by the VSP survey.

SP and DC lines across the Field of Pain are consistent and there appears to be a good correlation between the two different data types. The DC profile shows a deep geothermal anomaly of low resistivity which correlates well with the SP profile which has a pronounced anomaly in the same region. Also the resistivity profile shows a well defined anomaly to the north. Also this low resistivity anomaly suggests denser sediments of lower permeability which is also seen on the north side of the gravity profile.
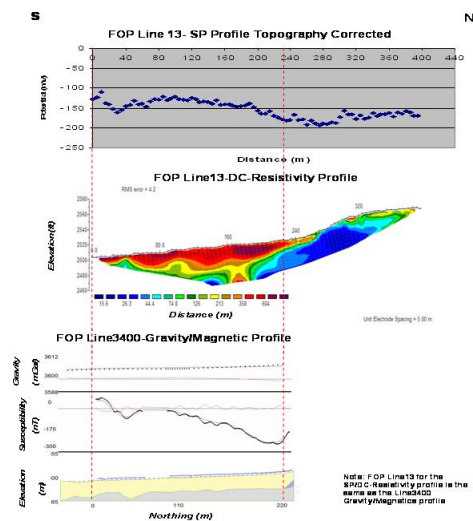
Figure 12.4: SP, DC-Resistivity and Gravity/Magnetic Profiles from the Field of Pain

12.4 Chalk Creek Valley

The DC resistivity data shows an anomaly along the long line P1 which extends to the base of the Chalk Cliffs. This anomaly is a low resistivity zone interpreted to be the shear zone created by the movement of the active fault system. The low resistivity response could be due to three different factors; the presence of water, fractured granite, or high clay volumes. However, the SP data obtained for the same lines show a positive response in the same area where the shear zone is considered to be present which is a direct indication of the water.
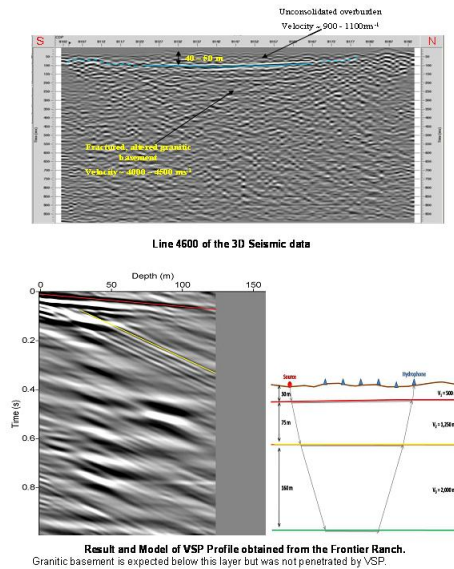
Figure 12.5: Line 4600 of the 3D seismic data and VSP profile from the Frontier Ranch

The temperature plot shows that the south side of the shear zone has a high temperature while the north side of it has a low or dropping temperature trend. One side is hotter than the other and this may be explained by the fact that hot water is flowing up the fractures and is moving to the area of shear zone on the south side. Moreover, passive seismic sensors recorded a series of events which were identified as possible microseismic events after analysis. It is assumed that the flow of water weakens the rocks in the shear zone and creates fractures that might be recorded by the passive seismic sensors.

12.5   South Side

Our south site consisted of lines along County Road 221, Highway 285, and an area south of Poncha Springs. Though there is a low amount of data collected, relative to our north site, there has been a lot of information received.

The magnetic and electromagnetic data collected along County Road 221 shows trends where a change in lithology occurs, changing from the Dry Union formation to a smaller formation only found in the upper Arkansas valley. The boundary between the two units runs along the road because the units show up alternatively as indicated by the green dotted lines in Figure 12.7.

Another magnetic line that ran from Highway 285 up to the Boy Scout Camp had data that produced some interesting results. Along this profile a gradual change from a low response to a higher response occurs, this correlates well with the USGS data collected in the area. But the aeromagnetic data does not have the sensitivity to see the fault and change in rock type that occurred along the line, as shown by the anomalies in the data. The data
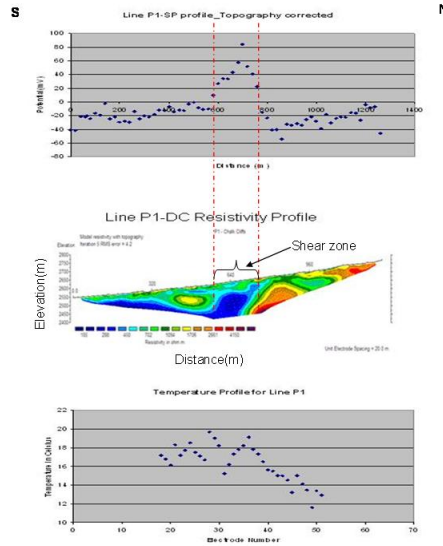
Figure 12.6: SP, DC-Resistivity profile for Line P1 extending to the chalk cliff
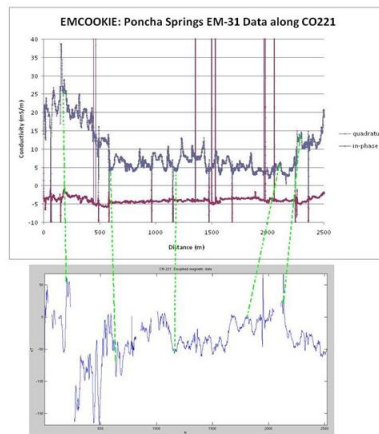
Figure 12.7: Magnetic correlation

is displayed in the figure below, with comments pointing out where the anomalies occurred.

The DC and SP data taken in the area around the Boy Scout Camp reveals how the hot water is distributed in the subsurface as shown by the high conductivity zones, or blue zones, in the DC profiles. The results are confirmed by the hot water shows at the surface that correlates well with the data taken along lines 100, 200, 300, and 1000. The figure below is the profile for line 200 the results show the hot water zones as mentioned earlier.

Though the results are still preliminary, the potential of what we could find out with

167
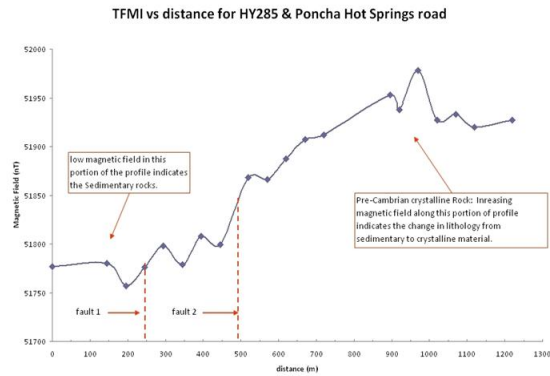
Figure 12.8: South site magnetic profile.
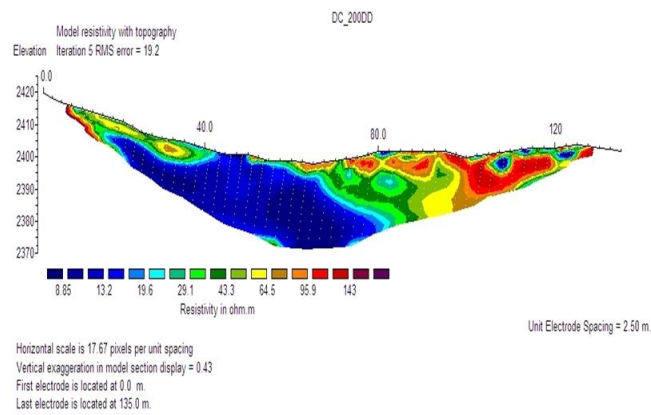
Figure 12.9: South site contour DC contour.

more data is very exciting. By collecting more data it may be possible to explain the local geology, complex faulting, and water table in the area.

12.6 Conclusions

In terms of geological interpretation, the integrated results suggest a two layer model with unconsolidated sedimentary rocks sitting on top of fractured granitic basement. This model was supported with all the geophysical methods used apart from the SP profile. The final model suggests an unconsolidated overburden section approximately 40 to 50 meters thick with a velocity ranging from 900 to 1100 $\frac{m}{s}s$, and an underlying fractured, altered granitic basement section with a velocity ranging from 4000 to 4500 $\frac{m}{s}$. The DC profile shows a deep geothermal anomaly of low resistivity which correlates well with the SP profile which has a pronounced anomaly in the same region.

The integrated results suggest the occurrence of a shear zone which extends from the north east to the south west running to the north far side of Mr Long's field, (also known as the Field of Pain) and extend just below the base of the Chalk Cliffs. The data also suggest an upward migration of the water through the fault system and then flowing along the porous sediments towards the South.

The data collected from the south site at Poncha Springs identified hot water distribution in the subsurface as shown by the high conductivity zones in EM data and low resistivity results in the DC profiles. According to the magnetic data which shows the change in lithology it is assumed that the fault exists near the Boy Scout camp and it is identified as a potential hot water source.

The main target of W-E line and N-S were to determine the depth to the basement, which was identified to be approximately 2000m. Two major faults were interpreted on West end as well as two minors at the East end of the cross-section. This study also aided in proving the existence of other major features such as alteration zone in between the faults and the possible Precambrian shear zone of a Northeast trend. Last, it was possible to determine approximate boundaries between some major layers that comprise the subsurface of the Upper Arkansas Valley.

Chapter 13

Future Planning

Incorporating previous years data as well as expert advice into the findings of the 2009 field camp, a plan for future projects in the Arkansas Valley has been developed. This section of the report is intended to be used as an advisory reference, in conjunction with the desires of sponsors, local councils and academic programs, for future survey proposals.

The Arkansas Valley has undergone extensive geophysical investigation in the past and it is believed that 2010 will be the final stage in the investigation carried out by the CSM. To that end, the 2010 field camp will be used to help tie together all currently available data and aim to solve a number of questions on the geology and hydrothermal potential of the region that remain unanswered.

Two deep seismic surveys could be conducted in 2010. The areas recommended for surveying are a North-South line on highway 221 (west of Salida) and an approximately North-South line to tie in with the 2006 and 2009 West-East seismic surveys (See Figure 13.1). The survey on highway 221 will be aimed at resolving the sub-surface geology of the southern section of the basin and allowing a tie to be made with the southern 2007 line. The northern survey would help resolve the anomaly detected on the 2009 West-East seismic data set. It is suggested that this site is the most suitable location for a well to be drilled as this would confirm the geological structure below the surface as well as give an accurate depth to basement rock value. Each survey can be approximately 8km in length, so the acquisition can be conducted within a one week period.

The 2009 results also confirm the presence of a rift running from the south-west to the north-east through Mt. Princeton. Further DC/SP lines to the west of those taken in 2009 and running perpendicular to the predicted rift direction into the valley would allow accurate modeling of the structure. This data will also tie in with the 2009 deep seismic line as well as the proposed 2010 northern line (see Figure 13.1).

To the East of the proposed 2010 southern deep seismic line is the relatively unknown area of Poncha Springs. Preliminary investigation of this area was carried out in the 2009
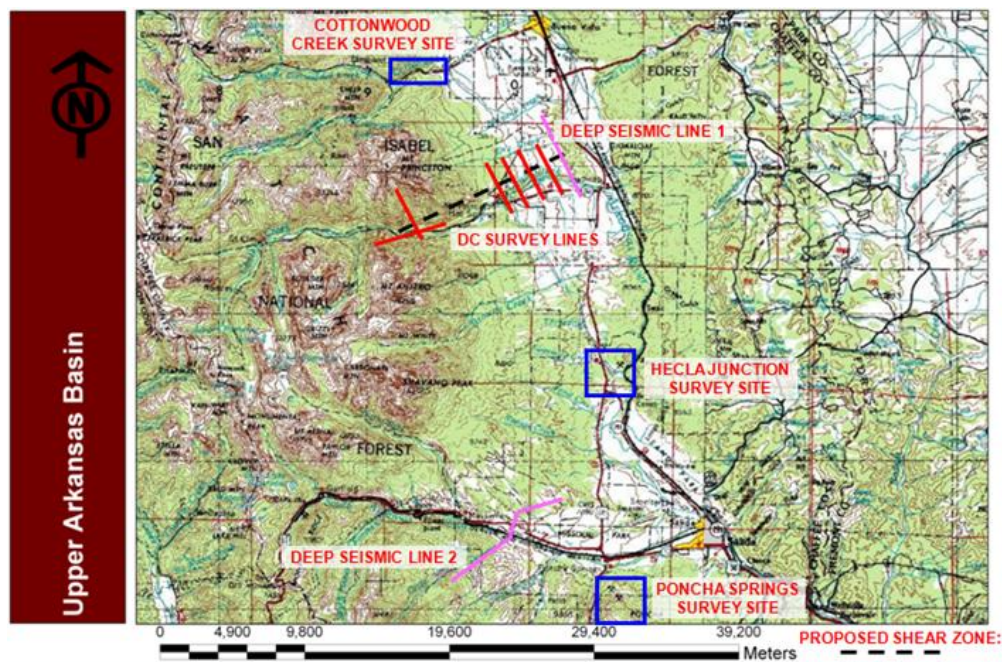
Figure 13.1: proposed sites for 2010 field camp in the Upper Arkansas River Valley

project suggesting there is complex geology that could be understood better with more in depth DC/SP, magnetic, passive seismic and gravity surveys. Two wells have been drilled in the area and attainment and analysis of the well cores and logs, as well as the implementation of VSP surveys, would allow for a highly developed understanding of the local geology.

The rights to the current know hot springs in the location have been sold and the locals of Poncha Springs are keen to determine if another spring exists in the area. First hand experience of the location dictates that it is not suitable for any seismic surveys due to its inaccessibility and the nature of the targets to be imaged. It would be a better use of time and resources to carry out a 3D seismic survey at a more convenient location.

One region of the valley that has yet to be investigated is the Hecla Junction Hot Springs which, uniquely, are on the Eastern side of the valley. The source of the hot springs is unknown, although geological modeling suggests that the hot rocks may extend from East to West across the extent of the valley. This offers a potential geothermal source which will be of great interest to the United States Department of Energy. Because of this it is proposed to run a Field of Pain style of acquisition over the Hot Springs area; including a 3D shallow seismic, DC/SP, magnetic, passive seismic and gravity surveys. These surveys will hopefully allow a full characterization of the Hecla Junction area and indicate its potential as an energy source. A developed geological model of the area could then be used as an analogy for similar east valley sites.

Due to the timely nature of acquiring land ownership information it was not possible to ascertain the ease of access to the proposed sites above. It is therefore imperative that any future group fully investigate this issue and determine the likelihood of permission for survey sites. An auxiliary site is therefore proposed in case these sites are found to be unsuitable. The area of Cottonwood Creek to the north of Mt. Princeton (see Figure 13.1 is of a similar geological nature to the rift at the Field of Pain site. A recreation of the Field of Pain surveys carried out in 2009 at this site would act as a useful analogy for the Mt. Princeton site as well as other similar sites along the western extent of the valley.

Other possibilities for further investigation are undertaking radial seismic to test for anisotropy in the subsurface granite in the field of pain, which could be achieved by placing geophones in the centre and then using shear wave vibroseis or thumper in increasing concentric circles around the geophone, and using geochemistry techniques providing the expertise is available to help characterize the surface make-up especially in the Hecla Junction area. A large scale gravity survey over the entire basin could be undertaken, but this has been attempted in the past, and the results have not been of a high quality and processing times are long.

In a practical sense, the 2010 survey should have a specific data analysis team formed at the start of the field trip, headed by a data boss responsible for collecting all data and saving it so it is quickly available to anybody. This team should undertake initial data processing whilst at the field camp, especially for the survey data to check it is of a suitable quality for use in the project. It is recommended that a team of approximately four people is assigned to this for the entire field trip. A team should also be assigned throughout the processing part of the project to reinterpret previous data and to try and create 3D and large scale models for the entire valley.
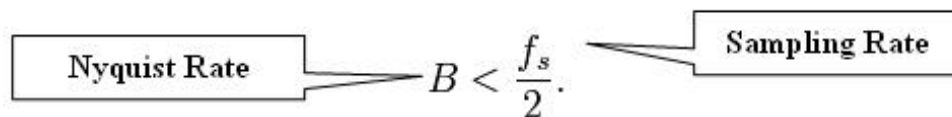
Appendix A

Seismic

A.1 Nyquist Theorem

The nyquist frequency theorem was developed by Harry Nyquist an American physicist and electrical and communications engineer.

The Nyquist Theorem states that the highest frequency which can be accurately represented within a data set (i.e. The Nyquist Rate) is less than half of the Sampling Rate. So the Sampling Rate must always be double the bandwidth to reduce noise within the data. If this is not done, a phenomenon called aliasing occurs. Multiple records of a data set are also taken to reduce high levels of aliasing.

Figure A.1: Nyquist Rate & Sampling Rate

The primary uses of the theorem involve noise reduction and signal analysis within geophysics and telecommunications specifically.

A.2 Huygens Principle

Huygens principle states that every point along a wave front acts as a secondary source and the wave front of a propagating wave of light at any instant is the envelope of spherical wavelets emanating from every point on the previous wave front.
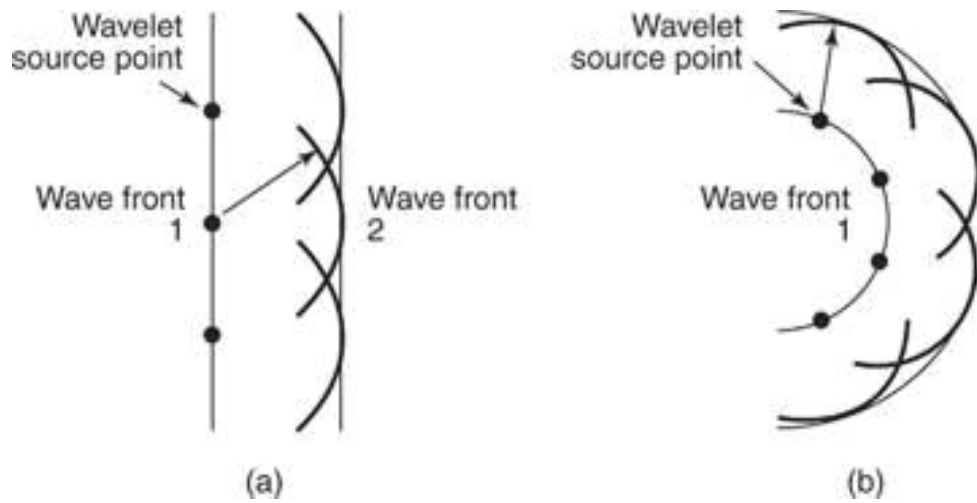
Figure A.2: Huygens Principle

Appendix B

Vertical Sesimic Profile

B.1 Processing Script

B.1.1 File Preparation

- Combine .DAT files:
  seg2segy startingfile .DAT number of files

- Convert files to Seismic Unix
  segyread tape= combinedfile .sgy > filename .su

B.1.2 Header Management Zero Offset

- Change Headers (Must determine for each file)
  sushw key=cdp a= starting depth b= hydrophone increment j= number of phones
  c= total increment < filename .su> filename cdp.su

- Sort Headers
  susort key=cdp < filename cdp.su> filename sorted.su

B.1.3 Header Management Radial Survey

susplit < ../ filename .su key=fldr

(*poundsymbol*)! /bin/sh
count=1
for i in 'ls split*'
do
sushw key=otrav a=$count < $ > 1$i
count = 'expr $count + 1'
if [$count -eq 8]

```
then
count =1
fi
done
count =1
for i in 'ls 1split*'
do
if [ $count -lt 8 ]
then
sushw key=sx a=10 < $i > 2$i
else sushw key=sx a=20 < $i > 2$i
fi
count ='expr $count + 1'
if [ $count -eq 15 ]
then
count=1
fi
done
start = 160
count = 1
for i in 'ls 21split*'
do
sushw key=gx a =$start b=.5 j=37 < $i > 3$i
count = 'expr $count +1'
if [ $count -eq 15 ]
then start='expr $start - 5'
count =1
fi
done
```

for i in 321*; do surange < $i; done — more

fcat 321* > filename .su

B.1.4   File Processing

- Stack Data
  sustack key=cdp < filename sorted.su> filename stacked.su

- Dip Filter
  sudipfilt < filename stacked.su slopes= determine 6 values amps= 6 values dx= determine
  > filename fk.su

B.1.5 Image Creation

- Create .ps Image
  supsimage perc=97 label1='<mark>label</mark>' label2='<mark>label</mark>' f2=<mark>lowest depth *not for dip*</mark>
  d2=<mark>phone increment</mark> title='<mark>title</mark>' < <mark>filename</mark> stacked.su> stackedvsp.ps

- Convert .ps to .pdf
  epstopdf stackedvsp.pdf

B.2   Figures
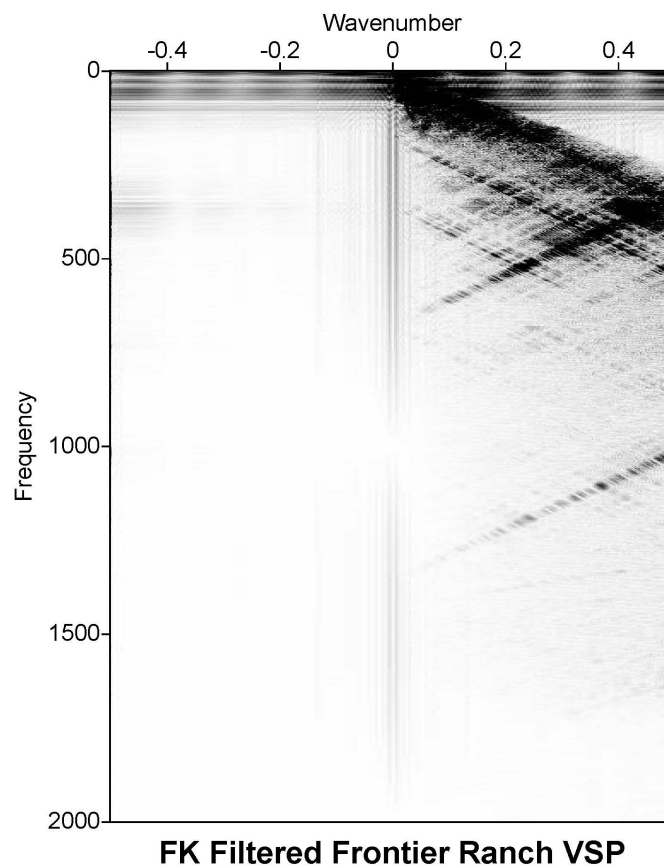
Figure B.1: FK Dip filter removing all negative dipping energy
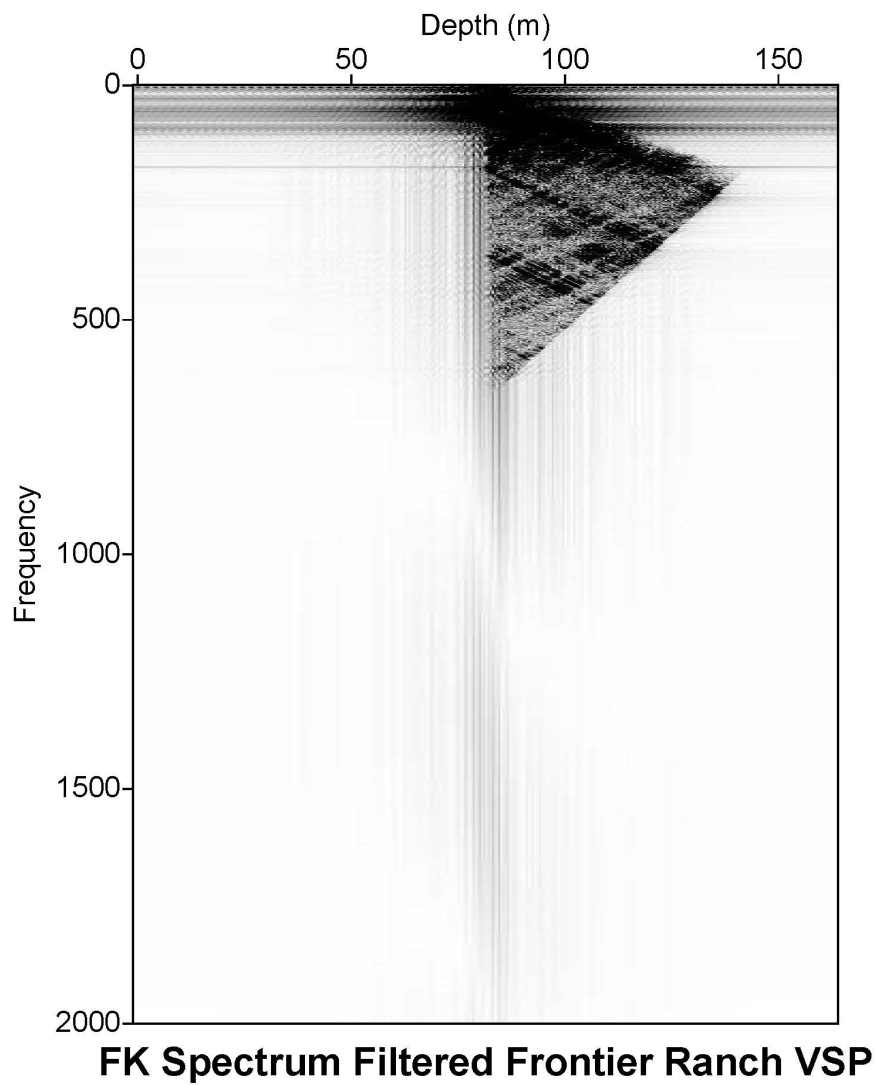
Figure B.2: Anti-Aliad FK Dip filter removing all energy at dips corresponding to slopes above Nyquist frequency
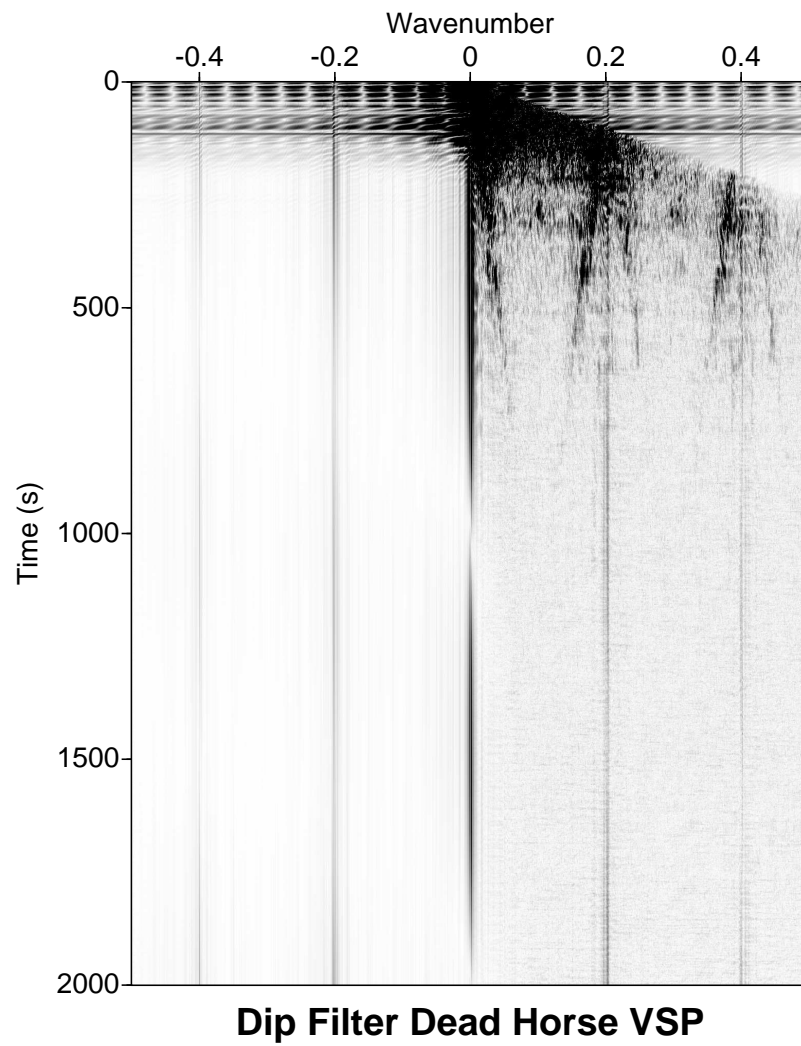
Figure B.3: FK Dip filter removing all negative dipping energy

180
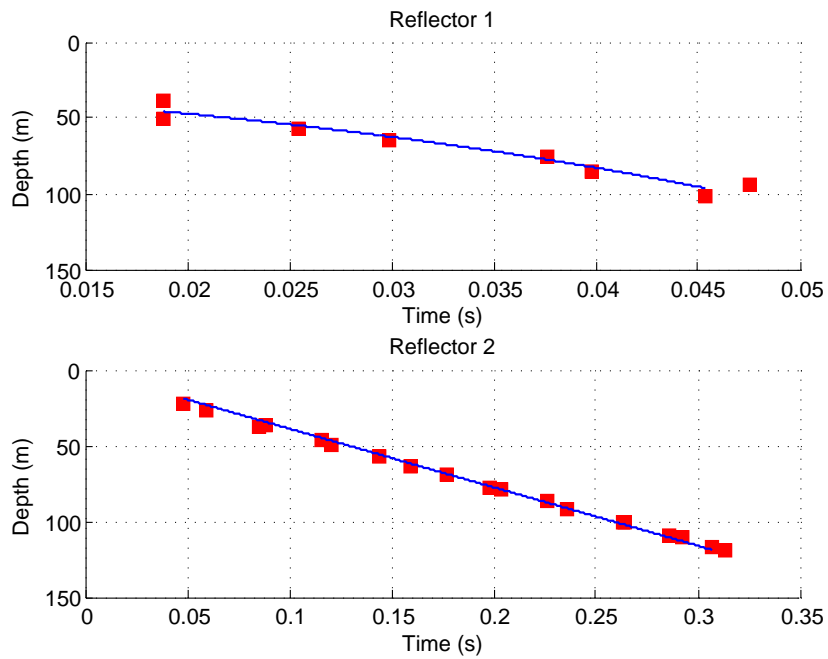
Figure B.4: Frontier Ranch: Velocity models of arrival picks from processed data.

181
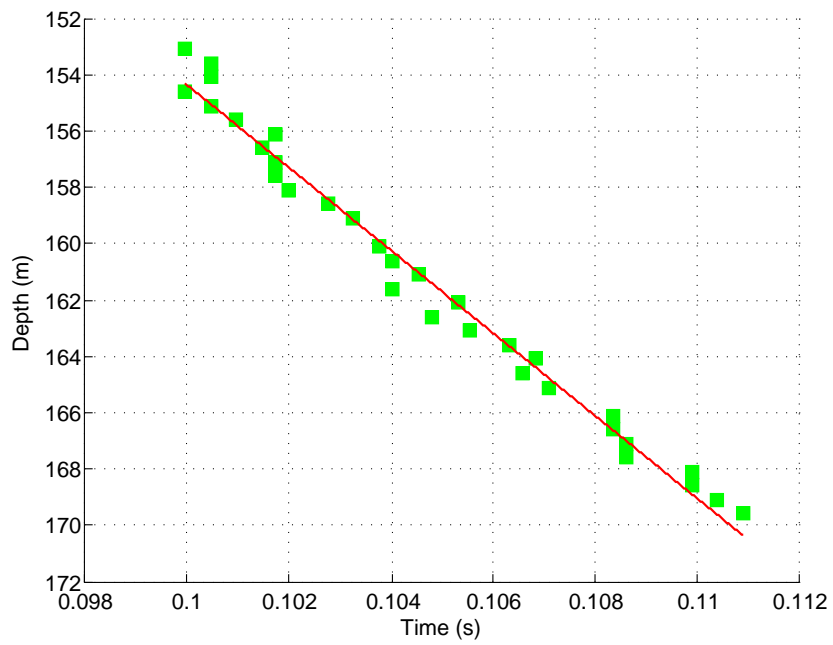
Figure B.5: Dead Horse Lake: Velocity models of arrival picks from processed data.
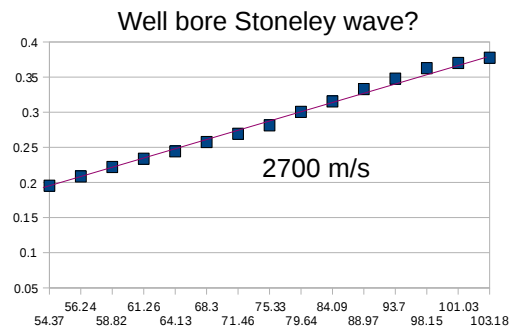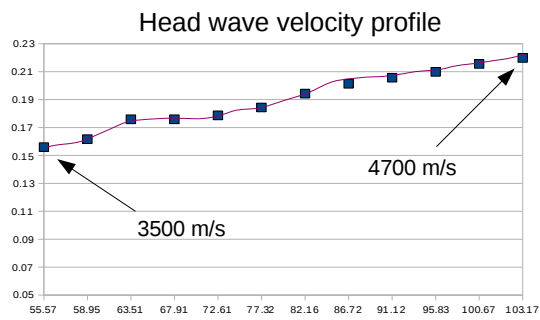
Figure B.6: Dead Horse Lake: Velocity models of arrival picks from processed data.

Appendix C

DC Resistivity & Self-Potential
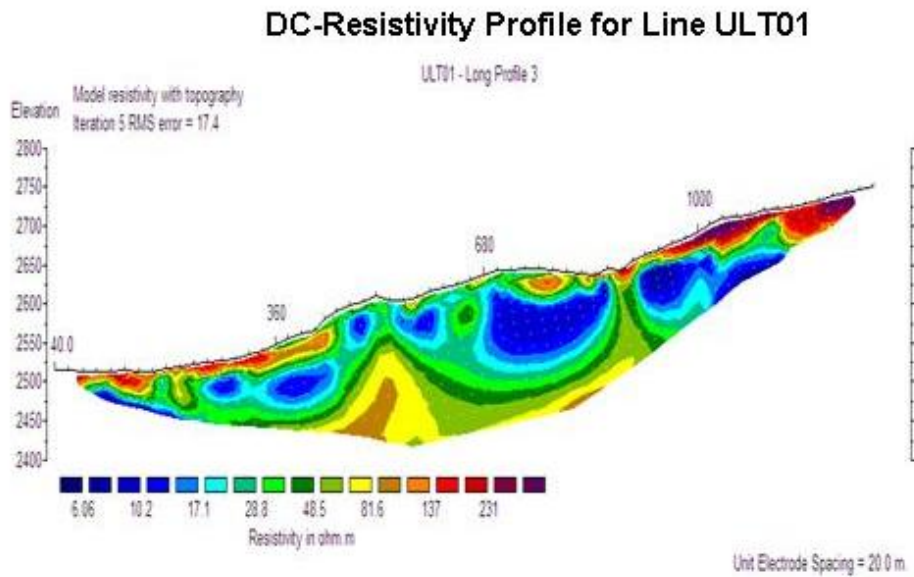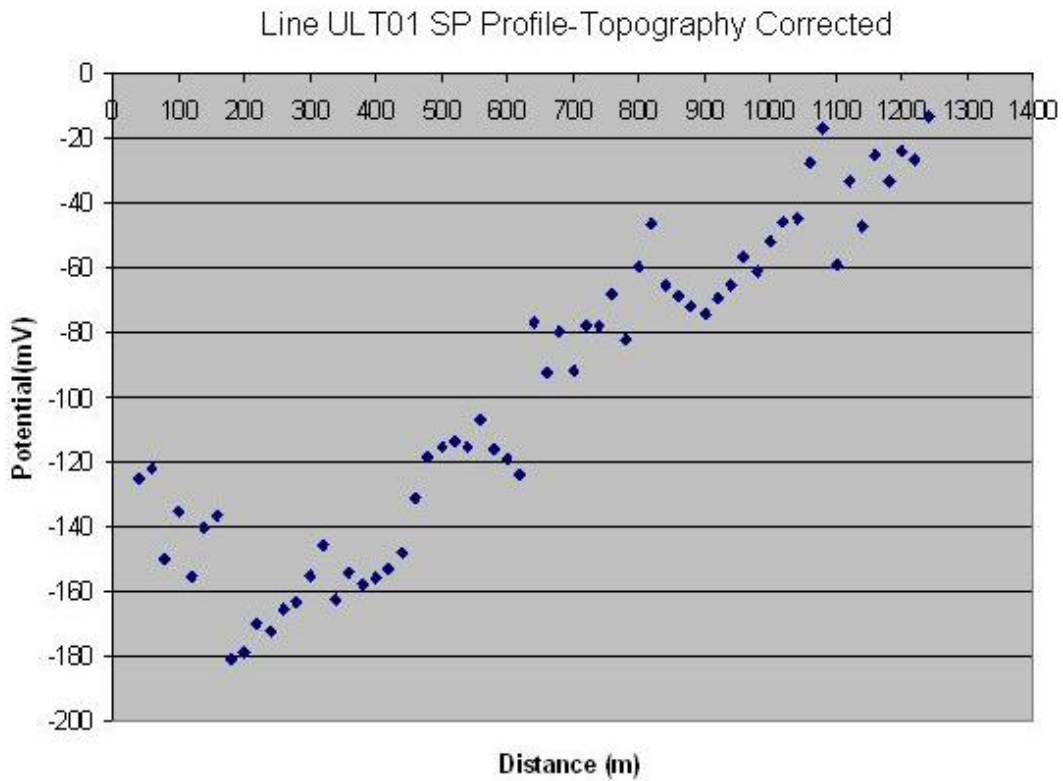
Figure C.1: SP profile for Line ULT01- Topography correction and DC resistivity profile

Line ULT2-SP profile_Topography corrected

DC-Resistivity Profile for Line ULT02
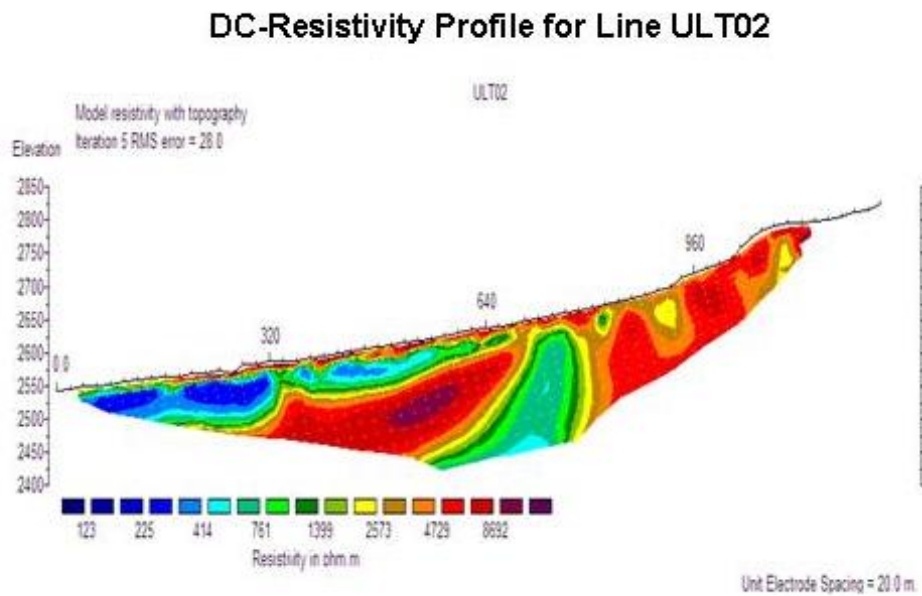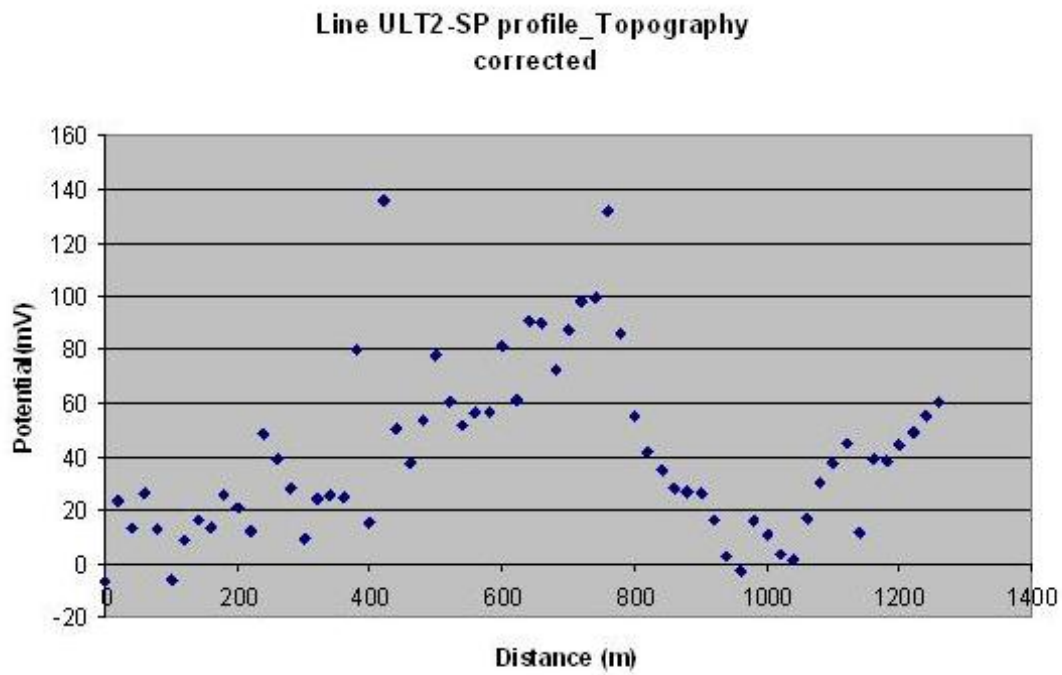
Figure C.2: SP profile for Line ULT02- Topography correction and DC resistivity profile

185
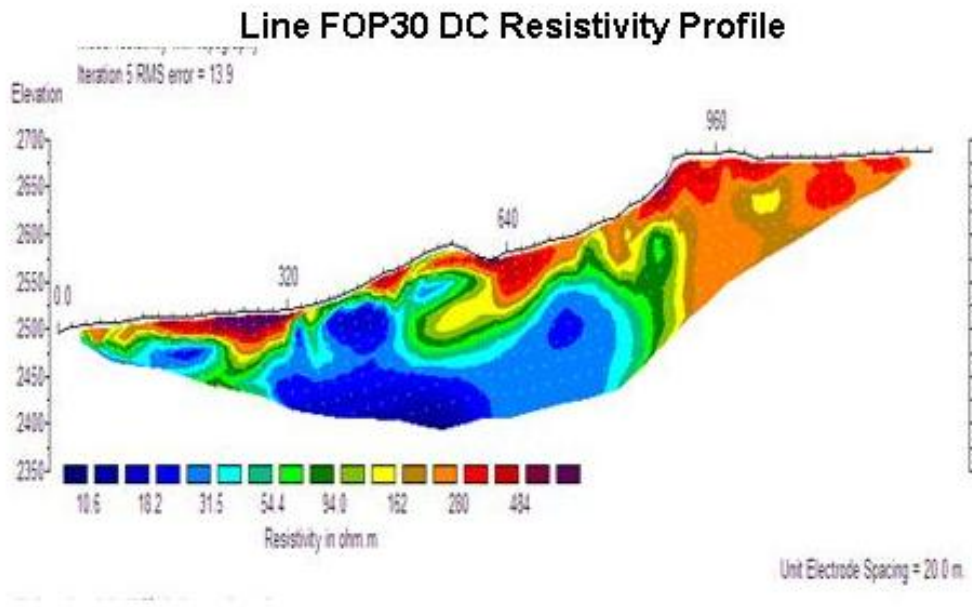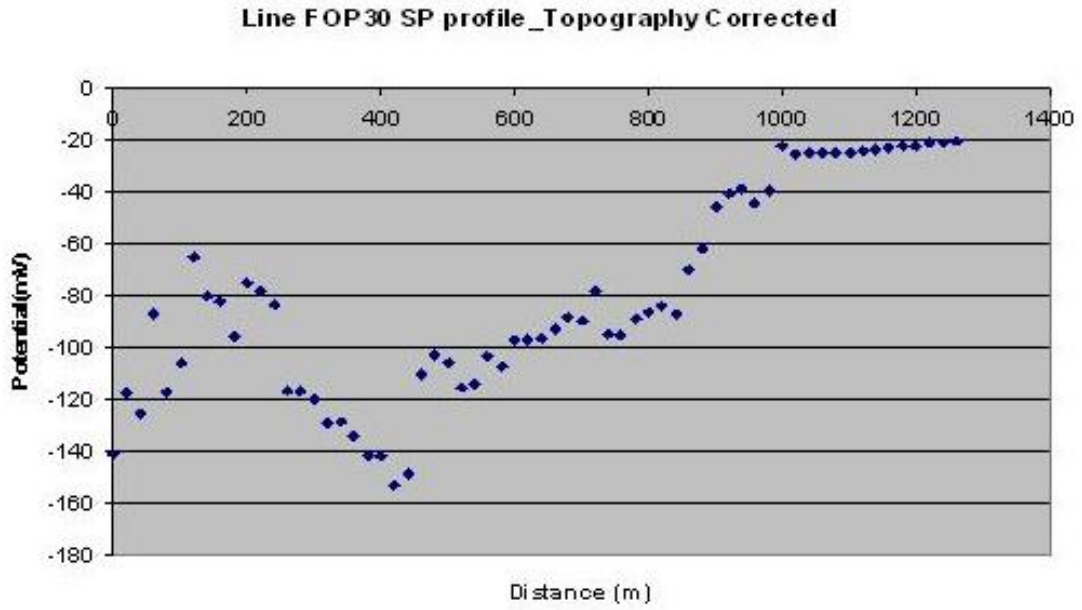
Figure C.3: SP profile for Line FOP30- Topography correction and DC resistivity profile
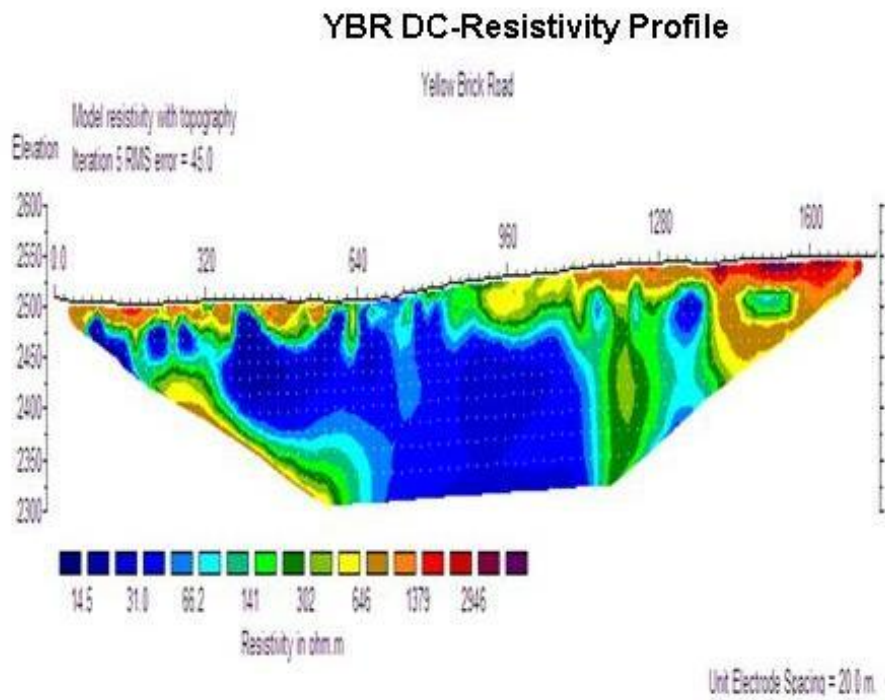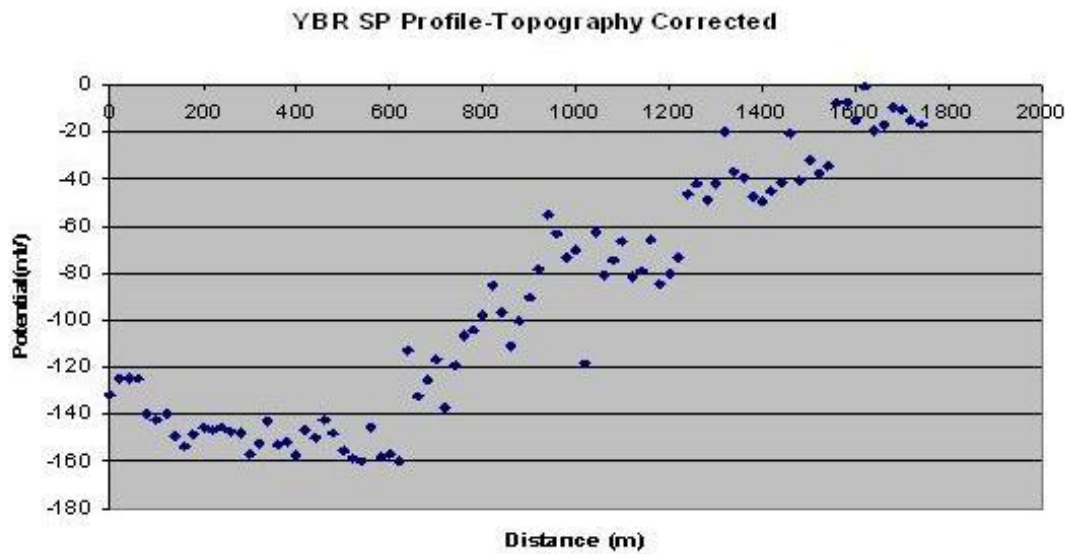
Figure C.4: SP profile for Line YBR- Topography correction and DC resistivity profile

Appendix D

Gravity

D.1 Data acquisition

CG-5:
1. Set the stand on a level patch of ground. Push the spikes into the ground until the stand is leveled. Then place the CG-5 onto the stand so that each foot of the stand is in the corresponding receptacle on the bottom of the instrument.
2. file setup procedures Tune the equipment on by pushing the on/off button. If it takes you to the STATION DESIGNATION screen, press number 4 to go to set up menu. Make sure the SURVEY icon is highlighted. Press F5 (OK) to enter the SURVEY HEADER screen. Make sure the SURVEY ID is highlighted. Press F3 to edit the ID name. Use the number keys to letters and arrow keys to advance to the next letter. The filename should be unique. When your new ID is entered, you press F3 to exit edit mode. There is no reason to edit the Customer and Operator names. Since the automatic corrections are turned off, you do not need to worry about updating the GRID REFERENCE values. Then press F5 to return to the set up menu.

Highlight the Autograv icon and press F5. Make sure all of the automatic corrections and filters are turned off and you only save raw data. If you need edit any of these fields, use arrow keys to highlight them and F3 to edit. Once everything is set correctly, press F5 (record) to return to the set up menu.

Highlight the Clock icon and press F5. Make sure the clock and date are set up correctly. If they are not, edit them the same way described above. Press F5 (OK) to return to the set up menu.
3. data acquisition Press the large yellow button MEASURE CLR to get to the STATION DESIGNATION screen. Press F1 (Option) to enter the DEFINE THE OPTIONS screen. For our surveys, we set the read time to be 60 seconds, the number of cycles to 2, the start delay to 10 seconds and the station separation to 30 meters. Depending on your survey, you may need to edit the line separation. Press F5 (OK) to return to the STATION DES-IGNATION screen. The Station icon should be highlighted. Then Press F3 to edit station number. If you have multiple lines, be sure to edit line numbers so that they correspond

with the right lines. Since the automatic corrections are turned off, you don't need to edit the Elevation. Then press F5 to enter the leveling screen. Use the dials on the stand to level the instrument. Look at the icons in the upper left and right corners of the leveling screen to determine which way the dials need to be turned. The X and Y values at the bottom of the screen indicate how close to the level you are. Zero means perfect leveling. Once the instrument is leveled, press F5 (READ GRAV) to enter the recording phase. Now you have a delay time of 10 seconds to get away (15 to 20 feet) from the instrument before it starts recording. Stay still and avoid any moving objects coming close to the instrument (like a passing truck). When it is recording, there is a blue light on the front of it that is illuminated. When it has finished recording the blue light will turn off and the instrument would beep once. The beep is very quiet and you may not always hear it. When it is done recording, it automatically goes to the AUTOGRAV FINAL DATA screen. From this screen, we hand recorded the time, gravity reading and standard deviation (S.D.) for the two measurements. Then press F5 to record the data in the instrument. After this it should take you back to the STATION DESIGNATION screen. You are now ready to move the instrument to the next station and repeat the data collection procedure. Be sure to update the station number for the new station.

helpful notes: on a hot sunny day, bring a sheet of paper and some tape to cover the screen of the instrument. This will prevent the screen from becoming dark and hard to read.

LaCoste and Romberg G-491 Geodetic Gravity Meter (LNR):
The LNR instrument is shown in figure 10.2
1. Level the meter using the three leveling screws.
2. Unlock the meter by tuning the locking knob counterclockwise all the way.
3. Tune on the light by the small switch to the right of the locking knob.
4. Look through the eye piece and turn the adjustment dial until the cross hair in the eye piece is at 2.4.
5. Record the reading:
In the reading window, the decimal point follows the first four digits. The fifth digit is the first number after the decimal point and this digit corresponds to the integer stamped on the adjustment dial. For example, if the reading window shows 31368 and the adjustment dial shows 8.5, then the correct recording should be 3136.85. Sometimes the fifth digit in the reading window may not be clear (i.e. between 8 and 9), for this reason, we recommend reading all decimal values from the adjustment dial. This reading will have to be converted into mGals before processing.
6. Turn off the light and lock the spring by turning the locking knob clockwise all the way before moving the instrument to the next station.

Base station: The measured value of an instrument changes with time. This phenomenon is called instrument drift. Therefore, the gravimeter would give different readings at different time. In order to measure the instrument drift and tidal affection, the gravity field at a base station needs to be measured repeatedly with certain time interval. Figure D.1 shows a
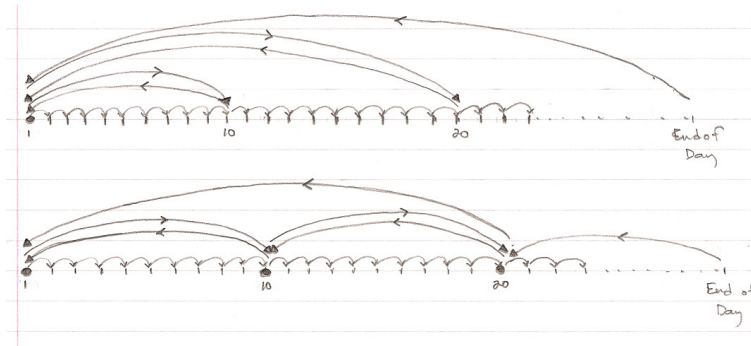
Figure D.1: diagram of three different base station design schemes. The first one is the ideal design, the second one is still valid and easier to realize when the acquisition line is long, and the third is an unaccepted design. Base stations are represented by the black dot.

diagram of three different base station design schemes. The first one is the ideal design; the second one is still valid and easier to realize when the acquisition line is long; the third one looks very similar with the second one, but an unaccepted design. The main point of design a base station is that the base station repeating loops need to be closed and connected to each other. Table D.1 is another presentation of figure D.1. The running time increases from top to the bottom of the table.

D.2   Data processing and software using

Collect all the data into a Excel spread sheet. This master sheet helps you to make files which Oasis Montaj needs in the processing. Oasis Montaj is the software we use to process gravity data.

D.2.1   Create a base file

This file contains the information from all your base stations. The format of the base file is : | station # | gravity | X | Y | elevation | The station # for each base station should be unique in this file. If you have multiple recordings for the same station, give them different station #. For example, if you have three readings for station # 1, you can name their station # in this file as # 1.1, # 1.2 and # 1.3. After copy these values in the spread sheet, save it as a .csv file. In this instruction, let's call it base.csv.

D.2.2   Create a location file

This is a file contains all the location information of the survey. The format of the location file is : | station # | X | Y | elevation | Here we are not very sure about if the stations should have unique station #. To be safe, make them different. After copy these values in the spread sheet, save it as a .csv file. In this instruction, let's call it location.csv.

station	station	station
1	**1**	**1**
2	2	2
...	...	...
9	9	9
10	**10**	10
1	**1**	**1**
11	**10**	**11**
12	11	12
...	...	...
20	**20**	20
1	**10**	**11**
21	**20**	**21**
22	21	22
...	...	...

Table D.1: diagram of three different base station design schemes. The first one is the ideal design, the second one is still valid and easier to realize when the acquisition line is long, and the third is an unaccepted design. Base stations are bold.

D.2.3 Create a survey file

This is a file contains all the data of the survey. The format of the survey file is :

Title								
gm=6	op=(name)	in=(i.e. cG5)	sf=	un=MMC	gf=1980	dn=2.67		
stn	Rdng	Time	Height	Date	Line	Longitude	Latitude	Elevation

where stn is the station #, Rdng is the gravity readings. Put the value of Height and Line to be zero. The format of Time is 00:00 and the format of data is yyyy/mm/dd. After copy these values in the spread sheet, save it as a .txt file. In this instruction, let's call it survey.txt

D.2.4 Create a project file in Oasis montaj

In this instruction, a commend in a clickable tab or drop down menu is shown in a box, e.g. $\boxed{\text{command}}$. "→" means next step. Open the software Oasis montaj. Click $\boxed{\text{Project}}$ → $\boxed{\text{new}}$ to create a project in the same folder where you saved all 3 previous files. Save the project as a .gpf. We use project.gpf in this instruction.

D.2.5 Load data in the project file and coordinate transfer

Click $\boxed{\text{GX}}$ → $\boxed{\text{load menu}}$. It should automatically takes you to the omn folder. Open a file called gravity.omn. This will create a drop down menu called $\boxed{\text{gravity}}$.

Next, we need to load the base station file. Click $\boxed{\text{gravity}}$ → $\boxed{\text{base station}}$ → $\boxed{\text{open/create base station}}$.

Give a name to your base station database.

create a new one?: ⊡yes⊡

load data?: ⊡yes⊡

Base station data source: choose ⊡text data file⊡ and ⊡next⊡

Base file load: click ⊡...⊡ and find your base.csv file. Open it and click ⊡ok⊡. This will load your base station database from base.csv into this project. Now you have X and Y in the work sheet. But in order to use this data base, we need to transfer X and Y to longitude and latitude.

Click ⊡coordinate⊡ → ⊡new projected coordinate system⊡. Choose ⊡existing X⊡ as X, ⊡existing Y⊡ as Y and ⊡process⊡ all lines. Click ⊡next⊡ and you are in another window. Choose ⊡current⊡ as projected (X,Y), ⊡length⊡ as meter, ⊡Datum⊡ as WGS84, ⊡Local datum transform⊡ as [WGS84] world and ⊡Projection method⊡ as UTM zone 13N. Click ⊡ok⊡ and you are in the next window. Choose ⊡longitude⊡ and ⊡latitude⊡. Click ⊡next⊡. Choose ⊡coordinate system⊡ as Geographic (Long,Lat), ⊡Datum⊡ as WGS84, ⊡local datum transform⊡ as [WGS84] world. Click ⊡ok⊡ and you will find the longitude and latitude columns in your work sheet are filled. Save the changes by clicking ⊡Database⊡ → ⊡save database changes⊡. Now you have done loading your base file.

Next we need to load the location file. Click ⊡gravity⊡ → ⊡location⊡ → ⊡open/create location database⊡. Give a name to your location database and click ⊡ok⊡.

Create a new one?: ⊡Yes⊡ Load file?: ⊡Yes⊡ Location data source?: ⊡text data file⊡ and ⊡next⊡

Location file load: click ⊡...⊡ and find your location.csv file. Open it and click ⊡ok⊡. This will load your location station database from location.csv into this project. Then do the coordinate transform (X,Y) → (Long, Lat) for this location work sheet as we did for the base work sheet. Save the changes by clicking ⊡Database⊡ → ⊡save database changes⊡. Location database has been loaded.

Next let's load the survey file. Click ⊡gravity⊡ → ⊡import⊡ → ⊡gravity survey⊡.

filename: click ⊡...⊡ and find file survey.txt. Choose ⊡filetype⊡ as Geosoft Raw File and click ⊡ok⊡. It takes you to the Survey parameter window. Put the start date of your survey in ⊡date⊡. Other parameters are read from your survey file or default. Click ⊡ok⊡. For this survey sheet, we need to do a transform of (Long, Lat) → (X,Y). Click ⊡coordinate⊡ → ⊡new projected coordinate system⊡. Choose ⊡current X⊡ as Longitude, ⊡current Y⊡ as Latitude and click ⊡next⊡. Then Choose ⊡coordinate system⊡ as Geographic (Long,Lat). Keep the other parameters as default and they should be the same as we used for the transformation of (Long,Lat) to (X,Y). Click ⊡ok⊡ and go to the next window. Choose ⊡new X⊡ as X and ⊡new Y⊡ as Y. Click ⊡next⊡ to the next window. Choose ⊡coordinate system⊡ as Projected (X,Y). Same datum and Projected method as we used above in the transformation of (Long,Lat) to (X,Y). Click ⊡ok⊡ and don't forget to save database. At this point, we have load all the data.
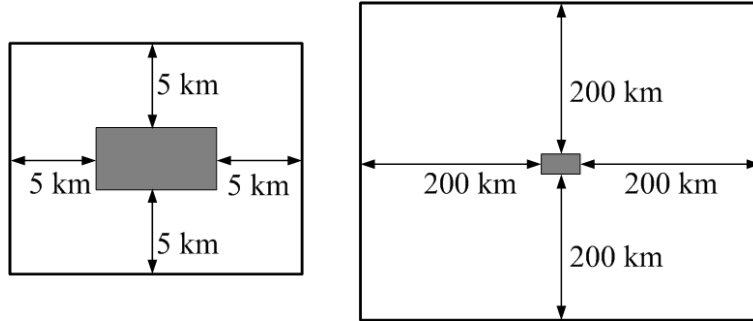
Figure D.2: Local (left) and regional (right) maps used in the terrain correction. Gray area in the center of the map represents the survey site.

D.2.6 Corrections

Click ⟨gravity⟩ → ⟨project information⟩ and fill all the information needed.

1. Drift correction
Click ⟨gravity⟩ → ⟨Drift⟩. Make sure you have correct file name. Click ⟨ok⟩. Check your work sheet. If no new columns are added (no display), right click the head cell of the new column and choose ⟨tidal correction⟩. Then you see a new column called Tidcorr.

2. Averaging
Click ⟨gravity⟩ → ⟨project repeats⟩. Data channel should be Reading/Gravity. Name an output such as Gravity_Avg. Repeats from ⟨station only⟩. Click ⟨ok⟩ and you will see a display of the statistics. You can save this as a report. Right click the head cell of the new column and choose Gravity_Avg to display it.

3. Terrain correction
First we need to load two topographic maps which include the survey area. One is local map and the other is regional map. Figure D.2 shows a diagram of these two maps. The local map has a resolution of 30 m and the regional map has a resolution of 90 m. Click ⟨DAP⟩ → ⟨find data⟩. At the bottom left, choose the position of the local map first. You need to know the minimum and maximum of the map coordinates X and Y. Click ⟨set⟩. On the right side of the window, Click ⟨Geosoft DAP data server (3D)⟩ under tap ⟨Results⟩. Then under ⟨SRTM⟩, choose 30 m resolution for the local map. Then go to ⟨resolution⟩ under ⟨get data⟩ tab. Click ⟨...⟩ and make the slider as low as possible (as close as 30 m). Next choose the coordinate of the regional map and do the same steps as we just did for the local map. Now we got two maps.

In the maps, there are some white dots represent missing data. We need to interpret these values first. Let's start from the local map. Highlight the local grid. Click ⟨Grid & imag⟩ → ⟨utilities⟩ → ⟨field grid dummies⟩. Name your input and output grid, such as 30m.grd

193

and 30m_dummyfilled.grd. Leave all the other parameters as defualt. Click $\boxed{\text{ok}}$ and you got a grid with no missing point. Next do the same step to fill all the missing points for the regional map.

Here we have a trick to display maps in a better way than the default. But you don't have to use it. Click $\boxed{\text{Grid \& imag}} \rightarrow \boxed{\text{display}} \rightarrow \boxed{\text{color shaded grid}}$. Choose the input file that has your map grid, e.g. 30_dummyfilled.grd. Make sure there is no scale factor.

Now we got the two maps for the terrain correction. Click $\boxed{\text{gravity}} \rightarrow \boxed{\text{Terrain correction}}$ $\rightarrow \boxed{\text{create regional correction grid}}$.

regional: your regional grid name (e.g. 90m_dummyfilled.grd)

local: your local grid name (e.g. 30m_dummyfilled.grd)

output: new output name (e.g. gravity_terrain)

outer distance: 166700

inner distance: 4000

Terrain density: 2.67

Optimization: faster

Don't use $\boxed{\text{scan X Y}}$ button because it screws the correction process somehow. Just leave X and Y values blank. Then click $\boxed{\text{ok}}$.

Click $\boxed{\text{gravity}} \rightarrow \boxed{\text{Terrain correction}} \rightarrow \boxed{\text{Terrain correction}}$. X channel: Longitude Y channel: Latitude

elevation: elevation

local slop channel: leave blank.

Leave other parameters as default. Click $\boxed{\text{ok}}$. Now your database may be sorted in a way you don't want. Click $\boxed{\text{database tool}} \rightarrow \boxed{\text{channel tools}} \rightarrow \boxed{\text{sort all by 2 channels}}$.

primary channel: data

sort: ascending

secondary channel: time

sort:ascending

only channels: yes

Click $\boxed{\text{ok}}$ and your data will be sorted ascending in time.

Click $\boxed{\text{Database}} \rightarrow \boxed{\text{Export}} \rightarrow \boxed{\text{CSV etc.}}$.

format: csv

filename: you choose a name

channels to save: all database channels

lines: all

Include dummies: Yes

Include channel name: Yes

Include line names as date: No

Click $\boxed{\text{ok}}$ and you are done.

Appendix E

Super Sting R8 IP

1. Make sure that the box is hooked up to electrode 28

2. Start survey at electrode 1

3. Hook up 2 batteries to allow for a better signal-to-noise ratio

4. TURN ON THE STING: Press STU 1 for Automatic mode

5. Press VWN to Create data file

6. Type in the file name, pressing each key for each respective number

    - Press F1 for the 1st letter (ex, S)
    - Press F2 for the 2nd letter (ex, T)
    - Press F3 for the 3rd letter (ex, U)

7. Press ENTR when complete

8. COMMAND FILE: Use the and + keys to move up and down

    - Available choices are Schlum28, DipDip28, or Wenner28

9. Put the cursor on the file name and press ENTR

10. Scaling factor is the distance between electrodes

11. Press ENTR for the defaults until you get to roll-along

12. If you want a roll-along, select the option with a Y

13. Enter the end address

    - 28 for your 1st survey

14. .Press MEN to exit setup

- This will take you back to Automatic mode menu

15. Press MEN again to take you back to the MAIN menu

16. Press POR6 for System Settings

17. Press VWN2 for cable address setup

    - The start address should be 1 (this is the starting electrode number)

18. Section 1 should be from 1 to 14 and Section 2 should be from 15 to 28

    - If not, clear the table by pressing VMX2
    - Create both sections accordingly by pressing STU1
    - Input the correct low and high electrode numbers
    - Press MEN twice to return to main menu
    - Survey setup should now be complete

19. Press YZ3 for Test mode

20. Press STU1 to test for contact resistance

    - The starting address should be the very 1st electrode (1 for 1st survey)
    - The end should be the last (28 for the 1st survey)

21. Press F1 to start the test

    - Make sure line is clear
    - Prepare to water electrodes that are above 1.2 k

22. Add salt water if you are getting an error

23. Press MEN twice to return to the main menu

24. Press STU1 for automatic mode

25. Press MEA to start taking measurements

    - The box will beep a few times and the time remaining will be at 0:00 when the survey is complete

26. FOR A ROLL-ALONG: Press ENT as prompted by the Sting

    - The box will shut off and you can leapfrog your cables

27. Turn the sting back on when you are ready

28. Enter the end address

    - Need information for end address

29. Press MEN and repeat the contact resistance test.

30. Go to the Automatic mode

31. Press MEA to start taking measurements

32. Enter Y or N for the roll-along

33. DOWNLOAD DATA: Turn on the Sting using the power source that plugs into the wall

34. Press any key on the box

35. Plug in the connector from the computer PC SERIAL COM port on the box

36. Open AGISSAdmin program from AGI

37. Click the computer icon in the upper right hand corner

38. Go to the Config menu and select the correct COM port and baud rate (38400 baud)

39. Click connect

    - The small box will go from red to green if you are connected correctly
    - If not, check all connections

40. The data files will be shown on the right

41. Right click your data file

42. Select Read File to save it to the disk

43. Click the CONV button and select Convert

44. Select Load File from the top menu

45. Select the file you just saved

    - FILENAME.stg

46. If message appears, Target does not support 3D data! Do you want to continue using only XY positions? select Yes

47. Select the correct type of survey

48. Make sure the Surfer for Windows option is chosen for the file output

49. Save converted file

50. The output will give you a file with 3 columns: X, Pseudo Depth, Apparent resistivity

Appendix F

Geometrics Model G-856 Proton Process Magnetometer

1. Use chart to find Gorean date.

2. CLOCK: Press 2 (Auto), then press 5 (Time), then press 0 (Shift). Use number keypad to enter Gorean date and military time consecutively (ex. June 2 at 2:38 pm will be entered as 1 5 3 1 4 3 8). Note: screen will go blank if left inactive for over 30 seconds.

3. TUNING: Press Read and when instrument beeps twice write down first three digits of reading in field/time display screen. Press 6 (Tune), then press 0 (Shift) and use number keypad to enter the three digits you wrote down. Press Enter.

4. LINE NUMBER: Press 5 (Time) and then press 0 (Shift). Use number keypad to enter number of line youre on. Press Enter. Note: Check by pressing 5 again (line number will display in station/day display screen).

5. SET AUTO STORE: Press 2 (Auto), then press 8 (Store) and then press Enter. This will be set almost always, but if it needs to be turned off: press 2 (Auto), then press 8 (Store), then press Clear.

6. SET AUTO RECORD (base station): Press 2 (Auto) then press 0 (Shift). Use number keypad to enter the time in seconds (three digits, with minimum 005) and then press Enter. The instrument will then begin recording at intervals of the time you just entered, and will continue measuring until the battery runs out. To stop auto recording press 2 (Auto) and then press Clear in rapid succession. TAKE A READING: If not in auto record mode, press 9 (Read) to take a reading. If not in auto store mode follow that by pressing 8 (Store).

7. DOWNLOAD DATA: Plug storage box into computer, run MagMap2000 and go to Import in the File menu. When prompted by the computer, press 1 (Output) and then Enter on the magnetometer. Follow on screen directions.

F.1 Notes

- RECALL A READING: To recall previous reading press 7 (Recall). To recall a specific station number press 7 (Recall), then press 0 (Shift). Use the number keypad to type in the station number and then press Enter.

- ERASE A READING: To erase last reading press 7 (Recall), then press 3 (Erase) twice.

  To erase readings after a specific station number press 7 (Recall), then press 0 (Shift), then use the number keypad to type in the station number you want to erase past, then press Enter and finish by pressing 3 (Erase) twice. To erase all readings press 7 (Recall), then press 0 (Shift) twice, then press Enter, then press 3 (Erase) twice.

- BATTERY CHECK: Every time you press 9 (Read), the field/time display screen will briefly say batt and the station/day display screen will give you the battery voltage. Change batteries before the display reaches 7.5 V. To change battery unsnap side black clasps and then replace D batteries (there are 9 in it).

Appendix G

Cesium Magnetometer

G.0.1   To Test Sensors

1. Turn on magnetometer

2. Magnetometer: System setup: Magnetometer test

    - Warmed up and ready when 1 and 2 are 50

G.0.2   Set Time

3. Turn on magnetometer

4. Magnetometer: System setup: Date and Time

5. Sync with GPS clock

G.0.3   Configure GPS Rover

6. Connect 5800 Rover to COM port

7. Use port 2 on rover and USB to Serial Port cable

8. Open GPS Config

    - Connect to 5800
    - Set COM port (My Computer: Properties: Hardware: Device Manager: Ports)
    - Baud rate = 38400

9. In set up menu go to serial outputs

    - Add: NMEA-GGK, Port 1, 1 Hz

- Port Settings: Port 1, Baud rate 19200
- Apply

10. Connect 5800 Rover to Magnetometer

    - Port 1 on rover
    - Must have null modem and gender changer

11. To check, turn on magnetometer

12. Magnetometer: System setup: Com + field: Chat Mode (if working will see GPS numbers)

G.0.4 Start Survey

13. Turn on magnetometer

14. Magnetometer: Simple Survey

    - Pick file 1-5
    - Survey mode = continuous
    - Cycle time = 1.0 seconds

15. Continue Survey or Start Survey

    - To Start hit "mark"
    - To end hit "end line"

G.0.5 To Download to Computer

16. Turn on magnetometer

17. Magnetometer: Data Transfer : PC Controlled transfer

18. On computer (MagMap)

19. Import

    - Make sure using correct com port
    - Pick files to download and where to save them

20. Download Now

Appendix H

Trimble DGPS

H.0.6   Setup GPS Antenna

1. Setup tripod, make sure to level

2. Screw on the dish (L1/L2 Antenna) to the tripod, adjust arrow on top to point North

3. Attach cable to dish (L1/L2 Antenna)

4. Other end will connect to 4700

H.0.7   Setup Base Station Antenna

5. Setup tripod

6. Put black disk on top of tripod

7. Connect satellite antenna on top of rod

   - Must screw together 3 pieces, bottom piece has cord that will connect to HPB450

8. Add rod by screwing into tripod

9. Clip on small battery, 4700 Transmitter and HPB450 to side of tripod

H.0.8   Controller Setup

10. Turn on hand held controller (TSC2)

    - Should be connected to 4700 base station

11. File: New Job: Enter new job name: Accept

12. Select 'Survey': 'RTK': 'Start Base Receiver'

13. Select 'point name'

14. Click right arrow: 'Key In...': 'Here'

15. If base station is location is known, type in position instead of push 'Here'

16. Click 'Accept'

17. Enter antenna height

18. Click 'Start'

19. Disconnect controller (TSC2) from receiver (4700)

H.0.9 Rover Setup

20. Turn on rover (5800)

   - Orange light = satellite connection
   - Yellow light = talking to base station
   - Green light = Rover Battery

21. Select 'Survey': 'RTK': 'Start Survey'

22. Wait for it to connect to the rover, if having problems check bluetooth on controller

23. Choose base station, Click 'Accept'

H.0.10 To collect points

24. Select 'Survey': 'Measure Points' or 'Continuous Topo'

25. Enter rover height

26. Select 'Measure'

27. When done measuring, select 'Store'

   - Point numbers are automatically incremented

H.0.11   To configure Bluetooth

28. Click 'Configuration': 'Controller': 'Bluetooth'

29. Click 'Config', Select both boxes

30. Push 'Esc'

31. Click 'Accept'

Appendix I

EM31-MK2

I.0.12   To Check Battery Level

1. MODE: OPER

2. RANGE: BATT

3. Datalogger: ON

4. Mode: 0

5. Execute Program File: EM31-MK2

6. Display two readings, both should be above 4.4

   - If not replace batteries

7. MODE: OFF

I.0.13   Zero Quadrature

8. Attach transmitter tube

9. MODE: OPER

10. RANGE: 1000

11. Datalogger: ON

12. Mode?: 0

13. Execute Program File: EM31-MK2

14. 'Q' should equal .000 mS/m 1 mS/m

15. MODE: OFF

16. Attach transmitter tube

I.0.14   Equipment Functional Checks

17. MODE: OPER

18. RANGE: 100

    - if Quad: 100, RANGE = 1000

19. Datalogger: ON

20. Mode?: 0

21. Execute Program File: EM31-MK2

    - 'I' should equal .000 ppt 0.1 ppt
    - If not, turn COARSE and FINE controls

22. MODE: PHASE

    - Note Q reading

23. COARSE control rotate one click clockwise

    - Q should NOT change more than 0.2
    - if Q stays within 0.2, phase correct
        - return COARSE to original position
    - if Q goes beyond 0.2
        - return COARSE to original position
        - adjust PHASE about turn clockwise
        - repeat phase test
        - if difference increase, turn PHASE counter-clockwise

24. MODE: COMP

25. COARSE: one click clockwise

    - Q change 22- 26 mS/m

I.0.15 Setup EM31 Datalogger

26. Connect new datalogger

27. Create new file, set all parameters

I.0.16 Measuring Data

Auto Mode

28. Stand at 1st station on 1st line

29. Face direction you are going to walking

30. Press ENTER and start walking

    - Data records at chosen TimeInterval

31. At end of line press ENTER to stop

    - Will pause until next time press ENTER

32. Hit orange trigger at markers

33. To change line number press 4 while paused

I.0.17 Auto Mode

34. Stand at 1st station on 1st line

35. Face direction you are going to walking

36. Press orange trigger

    - Reading taken and recorded
    - Move to next station after hear the beep

37. To change line number press 4

I.0.18 Download Data

38. Connect datalogger to computer

39. On computer run DAT31W.EXE

40. Open line to datalogger

41. DataTransfer: Download EM31 files from Polycorder 600

42. Choose Save In Directory

Bibliography

[1] L. Hart, "Hot springs eyed for renewable project." http://salidacitizen.com/2008/05/hot-springs-eyed-for-renewable-energy-project/, May 14 2008.

[2] E. B. C. M. Matters, "Rocky article on irea objection to renewable energy mandate ommited co-op's controversial funding of global warming critic." http://colorado.mediamatters.org/items/200702210004, June 03 2009.

[3] U. S. G. Survey, "Eros image gallery: States - ned shaded relief: Colorado." http://eros.usgs.gov/imagegallery/index.php/image/2505, May 29 2009.

[4] G. F. C. S. 2008, "Characterization of the upper arkansas river basin, chaffee county, colorado," tech. rep., Colorado School of Mines & Boise State, June 05 2008.

[5] T. Seismic, June 2009. http://www.terrexseismic.com/images/pics/what_is_seismic_01.jpg.

[6] G. BC, June 2009. http://www.geosciencebc.com/i/common/P1010057.jpg.

[7] E. Nemitz, "The dry union formation in howard, co: Documenting the sangre de cristo uplift."

[8] T. R. M. Bacon, R. Simm, *3-D Seismic Interpretation.* Cambridge University Press, 2007.

[9] J. Reynolds, *An Introduction to Applied and Environmental Geophysics.* John Wiley & Sons Ltd, 1997.

[10] A. Jardani, "Reconstruction of the water table from self potential data: A bayesian approach," *Ground Water 47*, vol. 2, pp. 213 – 227, March - April 2009.

[11] B. H. S. A. J. C.H, *Introduction to Applied Geophysics.* W.W. Norton & Company, 1992.

[12] S. A. Shapiro, M. Parotidis, S. Rentsch, and E. Rothert, "Reservoir characterization using passive seismic monitoring: Physical fundamentals and road ahead," *74th Annual International Meeting, SEG, Expanded Abstracts*, 2004.

[13] P. M. Duncan, "Passive seismic: Something old, something new," *Search and Discovery Article*, 2005.

[14] B. Artman, "Imaging passive seismic data," *Geophysics*, vol. 71, pp. SI177–SI187, 2006.

[15] J. Tan, H. Bland, and R. Stewart, "Passive seismic event-classification techniques applied to heavy oil production from Cold lake, Alberta," *77th Annual International Meeting, SEG, Expanded Abstracts*, pp. 1261–1265, 2007.

[16] S. C. Maxwell and T. I. Urbancic, "The role of passive microseismic monitoring in the instrumented oil field," *The Leading Edge*, pp. 636–639, 2001.

[17] E. Rothert and S. A. Shapiro, "Microseismic monitoring of borehole fluid injection: Data modeling and inversion for hydraulic properties of rocks," *Geophysics*, vol. 68, pp. 685–689, 2003.

[18] N. Shapiro, M. Campillo, L. Stehly, and M. Ritzwoller, "High-resolution surface wave tomography from ambient seismic noise," *Science*, vol. 307, pp. 1615–1618, 2005.

[19] J. Ellenberger and T. Bajpayee, "An evaluation of microseismic activity associated with major roof falls in a Limestone Mine," *2007 SME Annual Meeting Exhibit*, pp. 1–5, 2007.

[20] M. Fehler, A. Jupe, and H. Asanuma, "More than cloud: New techniques for characterizing reservoir structure using induced seismicity," *The Leading Edge*, pp. 324–328, 2001.

[21] J. T. Rutledge and W. S. Phillips, "Hydraulic stimulation of natural fractures as revealed by induced microearthquakes, Carthage Cotton Valley gas field, east Texas," *Geophysics*, vol. 68, pp. 441–452, 2003.

[22] P. R. McGillivray, "Microseismic and time-lapse monitoring of a heavy oil extraction process at Peace River," *74th Annual International Meeting, SEG, Expanded Abstracts*, 2004.

[23] H. Asanuma, H. Nozaki, H. Niitsuma, and D. Wyborn, "Interpretation of microseismic events with large magnitude collected at Cooper Basin, Australia," *GRC transactions*, vol. 29, pp. 87–91, 2005.

[24] L. Eisner, T. Fischer, and J. H. Calvez, "Detection of repeated hydraulic fracturing (out-of- zone growth) by microseismic monitoring," *The Leading Edge*, pp. 548–554, 2006.

[25] S. Turuntaev, V. Burchik, and D. Turuntaev, "Microseismic background study for gas field exploration," *77th Annual International Meeting, SEG, Expanded Abstracts*, pp. 115–119, 2007.

[26] F. Cerda and R. Alfaro, "The application of microseismic monitoring in E, P," *77th Annual International Meeting, SEG, Expanded Abstracts*, pp. 1312–1316, 2007.

[27] M. E. Willis, D. R. Burns, R. LU, M. N. Toksos, and N. J. House, "Fracture quality from integrating time-lapse VSP and microseismic data," *The Leading Edge*, pp. 1198–1202, 2007.

[28] M. Miyazawa, A. Venkataraman, R. Snieder, and M. A. Payne, "analysis of microearthquake data at Cold Lake and its application to reservoir monitoring," *Geophysics*, vol. 73, pp. O15–O21, 2008.

[29] Y. Kumano, H. Asanuma, A. Hotta, H. Niitsuma, U. Schanz, and M. Haring, "Reservoir structure delineation by microseismic multiplet analysis at Basel, Switzerland 2006," *77th Annual International Meeting, SEG, Expanded Abstracts*, pp. 1271–1276, 2007.

[30] "Recent earthquakes- last 8-30 days," *United States Geological Survey*, 2009.

[31] A. E. Mussett and M. A. Khan., "Looking into the earth: An introduction to geological geophysics," *Cambridge University*, p. 44, 2000.

[32] A. Hasegawa and A. Yamamoto, "Deep, low-frequency microearthquakes in or around seismic low-velocity zones beneath active volcanoes in northeastern japan," *Techtonophysics*, pp. 233–252, 1994.

[33] P. S. Ran Xuan

[34] J. S. J.P. McCaplin, "Colorado geological survey maps."

[35] O. Tweto, "Precambrian geology of colorado," *Colorado Geology*, p. 43.

List of Figures

216